



universität
wien

DISSERTATION / DOCTORAL THESIS

Titel der Dissertation / Title of the Doctoral Thesis

**„Metabolic Versatility of Nitrifiers Playing a Key Role
in Global Nitrogen Cycling“**

verfasst von / submitted by

Katharina Kitzinger, MSc, BSc

angestrebter akademischer Grad / in partial fulfilment of the requirements for the degree of

Doctor of Philosophy (PhD)

Wien, 2019 / Vienna 2019

Studienkennzahl lt. Studienblatt /
degree programme code as it appears on the student
record sheet:

A 794 685 437

Dissertationsgebiet lt. Studienblatt /
field of study as it appears on the student record sheet:

Biologie / Biology

Betreut von / Supervisor:

Univ.-Prof. Mag. Dr. Michael Wagner
Prof. Dr. Marcel Kuypers

Metabolic Versatility of Nitrifiers Playing a Key Role in Global Nitrogen Cycling



Dissertation

Zur Erlangung des Grades eines Doktors der Naturwissenschaften

- Dr. rer. nat. -

Im Fachbereich Geowissenschaften der



Katharina Kitzinger
Bremen, Mai 2019

Diese Doktorarbeit wurde in der Zeit von Mai 2015 bis Mai 2019 im Rahmen einer „Cotutelle de thèse“ Vereinbarung zwischen der Universität Bremen und der Universität Wien ausgeführt, assoziiert an das Programm “The international Max Planck Research School of Marine Microbiology” (MarMic). Die Ergebnisse dieser Arbeit wurden am Max-Planck-Institut für Marine Mikrobiologie in der Abteilung Biogeochemie, sowie der Universität Wien in der Abteilung für Mikrobielle Ökologie erarbeitet.

This doctoral thesis was conducted as a “Cotutelle de thèse” (joint PhD) between the University of Bremen and the University of Vienna from May 2015 to May 2019. The doctoral candidate is affiliated with the program “The international Max Planck Research School of Marine Microbiology” (MarMic). Experiments were conducted at the Max Planck Institute for Marine Microbiology, Biogeochemistry Department, and at the University of Vienna, Division of Microbial Ecology.

Autorin/Author:

Katharina Kitzinger

Universität Bremen

Max-Planck-Institut für Marine Mikrobiologie

Universität Wien

Abteilung für Mikrobielle Ökologie

Betreuer/Supervisors:

Prof. Dr. Marcel Kuypers

Universität Bremen

Max-Planck-Institut für Marine Mikrobiologie

Univ.-Prof. Mag. Dr. Michael Wagner

Universität Wien

Abteilung für Mikrobielle Ökologie

Gutachter/Reviewers:

Prof. Dr. Samantha B. Joye

Department of Marine Sciences, University of Georgia, Athens

Prof. Dr. Kai-Uwe Hinrichs

Marum, Universität Bremen

Contents

Acknowledgements	1
Summary	5
Zusammenfassung	7
Chapter 1	11
Introduction	
Aims and Outline	
Chapter 2	41
Characterization of the first " <i>Candidatus Nitrotoga</i> " isolate reveals metabolic versatility and separate evolution of widespread nitrite-oxidizing bacteria	
Chapter 3	85
Cyanate and urea are substrates for nitrification by Thaumarchaeota in the marine environment	
Chapter 4	141
Single cell analyses reveal contrasting life strategies of the two main nitrifiers in the ocean	
Chapter 5	177
Flow-through stable isotope probing (Flow-SIP) minimizes cross feeding in complex microbial communities	
Chapter 6	193
Synthesis and Outlook	
Author contributions	207

Acknowledgements

I would have never started this PhD (let alone finished) if it wasn't for a group of wonderful people who supported me all along the way. So, in a way, this is the most important section of the entire thesis (and you have to bear with me because it is rather long).

Doing a PhD between two institutes and countries and being supervised by four people isn't always easy. This being said, I would not want to miss the last years or go through this experience with anybody else than the four of you: Marcel, Michi, Hannah and Laura. Thank you all for making this joint endeavor happen and for putting up with all of it – the great and not so great aspects!

... Marcel Kuijpers – thank you for welcoming me into your group with open arms, for always having an open ear and giving me pep talks whenever I needed them. Your excitement about science is truly contagious. Thank you for giving me a wonderful Northern scientific home base, and for the opportunity to visit some of the most beautiful places I've been to. I have really enjoyed working with you (thanks to you, filling off exetainers in the middle of the night in a loud Peruvian lab full of fish was rather enjoyable, let alone trying to find those air splints). Thank you for all your support, trust and advice, especially during these last months of my PhD. I'm looking forward to what's to come.

... Michael Wagner – thanks to you I discovered my love for microbes and their crazily diverse metabolisms. Thank you for your unwavering support throughout the years, for putting so much trust into me and my abilities, for your insane ideas and for sometimes admitting that not everything is quite so straightforward, and – not the least – thank you for offering me to half-stay in Vienna, and half-go to Bremen for the PhD. I'm really glad I didn't entirely leave my Viennese scientific home base. Your door was always open for me (at times after insistent knocking, especially when facing bureaucratic problems) and I could not have wished for a better mentor.

... Hannah Marchant – I still remember giving my first presentation at Biogeo, before starting my PhD. I distinctly recall this one person smiling enthusiastically as I was talking. It was you that made me confident that going to Bremen was an excellent idea (I have not regretted it!). Thank you for introducing me to the intricacies of process rate measurements, showing me how much fun it is to work in the field and investigate environmental communities rather than just cultures (or WWTPs!). Thanks for all the smoking breaks (though I was not smoking – most of the times), scientific and emotional support, for always being there and for pointing out the bigger picture when I got too bogged down in details.

... Laura Bristow – thank you for taking greenhorn me to the first ship-based field trip, for showing me the wonders of low oxygen incubations, jointly working through nights and teaching me so much about biogeochemistry, nitrification and science in general. I learned a lot from you and I'm really grateful that you were always there for advice and support, even after having physically moved even further North.

... Holger Daims – as you were my supervisor in my very first practical, I feel that a substantial part of me being about to finish a PhD is thanks to you. Thank you for infecting me with your excitement about nitrification (especially about NOB of course!), for always having an open door and ear, scientific input and support. I'm really glad we finished the Nitrotoga project together!

... Frank Stewart and Cory Padilla – I could not have wished for better collaborators than the two of you. You were incredibly supportive, positive and excited about all of our joint projects, and did everything to make even the craziest ideas happen. It was really a pleasure to work with you.

Acknowledgements

... Maria – I would not have wanted to work on our Flow-SIP endeavor with anyone else than you! Thank you for the great time in Aalborg and Vienna, for putting up with me 24/7 for weeks, on top of all the lab stress and for always having an open ear and/or email box for me.

... Craig – I'm sorry for having bothered you so often for more of your miraculous bioinformatics data! I guess that's what you get when you're really good at the things you do. Being a nice human being on top makes this a quite a horrible combination. Thanks for working with me on pretty much all of my projects, for being so determined to find optimal solutions and for always going that extra mile.

... Petra – I'm really grateful you decided to take the opposite path to me and went from Bremen to Vienna, I would have hated not to get to know you. Your energy is inspiring (and sometimes frightening). Thank you for always having an open ear to my nagging about science and life, and for making me feel a bit better about both!

... Gabi, Daniela, Kirsten, Swantje – without all of you, my PhD would have been impossible. Thank you for all your support with measuring samples, teaching me new methods and helping with old ones, lending hands with cruise packing, fighting the HPLC and generally finding solutions to any problem I had.

... Sten, Arno and Abiel – thank you for all your time and energy that you put into measuring our nanoSIMS samples and getting the highest quality data out of these tricky microbes that I've forced us to work with!

... Ulrike, Nadja & Barbara – without your support in Bremen and Vienna, I would have probably stumbled across a hundred bureaucratic obstacles. Thank you for all your help in organizing, communicating and problem solving and for always taking time for me!

... Susanne Steinfeld & Christian Kolowrat – I'm grateful for all your help and support in aligning Uni Bremen and Uni Wien interests to make this joint PhD happen, I would never have managed on my own.

... Philipp – thank you for having been a great colleague (and measuring all of my thousands of mass spec samples) and, more importantly, thank you for being a friend, I'm glad to have you!

... Miri, Julia and Niek a.k.a. the jungle inhabitants – I would not have swapped office mates for anything. You make my time in Bremen extremely enjoyable and I'm really grateful to have friends (and colleagues) like you!

... Babsi, Bela, Steph – you're a major reason why I always feel at home in Vienna. Thank you for being there. Babsi, thanks for being my marine AOA Vienna discussion buddy!

... Niels and Helga – I'm really happy we had this joint time in Bremen, with all the breakfasts, lunches, dinners, teas and coffees, cycling, knitting, laughing (and at times complaining). Spending time with you was always like a mini holiday from everyday stress.

... Sina – I'm really happy you are here. Not only would I lack my favorite fish lab late night exetainer filling buddy and field trip roommate, but nobody would force me to do sports every now and again (and share the sore muscles afterwards!)

... Nadine – thank you for always being there, the great time at Elba fieldtrips, and especially our island-roadtrip-one-day-holiday.

Acknowledgements

... Jasmine – thank you for making the transition from Vienna to Bremen so enjoyable and for sharing friendship, plants, strawberries, elder syrup and furniture with me so readily.

... Clarissa – thank you for the great times in Bremen, Puerto Rico and Peru, for forest hikes, very early and late evening swims, and many great cocktails and dinners.

... Anna – thanks a lot for the nice time in Vienna, Bremen and Peru – I'm happy to have a Nitrospinae buddy like you.

... David and Jan – thanks for being the best first and second master students ever.

... Wiebke – thanks for company, advice and conversations on the many lab-Sundays, late evenings and throughout normal working hours when meeting in the tea kitchen.

... Boran – thanks for your hard-core N-cycling network (!) physiology enthusiasm – it's contagious! Also, I really appreciate your (sometimes grudgingly given) encouragement when I'm in a bad mood.

... Julia – despite the fact that our stay in GB made us suffer quite a bit, I'm happy we suffered together! Thanks for taking me along your AOA/AOB oil refinery adventures and for always being there for me.

... Biogeos & Nitrification group (current and former) – thanks for being such great groups of people to work and be around with, Bremen and Vienna wouldn't feel like home without you!

... Basti – thank you for teaching me pretty much all I know about NOB genome annotation. Thank you for making me feel so welcome during the time I spent with you in Nijmegen.

... Hanna – Without you, I would probably not be doing what I'm doing. I'm glad to have a friend and shining example (!) like you – and I'm happy you're back to the N-cycling world.

... Michi – whenever I come back to Vienna, meeting you is on top of my to do list. Thank you for your friendship during the last six years (time flies!). I'm really grateful you're always there (especially to tell me when I'm being stupid).

... The Mopeds incl. associated members – having you as non-work friends to rely on kept me sane during the last four years. Thank you.

... Karo – having you as a friend, even if physically rather far away, means a lot. Thank you.

... Alven – Ich kann schwer in Worte fassen, wie viel es mir bedeutet, Dich an meiner Seite zu haben. Du hast mir durch all die Jahre den Rücken freigehalten, mich unterstützt, zum Lachen und zum Pausen-Einlegen gebracht, und Du machst mich glücklich. Danke für alles.

... Mama und Papa – Ohne Euch und Eure grenzenlose (im wahrsten Sinn des Wortes) Unterstützung hätte ich das alles nie geschafft. Ihr seid die beste Familie, die ich mir vorstellen kann, und ich bin sehr glücklich, dass ich Euch habe. Danke.

Summary

Nitrification, the stepwise oxidation of ammonia to nitrate via nitrite, is a key process in global biogeochemical nitrogen (N) cycling. Nitrification is carried out by specialized chemolithoautotrophic microorganisms; the ammonia oxidizing bacteria and archaea (AOB and AOA), the nitrite oxidizing bacteria (NOB), and complete ammonia oxidizers (comammox), collectively termed nitrifiers. Despite the importance of nitrifiers in both man-made and natural systems, many aspects of their physiology and *in situ* activity are still poorly understood. Previous studies on nitrifiers in culture and the environment have indicated that metabolic versatility may be a key aspect explaining their success in nature. Both ammonia and nitrite oxidizers can use alternative substrates such as hydrogen, reduced sulfur compounds and organic carbon compounds.

This thesis combines different cultivation-dependent as well as cultivation-independent approaches to study nitrifier metabolic versatility and their environmental importance on different process levels, from single cells to the bulk community.

In **Chapter 2**, the isolation of a new NOB from a municipal wastewater treatment plant provided unprecedented insight into the physiology of key NOB in man-made systems. The organism, *Candidatus Nitrotoga fabula*, is the first isolate from the *Ca. Nitrotoga* genus. Physiological and genomic characterization revealed a separate evolutionary history of nitrite oxidation for this genus, as the key enzyme for nitrite oxidation, nitrite oxidoreductase, of *Ca. Nitrotoga* is only distantly related to nitrite oxidoreductase genes in other known NOB. Intriguingly, the nitrite oxidoreductase of *Ca. Nitrotoga* is affiliated with a clade of uncharacterized genes previously classified as nitrate reductases. These genes are found in physiologically uncharacterized microorganisms, hinting at the presence of yet unknown nitrite oxidizers in both the bacterial and archaeal domain. Furthermore, the genome of *Ca. N. fabula* indicates that in addition to nitrite, hydrogen and sulfite can be used as alternative electron donors. This metabolic versatility may enable *Ca. Nitrotoga* to remain active in the environment even under nitrite deplete conditions.

Metabolic versatility is not restricted to nitrifiers in man-made systems but also characterizes marine nitrifiers. Unlike in man-made systems, ammonium, the primary substrate for nitrification, is hardly detectable in the marine environment. Despite this, AOA, the main ammonia oxidizers in the ocean, can constitute up to forty percent of the microbial community. In contrast to ammonium, dissolved organic nitrogen (DON) is highly abundant in the ocean and previous studies have indicated that some AOA are able to use DON compounds, such as urea and cyanate, as additional energy and N-sources for assimilation. In **Chapter 3**, the environmental relevance of urea and cyanate for marine AOA in the Gulf of Mexico was investigated by combining stable isotope labeling incubations with pure culture experiments and metagenomics. AOA utilized urea and cyanate both directly and indirectly as additional energy and N-sources for assimilation. Especially the finding that cyanate was used by AOA is intriguing, as the genomes of marine AOA lack known enzymes for cyanate utilization. Taken together, these results show that metagenomic analyses alone can be insufficient to infer physiological functions and highlight the importance of *in situ* and activity-based studies. The utilization of urea and cyanate as additional substrates has important implications for the

environment, as it may allow AOA to remain active, even when ammonium is depleted and to evade competition for ammonium with other microorganisms.

In contrast to the highly abundant AOA, the main marine nitrite oxidizers, Nitrospinae, are rare, with a ten-fold lower abundance in most oceanic regions. Nevertheless, the fact that nitrite does not accumulate in the ocean and the vast majority of inorganic N is present as nitrate implies that Nitrospinae are highly active. However, the factors that allow them to keep pace with the AOA are largely unconstrained. In **Chapter 4**, *in situ* growth rates, activity and N-assimilation strategies of Nitrospinae were compared to those of the AOA in the Gulf of Mexico. In the Gulf of Mexico, AOA outnumbered Nitrospinae ten to one, even though ammonia and nitrite oxidation rates were similar and Nitrospinae had five-times higher *in situ* growth rates than AOA. While AOA mainly assimilated ammonium, more than half of the cellular N-demand of Nitrospinae was met by urea and cyanate. Additionally, Nitrospinae had a substantially higher energy yield than AOA, indicating that Nitrospinae are much more efficient in translating the energy from nitrite oxidation into fixed carbon. The high growth rates combined with the low abundance of Nitrospinae *in situ* indicate that their population size is strongly controlled by mortality, possibly transferring a large proportion of fixed carbon into the marine food web. The high energy yield and utilization of organic N-sources by Nitrospinae are likely important factors for their success in the oceans.

Stable isotope labeling experiments yield important insights into substrate utilization patterns in the environment, however, cross-feeding (indirect substrate utilization) can strongly confound the results. In **Chapter 5**, a novel approach, flow-through stable isotope labeling (Flow-SIP), was developed to limit cross-feeding in stable isotope incubations. In this setup, cross-feeding is largely excluded by trapping microbial cells on a filter membrane and supplying a continuous flow of stable isotope labeled substrate, while continuously removing metabolites or breakdown products. This method allows to link specific microorganisms to substrate turnover in the environment and thereby significantly expands the toolbox of microbial ecologists and biogeochemists.

Chapter 6 puts the results obtained in this thesis into a global perspective and provides an outlook on future directions of research on nitrifier metabolic versatility, which will be key to gain a deeper understanding of the physiology, distribution and activity of these important N-cycling microorganisms.

Zusammenfassung

Nitrifikation, die schrittweise Oxidation von Ammoniak zu Nitrat über Nitrit, ist ein Schlüsselprozess im globalen biogeochemischen Stickstoffkreislauf (N). Dieser Prozess wird von spezialisierten chemolithoautotrophen Mikroorganismen ausgeführt, den Ammoniak-oxidierenden Bakterien und Archaeen (AOB und AOA), den Nitrit-oxidierenden Bakterien (NOB) und Comammox-Bakterien, welche Ammoniak in einer Zelle zu Nitrat oxidieren. Gemeinsam werden diese Mikroorganismen als Nitrifikanten bezeichnet. Trotz der Bedeutung von Nitrifikanten für sowohl künstliche als auch natürliche Systeme sind viele Aspekte ihrer Physiologie und ihrer *in-situ*-Aktivität noch immer wenig erforscht. Frühere Studien zu Nitrifikanten in Kultur und Umwelt haben gezeigt, dass metabolische Vielseitigkeit ein Schlüsselaspekt sein kann, der zu ihrem Erfolg in der Umwelt beiträgt, denn sowohl Ammoniak- als auch Nitrit-Oxidierer können alternative Substrate wie Wasserstoff, reduzierte Schwefelverbindungen und organische Kohlenstoffverbindungen verwenden.

In dieser Dissertation wurden verschiedene kultivierungsabhängige und kultivierungsunabhängige Ansätze kombiniert, um die metabolische Vielseitigkeit von Nitrifikanten und ihre Relevanz in der Umwelt auf verschiedenen Prozessebenen zu untersuchen – von einzelnen Zellen bis hin zur mikrobiellen Gemeinschaft.

In **Kapitel 2** lieferte die Isolierung eines neuen NOB aus einer kommunalen Kläranlage wichtige Einblicke in die Physiologie eines Nitrit-oxidierenden Schlüsselorganismus in künstlichen Systemen. *Candidatus Nitrotoga fabula* ist die erste Reinkultur der Gattung *Ca. Nitrotoga*. Die physiologische und genomische Charakterisierung von *Ca. N. fabula* enthüllte die separate Evolutionsgeschichte der Nitrit-Oxidation für diese Gattung, da das Schlüsselenzym für die Nitrit-Oxidation, Nitrit Oxidoreduktase, von *Ca. Nitrotoga* nur entfernt mit Nitrit-Oxidoreduktase-Genen in anderen bekannten NOB verwandt ist. Interessanterweise gehört die Nitrit-Oxidoreduktase von *Ca. Nitrotoga* zu einer Gruppe nicht charakterisierter Gene, die zuvor als Nitrat-Reduktasen klassifiziert wurden. Diese Gene finden sich in physiologisch nicht charakterisierten Mikroorganismen, was auf das Vorhandensein noch unbekannter, sowohl bakterieller als auch archaeeller Nitrit-Oxidierer hindeutet. Darüber hinaus enthält das Genom von *Ca. N. fabula* neben Genen für die Nitrit-Oxidation auch Gene für die Verwendung von Wasserstoff und Sulfit als alternative Elektronendonoren. Diese metabolische Vielseitigkeit könnte es *Ca. Nitrotoga* ermöglichen, auch in Abwesenheit von Nitrit in der Umwelt aktiv zu bleiben.

Metabolische Vielseitigkeit ist jedoch nicht auf Nitrifikanten in künstlichen Systemen beschränkt, sondern ist auch für marine Nitrifikanten wichtig. Im Gegensatz zu künstlichen Systemen ist Ammonium, das primäre Substrat für die Nitrifikation, in den Ozeanen kaum nachweisbar. Trotzdem können AOA, die wichtigsten Ammoniak-Oxidierer im Ozean, bis zu vierzig Prozent der mikrobiellen Gemeinschaft ausmachen. Im Gegensatz zu Ammonium kommt gelöster organischer Stickstoff (DON) im Ozean in hohen Konzentrationen vor, und frühere Studien haben gezeigt, dass einige AOA die DON-Verbindungen Harnstoff und Cyanat als zusätzliche Energie- und N-Quellen für Assimilation verwenden können. In **Kapitel 3** wurde die Umweltrelevanz von Harnstoff und Cyanat für marine AOA im Golf von Mexiko untersucht, indem Inkubationen mit stabilen Isotopen mit Reinkultur-Experimenten und Metagenomik kombiniert wurden. AOA nutzten Harnstoff und Cyanat sowohl direkt als auch indirekt als zusätzliche Energie- und N-Quellen zur Assimilation. Insbesondere die

Verwendung von Cyanat durch AOA ist interessant, da die Genome von marinen AOA keine bekannten Enzyme für Cyanat-Abbau aufweisen. Diese Ergebnisse zeigen, dass Metagenom-Analysen allein nicht immer ausreichen, um auf physiologische Funktionen zu schließen, und heben die Bedeutung von *in-situ*- und aktivitätsbasierten Studien hervor. Die Verwendung von Harnstoff und Cyanat als zusätzliche Substrate hat wichtige Auswirkungen auf die Umwelt, da AOA dadurch selbst dann aktiv bleiben können, wenn kein Ammonium verfügbar ist, und Konkurrenz um Ammonium mit anderen Mikroorganismen vermeiden können.

Im Gegensatz zu den sehr abundanten AOA sind Nitrospinae, die wichtigsten marinen Nitrit-Oxidierer, in den meisten Ozean-Regionen etwa zehnmalseltener. Trotzdem ist Nitrit im Ozean nicht angereichert, und der größte Teil an anorganischem N liegt als Nitrat vor. Das impliziert, dass Nitrospinae trotz ihrer niedrigen Abundanz hochaktiv sind. Die Faktoren, die es ihnen ermöglichen, mit den AOA Schritt zu halten, sind jedoch weitgehend unerforscht. In **Kapitel 4** wurden die *in-situ*-Wachstumsraten, Aktivitäten und N-Assimilationsstrategien von Nitrospinae mit jenen der AOA im Golf von Mexiko verglichen. Im Golf von Mexiko waren AOA zehnmals häufiger als Nitrospinae, obwohl die Oxidationsraten von Ammoniak und Nitrit ähnlich waren. Außerdem wiesen Nitrospinae fünfmal höhere *in-situ*-Wachstumsraten auf als AOA. Während AOA hauptsächlich Ammonium assimilierten, wurde mehr als die Hälfte des zellulären N-Bedarfs von Nitrospinae durch Harnstoff und Cyanat gedeckt. Des Weiteren hatten Nitrospinae eine wesentlich höhere Energieausbeute als AOA, was darauf hinweist, dass Nitrospinae die Energie aus der Nitrit-Oxidation wesentlich effizienter in fixierten Kohlenstoff, also Biomasse, umwandeln. Die hohen Wachstumsraten in Kombination mit der geringen Abundanz von Nitrospinae *in-situ* lassen darauf schließen, dass ihre Populationsgröße stark durch Mortalität kontrolliert wird und dadurch möglicherweise ein hoher Anteil an fixiertem Kohlenstoff in das marine Nahrungsnetz übergeht. Die hohe Energieausbeute und die Nutzung organischer N-Quellen durch Nitrospinae sind wahrscheinlich wichtige Faktoren für ihren Erfolg in den Ozeanen.

Experimente mit stabilen Isotopen liefern wichtige Erkenntnisse über Substratnutzung durch Mikroorganismen in der Umwelt. Allerdings kann Cross-Feeding (indirekte Substratnutzung) die Ergebnisse verfälschen. In **Kapitel 5** wurde ein neuartiger Ansatz entwickelt, Flow-through stable isotope labeling (Flow-SIP), um Cross-Feeding in Inkubationen mit stabilen Isotopen einzuschränken. In diesem Ansatz wird Cross-Feeding weitgehend ausgeschlossen, indem Mikroorganismen auf einer Filtermembran platziert werden und ein kontinuierlicher Fluss von mit stabilen Isotopen markiertem Substrat zugeführt wird, während gleichzeitig Metabolite oder Abbauprodukte kontinuierlich entfernt werden. Diese Methode ermöglicht die Identifikation spezifischer Mikroorganismen, die ein bestimmtes Substrat in der Umwelt umwandeln, und erweitert damit den „Werkzeugkasten“ der mikrobiellen Ökologen und Biogeochemiker.

Kapitel 6 stellt die in dieser Arbeit erzielten Ergebnisse in einen globalen Kontext und gibt einen Ausblick auf zukünftige Fragestellungen zur metabolischen Vielseitigkeit von Nitrifikanten, die für ein tieferes Verständnis der Physiologie, Verteilung und Aktivität dieser wichtigen Mikroorganismen im Stickstoff-Kreislauf von entscheidender Bedeutung sind.

“... the soil is a complicated microbiological medium, and the study of this complex could not be based solely upon the isolation of a certain number of organisms in pure culture. It must be studied as a whole and in the soil itself ...”

Sergej N. Winogradsky (Waksman 1946)

...the same holds true for any environment

Chapter 1

Introduction

All life forms depend on the availability of nitrogen (N), as N is a key element in proteins, nucleic acids and many cofactors and vitamins. N occurs in eight redox states, ranging from -3 (ammonium/ammonia, $\text{NH}_4^+/\text{NH}_3$; and many organic N compounds) to +5 (nitrate, NO_3^-) (Figure 1). Several of the interconversions between N redox-states are exclusively carried out by specialized microorganisms, many of which make a living off the energy gained from N-oxidations and reductions (Kuypers et al. 2018). The N-interconversions catalyzed by microorganisms are tightly linked to the cycling of other elements. This linking occurs both via incorporation of different elements into biomass and via direct coupling of element transformations in respiratory processes (Falkowski et al. 2008).

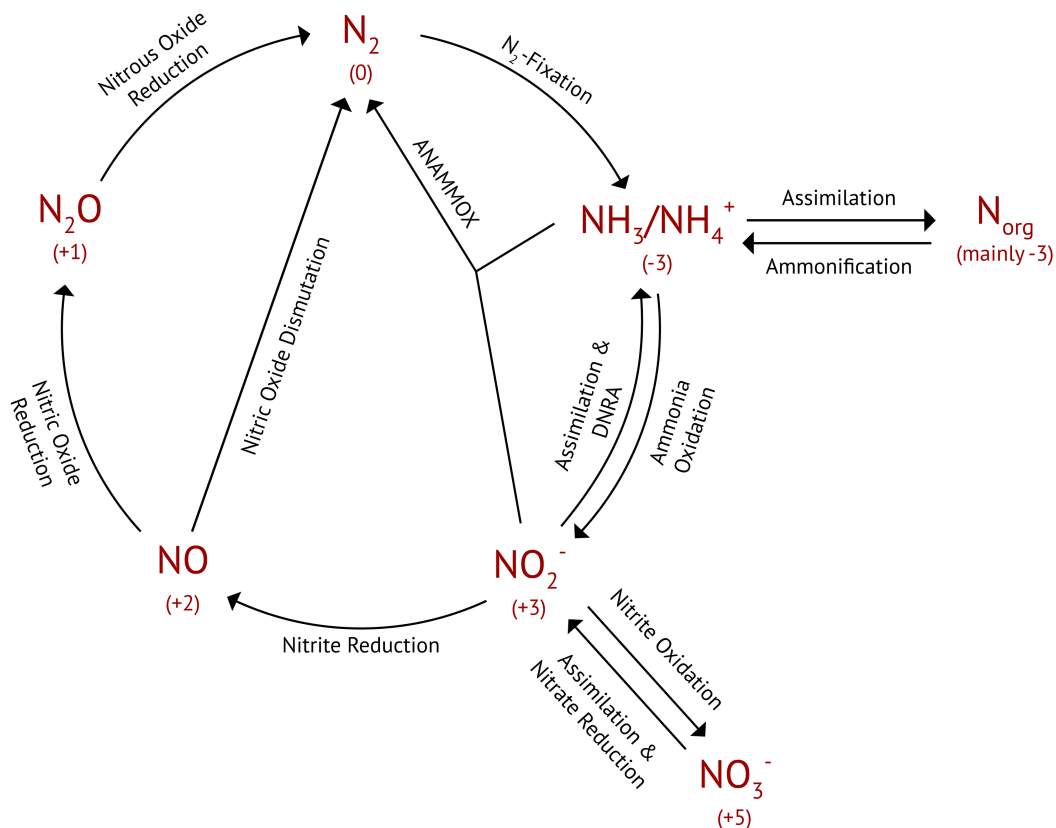


Figure 1 Schematic representation of biogeochemical N-cycling and microbially catalyzed processes. The different N-compounds and their redox state are printed in bold red, process names in black, arrows depict process directionality. Dashed lines indicate processes leading to the formation of gaseous N-compounds and thus conversion to non-bioavailable forms of N. Nitrification encompasses ammonia and nitrite oxidation, denitrification encompasses nitrate, nitrite, nitric oxide and nitrous oxide reduction. ANAMMOX, anaerobic ammonium oxidation; DNRA, dissimilatory nitrate reduction to ammonium.

During the last decades, humans have altered global N-cycling beyond a safe operating space via the massive addition of reactive, bioavailable N to the environment (Rockström et al. 2009). The yearly anthropogenic input of reactive N from the Haber-Bosch process, legume cultivation and fossil fuel burning almost equals the yearly amount of biological dinitrogen (N₂) fixation in terrestrial and marine systems (Canfield et al. 2010). Understanding the physiology of N-cycling microorganisms, and how they react to the anthropogenic changes in the reactive N-budget is vital to counteract negative effects of human activities.

1.1. Key microbial processes in biogeochemical N-cycling

1.1.1. N₂-fixation, N-assimilation and ammonification

The largest inventory of accessible N is atmospheric N₂. N₂ is chemically rather unreactive, due to the stable triple bond between its two N-atoms. While N₂ can be transformed into more reactive, bioavailable N-forms via lightning (Schumann & Huntrieser 2007) and volcanism (Mather et al. 2004), the main natural input of bioavailable N occurs via biological N₂-fixation (Gruber & Galloway 2008; Galloway et al. 2013). During this energetically costly process, N₂ is reduced to ammonia at the expense of eight reducing equivalents and at least 16 ATPs (Bothe et al. 2010). N₂-fixation is exclusively carried out by specialized, but phylogenetically and physiologically diverse microorganisms called diazotrophs, found among bacteria and archaea (Raymond et al. 2004).

The ammonium resulting from N₂-fixation can be directly assimilated by most organisms. In addition to ammonium, many organisms can assimilate nitrate and nitrite (NO₂⁻) via assimilatory reduction to ammonium. Some plants appear to even preferentially assimilate nitrate over ammonium (Britto & Kronzucker 2013). The assimilation of inorganic N into organic N and its liberation from organic N (ammonification) represent the by far largest fluxes in biogeochemical N-cycling (Kuypers et al. 2018) (Figure 1). However, unlike the processes described below, these reactions are not involved in dissimilatory processes.

1.1.2. N-oxide respiration: Reductive pathways in microbial N-cycling

Dissimilatory nitrate reduction to nitrite In the absence of oxygen, nitrate is an important alternative terminal electron acceptor for anaerobic respiration. Due to its positive redox potential, nitrate is among the most energetically favorable terminal electron acceptors after oxygen (Madigan et al. 2012).

Nitrate can be reduced to nitrite by diverse microorganisms found among bacteria, archaea and even eukaryotes (Risgaard-Petersen et al. 2006; Kamp et al. 2015). Electrons for nitrate reduction can be derived from organic and sulfur compounds, hydrogen, or reduced metals (Ehrich et al. 1995; Straub et al. 1996; Gevertz et al. 2000). Nitrate reduction can be a standalone process, releasing nitrite as end product (Gevertz et al. 2000; Tsementzi et al. 2016; Roco et al. 2017), or nitrite can be further reduced. The fate of nitrite has important implications for the environment – denitrification, nitric oxide (NO) dismutation and anaerobic ammonium oxidation (anammox) lead to conversion of nitrite into gaseous forms, and thereby to N-loss from the environment. Alternatively, nitrite can be further reduced to ammonium in a process called dissimilatory nitrate reduction to ammonium (DNRA), which retains N in bioavailable forms.

Denitrification During denitrification, nitrate and nitrite are reduced to gaseous N-compounds in a stepwise fashion, from nitrate reduction to nitrite (see above), nitrite reduction to NO, nitrous oxide (N₂O) and finally to N₂. Phylogenetically diverse microorganisms from all domains of life can denitrify, however, those able to reduce nitrate all the way to N₂ (complete denitrifiers) might be more an exception than the rule (Sanford et al. 2012; Graf et al. 2014; Kamp et al. 2015; Kuypers et al. 2018;

Marchant et al. 2018). Denitrification can be coupled to the oxidation of organic and sulfur compounds, metals, or hydrogen (Nokhal & Schlegel 1983; Straub et al. 1996; Sorokin et al. 2004; Cardoso et al. 2006).

Dissimilatory nitrate reduction to ammonium Unlike denitrification, dissimilatory nitrate (and nitrite) reduction to ammonium (DNRA) retains N in bioavailable forms. DNRA is carried out by phylogenetically diverse bacteria, archaea, and some fungi (Kamp et al. 2015; Kuypers et al. 2018). Electrons for DNRA can – as for denitrification – stem from organic and sulfur compounds, metals or hydrogen (Seitz & Cypionka 1986; Tiedje 1988; Brunet & Garcia-Gil 1996; Robertson et al. 2016).

Nitric oxide dismutation A recently discovered, specialized group of microorganisms in the NC10 phylum appears to be able to carry out nitrite reduction to NO followed by NO-dismutation. This allows for generating N₂ and molecular oxygen (O₂), where the latter is required for the intra-aerobic oxidation of methane by these microorganisms (Ettwig et al. 2010). Thereby, NC10, which thrive in anaerobic environments (Ettwig et al. 2010; Padilla et al. 2016; Graf et al. 2018), carry out one of the few biological reactions generating molecular oxygen.

Anaerobic ammonium oxidation In addition to denitrification and NO-dismutation, a third pathway leads to the formation of N₂. Anaerobic ammonium oxidizing (anammox) Planctomycetes combine the reduction of nitrite with the oxidation of ammonium, producing N₂ (Mulder et al. 1995; Kartal et al. 2011). In addition to N₂, anammox bacteria also produce nitrate when growing on ammonium and nitrite. Oxidation of nitrite to nitrate was long thought to be required for the generation of reducing equivalents for autotrophic carbon (C) fixation (van de Graaf et al. 1997). However, recently, it was shown that nitrate was not produced by anammox bacteria when NO was supplied instead of nitrite (Hu et al. 2019). It was suggested that also under growth on nitrite and ammonium, electrons for C-fixation are derived from hydrazine oxidation to N₂, while nitrite oxidation to nitrate is coupled to nitrite reduction to NO (Hu et al. 2019).

1.1.3. Oxidative pathways in microbial N-cycling – ammonia and nitrite oxidation

All reductive N-cycling respiratory processes rely on the supply of oxidized N, of which nitrite and nitrate are the most common forms. These two oxidized N-compounds are supplied mainly by the activity of aerobic nitrifying microorganisms.

Ammonia resulting from ammonification or N₂-fixation serves as electron donor for ammonia oxidizing microorganisms, which oxidize ammonia to nitrite, using oxygen as terminal electron acceptor. The resulting nitrite can serve as substrate for nitrite oxidizing microorganisms, which gain energy from the aerobic oxidation of nitrite to nitrate. Both ammonia and nitrite oxidizing microorganisms are chemolithoautotrophs and generate reducing equivalents for C-fixation from the oxidation of ammonia and nitrite, respectively. The two processes, ammonia and nitrite oxidation, are collectively termed nitrification and are described in detail in the following sections.

1.2. Nitrification as a key process in global N-cycling

Nitrification plays a key role in the global biogeochemical cycling of N, linking the most reduced N-compound, ammonium/ammonia, with the most oxidized, nitrate. Thereby, ammonia and nitrite oxidation generate key electron acceptors for anaerobic, reductive N-cycling processes and have a strong impact on the availability of N in the environment.

To sustain the human population, efficient fertilization of crops is vital (Erismann et al. 2008). For plant nutrition, reduced, bioavailable N generated via the Haber-Bosch-Process is applied to fields in form of urea or ammonium (Figure 2). Ammonium, as a cation, is well retained in soil due to its binding to negatively charged soil particles, and ammonium can be readily assimilated by plants (Prosser 2011;

Ward 2013). Yet, only a small percentage of the supplied N is actually used for plant growth (UNEP & WHRC 2007), the rest of the applied ammonium is nitrified to nitrate. The produced nitrate can be lost from soil both via conversion to gaseous N-compounds, or via leaching due to its negative charge (Prosser 2011; Ward 2013). Thereby, nitrification is one major cause for the low efficiency of applied N-fertilizer (Erisman et al. 2008; Galloway et al. 2008).

The increased runoff of reactive N-compounds from agriculture has far-reaching consequences, beyond merely influencing the efficiency of agricultural fertilization. N leaching from agricultural fields increases the reactive N-concentration in natural water bodies, leading to eutrophication of freshwater lakes and rivers (Smith 2003). The increased riverine nutrient load strongly affects coastal marine areas (Gruber & Galloway 2008), fueling large algal blooms. As the phototrophic biomass dies off and heterotrophic microorganisms degrade the organic matter, oxygen is gradually depleted, leading to the formation of hypoxic or anoxic waters. During the last decades, both the riverine N-input and the occurrence of hypoxic zones in coastal regions have multiplied, especially at densely populated watersheds (Rabalais et al. 2001; Diaz & Rosenberg 2008). These low-oxygen areas are hotspots of N-cycling processes and act as a buffer zone for anthropogenic N, as the open ocean appears to be much less affected by anthropogenic N-inputs (Gruber & Galloway 2008).

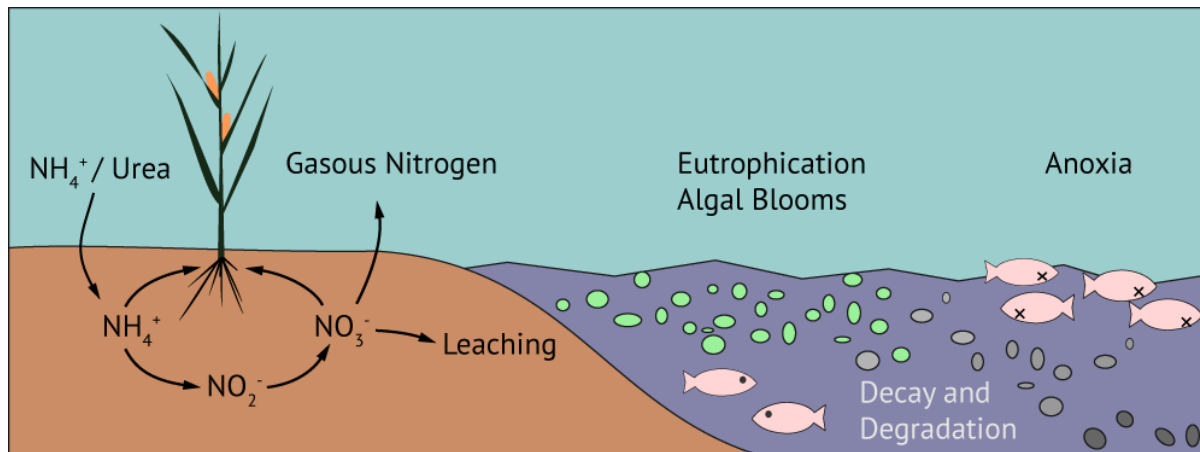


Figure 2 Schematic of the fate of anthropogenic N applied as fertilizer.

Despite the nitrifiers' inherent dependence on oxygen, they are frequently found and highly active in low-oxygen environments – especially in marine systems (Pitcher et al. 2011; Füssel et al. 2012; Beman et al. 2013; Berg et al. 2015; Bristow et al. 2015; Ngugi et al. 2016). Two recent studies revealed an exceptionally high affinity of ammonia and nitrite oxidizers for oxygen in marine oxygen minimum zones (OMZ) and showed that nitrification was sustained even at low nanomolar oxygen concentrations (Bristow et al. 2016; Sun et al. 2017). This has major implications for marine N-cycling. The activity of nitrifiers at the fringes of low oxygen waters retains N in bioavailable forms, as all substrates and products of nitrification are important N-sources that can readily be assimilated. Therefore, the activity and efficiency of the microorganisms catalyzing ammonia and nitrite oxidation strongly impact the availability of N in the environment.

From a human perspective, nitrification can have detrimental effects in agriculture, however, ammonia and nitrite oxidation are also key processes in reducing the impact of human waste products on the environment. Wastewater is strongly enriched in bioavailable N-forms, mainly ammonium from breakdown of organic N-compounds (Wagner & Loy 2002). To avoid eutrophication of natural water bodies due to the release of untreated wastewater into the environment, reactive N

has to be removed prior to discharge. To achieve N-removal, most wastewater treatment plants (WWTP) employ the combined action of nitrifying and denitrifying microorganisms. Under aerobic conditions, nitrifiers oxidize ammonium to nitrate, which is denitrified to N_2 in a second step under anaerobic conditions.

Thus, both in natural and engineered systems, ammonia and nitrite oxidation play a major role. In the following sections, I discuss the phylogenetic and metabolic diversity of the microorganisms carrying out these vital processes.

1.3. Phylogenetic diversity of chemolithoautotrophic nitrifying microorganisms

1.3.1. The discovery of chemolithoautotrophic nitrifiers

After long debate over whether nitrification is a biological process or occurs abiotically (Winogradsky 1890; Waksman 1946), its dependence on the activity of microorganisms was confirmed in the late 19th century by Schloesing and Müntz (1877). Almost at the same time, Frankland and Frankland, Warington, and Winogradsky, published results on the enrichment and/or isolation of the first chemolithoautotrophic nitrifiers (Frankland & Frankland 1890; Winogradsky 1890; Warington 1891). Originally, it was thought that one organism would carry out ammonia oxidation to nitrate, however, finally two distinct microorganisms were isolated – ammonia oxidizing bacteria (AOB) of the genera *Nitrosomonas/Nitrosococcus* and nitrite oxidizing bacteria (NOB) of the genus *Nitrobacter* (Waksman 1946) (Figure 3). For decades, the study of nitrification has focused on these bacterial groups.

Only in the 1970s, NOB other than *Nitrobacter* were discovered – the marine *Nitrospina gracilis* and *Nitrococcus mobilis* (Watson & Waterbury 1971), and later *Nitrospira marina* (Watson et al. 1986).

One major conundrum in nitrification research – why so few AOB were found in marine systems – was only solved in the 2000s. It had been known for some years that mesophilic archaeal groups were a major component of the marine microbial community, however, their physiology was unknown (DeLong 1992; Fuhrman et al. 1992; Delong et al. 1994). Two studies by Treusch *et al.* and Venter *et al.* showed that some of these archaea may be ammonia oxidizers by identifying an ammonia monooxygenase gene, encoding for the key enzyme for ammonia oxidation (see below) on an archaeal metagenomic fosmid (Treusch et al. 2005) or scaffold (Venter et al. 2004). Direct proof for the existence of ammonia oxidizing archaea (AOA) came from the isolation of the marine AOA *Nitrosopumilus maritimus* (Könneke et al. 2005). This discovery revealed that the marine group I archaea, which are highly abundant in the ocean (DeLong et al. 1994; Treusch et al. 2005; Francis et al. 2005; Wuchter et al. 2006), are indeed ammonia oxidizers.

Only recently, another discovery changed the field of nitrification. For over a century, it was assumed that the oxidation of ammonia via nitrite to nitrate always occurs by the concerted action of two distinct microorganisms. Yet, some members of the genus *Nitrospira* (previously assumed to all be nitrite oxidizers) are complete ammonia oxidizers (comammox). These microbes are able to catalyze both ammonia and nitrite oxidation in one cell (Daims et al. 2015; van Kessel et al. 2015).

1.3.2. The currently known phylogenetic diversity of chemolithoautotrophic nitrifiers

To date, ammonia oxidizers have been described in three phyla (Figure 3) – the Thaumarchaeota (or Crenarchaeota, see below), containing the AOA (Brochier-Armanet et al. 2008), the Proteobacteria (AOB) and the Nitrospirae (comammox). Both AOA and AOB occur in a wide range of both marine and terrestrial environments, with AOA dominating especially in environments with low substrate availability (Martens-Habbena et al. 2009; Horak et al. 2013). While comammox also appear to be adapted to low substrate concentration (Kits et al. 2017), to date, they have only been detected in terrestrial environments (Daims et al. 2015; van Kessel et al. 2015; Pjevac et al. 2017).

Currently, all known nitrite oxidizers are bacteria – yet, they are phylogenetically highly diverse (Figure 3). NOB are found in eight genera (*Nitrospira*, *Nitrospina*, *Ca. Nitromaritima*/Nitrospinae Clade 1, Nitrospinae Clade 2, *Nitrococcus*, *Nitrobacter*, *Nitrotoga* and *Nitrolancea*) (Watson et al. 1986; Ehrich et al. 1995; Watson & Waterbury 1971; Lücker et al. 2013; Alawi et al. 2007; Sorokin et al. 2012), distributed over four phyla (Nitrospirae, Nitrospinae, Proteobacteria and Chloroflexi). *Nitrospina*, *Ca. Nitromaritima*, Nitrospinae Clade 2 and *Nitrococcus* are exclusively marine genera, while *Nitrospira* and *Nitrobacter* occur in both marine and terrestrial environments. *Nitrotoga* and *Nitrolancea* have to date only been detected in terrestrial environments.

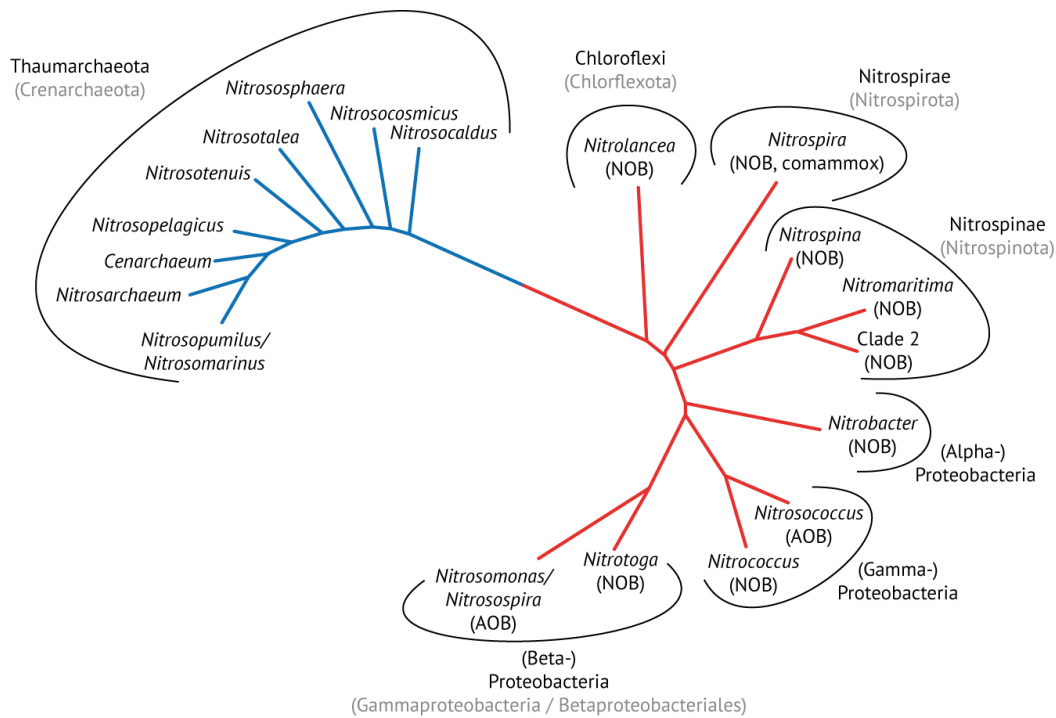


Figure 3 Schematic phylogenetic distribution of currently known genera containing aerobic chemolithoautotrophic nitrifiers. Tree branches correspond to nitrifying genera, corresponding phyla are printed in bold. Archaeal nitrifiers are depicted as blue, bacterial nitrifiers as red branches. All depicted Thaumarchaeota genera contain AOA. The new taxonomic nomenclature proposed by Parks et al. (2018) is given in parenthesis and printed in grey.

1.3.3. Recent changes to nitrifier taxonomy

The taxonomy of microorganisms has long been based primarily on 16S rRNA gene sequence identity, and this gene is still widely used to classify bacteria and archaea. With rapidly increasing numbers of full-length microbial genome sequences, taxonomic classification has shifted towards comparisons of entire genomes (e.g. Konstantinidis et al. 2005) or a set of concatenated universal marker genes (Delsuc et al. 2005), rather than a single gene sequence. Recently, a new taxonomy (Genome Taxonomy Database GTDB, <http://gtdb.ecogenomic.org>) has been proposed (Parks et al. 2018). This taxonomy has led to substantial changes in the classification of bacterial and archaeal taxonomic ranks and is based on relative evolutionary divergence, thereby correcting for lineage-specific rates of evolution (Parks et al. 2018). This has for example led to reclassification of the former class Betaproteobacteria to the family Betaproteobacteriales within the class Gammaproteobacteria, and the former phylum Thaumarchaeota to the class Nitrososphaeria within the phylum Crenarchaeota. Additionally, the phyla Nitrospinae, Nitrospirae and Chloroflexi have been renamed Nitrospinota, Nitrospirota and Chloroflexota, and the genus *Nitrospira* has been split into several genera

(<http://gtdb.ecogenomic.org>, Parks et al. 2018). In this thesis, this new taxonomy has not been implemented for consistency between the (partly published) chapters.

1.4. Metabolic diversity of nitrifying microorganisms

1.4.1. Canonical metabolism of chemolithoautotrophic nitrifiers

Chemolithoautotrophic ammonia oxidation

Canonical, chemolithoautotrophic nitrifying microorganisms have evolved a complex enzymatic machinery involved in ammonia and nitrite oxidation, which is still not fully understood (Kuypers et al. 2018; Lancaster et al. 2018).

In AOB, AOA and comammox, the enzyme ammonia monooxygenase (AMO) converts ammonia to hydroxylamine (Hooper et al. 1997; Vajjala et al. 2013) (Figure 4a). In addition to AMO, methane monooxygenase (MMO), an enzyme closely related to AMO found in methanotrophs, also catalyzes the conversion of ammonia to hydroxylamine, although less efficiently than AMO; likewise, AMO can (inefficiently) convert methane to methanol (Kuypers et al. 2018).

The first step of the ammonia oxidation pathway, the conversion of ammonium to hydroxylamine is endergonic and requires molecular oxygen and two electrons, which stem from hydroxylamine/NO oxidation later in the pathway. Hydroxylamine is further oxidized, finally resulting in the formation of nitrite. For a long time, it was assumed that hydroxylamine oxidoreductase (HAO) directly oxidizes hydroxylamine to nitrite. However, recently, it was shown that the HAO from AOB forms NO, rather than nitrite as end product (Caranto & Lancaster 2017) (Figure 4a). As comammox *Nitrospira* possess an enzymatic machinery closely related to that of AOB (Daims et al. 2015; van Kessel et al. 2015), these results likely extend to comammox HAO (Lancaster et al. 2018). To date, the enzyme in AOB (and comammox) responsible for oxidation of NO to nitrite (nitric oxide oxidoreductase, NOO) has not been unambiguously identified (Lancaster et al. 2018; Stein 2019). For AOA, which lack a HAO homologue, the enzymes involved in hydroxylamine oxidation are entirely unknown. Nonetheless, NO also appears to be an obligate intermediate in the ammonia oxidation pathway of AOA (Kozłowski et al. 2016) (Figure 4b).

Under low oxygen conditions, AOB release substantial amounts of NO and N₂O as a result of a process termed “nitrifier denitrification”. This process has been implicated as electron sink under low oxygen conditions (Cantera & Stein 2007). In AOB, N₂O production increases with decreasing oxygen concentration. AOA also release N₂O, however, this appears to be due to abiotic reactions of the metabolic intermediate NO, rather than an enzymatically catalyzed reaction (Stieglmeier et al. 2014). Conflicting results have been obtained whether N₂O production by AOA increases with decreasing oxygen conditions (Löscher et al. 2012; Qin et al. 2017) or not (Stieglmeier et al. 2014). This is highly relevant to predict future emissions of N₂O, a potent greenhouse gas, because low oxygen waters will likely expand in the marine environment due to global warming (Pörtner et al. 2014). If the highly abundant marine AOA release more N₂O at decreased oxygen concentrations, they could substantially affect future marine greenhouse gas emissions.

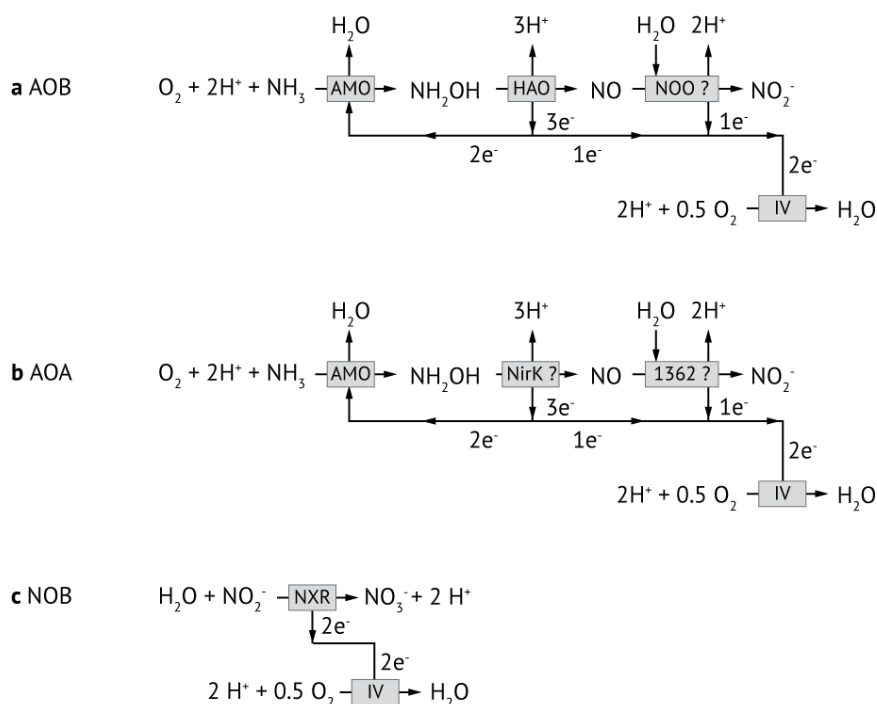


Figure 4 Scheme of ammonia and nitrite oxidation pathways in AOB (a), AOA (b) and NOB (c). Enzymes are depicted as grey boxes. AMO, ammonia monooxygenase; HAO, hydroxylamine oxidoreductase; IV, complex IV (terminal oxidase); NirK, nitrite reductase; NOO, putative NO oxidoreductase; NXR, nitrite oxidoreductase; 1362, a membrane-anchored Cu metalloenzyme (T478_1362); ? indicates hypothetical enzyme function/enzyme. The ammonia oxidation pathway for AOB was modified from Lancaster *et al.* (2018), for AOA from Carini *et al.* (2018). Alternative ammonia oxidation pathways have been suggested for AOA (e.g. Kozłowski *et al.* 2016). The nitrite oxidation pathway of NOB is depicted as in e.g. Lückner *et al.* (2010).

Chemolithoautotrophic nitrite oxidation

While ammonia oxidation to nitrite requires the action of many enzymes, nitrite oxidation to nitrate requires only one enzyme. In nitrite oxidizing bacteria, the enzyme nitrite oxidoreductase (NXR) oxidizes nitrite to nitrate in a single reaction. It is noteworthy that the oxygen atom in nitrate is derived from water, rather than from molecular oxygen. Unlike ammonia oxidizers, NOB use molecular oxygen only as terminal electron acceptor (Hussain Allem & Sewell 1981; Kumar *et al.* 1983) (Figure 4c). There are two possible orientations of the NXR enzyme, which is thought to be anchored in, or associated to, the cytoplasmic membrane in NOB. The NXR active site can face the cytoplasm, as in *Nitrobacter*, *Nitrolancea*, *Nitrococcus* – and, in a divergent form – in the phototroph *Thiocapsa* (Meinke *et al.* 1992; Sorokin *et al.* 2012; Hemp *et al.* 2016). Alternatively, NXR can face the periplasm, as in *Nitrospira* and *Nitrospina* (Spieck *et al.* 1998; Bartosch *et al.* 1999; Lückner *et al.* 2010). For *Nitrotoga*, it is unknown how NXR is oriented.

The orientation of the NXR active site is important, as it has energetic consequences for NOB. During nitrite oxidation, protons are generated (Figure 4c). When NXR is oriented toward the periplasm, the generated protons directly contribute to the proton motive force across the cytoplasmic membrane, thereby contributing to ATP synthesis (Lückner *et al.* 2010). Thus, nitrite oxidation in *Nitrospira* and *Nitrospina* is considered to be more energy efficient than in other NOB, which generate protons on the energetically “wrong” side of the membrane.

Carbon fixation pathways in AOB, AOA and NOB

Aerobic chemolithoautotrophic nitrifiers employ a wide variety of C-fixation pathways: genome-sequenced proteobacterial nitrifiers (all known AOB, *Nitrobacter* and *Nitrococcus*) and *Nitrolancea*

encode genes for the Calvin-Benson-Bessham cycle (Klotz et al. 2006; Starkenburg et al. 2008; Sorokin et al. 2012; Bollmann et al. 2013; Füssel et al. 2017), *Nitrospira* and Nitrospinae NOB for the reverse tricarboxylic acid (rTCA) cycle (Lücker et al. 2010; Lücker et al. 2013; Koch et al. 2015; Ngugi et al. 2016; Pachiadaki et al. 2017), and AOA use a highly energy-efficient modification of the hydroxypropionate/hydroxybutyrate (HP-HB) cycle (Könneke et al. 2014).

All nitrifiers face the problem that the electrons generated from ammonia and nitrite oxidation are too electropositive to be directly transferred to NAD(P)H (Madigan et al. 2012). As chemolithoautotrophic nitrifiers require NAD(P)H or other reducing equivalents for fixation of inorganic C, reducing equivalents have to be generated via reverse electron transport.

1.4.2. Heterotrophic, anaerobic and photolithoautotrophic nitrifiers

Most research on nitrifying microorganisms has focused on chemolithoautotrophic nitrifiers that oxidize ammonia to nitrite and nitrate with oxygen as terminal electron acceptor. Yet, there are also heterotrophic organisms that nitrify as a side reaction of their metabolism. These organisms don't necessarily oxidize ammonia to nitrite/nitrate, but more generally convert a more reduced to a more oxidized N-compound (Stein 2011). In heterotrophic nitrifiers, which are found among bacteria, archaea, algae and fungi (Bock & Wagner 2006), these oxidations are not linked to energy conservation (Stein 2011).

Other microorganisms (*Thiocapsa* and *Rhodospseudomonas*) use nitrite as electron donor for anoxygenic photosynthesis (Griffin et al. 2007; Schott et al. 2010; Hemp et al. 2016), thereby decoupling nitrite oxidation from the availability of oxygen. Unlike heterotrophic nitrifiers, phototrophic nitrite oxidizers use an NXR related to cytoplasmic nitrate reductases (NAR) to oxidize nitrite to nitrate (Hemp et al. 2016). Anammox bacteria also oxidize nitrite to nitrate anaerobically (see above), and use NXR enzymes closely related to those of Nitrospinae and Nitrospirae (Lücker et al. 2010; Lücker et al. 2013). Anammox bacteria can contribute substantially to nitrate formation in the environment, as up to 20% of the total nitrite turnover are oxidized to nitrate (van de Graaf et al. 1997). The contributions to N-cycling from heterotrophic and photolithoautotrophic nitrifiers are to date not well constrained, but are considered to constitute only a minor fraction in most environments (Stein 2011).

1.4.3. Non-canonical nitrifier metabolism

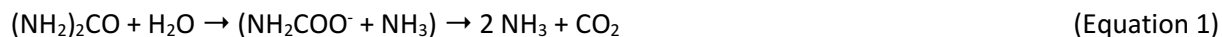
For most of the last century, chemolithoautotrophic nitrifiers were considered to be exceptionally specialized microorganisms, making use only of ammonium/ammonia and nitrite. Recent studies, however, challenge this view and started to uncover a much more diverse metabolism in many nitrifiers, which may contribute to their environmental distribution and success (Daims et al. 2016) (Figure 5). Below, a brief overview of the known alternative metabolisms in nitrifiers is given.

Dissolved organic N as alternative energy and N-source for nitrifiers

The largest pool of reduced bioavailable N in the environment is dissolved organic N (DON, here defined as compounds containing both C and N atoms), while ammonium rarely accumulates (e.g. Gruber 2008). Therefore, it may be beneficial for ammonia oxidizers to invest into the use DON as additional source of ammonia when ammonium is limiting.

Indeed, urea, a simple DON compound, has long been known to serve as additional energy source for ammonia oxidizers. The cytoplasmic enzyme urease allows for the breakdown of urea into ammonium and CO₂, thereby providing ammonia oxidizers with their primary substrates. Urease first catalyzes the hydrolysis of urea to one molecule ammonia and one molecule of carbamate, which spontaneously decays into another molecule of ammonia and CO₂ (Equation 1, Mobley et al. 1995).

Urea use by ammonia oxidizers has been shown both in pure culture (Koops et al. 1991; Tourna et al. 2011; Spang et al. 2012; Qin et al. 2014; Bayer et al. 2016) and the environment.



Many AOA in marine systems can cover part of their energy requirement from the use of urea (Alonso-Saez et al. 2012; Connelly et al. 2014; Seyler et al. 2014; Tolar et al. 2017; Seyler et al. 2018), and urea-derived ammonia oxidation rates can even equal the ammonia oxidation rates (Santoro et al. 2017) (Figure 5d). Urea use has also been suggested to be important for ammonia oxidizers in acidic soils, where use of urea circumvents the low ammonia availability at low pH (De Boer et al. 1989; Allison & Prosser 1991; Burton & Prosser 2001; Lu et al. 2012).

Also cyanate, another simple DON compound, was shown to serve as an alternative substrate for the terrestrial hot-spring AOA isolate *Nitrososphaera gargensis* (Palatinszky et al. 2015) (Figure 5d). Similar to urea, cyanate is broken down to ammonium and CO₂ by an intracellular enzyme – cyanase. This reaction is bicarbonate dependent, and also occurs via an instable intermediate, carbamate, which spontaneously decays to ammonium and CO₂ (Johnson & Anderson 1987) (Equation 2).



The cyanase encoded by *N. gargensis* appears to have been acquired via lateral gene transfer and is closely related to cyanases of *Nitrospira* NOB (Spang et al. 2012; Palatinszky et al. 2015). Similar cyanases were found in metagenomic data of peat soil and permafrost, yet, they could not unambiguously be assigned to AOA (Palatinszky et al. 2015). To date, it is unknown whether cyanate is also used by ammonia oxidizers in the environment.

A recent study reported NO_x production from polyamines and amino acids by marine AOA (Damashek et al. 2019) (Figure 5d). However, it is unknown whether AOA can use these substrates directly.

Apart from direct use of DON, ammonia oxidizers can also make use of DON-derived ammonium indirectly via cross feeding, where other microorganisms degrade DON and release ammonium, which is subsequently used as substrate by the AOA.

This cross-feeding can be unidirectional, where one microorganism breaks down DON to ammonium, feeding an ammonia oxidizer unable to directly utilize DON, or bidirectional (Koch et al. 2015; Palatinszky et al. 2015). Recent experiments using cocultures of ammonia and nitrite oxidizers, showed that ammonia oxidizers, which could not directly use the DON compounds urea and cyanate, were able to grow on ammonium released from urea or cyanate by NOB containing ureases and/or cyanases. The nitrite formed by the ammonia oxidizers in return provided the substrate for NOB in a “reciprocal feeding scenario” (Koch et al. 2015; Palatinszky et al. 2015) (Figure 5b). Although genomic data indicates that the use of simple DON as N-source is widespread in cultured and environmental NOB (Koch et al. 2015; Palatinszky et al. 2015; Ngugi et al. 2016; Pachiadaki et al. 2017), so far, there is no data on the relevance of DON for NOB in the environment.

Mixotrophy in nitrifiers

In addition to chemolithoautotrophy, some nitrifiers are able to grow mixotrophically. Marine AOA have been shown to incorporate amino acids (Ouverney & Fuhrman 2000; Teira et al. 2006), although it remains unclear if this represents a mixotrophic or heterotrophic lifestyle. Also a marine AOA sponge-symbiont has been implicated to use amino acids mixotrophically (Moeller et al. 2019).

Moreover, enhanced growth of some AOA isolates was reported when incubated with ammonium in presence of alpha-keto acids (Tourna et al. 2011; Qin et al. 2014). However, this was recently shown to be due to the hydrogen peroxide (H₂O₂)-scavenging activity of alpha-keto acids, rather than mixotrophy (i.e. the assimilation of the alpha-keto acids) of the AOA (Kim et al. 2016; Qin et al. 2017; Bayer et al. 2019). Indeed, known AOA genomes lack genes encoding for canonical catalase, which would allow to detoxify H₂O₂ (Kim et al. 2016; Qin et al. 2017; Bayer et al. 2019), and activity of both cultures and environmental AOA is inhibited by H₂O₂ (Kim et al. 2016; Qin et al. 2017; Tolar et al. 2016; Bayer et al. 2019).

Growth of several AOB isolates was promoted by concurrent incubation with ammonium and organic substrates (Clark & Schmidt 1966; Clark & Schmidt 1967; Krümmel & Harms 1982; Hommes et al. 2003), and also growth of many NOB was stimulated by addition of nitrite and organics both in culture (Watson et al. 1986; Spieck et al. 2006; Keuter et al. 2011; Spieck et al. 2014) and in WWTPs (Daims et al. 2001; Gruber-Dorninger et al. 2015).

Anaerobic metabolism and reactions outside N-cycling

In addition to their canonical, aerobic lifestyle, some nitrifiers can also thrive under anoxic conditions. For example, AOB of the genus *Nitrosomonas* were shown to perform nitrite reduction to gaseous N-compounds coupled to hydrogen oxidation (Bock et al. 1995) (Figure 5e).

In many (and possibly all) NOB, the key enzyme NXR can also work in reverse, reducing nitrate to nitrite. Depending on the genetic repertoire of a given NOB, the electrons for this reaction can be obtained from the oxidation of organic compounds, e.g. formate, acetate, pyruvate (Freitag et al. 1987; Sorokin et al. 2012; Sorokin et al. 2014; Koch et al. 2015; Füssel et al. 2017) (Figure 5f) or hydrogen (Ehrich et al. 1995) (Figure 5f).

Some nitrifiers can also gain energy from electron donors other than N-compounds. For example, AOA in an oil refinery treatment plant appear to neither use ammonia as energy source nor grow autotrophically (Mußmann et al. 2011). *Nitrobacter* NOB can grow heterotrophically (Bock 1976; Bock et al. 1983; Bock et al. 1990) (Figure 5f) and some NOB can gain their energy and reducing equivalents from different chemolithoautotrophic growth modes. *Nitrospira moscoviensis* can perform aerobic formate oxidation (Koch et al. 2015) (Figure 5f) and aerobic hydrogen oxidation (Koch et al. 2014) (Figure 5f), and *Nitrococcus mobilis* aerobically oxidizes sulfide (Füssel et al. 2017) (Figure 5f).

The large metabolic diversity of nitrifiers implies that the mere presence of nitrifying microorganisms in the environment does not necessarily indicate they perform ammonia or nitrite oxidation (Daims et al. 2016). Therefore, activity measurements are vital to determine their actual function. Many studies on alternative metabolisms have found a vital role of DON, as both energy and N-source, and have indicated that this may be especially important for nitrifiers in marine systems. Most of these studies, however, investigated DON use by nitrifier pure cultures or based on presence of DON-utilization genes, while the environmental importance of DON for nitrifiers is still understudied.

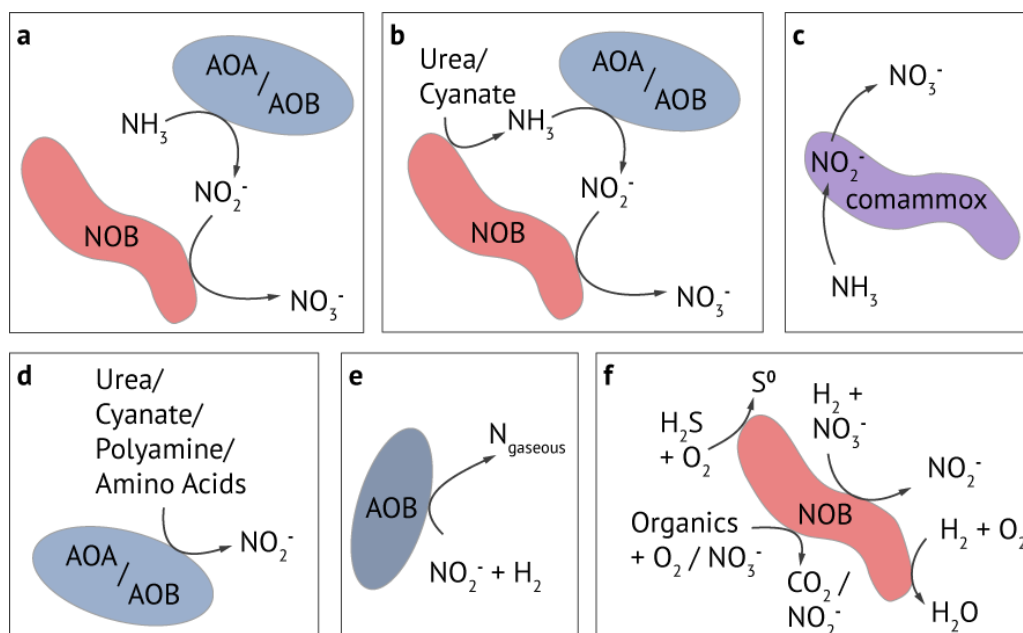


Figure 5 Canonical and non-canonical metabolism of nitrifiers. a) Canonical, coupled ammonia and nitrite oxidation, b) Reciprocal feeding between urea or cyanate degrading NOB and non-urea or -cyanate degrading ammonia oxidizers (Koch et al. 2015; Palatinszky et al. 2015), c) Comammox (Daims et al. 2015; van Kessel et al. 2015), d) Urea, cyanate, polyamine or amino acid use as additional energy source by ammonia oxidizers (e.g. Koops et al. 1991; Palatinszky et al. 2015; Bayer et al. 2016; Tolar et al. 2017; Damashek et al. 2019), e) Anaerobic ammonia or hydrogen oxidation coupled to nitrogen dioxide (NO_2^-) or nitrite by AOB (Bock et al. 1995), f) Alternative metabolisms in NOB, anaerobic nitrate reduction coupled to oxidation of organics (Freitag et al. 1987; Sorokin et al. 2012; Sorokin et al. 2014; Koch et al. 2015; Füssel et al. 2017) or hydrogen (Ehrlich et al. 1995), oxidation of organics (Bock 1976; Bock et al. 1983; Bock et al. 1990; Koch et al. 2015), aerobic hydrogen oxidation (Koch et al. 2014), and aerobic sulfide oxidation (Füssel et al. 2017).

1.5. Dissolved organic N in the marine environment

Apart from dissolved N_2 , which is not readily bioavailable, DON is the most abundant reduced N-source in the ocean (Gruber 2008). Yet, its importance for marine nutrient cycling has long been overlooked (Mulholland & Lomas 2008). DON comprises a plethora of different compounds of different chemical properties, molecular sizes and vastly different turnover times. DON is partly highly recalcitrant with turnover times of years, while some DON compounds, especially low molecular weight compounds (<1kDa), are turned over within minutes to days (Antia et al. 1991; Bronk 2002).

Most DON compounds can be used by microorganisms as both C- and N-source for assimilation into biomass. One example for DON serving as both organic C- and N-source are amino acids, where after deamination, both the resulting ammonium and the remaining keto-acid can be directly assimilated. However, some DON compounds serve only as N-source but not as organic C-source, because their breakdown products are ammonium and CO_2 – this is the case for urea and cyanate (Equations 1 and 2).

The simple DON compounds urea and cyanate, which have been found to serve as energy and/or N-source for nitrifiers (see above), appear to be ubiquitous components of DON in the marine environment (Antia et al. 1991; Widner et al. 2013; Widner et al. 2016; Widner & Mulholland 2017; Widner et al. 2018a; Widner et al. 2018b; Sipler & Bronk 2015).

The role of urea for the bulk microbial community in the marine environment has been studied quite extensively (summarized in Antia et al. 1991; Bronk 2002; Sipler & Bronk 2014). Urea is introduced

into marine systems both by runoff from terrestrial systems and discharge of rivers, and via excretion by diverse marine biota, such as microorganisms, zooplankton and fish (Antia et al. 1991; Solomon et al. 2010). Uptake of urea into cells is mediated either passively by diffusion (Siewe et al. 1998), by presence of porins or channel proteins (Weeks et al. 2000; Minocha et al. 2003; Sachs et al. 2006), or by ATP-dependent uptake via a dedicated ABC-transporter (Valladares et al. 2002). The cytoplasmic enzyme urease allows for ATP-independent cleavage of urea into ammonia and carbamate, and is present in many nitrifiers, phytoplankton, other microorganisms, as well as an anammox metagenome-assembled genome (e.g. Solomon & Glibert 2008; Solomon et al. 2010; Qin et al. 2014; Ngugi et al. 2016; Bayer et al. 2016; Pachiadaki et al. 2017).

Compared to urea, still very little is known about cyanate and its relevance for microorganisms in the marine environment. First indications that cyanate might be a relevant N-source came from genome analyses of marine Cyanobacteria of the genera *Synechococcus* and *Prochlorococcus* (Palenik et al. 2003; Rocap et al. 2003). These analyses revealed that some *Synechococcus* and *Prochlorococcus* strains contained cyanase, the enzyme converting cyanate to ammonium and CO₂ (Equation 2). Both marine *Synechococcus* and *Prochlorococcus* strains were later shown to use cyanate as N-source (Kamennaya et al. 2008; Kamennaya & Post 2011; Kamennaya & Post 2013), a marine dinoflagellate could use cyanate as N-source (Hu et al. 2012). Furthermore, some anammox bacteria encode for cyanases (Van de Vossenberg et al. 2013; Ganesh et al. 2018) and there is experimental evidence that cyanate is used as energy source by marine anammox bacteria *in situ* (Babbin et al. 2017).

Methods to detect nanomolar cyanate concentrations in seawater only became available recently (Widner et al. 2013). Since then, cyanate was found to have similar depth distributions as ammonium, with concentrations at or below detection limit in the surface waters to tens of nM at depth (Widner et al. 2016; Widner & Mulholland 2017; Widner et al. 2018a; Widner et al. 2018b). Additionally, cyanate was shown to serve as an N-source for some marine microbial communities (Widner & Mulholland 2017; Widner et al. 2018a; Widner et al. 2018b). In these studies, bulk community cyanate uptake was lower than urea and ammonium uptake (Widner et al. 2018a; Widner et al. 2018b).

At low concentrations, cyanate uptake appears to be dependent on transporters. These can either be ABC-type transporters as e.g. in *Cyanobacteria*, (Kamennaya et al. 2008), or, alternatively, the putative cyanate/nitrite/formate transporters as found e.g. in *N. gargensis* (Palatinszky et al. 2015). Cyanate use as an N-source is thought to be dependent on the presence of cytoplasmic cyanases. Apart from the canonical cyanases encoded by *cynS*, a new type of cyanase (*cynH*) has recently been described in *Synechococcus*. *cynH* lacks homology to *cynS* but also catalyzes cyanate degradation to ammonium (Kamennaya & Post 2011).

Cyanate is released to the environment as a result of spontaneous urea (Dirnhuber & Schütz 1948) or carbamoyl phosphate breakdown (Allen & Jones 1964) or by microbial thiocyanate breakdown (Sorokin et al. 2001). Additionally, cyanate formation has been reported for senescent diatom cultures of *Thalassiosira* species and from photoproduction in sterile filtered surface waters upon UV irradiation (Widner et al. 2016).

From a nitrifier perspective, utilization of DON as N- and/or energy source in addition to inorganic N may be highly advantageous. Ammonium is often a limiting nutrient in the marine environment, because it is a highly sought-after resource and serves as N-source for almost all microorganisms. Competition for ammonium between ammonia oxidizers and phytoplankton has been suggested to be a main cause for the relatively low ammonia oxidation rates in surface seawater (Smith et al. 2014), together with light and H₂O₂ inhibition (e.g. Horak et al. 2018). Therefore, it may be advantageous for ammonia oxidizers to tap other N-resources to gain energy and biomass-N when

ammonium is scarce – i.e. to use DON as source of ammonium. However, also for NOB, the use of DON rather than ammonium as an N-source may be advantageous. When NOB assimilate ammonium, they reduce the substrate availability for ammonia oxidizers – the microorganisms whose activity supplies NOB with their substrate, nitrite. Thus, NOB may use DON to minimize competition with ammonia oxidizers for ammonium, thereby concomitantly maximizing nitrite supply. Furthermore, the differential use of DON by co-occurring nitrifiers may be beneficial, as it could allow for niche partitioning by the use of different substrates and thereby reduce inter-clade competition.

1.6. Determining DON utilization by nitrifiers

1.6.1. DON use in cultures

DON use has mainly been studied in nitrifier pure cultures or on basis of environmental (meta-)genomics. These studies have substantially expanded our knowledge on DON-use.

Pure culture studies allow for testing of new metabolisms under strictly controlled conditions and to pinpoint the effect of variables such as substrate concentration, pH and temperature. The observed activity – be it measurements of DON-derived ammonia oxidation, or measurements of DON assimilation – can be unambiguously linked to a specific isolate and microorganism. Confounding factors like cross-feeding, that play a large role in complex environmental communities (see below), can be excluded. However, nitrifiers are notoriously difficult to isolate (Speick & Lipski 2011; Prosser & Nicol 2012), and many environmentally widespread nitrifier groups lack isolated representatives (e.g. some environmentally widespread Thaumarchaeota clades, *Ca.* Nitromaritima, Nitrospinae Clade 2, *Nitrotoga*). Additionally, the employed cultivation techniques may not select for metabolically versatile organisms. Conventional cultivation conditions for nitrifiers rely on cultivation with ammonium or nitrite as sole substrate, rather than organic N. These conditions give a selective advantage to autotrophic nitrifiers over other e.g. heterotrophic organisms that use DON as both N and C-source, but might result in isolation of nitrifiers not able to use DON. Furthermore, the environmental relevance of a given metabolism cannot easily be assessed by investigating pure cultures (Prosser & Nicol 2012).

1.6.2. DON use based on presence and transcription of DON-utilization genes

Several studies have investigated DON-use by nitrifiers based on the presence of the genes encoding for DON-degrading enzymes, like urease or cyanase. This approach has revealed that many environmental marine AOA encode ureases (Hallam et al. 2006), and many Nitrospinae encode both ureases and cyanases (Ngugi et al. 2016; Pachiadaki et al. 2017). Analysis of the transcription levels of these genes hints at active use of these enzymes *in situ*. However, in metagenomics and -transcriptomics based studies, gene functions can only be assigned based on previous knowledge, e.g. novel cyanases without close phylogenetic relationship to other known cyanases cannot be detected. For genes that frequently undergo horizontal gene transfer, it can be difficult to assign genes to specific organisms when metagenomic contigs lack additional phylogenetic information. Furthermore, even when genes are transcribed, their *in situ* activity levels can only be determined experimentally.

1.6.3. Determining DON utilization rates in the environment

Activity of ammonia and nitrite oxidizers in the environment is typically assessed by rate measurements using ^{15}N stable isotope tracer approaches. For example, for ammonia oxidation rate measurements, ^{15}N -ammonium is supplied, and combined ^{15}N -nitrite and ^{15}N -nitrate production is

measured either as a single end-point measurement, or over a time course. Natural isotope abundance nitrite is sometimes added to avoid loss of ^{15}N -nitrite e.g. due to further oxidation to ^{15}N -nitrate, thereby trapping ^{15}N -nitrite by dilution in the ^{14}N -nitrite pool.

For measurement of ^{15}N -DON-derived ammonia oxidation rates, the interpretation of ^{15}N -tracer experiments is less straightforward. Not all ^{15}N -nitrite that is produced upon addition of ^{15}N -DON may result from direct use of the DON by ammonia oxidizers, as ammonia oxidizers are rarely the only microorganisms that can break down DON in complex environmental samples. Instead, parts of the measured ^{15}N -nitrite may result from indirect DON-use or cross-feeding. In this scenario, other microorganisms break down ^{15}N -DON to ^{15}N -ammonium, which can be oxidized to ^{15}N -nitrite by ammonia oxidizers unable to use the originally supplied DON (Figure 6). Cyanate, and, to a lesser extent urea, also undergo abiotic breakdown to ammonium in a pH, temperature and salt dependent manner (Dirnhuber & Schütz 1948; Lister 1954; Kamennaya et al. 2008; Palatinszky et al. 2015), further complicating interpretation results of ^{15}N -labeling experiments.

Urea-, amino acid- and polyamine-derived ammonia oxidation rates have been measured in the marine environment (Tolar et al. 2017; Santoro et al. 2017; Damashek et al. 2019). However, to date, abiotic and biotic breakdown rates of ^{15}N -DON to ^{15}N -ammonium have not been systematically measured at the same time. Incubations to assess direct vs. indirect uptake of DON by ammonia oxidizers were only performed in one study focusing on the use of urea by AOA (Tolar et al. 2017). Therefore, most DON-derived ammonia oxidation rates reported to date likely overestimate direct DON-use by ammonia oxidizers.

Control incubations to constrain direct vs. indirect DON-use are therefore crucial to better assess the importance of a given DON compound for ammonia oxidizers. Direct vs. indirect DON-use can be differentiated by setting up parallel incubations: One with the addition of ^{15}N -DON and ^{14}N -nitrite (to trap ^{15}N -nitrite resulting from DON-derived ammonia oxidation), and a second incubation (pool incubation), where an additional ^{14}N -ammonium pool is added (Figure 6). In these pool incubations, ^{15}N -ammonium released from the breakdown of ^{15}N -DON by non-ammonia oxidizers is diluted into the ^{14}N -ammonium pool. Thus, the produced ^{15}N -ammonium is less likely further oxidized to ^{15}N -nitrite by ammonia oxidizers and the measured ^{15}N -nitrite production rates more likely reflect true direct DON utilization by ammonia oxidizers. Additionally, time course experiments allow more insight into the fate of ^{15}N -DON. Indirect use of ^{15}N -DON by ammonia oxidizers results in an exponential increase in ^{15}N -nitrite with time due to the increasing labeling percentage of the ammonium pool with time. In contrast, direct ^{15}N -DON use by ammonia oxidizers leads to a linear increase in ^{15}N -nitrite (Figure 6).

Although pool incubations can yield valuable insights into direct vs. indirect utilization patterns, they may lead to an underestimation of the direct DON-derived ammonia oxidation rates, as the addition of the ^{14}N -ammonium pool might cause preferential oxidation of the added ammonium rather than DON by ammonia oxidizers (Figure 6).

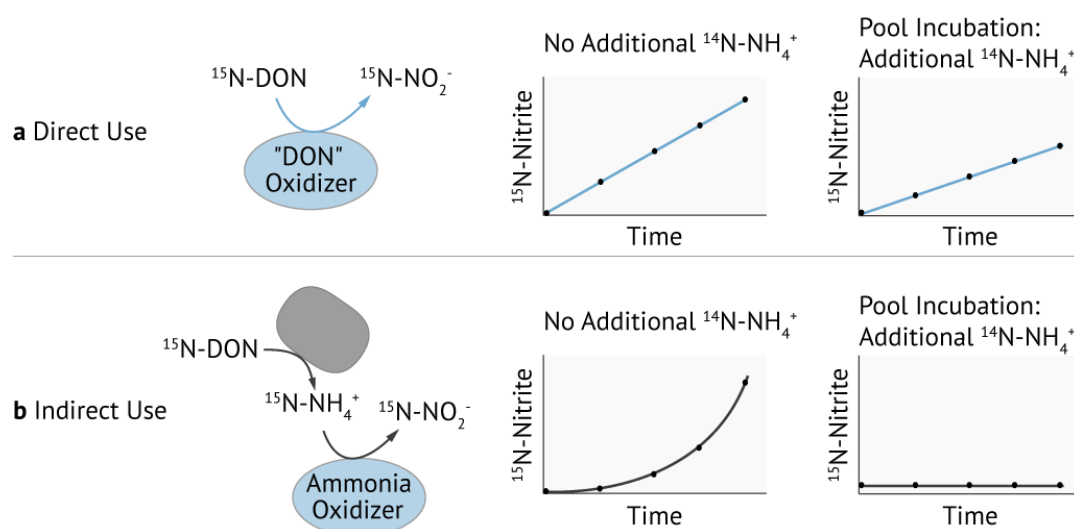


Figure 6 Scheme of DON-derived ammonia oxidation rates resulting from direct (a) or indirect DON-use by ammonia oxidizers (b).

1.6.4. Determining DON assimilation rates

Stable isotope incubations are also frequently employed to investigate DON assimilation rates. In the case of DON, the fate of stable isotope labeled DON can be studied via tracking the incorporation of the stable isotope into biomass of a specific microorganism. This can be achieved by methods like DNA-, RNA-, protein- or lipid-stable isotope probing (SIP) (Boschker et al. 1998; Radajewski et al. 2000; Manefield et al. 2002; Jehmlich et al. 2008). Alternatively, single cell isotope incorporation can be visualized by combining fluorescence *in situ* hybridization (FISH) with raman or nanoscale secondary ion mass spectroscopy (nanoSIMS) (Orphan et al. 2001; Huang et al. 2007). These SIP approaches allow to gain insights into which organisms are responsible for biogeochemical transformations in the environment and have thus greatly enhanced our understanding of microbial activity, independent of the availability of pure cultures and/or genomic information.

However, also when looking at the incorporation of stable isotopes by specific microorganisms, cross-feeding can confound results. The stable isotope labeled compound can undergo transformations by the microbial community – e.g. ^{15}N -ammonium from ^{15}N -DON degradation can be released and incorporated by another microorganism, or a microorganism able of direct use of ^{15}N -DON incorporates the ^{15}N into biomass and lyses, releasing ^{15}N -DON to the environment. To a certain extent, time course experiments allow to differentiate between direct vs. indirect uptake, as microorganisms capable of direct uptake will likely incorporate the stable isotope first. However, it is difficult to distinguish slow growing organisms able to directly use the supplied DON from fast growing organisms that use DON indirectly in a complex community.

To minimize cross-feeding, the breakdown products of ^{15}N -DON would need to be continuously removed, to identify cells directly using the supplied ^{15}N -labelled substrates. Retentostat-like systems, where cells are retained on a membrane at low cell densities, could in principle be used to achieve both continuous supply of fresh ^{15}N -DON at constant concentration and constant removal of ^{15}N -DON breakdown products, thereby limiting cross-feeding effects.

Aims and Outline

Most insights into the metabolic capacity of nitrifiers come from culture-dependent studies using the few nitrifier isolates that are available. As a result, the environmental importance of many alternative nitrifier metabolisms is still poorly constrained. Yet, understanding nitrifier metabolic versatility is key to understanding how these microorganisms make a living and how they cope with fluctuating conditions in both man-made and natural systems. In this thesis, I combined different approaches of both cultivation-dependent and cultivation-independent experiments to study the metabolic versatility of globally distributed nitrifiers and their environmental relevance.

To date, few environmentally relevant nitrite oxidizers have been isolated and characterized, however, pure culture model organisms are vital for studying NOB physiology under controlled experimental conditions. In **Chapter 2**, we aimed to gain insights into the physiology of key NOB from wastewater treatment plants (WWTP) by using a cultivation and genome-based approach. We isolated and characterized a member of the NOB genus *Nitrotoga*, which plays a key role in many engineered systems (Lücker et al. 2015; Saunders et al. 2016). The functioning of most WWTPs relies on the efficient conversion of ammonium to nitrate by nitrifiers, yet, nitrification activity in engineered systems can be difficult to maintain (Daims et al. 2009). To ensure stable nitrification activity, it is imperative to go beyond treating the microorganisms in WWTPs as a “black box” and to gain more knowledge on the physiology of key nitrifiers within WWTPs. The isolated NOB, which we named *Candidatus Nitrotoga fabula*, was obtained from a municipal WWTP and is the first *Nitrotoga* pure culture available. *Ca. N. fabula* is physiologically different to previously described *Nitrotoga* enrichments, tolerating both higher pH, temperature and substrate concentrations, which makes it ideally suited to WWTPs. Additionally, *Ca. N. fabula* encodes for an NXR that is different to previously known NXRs of NOB. Intriguingly, closely related enzymes are present in physiologically uncharacterized bacteria and archaea, hinting at an even larger diversity of nitrite oxidizers in nature than is currently known. In addition to nitrite oxidation, the genome of *Ca. N. fabula* implies that both hydrogen and sulfite can serve as alternative electron donors to nitrite. This metabolic versatility may allow *Ca. N. fabula* to remain active irrespective of the availability of nitrite.

Metabolic versatility has also been hypothesized to play a role in the success of nitrifiers in natural ecosystems. In contrast to most man-made systems, in marine systems ammonium is a limiting nutrient. Competition for ammonium in the ocean can be high, as it is the preferred N-source for most organisms. Despite this high competition for ammonium, nitrifiers are widely distributed and active in the world’s ocean. Previous studies, which mainly used nitrifier isolates, have shown that some nitrifiers can utilize the simple dissolved organic N (DON) compounds urea and cyanate to supplement their N-requirements for both energy generation and growth (e.g. Alonso-Saez et al. 2012; Koch et al. 2015; Palatinszky et al. 2015; Bayer et al. 2016). As DON is the most abundant reduced form of N in the oceans (Antia et al. 1991; Gruber 2008; Sipler & Bronk 2015), we hypothesized that the utilization of DON in addition to ammonium may be an important trait for nitrifiers in the environment. Therefore, in this thesis we aimed to investigate how DON utilization might contribute to this ecological success of ammonia (**Chapter 3**) and nitrite oxidizers (**Chapter 4**). These studies were carried out in the Louisiana shelf waters of the Gulf of Mexico (GoM), which is an ideal region to investigate nitrifier DON utilization and ecophysiology as it is a hotspot of both ammonia and nitrite oxidation activity (Bristow et al. 2015). Additionally, the GoM has been reported to be dominated by two nitrifier groups – ammonia oxidizing archaea (AOA) and Nitrospinae (Tolar et al. 2013; Bristow et al. 2015), which makes it easier to link the measured activity to specific nitrifier

groups. Furthermore, AOA and Nitrospinae are the main players in nitrification in the vast majority of the world's ocean.

In **Chapter 3**, we aimed to gain insights into the *in situ* use of urea and cyanate as energy and N-sources by marine AOA. This was achieved by employing a combination of *in situ* experiments, (meta-) genomics, single cell analyses and cultivation-based experiments. This chapter highlights the importance of activity-based studies, as environmental AOA and the tested AOA isolate were able to use cyanate as substrate despite lacking canonical cyanases. Additionally, this study introduces a set of control incubations to differentiate between direct and indirect use of substrates for the first time. In **Chapter 4**, we aimed to gain deeper understanding of the ecophysiology of Nitrospinae compared to the AOA, especially regarding their *in situ* growth rates and their ability to utilize DON compounds. To achieve this, a combination of *in situ* rate measurements, metagenomics and single cell analyses was used. Our analyses revealed that despite their low abundance, Nitrospinae catalyzed high nitrite oxidation rates and showed surprisingly high *in situ* growth rates. Nitrospinae met a large part of their N-demand for their growth by using urea and cyanate as N-sources. Intriguingly, Nitrospinae growth rates were higher than those of the far more abundant AOA, a mismatch that could not be explained even when considering differences in energy gain per population based on thermodynamic modelling. This indicates that the Nitrospinae are highly efficient in translating the energy into growth, and/or, that they can gain additional energy from alternative metabolic pathways. This study suggests that the energy efficiency and potential metabolic flexibility of Nitrospinae give them a competitive advantage which could explain their success as nitrite oxidizers in the world's ocean.

One key methodological issue that we had to address in **Chapter 3** was whether and to which extent cross-feeding was occurring between the AOA and other members of the microbial community. By carrying out careful control incubations, we could indeed show that both urea and cyanate were utilized directly by the AOA in addition to indirect utilization via cross-feeding. However, ideally, cross-feeding should be entirely excluded to unequivocally link the activity of a specific microorganism to substrate turnover in the environment.

In **Chapter 5**, we aimed to develop a new method to overcome cross-feeding in stable isotope incubations. The newly developed method Flow-through stable isotope probing (Flow-SIP) allowed us to identify the microorganisms capable of direct substrate utilization in complex environmental samples. Flow-SIP eliminates cross-feeding by trapping microbial cells on a membrane and continuously supplying a flow of stable isotope labeled substrate. At the same time, any secreted metabolites are removed, thereby limiting confounding cross-feeding effects. In future studies, this new method, as well as those that were successfully applied for the first time in **Chapter 3**, might also provide unprecedented insight into the ecophysiology of nitrifying microorganisms in both engineered systems and the highly oligotrophic waters which constitute the majority of the world's ocean.

Chapter 2 and **Chapter 3** have been published, **Chapter 4** and **Chapter 5** are in preparation for submission to international peer reviewed scientific journals.

References

- Alawi M., Lipski A., Sanders T., Pfeiffer E.M. and Spieck E. 2007. Cultivation of a Novel Cold-Adapted Nitrite Oxidizing Betaproteobacterium from the Siberian Arctic. *The ISME Journal* 1 (3): 256–64. doi:10.1038/ismej.2007.34.
- Allen C.M. and Jones M.E. 1964. Decomposition of Carbamylphosphate in Aqueous Solutions. *Biochemistry* 3 (9): 1238–47. doi:10.1021/bi00897a010.
- Allison S.M. and Prosser J.I. 1991. Urease Activity in Neutrophilic Bacteria From Acid Soils. *Soil Biology and Biochemistry* 23 (1): 45–51.
- Alonso-Saez L., Waller A.S., Mende D.R., Bakker K., Farnelid H., Yager P.L., Lovejoy C., Tremblay J.-E., Potvin M., Heinrich F., Estrada M., Riemann L., Bork P., Pedros-Alio C. and Bertilsson S. 2012. Role for Urea in Nitrification by Polar Marine Archaea. *Proceedings of the National Academy of Sciences of the United States of America* 109 (44): 17989–94. doi:10.1073/pnas.1201914109.
- Antia N.J., Harrison P.J. and Oliveira L. 1991. The Role of Dissolved Organic Nitrogen in Phytoplankton Nutrition, Cell Biology and Ecology. *Phycologia* 30 (1): 1–89. doi:10.2216/i0031-8884-30-1-1.1.
- Babbin A.R., Peters B.D., Mordy C.W., Widner B., Casciotti K.L. and Ward B.B. 2017. Multiple Metabolisms Constrain the Anaerobic Nitrite Budget in the Eastern Tropical South Pacific. *Global Biogeochemical Cycles* 31: 258–71. doi:10.1002/2016GB005407.
- Bartosch S., Wolgast I., Spieck E. and Bock E. 1999. Identification of Nitrite-Oxidizing Bacteria with Monoclonal Antibodies Recognizing the Nitrite Oxidoreductase. *Applied and Environmental Microbiology* 65 (9): 4126–33.
- Bayer B., Vojvoda J., Offre P., Alves R.J.E., Elisabeth N.H., Garcia J. AL, Volland J.-M., Srivastava A., Schleper C. and Herndl G.J. 2016. Physiological and Genomic Characterization of Two Novel Marine Thaumarchaeal Strains Indicates Niche Differentiation. *The ISME Journal* 10. Nature Publishing Group: 1051–63. doi:10.1038/ismej.2015.200.
- Bayer B., Vojvoda J., Reinthaler T., Reyes C., Pinto M. and Herndl G.J. 2019. Nitrosopumilus Adriaticus Sp. Nov. and Nitrosopumilus Piranensis Sp. Nov., Two Ammonia-Oxidizing Archaea from the Adriatic Sea and Members of the Class Nitrososphaeria. *International Journal of Systematic and Evolutionary Microbiology*, 1–11. doi:10.1099/ijsem.0.003360.
- Beman J.M., Leilei Shih J. and Popp B.N. 2013. Nitrite Oxidation in the Upper Water Column and Oxygen Minimum Zone of the Eastern Tropical North Pacific Ocean. *The ISME Journal* 7. Nature Publishing Group: 2192–2205. doi:10.1038/ismej.2013.96.
- Berg C., Vandieken V., Thamdrup B. and Jürgens K. 2015. Significance of Archaeal Nitrification in Hypoxic Waters of the Baltic Sea. *The ISME Journal* 9: 1319–32. doi:10.1038/ismej.2014.218.
- Bock E. 1976. Growth of Nitrobacter in Presence of Organic Matter II. Chemoorganotrophic Growth of Nitrobacter Agilis. *Archives Of Microbiology* 108: 305–12. doi:10.1007/bf00454857.
- Bock E., Koops H.-P., Möller U.C. and Rudert M. 1990. A New Facultatively Nitrite Oxidizing Bacterium, Nitrobacter Vulgaris Sp. Nov. *Archives of Microbiology* 153 (2): 105–10.
- Bock E., Schmidt I., Stüven R. and Zart D. 1995. Nitrogen Loss Caused by Denitrifying Nitrosomonas Cells Using Ammonium or Hydrogen as Electron Donors and Nitrite as Electron Acceptor. *Archives of Microbiology* 163: 16–20. doi:10.1007/BF00262198.
- Bock E., Sundermeyer-Klinger H. and Stackebrandt E. 1983. New Facultative Lithoautotrophic Nitrite-Oxidizing Bacteria. *Archives of Microbiology* 136: 281–84. doi:10.1007/BF00425217.
- Bock E. and Wagner M. 2006. Oxidation of Inorganic Nitrogen Compounds as an Energy Source. In *The Prokaryotes: Prokaryotic Physiology and Biochemistry*, edited by Eugene Rosenberg, Edward F Delong, Stephen Lory, Erko Stackebrandt, and Fabiano Thompson, 4th ed., 83–118. doi:10.1007/978-3-642-30141-4.
- Bollmann A., Sedlacek C.J., Norton J., Laanbroek H.J., Suwa Y., Stein L.Y., Klotz M.G., Arp D., Sayavedra-Soto L., Lu M., Bruce D., Detter C., Tapia R., Han J., Woyke T., Lucas S.M., Pitluck S., Pennacchio L., Nolan M., et al. 2013. Complete Genome Sequence of Nitrosomonas Sp. Is79, an Ammonia Oxidizing Bacterium Adapted to Low Ammonium Concentrations. *Standards in Genomic Sciences* 7: 469–82. doi:10.4056/sigs.3517166.
- Boschker H.T.S., Nold S.C., Wellsbury P., Bos D., De Graaf W., Pel R., Parkes R.J. and Cappenberg T.E. 1998. Direct Linking of Microbial Populations to Specific Biogeochemical Processes by ¹³C-Labeling of Biomarkers. *Nature* 392: 801–4. doi:10.1038/33900.
- Bothe H., Schmitz O., Yates M.G. and Newton W.E. 2010. Nitrogen Fixation and Hydrogen Metabolism in Cyanobacteria. *Microbiology and Molecular Biology Reviews* 74 (4): 529–51. doi:10.1128/MMBR.00033-10.

- Bristow L.A., Dalsgaard T., Tiano L., Mills D.B., Bertagnolli A.D., Wright J.J., Hallam S.J., Ulloa O., Canfield D.E., Revsbech N.P. and Thamdrup B. 2016. Ammonium and Nitrite Oxidation at Nanomolar Oxygen Concentrations in Oxygen Minimum Zone Waters. *Proceedings of the National Academy of Sciences* 113 (38): 10601–6. doi:10.1073/pnas.1600359113.
- Bristow L.A., Sarode N., Cartee J., Caro-Quintero A., Thamdrup B. and Stewart F.J. 2015. Biogeochemical and Metagenomic Analysis of Nitrite Accumulation in the Gulf of Mexico Hypoxic Zone. *Limnology and Oceanography* 60 (5): 1733–50. doi:10.1002/lno.10130.
- Britto D.T. and Kronzucker H.J. 2013. Ecological Significance and Complexity of N-Source Preference in Plants. *Annals of Botany* 112: 957–63. doi:10.1093/aob/mct157.
- Brochier-Armanet C., Boussau B., Gribaldo S. and Forterre P. 2008. Mesophilic Crenarchaeota: Proposal for a Third Archaeal Phylum, the Thaumarchaeota. *Nature Reviews Microbiology* 6: 245–52. doi:10.1038/nrmicro1852.
- Bronk D.A. 2002. Dynamics of DON. In *Biogeochemistry of Marine Dissolved Organic Matter*, edited by Dennis A. Hansell and Craig A. Carlson, 153–247. ACADEMIC PRESS, INC. doi:10.1016/B978-012323841-2/50007-5.
- Brunet R.C. and Garcia-Gil L.J. 1996. Sulfide-Induced Dissimilatory Nitrate Reduction to Ammonia in Anaerobic Freshwater Sediments. *FEMS Microbiology Ecology* 21: 131–38. doi:10.1016/0168-6496(96)00051-7.
- Burton S.A.Q. and Prosser J.I.M.I. 2001. Autotrophic Ammonia Oxidation at Low PH through Urea Hydrolysis. *Applied and Environmental Microbiology* 67 (7): 2952–57. doi:10.1128/AEM.67.7.2952.
- Canfield D.E., Glazer A.N. and Falkowski P.G. 2010. The Evolution and Future of Earth's Nitrogen Cycle. *Science* 330 (October): 192–96. doi:10.1126/science.1186120.
- Cantera J.J.L. and Stein L.Y. 2007. Role of Nitrite Reductase in the Ammonia-Oxidizing Pathway of Nitrosomonas Europaea. *Archives of Microbiology* 188: 349–54. doi:10.1007/s00203-007-0255-4.
- Caranto J.D. and Lancaster K.M. 2017. Nitric Oxide Is an Obligate Bacterial Nitrification Intermediate Produced by Hydroxylamine Oxidoreductase. *Proceedings of the National Academy of Sciences of the United States of America* 114 (31): 8217–22. doi:10.1073/pnas.1704504114.
- Cardoso R.B., Sierra-Alvares R., Rowlette P., Flores E.R., Gómez J. and Field J.A. 2006. Sulfide Oxidation Under Chemolithoautotrophic Denitrifying Conditions. *Biotechnology and Bioengineering* 95 (6): 1148–57. doi:10.1002/bit.
- Carini P., Dupont C.L. and Santoro A.E. 2018. Patterns of Thaumarchaeal Gene Expression in Culture and Diverse Marine Environments. *Environmental Microbiology* 20 (6): 2112–24. doi:10.1111/1462-2920.14107.
- Clark C. and Schmidt E.L. 1966. Effect of Mixed Culture on Nitrosomonas Europaea Simulated by Uptake and Utilization of Pyruvate. *Journal of Bacteriology* 91 (1): 367–73.
- Clark C. and Schmidt E.L. 1967. Growth Response of Nitrosomonas Europaea to Amino Acids. *Journal of Bacteriology* 93 (4): 1302–8.
- Connelly T.L., Baer S.E., Cooper J.T., Bronk D.A. and Wawrik B. 2014. Urea Uptake and Carbon Fixation by Marine Pelagic Bacteria and Archaea During the Arctic Summer and Winter Seasons. *Applied and Environmental Microbiology* 80 (19): 6013–22. doi:10.1128/AEM.01431-14.
- Daims H., Lebedeva E. V., Pjevac P., Han P., Herbold C., Albertsen M., Jehmlich N., Palatinszky M., Vierheilig J., Bulaev A., Kirkegaard R.H., von Bergen M., Rattei T., Bendinger B., Nielsen P.H. and Wagner M. 2015. Complete Nitrification by Nitrospira Bacteria. *Nature* 528 (7583): 504–9. doi:10.1038/nature16461.
- Daims H., Lückner S. and Wagner M. 2016. A New Perspective on Microbes Formerly Known as Nitrite-Oxidizing Bacteria. *Trends in Microbiology* 24 (9): 699–712. doi:10.1016/j.tim.2016.05.004.
- Daims H., Maixner F. and Schmid M. 2009. The Nitrifying Microbes: Ammonia Oxidizers, Nitrite Oxidizers, and Anaerobic Ammonium Oxidizers. In *FISH Handbook for Biological Wastewater Treatment - Identification and Quantification of Microorganisms in Activated Sludge and Biofilms by FISH*, edited by Per Halkjær Nielsen, Holger Daims, and H Lemmer. London: IWA Publishing.
- Daims H., Nielsen J., Nielsen P.H., Schleifer K.-H. and Wagner M. 2001. In Situ Characterization of Nitrospira-Like Nitrite-Oxidizing Bacteria Active in Wastewater Treatment Plants. *Applied and Environmental Microbiology* 67 (11): 5273–84. doi:10.1128/AEM.67.11.5273.
- Damashek J., Tolar B.B., Liu Q., Okotie-Oyekan A.O., Wallsgrove N.J., Popp B.N. and Hollibaugh J.T. 2019. Microbial Oxidation of Nitrogen Supplied as Selected Organic Nitrogen Compounds in the South Atlantic Bight. *Limnology and Oceanography* 64 (3): 982–95. doi:10.1002/lno.11089.

- De Boer W., Duyts H. and Laanbroek H.J. 1989. Urea Stimulated Autotrophic Nitrification in Suspensions of Fertilized, Acid Heath Soil. *Soil Biology and Biochemistry* 21 (3): 349–54. doi:10.1016/0038-0717(89)90142-9.
- DeLong E.F. 1992. Archaea in Coastal Marine Environments. *Proceedings of the National Academy of Sciences of the United States of America* 89 (June): 5685–89.
- DeLong E.F., Wu K.Y., Prezelin B.B. and Jovine R.V.M. 1994. High Abundance of Archaea in Antarctic Marine Picoplankton. *Nature* 371: 695–97.
- Delsuc F., Brinkmann H. and Philippe H. 2005. Phylogenomics and the Reconstruction of the Tree of Life. *Nature Reviews Genetics* 6: 361–75. doi:10.1038/nrg1603.
- Diaz R.J. and Rosenberg R. 2008. Spreading Dead Zones and Consequences for Marine Ecosystems. *Science* 321: 926–29. doi:10.1126/science.1156401.
- Dirnhuber P. and Schütz F. 1948. The Isomeric Transformation of Urea into Ammonium Cyanate in Aqueous Solutions. *Biochemical Journal* 42 (4): 628–32.
- Ehrich S., Behrens D., Lebedeva E., Ludwig W. and Bock E. 1995. A New Obligately Chemolithoautotrophic, Nitrite-Oxidizing Bacterium, *Nitrospira Moscoviensis* Sp. Nov. and Its Phylogenetic Relationship. *Archives of Microbiology* 164: 16–23.
- Erisman J.W., Sutton M.A., Galloway J., Klimont Z. and Winiwarter W. 2008. How a Century of Ammonia Synthesis Changed the World. *Nature Geoscience* 1: 636–39. doi:10.1038/ngeo325.
- Ettwig K.F., Butler M.K., Le Paslier D., Pelletier E., Mangenot S., Kuypers M.M.M., Schreiber F., Dutilh B.E., Zedelius J., de Beer D., Gloerich J., Wessels H.J.C.T., van Alen T., Luesken F., Wu M.L., van de Pas-Schoonen K.T., Op den Camp H.J.M., Janssen-Megens E.M., Francoijs K.-J., et al. 2010. Nitrite-Driven Anaerobic Methane Oxidation by Oxygenic Bacteria. *Nature* 464 (March): 543–48. doi:10.1038/nature08883.
- Falkowski P.G., Fenchel T. and DeLong E.F. 2008. The Microbial Engines That Drive Earth’s Biogeochemical Cycles. *Science* 320 (May): 1034–39. doi:10.1126/science.1153213.
- Francis C.A., Roberts K.J., Beman J.M., Santoro A.E. and Oakley B.B. 2005. Ubiquity and Diversity of Ammonia-Oxidizing Archaea in Water Columns and Sediments of the Ocean. *Proceedings of the National Academy of Sciences of the United States of America* 102 (41): 14683–88. doi:10.1073/pnas.0506625102.
- Frankland P.F. and Frankland G.C. 1890. The Nitrifying Process and Its Specific Ferment. Part I. *Philosophical Transactions of the Royal Society of London. B* 181: 107–28.
- Freitag A., Rudert M. and Bock E. 1987. Growth of *Nitrobacter* by Dissimilatoric Nitrate Reduction. *FEMS Microbiology Letters* 48: 105–9. doi:10.1111/j.1574-6968.1987.tb02524.x.
- Fuhrman J.A., McCallum K. and Davis A.A. 1992. Novel Major Archaeobacterial Group from Marine Plankton. *Nature* 356: 148–49.
- Füssel J., Lam P., Lavik G., Jensen M.M., Holtappels M., Günter M. and Kuypers M.M.M. 2012. Nitrite Oxidation in the Namibian Oxygen Minimum Zone. *The ISME Journal* 6: 1200–1209. doi:10.1038/ismej.2011.178.
- Füssel J., Lücker S., Yilmaz P., Nowka B., van Kessel M.A.H.J., Bourceau P., Hach P.F., Littmann S., Berg J., Spieck E., Daims H., Kuypers M.M.M. and Lam P. 2017. Adaptability as the Key to Success for the Ubiquitous Marine Nitrite Oxidizer *Nitrococcus*. *Science Advances* 3: 1–9. doi:10.1126/sciadv.1700807.
- Galloway J.N., Leach A.M., Bleeker A. and Erisman J.W. 2013. A Chronology of Human Understanding of the Nitrogen Cycle. *Philosophical Transactions of the Royal Society of London. B* 368 (20130120): 1–11. doi:10.1098/rstb.2013.0120.
- Galloway J.N., Townsend A.R., Erisman J.W., Bekunda M., Cai Z., Freney J.R., Martinelli L. a, Seitzinger S.P. and Sutton M. a. 2008. Transformation of the Nitrogen Cycle: Recent Trends, Questions, and Potential Solutions. *Science* 320 (May): 889–92. doi:10.1126/science.1136674.
- Ganesh S., Bertagnolli A.D., Bristow L.A., Padilla C.C., Blackwood N., Aldunate M., Bourbonnais A., Altabet M.A., Malmstrom R.R., Woyke T., Ulloa O., Konstantinidis K.T., Thamdrup B. and Stewart F.J. 2018. Single Cell Genomic and Transcriptomic Evidence for the Use of Alternative Nitrogen Substrates by Anammox Bacteria. *The ISME Journal* 12: 2706–22. doi:10.1038/s41396-018-0223-9.
- Gevertz D., Telang A.J., Voordouw G. and Jennemann G.E. 2000. Isolation and Characterization of Strains CVO and FWKO B, Two Novel Bacteria Isolated from Oil Field Brine. *Applied and Environmental Microbiology* 66 (6): 2491–2501. doi:10.1128/AEM.66.6.2491-2501.2000.Updated.
- Graf D.R.H., Jones C.M. and Hallin S. 2014. Intergenomic Comparisons Highlight Modularity of the Denitrification Pathway and Underpin the Importance of Community Structure for N₂O Emissions. *PLoS ONE* 9 (12): 1–20. doi:10.1371/journal.pone.0114118.

- Graf J.S., Mayr M.J., Marchant H.K., Tienken D., Hach P.F., Brand A., Schubert C.J., Kuypers M.M.M. and Milucka J. 2018. Bloom of a Denitrifying Methanotroph, “Candidatus Methyloirabilis Limnetica”, in a Deep Stratified Lake. *Environmental Microbiology* 20 (7): 2598–2614. doi:10.1111/1462-2920.14285.
- Griffin B.M., Schott J. and Schink B. 2007. Nitrite, an Electron Donor for Anoxygenic Photosynthesis. *Science* 316: 1870. doi:10.1126/science.1139478.
- Gruber-Dorninger C., Pester M., Kitzinger K., Savio D.F., Loy A., Rattei T., Wagner M. and Daims H. 2015. Functionally Relevant Diversity of Closely Related Nitrospira in Activated Sludge. *The ISME Journal* 9 (August): 643–55. doi:10.1038/ismej.2014.156.
- Gruber N. 2008. The Marine Nitrogen Cycle: Overview and Challenges. In *Nitrogen in the Marine Environment*, edited by Douglas G Capone, Deborah A Bronk, Margaret R Mulholland, and Edward J Carpenter, 2nd ed., 3:1–50. Elsevier. doi:10.1128/microbe.3.186.1.
- Gruber N. and Galloway J.N. 2008. An Earth-System Perspective of the Global Nitrogen Cycle. *Nature* 451 (January): 293–96. doi:10.1038/nature06592.
- Hallam S.J., Konstantinidis K.T., Putnam N., Schleper C., Watanabe Y., Sugahara J., Preston C., de la Torre J., Richardson P.M. and DeLong E.F. 2006. Genomic Analysis of the Uncultivated Marine Crenarchaeote Cenarchaeum Symbiosum. *Proceedings of the National Academy of Sciences of the United States of America* 103 (48): 18296–301. doi:10.1073/pnas.0608549103.
- Hemp J., Lückner S., Schott J., Pace L.A., Johnson J.E., Schink B., Daims H. and Fischer W.W. 2016. Genomics of a Phototrophic Nitrite Oxidizer: Insights into the Evolution of Photosynthesis and Nitrification. *The ISME Journal* 10: 1–10. doi:10.1038/ismej.2016.56.
- Hommel N.G., Sayavedra-Soto L.A. and Arp D.J. 2003. Chemolithoorganotrophic Growth of Nitrosomonas Europaea on Fructose. *Journal of Bacteriology* 185 (23): 6809–14. doi:10.1128/JB.185.23.6809-6814.2003.
- Hooper A.B., Vannelli T., Bergmann D.J. and Arciero D.M. 1997. Enzymology of the Oxidation of Ammonia to Nitrite by Bacteria. *Antonie van Leeuwenhoek* 71: 59–67.
- Horak R.E.A., Qin W., Bertagnolli A.D., Nelson A., Heal K.R., Han H., Heller M., Schauer A.J., Jeffrey W.H., Armbrust E.V., Moffett J.W., Ingalls A.E., Stahl D.A. and Devol A.H. 2018. Relative Impacts of Light, Temperature, and Reactive Oxygen on Thaumarchaeal Ammonia Oxidation in the North Pacific Ocean. *Limnology and Oceanography* 63 (2): 741–57. doi:10.1002/lno.10665.
- Horak R.E.A., Qin W., Schauer A.J., Armbrust E.V., Ingalls A.E., Moffett J.W., Stahl D.A. and Devol A.H. 2013. Ammonia Oxidation Kinetics and Temperature Sensitivity of a Natural Marine Community Dominated by Archaea. *The ISME Journal* 7: 2023–33. doi:10.1038/ismej.2013.75.
- Hu Z., Mulholland M.R., Duan S. and Xu N. 2012. Effects of Nitrogen Supply and Its Composition on the Growth of Proocentrum Donghaiense. *Harmful Algae* 13: 72–82. doi:10.1016/j.hal.2011.10.004.
- Hu Z., Wessels H.J.C.T., van Alen T., Jetten M.S.M. and Kartal B. 2019. Nitric Oxide-Dependent Anaerobic Ammonium Oxidation. *Nature Communications* 10 (1): 1244. doi:10.1038/s41467-019-09268-w.
- Huang W.E., Stoecker K., Griffiths R., Newbold L., Daims H., Whiteley A.S. and Wagner M. 2007. Raman-FISH: Combining Stable-Isotope Raman Spectroscopy and Fluorescence in Situ Hybridization for the Single Cell Analysis of Identity and Function. *Environmental Microbiology* 9 (8): 1878–89. doi:10.1111/j.1462-2920.2007.01352.x.
- Hussain Allem M.I. and Sewell D.L. 1981. Mechanism of Nitrite Oxidation and Oxidoreductase Systems in Nitrobacter Agilis. *Current Microbiology* 5: 267–72. doi:10.1007/BF01567916.
- Jehmlich N., Schmidt F., Von Bergen M., Richnow H.H. and Vogt C. 2008. Protein-Based Stable Isotope Probing (Protein-SIP) Reveals Active Species within Anoxic Mixed Cultures. *The ISME Journal* 2: 1122–33. doi:10.1038/ismej.2008.64.
- Johnson W. V. and Anderson P.M. 1987. Bicarbonate Is a Recycling Substrate for Cyanase. *Journal of Biological Chemistry* 262 (19): 9021–25.
- Kamennaya N.A., Chernihovsky M. and Post A.F. 2008. The Cyanate Utilization Capacity of Marine Unicellular Cyanobacteria. *Limnology and Oceanography* 53 (6): 2485–94. doi:10.4319/lo.2008.53.6.2485.
- Kamennaya N.A. and Post A.F. 2011. Characterization of Cyanate Metabolism in Marine Synechococcus and Prochlorococcus Spp. *Applied and Environmental Microbiology* 77 (1): 291–301. doi:10.1128/AEM.01272-10.
- Kamennaya N.A. and Post A.F. 2013. Distribution and Expression of the Cyanate Acquisition Potential among Cyanobacterial Populations in Oligotrophic Marine Waters. *Limnology and Oceanography* 58 (6): 1959–71. doi:10.4319/lo.2013.58.6.1959.

- Kamp A., Høgslund S., Risgaard-Petersen N. and Stief P. 2015. Nitrate Storage and Dissimilatory Nitrate Reduction by Eukaryotic Microbes. *Frontiers in Microbiology* 6 (1492): 1–15. doi:10.3389/fmicb.2015.01492.
- Kartal B., Maalcke W.J., de Almeida N.M., Cirpus I., Gloerich J., Geerts W., Op den Camp H.J.M., Harhangi H.R., Janssen-Megens E.M., Francoijs K.-J., Stunnenberg H.G., Keltjens J.T., Jetten M.S.M. and Strous M. 2011. Molecular Mechanism of Anaerobic Ammonium Oxidation. *Nature* 479 (November): 127–30. doi:10.1038/nature10453.
- Keuter S., Kruse M., Lipski A. and Spieck E. 2011. Relevance of Nitrospira for Nitrite Oxidation in a Marine Recirculation Aquaculture System and Physiological Features of a Nitrospira Marina-like Isolate. *Environmental Microbiology* 13 (9): 2536–47. doi:10.1111/j.1462-2920.2011.02525.x.
- Kim J.-G., Park S.-J., Damsté J.S.S., Schouten S., Rijpstra W.I.C., Jung M.-Y., Kim S.-J., Gwak J.-H., Hong H., Si O.-J., Lee S., Madsen E.L. and Rhee S.-K. 2016. Hydrogen Peroxide Detoxification Is a Key Mechanism for Growth of Ammonia-Oxidizing Archaea. *Proceedings of the National Academy of Sciences of the United States of America* 113 (28): 7888–93. doi:10.1073/PNAS.1605501113.
- Kits D.K., Sedlacek C.J., Lebedeva E. V., Han P., Bulaev A., Pjevac P., Daebeler A., Romano S., Albertsen M., Stein L.Y., Daims H. and Wagner M. 2017. Kinetic Analysis of a Complete Nitrifier Reveals an Oligotrophic Lifestyle. *Nature* 549: 269–72. doi:10.1038/nature23679.
- Klotz M.G., Arp D.J., Chain P.S.G., El-Sheikh A.F., Hauser L.J., Hommes N.G., Larimer F.W., Malfatti S.A., Norton J.M., Poret-Peterson A.T., Vergez L.M. and Ward B.B. 2006. Complete Genome Sequence of the Marine, Chemolithoautotrophic, Ammonia-Oxidizing Bacterium Nitrosococcus Oceani ATCC 19707. *Applied and Environmental Microbiology* 72 (9): 6299–6315. doi:10.1128/AEM.00463-06.
- Koch H., Galushko A., Albertsen M., Schintlmeister A., Gruber-Dorninger C., Lüscher S., Pelletier E., Le Paslier D., Spieck E., Richter A., Nielsen P.H., Wagner M. and Daims H. 2014. Growth of Nitrite-Oxidizing Bacteria by Aerobic Hydrogen Oxidation. *Science* 345 (6200): 761–63.
- Koch H., Lüscher S., Albertsen M., Kitzinger K., Herbold C., Spieck E., Nielsen P.H., Wagner M. and Daims H. 2015. Expanded Metabolic Versatility of Ubiquitous Nitrite-Oxidizing Bacteria from the Genus Nitrospira. *Proceedings of the National Academy of Sciences of the United States of America* 112 (36): 11371–76. doi:10.1073/pnas.1506533112.
- Könneke M., Bernhard A.E., de la Torre J.R., Walker C.B., Waterbury J.B. and Stahl D.A. 2005. Isolation of an Autotrophic Ammonia-Oxidizing Marine Archaeon. *Nature* 437: 543–46. doi:10.1038/nature03911.
- Könneke M., Schubert D.M., Brown P.C., Hügler M., Standfest S., Schwander T., Schada von Borzyskowski L., Erb T.J., Stahl D.A. and Berg I.A. 2014. Ammonia-Oxidizing Archaea Use the Most Energy-Efficient Aerobic Pathway for CO₂ Fixation. *Proceedings of the National Academy of Sciences of the United States of America* 111 (22): 8239–44. doi:10.1073/pnas.1402028111.
- Konstantinidis K.T. and Tiedje J.M. 2005. Towards a Genome-Based Taxonomy for Prokaryotes. *Journal of Bacteriology* 187 (18): 6258–64. doi:10.1128/JB.187.18.6258.
- Koops H.-P., Böttcher B., Möller U.C., Pommerening-Röser A. and Stehr G. 1991. Classification of Eight New Species of Ammonia-Oxidizing Bacteria: Nitrosomonas Communis Sp. Nov., Nitrosomonas Ureae Sp. Nov., Nitrosomonas Aestuarii Sp. Nov., Nitrosomonas Marina Sp. Nov., Nitrosomonas Nitrosa Sp. Nov., Nitrosomonas Eutropha Sp. Nov., N. *Journal of General Microbiology* 137: 1689–99. doi:10.1099/00221287-137-7-1689.
- Kozłowski J.A., Stieglmeier M., Schleper C., Klotz M.G. and Stein L.Y. 2016. Pathways and Key Intermediates Required for Obligate Aerobic Ammonia-Dependent Chemolithotrophy in Bacteria and Thaumarchaeota. *The ISME Journal* 10: 1–10. doi:10.1038/ismej.2016.2.
- Krümme A. and Harms H. 1982. Effect of Organic Matter on Growth and Cell Yield of Ammonia-Oxidizing Bacteria. *Archives of Microbiology* 133: 50–54.
- Kumar S., Nicholas D.J.D. and Williams E.H. 1983. Definitive ¹⁵N NMR Evidence That Water Serves as a Source of “O” during Nitrite Oxidation by Nitrobacter Agilis. *FEBS Letters* 152 (1): 71–74. doi:10.1016/0014-5793(83)80484-0.
- Kuypers M.M.M., Marchant H.K. and Kartal B. 2018. The Microbial Nitrogen-Cycling Network. *Nature Reviews Microbiology* 16 (5): 263–76. doi:10.1038/nrmicro.2018.9.
- Lancaster K.M., Caranto J.D., Majer S.H. and Smith M.A. 2018. Alternative Bioenergy: Updates to and Challenges in Nitrification Metalloenzymology. *Joule* 2: 421–41. doi:10.1016/j.joule.2018.01.018.
- Lister M.W. 1954. Some Observations on Cyanic Acid and Cyanates. *Canadian Journal of Chemistry* 33 (2): 426–40.

- Löscher C.R., Kock A., Könneke M., Laroche J., Bange H.W. and Schmitz R. a. 2012. Production of Oceanic Nitrous Oxide by Ammonia-Oxidizing Archaea. *Biogeosciences* 9: 2419–29. doi:10.5194/bg-9-2419-2012.
- Lu L., Han W., Zhang J., Wu Y., Wang B., Lin X., Zhu J., Cai Z. and Jia Z. 2012. Nitrification of Archaeal Ammonia Oxidizers in Acid Soils Is Supported by Hydrolysis of Urea. *The ISME Journal* 6: 1978–84. doi:10.1038/ismej.2012.45.
- Lücker S., Nowka B., Rattei T., Spieck E. and Daims H. 2013. The Genome of Nitrospina Gracilis Illuminates the Metabolism and Evolution of the Major Marine Nitrite Oxidizer. *Frontiers in Microbiology* 4 (27): 1–19. doi:10.3389/fmicb.2013.00027.
- Lücker S., Schwarz J., Gruber-Dorninger C., Spieck E., Wagner M. and Daims H. 2015. Nitrotoga-like Bacteria Are Previously Unrecognized Key Nitrite Oxidizers in Full-Scale Wastewater Treatment Plants. *The ISME Journal* 9: 708–20. doi:10.1038/ismej.2014.158.
- Lücker S., Wagner M., Maixner F., Pelletier E., Koch H., Vacherie B., Rattei T., Sinninghe Damsté J.S., Spieck E., Le Paslier D. and Daims H. 2010. A Nitrospira Metagenome Illuminates the Physiology and Evolution of Globally Important Nitrite-Oxidizing Bacteria. *Proceedings of the National Academy of Sciences of the United States of America* 107 (30): 13479–84. doi:10.1073/pnas.1003860107.
- Madigan M.T., Martinko J.M., Stahl D.A. and Clarke D.P. 2012. *Brock Biology of Microorganisms*. 13th ed. Pearson Education.
- Manefield M., Whiteley A.S., Griffiths R.I. and Bailey M.J. 2002. RNA Stable Isotope Probing, a Novel Means of Linking Microbial Community Function to Phylogeny. *Applied and Environmental Microbiology* 68 (11): 5367–73. doi:10.1128/AEM.68.11.5367.
- Marchant H.K., Tegetmeyer H.E., Ahmerkamp S., Holtappels M., Lavik G., Graf J., Schreiber F., Mussmann M., Strous M. and Kuypers M.M.M. 2018. Metabolic Specialization of Denitrifiers in Permeable Sediments Controls N₂O Emissions. *Environmental Microbiology* 20 (12): 4486–4502. doi:10.1111/1462-2920.14385.
- Martens-Habbena W., Berube P.M., Urakawa H., de la Torre J.R. and Stahl D.A. 2009. Ammonia Oxidation Kinetics Determine Niche Separation of Nitrifying Archaea and Bacteria. *Nature* 461: 976–79. doi:10.1038/nature08465.
- Mather T.A., Pyle D.M. and Allen A.G. 2004. Volcanic Source for Fixed Nitrogen in the Early Earth's Atmosphere. *Geology* 32 (10): 905–8. doi:10.1130/G20679.1.
- Meincke M., Bock E., Kastrau D. and Kroneck P.M.H. 1992. Nitrite Oxidoreductase from Nitrobacter Hamburgensis: Redox Centers and Their Catalytic Role. *Archives of Microbiology* 158: 127–31. doi:10.1007/BF00245215.
- Minocha R., Studley K. and Saier M.H. 2003. The Urea Transporter (UT) Family: Bioinformatic Analyses Leading to Structural, Functional, and Evolutionary Predictions. *Receptors and Channels* 9 (6): 345–52. doi:10.3109/714041015.
- Mobley H.L., Island M.D. and Hausinger R.P. 1995. Molecular Biology of Microbial Ureas. *Microbiological Reviews* 59 (3): 451–80. doi:10.2741/1350.
- Moeller F.U., Webster N.S., Herbold C.W., Behnam F., Domman D., Albertsen M., Mooshammer M., Markert S., Turaev D., Becher D., Rattei T., Schweder T., Richter A., Watzka M., Nielsen P.H. and Wagner M. 2019. Characterization of a Thaumarchaeal Symbiont That Drives Incomplete Nitrification in the Tropical Sponge *Ianthella Basta*. *BioRxiv*, 1–56. doi:10.1101/527234.
- Mulder A., Graaf A.A. Van De, Robertson L.A. and Kuenen J.G. 1995. Anaerobic Ammonium Oxidation Discovered in a Denitrifying Fluidized Bed Reactor. *FEMS Microbiology Ecology* 16: 177–83. doi:10.1111/j.1574-6941.1995.tb00281.x.
- Mulholland M.R. and Lomas M.W. 2008. Nitrogen Uptake and Assimilation. In *Nitrogen in the Marine Environment*, 303–84. doi:10.1016/B978-0-12-372522-6.00007-4.
- Mußmann M., Brito I., Pitcher A., Sinninghe Damsté J.S., Hatzepichler R., Richter A., Nielsen J.L., Nielsen P.H., Müller A., Daims H., Wagner M. and Head I.M. 2011. Thaumarchaeotes Abundant in Refinery Nitrifying Sludges Express AmoA but Are Not Obligate Autotrophic Ammonia Oxidizers. *Proceedings of the National Academy of Sciences of the United States of America* 108 (40): 16771–76. doi:10.1073/pnas.1106427108.
- Ngugi D.K., Blom J., Stepanauskas R. and Stingl U. 2016. Diversification and Niche Adaptations of Nitrospina-like Bacteria in the Polyextreme Interfaces of Red Sea Brines. *The ISME Journal* 10: 1383–99. doi:10.1038/ismej.2015.214.
- Nokhal T.-H. and Schlegel H.G. 1983. Taxonomic Study of Paracoccus Denitrificans. *International Journal of Systematic Bacteriology* 33 (1): 26–37.

- Orphan V.J., House C.H., Hinrichs K.-U., McKeegan K. and Delong E.F. 2001. Methane-Consuming Archaea Revealed by Directly Coupled Isotopic and Phylogenetic Analysis. *Science* 293: 484–86. doi:10.1126/science.1061338.
- Ouverney C.C. and Fuhrman J. a. 2000. Marine Planktonic Archaea Take up Amino Acids. *Applied and Environmental Microbiology* 66 (11): 4829–33. doi:10.1128/AEM.66.11.4829-4833.2000.
- Pachiadaki M.G., Sintés E., Bergauer K., Brown J.M., Record N.R., Swan B.K., Mathyer M.E., Hallam S.J., Lopez-Garcia P., Takaki Y., Nunoura T., Woyke T., Herndl G.J. and Stepanauskas R. 2017. Major Role of Nitrite-Oxidizing Bacteria in Dark Ocean Carbon Fixation. *Science* 358: 1046–51. doi:10.1126/science.aan8260.
- Padilla C.C., Bristow L.A., Sarode N., Garcia-Robledo E., Gómez Ramírez E., Benson C.R., Bourbonnais A., Altabet M.A., Girguis P.R., Thamdrup B. and Stewart F.J. 2016. NC10 Bacteria in Marine Oxygen Minimum Zones. *The ISME Journal* 10: 2067–71. doi:10.1038/ismej.2015.262.
- Palatinszky M., Herbold C., Jehmlich N., Pogoda M., Han P., Bergen M. Von, Lagkouvardos I., Karst S.M., Galushko A., Koch H., Berry D., Daims H. and Wagner M. 2015. Cyanate as an Energy Source for Nitrifiers. *Nature* 524: 105–8. doi:10.1038/nature14856.
- Palenik B., Brahamsha B., Larimer F.W., Land M., Hauser L., Chain P., Lamerdin J., Regala W., Allen E.E., McCarren J., Paulsen I., Dufresne A., Partensky F., Webb E.A. and Waterbury J. 2003. The Genome of a Motile Marine Synechococcus. *Nature* 424: 1037–42. doi:10.1038/nature01883.1.
- Parks D.H., Chuvochina M., Waite D.W., Rinke C., Skarshewski A., Chaumeil P.A. and Hugenholtz P. 2018. A Standardized Bacterial Taxonomy Based on Genome Phylogeny Substantially Revises the Tree of Life. *Nature Biotechnology* 36 (10): 996–1004. doi:10.1038/nbt.4229.
- Pitcher A., Villanueva L., Hopmans E.C., Schouten S., Reichart G.-J. and Sinninghe Damsté J.S. 2011. Niche Segregation of Ammonia-Oxidizing Archaea and Anammox Bacteria in the Arabian Sea Oxygen Minimum Zone. *The ISME Journal* 5: 1896–1904. doi:10.1038/ismej.2011.60.
- Pjevac P., Schauburger C., Poghosyan L., Herbold C.W., van Kessel M.A.H.J., Daebeler A., Steinberger M., Jetten M.S.M., Lückner S., Wagner M. and Daims H. 2017. AmoA-Targeted Polymerase Chain Reaction Primers for the Specific Detection and Quantification of Comammox Nitrospira in the Environment. *Frontiers in Microbiology* 8 (1508): 1–11. doi:10.1101/096891.
- Pörtner H.-O., Karl D.M., Boyd P.W., Cheung W.W.L., Lluch-Cota S.E., Nojiri Y., Schmidt D.N. and Zavialov P.O. 2014. Ocean Systems. In *Climate Change 2014: Impacts, Adaptation, and Vulnerability. Part A: Global and Sectoral Aspects. Contribution of Working Group II to the Fifth Assessment Report of the Intergovernmental Panel on Climate Change*, edited by C.B. Field, V.R. Barros, D.J. Dokken, K.J. Mach, M.D. Mastrandrea, T.E. Bilir, M. Chatterjee, et al., 411–84. Cambridge: Cambridge University Press. doi:10.1017/CBO9781107415379.011.
- Prosser J.I. 2011. Soil Nitrifiers and Nitrification. In *Nitrification*, edited by Bess B Ward, Daniel J Arp, and Martin G Klotz, 347–83. Washington: ASM Press, Washington DC. doi:10.1128/9781555817145.
- Prosser J.I. and Nicol G.W. 2012. Archaeal and Bacterial Ammonia-Oxidisers in Soil: The Quest for Niche Specialisation and Differentiation. *Trends in Microbiology* 20 (11): 523–31. doi:10.1016/j.tim.2012.08.001.
- Qin W., Amin S.A., Martens-Habbena W., Walker C.B., Urakawa H., Devol A.H., Ingalls A.E., Moffett J.W., Armbrust E.V. and Stahl D.A. 2014. Marine Ammonia-Oxidizing Archaeal Isolates Display Obligate Mixotrophy and Wide Ecotypic Variation. *Proceedings of the National Academy of Sciences of the United States of America* 111 (34): 12504–9. doi:10.1073/pnas.1324115111.
- Qin W., Meinhardt K.A., Moffett J.W., Devol A.H., Virginia Armbrust E., Ingalls A.E. and Stahl D.A. 2017. Influence of Oxygen Availability on the Activities of Ammonia-Oxidizing Archaea. *Environmental Microbiology Reports* 9 (3): 250–56. doi:10.1111/1758-2229.12525.
- Rabalais N.N., Turner R.E. and Wiseman W.J. 2001. Hypoxia in the Gulf of Mexico. *Journal of Environment Quality* 30: 320–29. doi:10.2134/jeq2001.302320x.
- Radajewski S., Ineson P., Parekh N.R. and Murrell J.C. 2000. Stable-Isotope Probing as a Tool in Microbial Ecology. *Nature* 403: 646–49. doi:10.1038/35001054.
- Raymond J., Siefert J.L., Staples C.R. and Blankenship R.E. 2004. The Natural History of Nitrogen Fixation. *Molecular Biology and Evolution* 21 (3): 541–54. doi:10.1093/molbev/msh047.
- Risgaard-Petersen N., Langezaal A.M., Ingvarsdén S., Schmid M.C., Jetten M.S.M., Op den Camp H.J.M., Derksen J.W.M., Piña-Ochoa E., Eriksson S.P., Nielsen L.P., Revsbech N.P., Cedhagen T. and van der Zwaan G.J. 2006. Evidence for Complete Denitrification in a Benthic Foraminifer. *Nature* 443: 93–96. doi:10.1038/nature05070.

- Robertson E.K., Roberts K.L., Burdorf L.D.W., Cook P. and Thamdrup B. 2016. Dissimilatory Nitrate Reduction to Ammonium Coupled to Fe(II) Oxidation in Sediments of a Periodically Hypoxic Estuary. *Limnology and Oceanography* 61: 365–81. doi:10.1002/lno.10220.
- Rocap G., Larimer F.W., Lamerdin J., Malfatti S., Chain P., Ahlgren N.A., Arellano A., Coleman M., Hauser L., Hess W.R., Johnson Z.I., Land M., Lindell D., Post A.F., Regala W., Shah M., Shaw S.L., Steglich C., Sullivan M.B., et al. 2003. Genome Divergence in Two Prochlorococcus Ecotypes Reflects Oceanic Niche Differentiation. *Nature* 424: 1042–47. doi:10.1038/nature01947.
- Rockström J., Steffen W., Noone K., Persson Å., Chapin III F.S., Lambin E.F., Lenton T.M., Scheffer M., Folke C., Schellnhuber H.J., Nykvist B., de Wit C., Hughes T., van der Leeuw S., Rodhe H., Sörlin S., Snyder P.K., Costanza R., Svedin U., et al. 2009. A Safe Operating Space for Humanity. *Nature* 461: 472–475. doi:10.1016/j.jen.2014.01.005.
- Roco C.A., Bergaust L.L., Bakken L.R., Yavitt J.B. and Shapleigh J.P. 2017. Modularity of Nitrogen-Oxide Reducing Soil Bacteria: Linking Phenotype to Genotype. *Environmental Microbiology* 19 (6): 2507–19. doi:10.1111/1462-2920.13250.
- Sachs G., Kraut J.A., Wen Y., Feng J. and Scott D.R. 2006. Urea Transport in Bacteria: Acid Acclimation by Gastric Helicobacter Spp. *Journal of Membrane Biology* 212: 71–82. doi:10.1007/s00232-006-0867-7.
- Sanford R.A., Wagner D.D., Wu Q., Chee-Sanford J.C., Thomas S.H., Cruz-Garcia C., Rodriguez G., Massol-Deya A., Krishnani K.K., Ritalahti K.M., Nissen S., Konstantinidis K.T. and Löffler F.E. 2012. Unexpected Nondenitrifier Nitrous Oxide Reductase Gene Diversity and Abundance in Soils. *Proceedings of the National Academy of Sciences of the United States of America* 109 (48): 19709–14. doi:10.1073/pnas.1211238109.
- Santoro A.E., Saito M.A., Goepfert T.J., Lamborg C.H., Dupont C.L. and Ditullio G.R. 2017. Thaumarchaeal Ecotype Distributions across the Equatorial Pacific Ocean and Their Potential Roles in Nitrification and Sinking Flux Attenuation. *Limnology and Oceanography* 62: 1984–2003. doi:10.1002/lno.10547.
- Saunders A.M., Albertsen M., Vollesen J. and Nielsen P.H. 2016. The Activated Sludge Ecosystem Contains a Core Community of Abundant Organisms. *The ISME Journal* 10 (1): 11–20. doi:10.1038/ismej.2015.117.
- Schloesing T. and Muntz A. 1877. Sur La Nitrification Par Les Ferments Organises. *Comptes Rendus Hebdomadaires Des Séances de l'Academie Des Sciences* 84: 301–3.
- Schott J., Griffin B.M. and Schink B. 2010. Anaerobic Phototrophic Nitrite Oxidation by Thiocapsa Sp. Strain KS1 and Rhodospseudomonas Sp. Strain LQ17. *Microbiology* 156: 2428–37. doi:10.1099/mic.0.036004-0.
- Schumann U. and Huntrieser H. 2007. The Global Lightning-Induced Nitrogen Oxides Source. *Atmospheric Chemistry and Physics Discussions* 7: 2623–2818. doi:10.5194/acpd-7-2623-2007.
- Seitz H.J. and Cypionka H. 1986. Chemolithotrophic Growth of Desulfovibrio Desulfuricans with Hydrogen Coupled to Ammonification of Nitrate or Nitrite. *Archives of Microbiology* 146: 63–67. doi:10.1007/BF00690160.
- Seyler L.M., McGuinness L.M. and Kerkhof L.J. 2014. Crenarchaeal Heterotrophy in Salt Marsh Sediments. *The ISME Journal* 8: 1534–43. doi:10.1038/ismej.2014.15.
- Seyler L.M., McGuinness L.R., Gilbert J.A., Biddle J.F., Gong D. and Kerkhof L.J. 2018. Discerning Autotrophy, Mixotrophy and Heterotrophy in Marine TACK Archaea from the North Atlantic. *FEMS Microbiology Ecology* 94 (3): 1–10. doi:10.1093/femsec/fiy014.
- Siewe R.M., Weil B., Burkovski A., Eggeling L., Krämer R. and Jahns T. 1998. Urea Uptake and Urease Activity in Corynebacterium Glutamicum. *Archives of Microbiology* 169: 411–16. doi:10.1007/s002030050591.
- Sipler R.E. and Bronk D.A. 2015. Dynamics of Dissolved Organic Nitrogen. In *Biogeochemistry of Marine Dissolved Organic Matter: Second Edition*, edited by Dennis A. Hansell and Craig A. Carlson, Second Edi, 127–232. ACADEMIC PRESS, INC. doi:10.1016/B978-0-12-405940-5.00004-2.
- Smith J.M., Chavez F.P. and Francis C.A. 2014. Ammonium Uptake by Phytoplankton Regulates Nitrification in the Sunlit Ocean. *PLoS ONE* 9 (9): e108173. doi:10.1371/journal.pone.0108173.
- Smith V.H. 2003. Eutrophication of Freshwater and Coastal Marine Ecosystems - A Global Problem. *Environmental Science and Pollution Research* 10 (2): 126–39. doi:10.17660/ActaHortic.2017.1170.71.
- Solomon C.M., Collier J.L., Berg G.M. and Glibert P.M. 2010. Role of Urea in Microbial Metabolism in Aquatic Systems: A Biochemical and Molecular Review. *Aquatic Microbial Ecology* 59: 67–88. doi:10.3354/ame01390.
- Solomon C.M. and Glibert P.M. 2008. Urease Activity in Five Phytoplankton Species. *Aquatic Microbial Ecology* 52: 149–57. doi:10.3354/ame01213.

- Sorokin D.Y., Lücker S., Vejmelkova D., Kostrikina N. a, Kleerebezem R., Rijpstra W.I.C., Damsté J.S.S., Le Paslier D., Muyzer G., Wagner M., van Loosdrecht M.C.M. and Daims H. 2012. Nitrification Expanded: Discovery, Physiology and Genomics of a Nitrite-Oxidizing Bacterium from the Phylum Chloroflexi. *The ISME Journal* 6: 2245–56. doi:10.1038/ismej.2012.70.
- Sorokin D.Y., Tourova T.P., Antipov A.N., Muyzer G. and Kuenen J.G. 2004. Anaerobic Growth of the Haloalkaliphilic Denitrifying Sulfur-Oxidizing Bacterium *Thialkalivibrio Thiocyanodenitrificans* Sp. Nov. with Thiocyanate. *Microbiology* 150: 2435–42. doi:10.1099/mic.0.27015-0.
- Sorokin D.Y., Tourova T.P., Lysenko a. M. and Kuenen J.G. 2001. Microbial Thiocyanate Utilization under Highly Alkaline Conditions. *Applied and Environmental Microbiology* 67 (2): 528–38. doi:10.1128/AEM.67.2.528-538.2001.
- Sorokin D.Y., Vejmelkova D., Lücker S., Streshinskaya G.M., Rijpstra W.I.C., Damsté J.S.S., Kleerbezem R., van Loosdrecht M., Muyzer G. and Daims H. 2014. *Nitrolancea Hollandica* Gen. Nov., Sp. Nov., a Chemolithoautotrophic Nitrite-Oxidizing Bacterium Isolated from a Bioreactor Belonging to the Phylum Chloroflexi. *International Journal of Systematic and Evolutionary Microbiology* 64: 1859–65. doi:10.1099/ijs.0.062232-0.
- Spang A., Poehlein A., Offre P., Zumbrägel S., Haider S., Rychlik N., Nowka B., Schmeisser C., Lebedeva E. V., Rattei T., Böhm C., Schmid M., Galushko A., Hatzenpichler R., Weinmaier T., Daniel R., Schleper C., Spieck E., Streit W., et al. 2012. The Genome of the Ammonia-Oxidizing Candidatus *Nitrososphaera Gargensis*: Insights into Metabolic Versatility and Environmental Adaptations. *Environmental Microbiology* 14 (12): 3122–45. doi:10.1111/j.1462-2920.2012.02893.x.
- Spieck E., Ehrich S., Aamand J. and Bock E. 1998. Isolation and Immunocytochemical Location of the Nitrite-Oxidizing System in *Nitrospira Moscoviensis*. *Archives of Microbiology* 169: 225–30. doi:10.1007/s002030050565.
- Spieck E., Hartwig C., McCormack I., Maixner F., Wagner M., Lipski A. and Daims H. 2006. Selective Enrichment and Molecular Characterization of a Previously Uncultured *Nitrospira*-like Bacterium from Activated Sludge. *Environmental Microbiology* 8 (3): 405–15. doi:10.1111/j.1462-2920.2005.00905.x.
- Spieck E., Keuter S., Wenzel T., Bock E. and Ludwig W. 2014. Characterization of a New Marine Nitrite Oxidizing Bacterium, *Nitrospina Watsonii* Sp. Nov., a Member of the Newly Proposed Phylum “Nitrospinae.” *Systematic and Applied Microbiology* 37: 170–76. doi:10.1016/j.syapm.2013.12.005.
- Spieck E. and Lipski A. 2011. Cultivation, Growth Physiology, and Chemotaxonomy of Nitrite-Oxidizing Bacteria. In *Methods in Enzymology*, edited by Martin G. Klotz, 1st ed., 486:109–30. Elsevier Inc. doi:10.1016/B978-0-12-381294-0.00005-5.
- Starkenburger S.R., Larimer F.W., Stein L.Y., Klotz M.G., Chain P.S.G., Sayavedra-Soto L. a., Poret-Peterson A.T., Gentry M.E., Arp D.J., Ward B. and Bottomley P.J. 2008. Complete Genome Sequence of *Nitrobacter Hamburgensis* X14 and Comparative Genomic Analysis of Species within the Genus *Nitrobacter*. *Applied and Environmental Microbiology* 74 (9): 2852–63. doi:10.1128/AEM.02311-07.
- Stein L.Y. 2011. Heterotrophic Nitrification and Nitrifier Denitrification. In *Nitrification*, edited by Bess B Ward, Daniel J Arp, and Martin G. Klotz, 95–114. Washington DC: ASM Press, Washington DC. doi:10.1128/9781555817145.ch5.
- Stein L.Y. 2019. Insights into the Physiology of Ammonia-Oxidizing Microorganisms. *Current Opinion in Chemical Biology* 49: 9–15. doi:10.1016/j.cbpa.2018.09.003.
- Stieglmeier M., Mooshammer M., Kitzler B., Wanek W., Zechmeister-Boltenstern S., Richter A. and Schleper C. 2014. Aerobic Nitrous Oxide Production through N-Nitrosating Hybrid Formation in Ammonia-Oxidizing Archaea. *The ISME Journal* 8: 1135–46. doi:10.1038/ismej.2013.220.
- Straub K.L., Benz M., Schink B. and Widdel F. 1996. Anaerobic, Nitrate-Dependent Microbial Oxidation of Ferrous Iron. *Applied and Environmental Microbiology* 62 (4): 1458–60. doi:10.1128/AEM.62.4.1458-1460.1996.
- Sun X., Ji Q., Jayakumar A. and Ward B.B. 2017. Dependence of Nitrite Oxidation on Nitrite and Oxygen in Low-Oxygen Seawater. *Geophysical Research Letters* 44 (15): 7883–91. doi:10.1002/2017GL074355.
- Teira E., van Aken H., Veth C. and Herndl G.J. 2006. Archaeal Uptake of Enantiomeric Amino Acids in the Meso- and Bathypelagic Waters of the North Atlantic. *Limnology and Oceanography* 51 (1): 60–69. doi:10.4319/lo.2006.51.1.0060.
- Tiedje J.M. 1988. Ecology of Denitrification and Dissimilatory Nitrate Reduction to Ammonium. In *Environmental Microbiology of Anaerobes*, edited by A J B Zehnder, 179–244. New York: John Wiley & Sons Ltd.

- Tolar B.B., King G.M. and Hollibaugh J.T. 2013. An Analysis of Thaumarchaeota Populations from the Northern Gulf of Mexico. *Frontiers in Microbiology* 4 (72): 1–36. doi:10.3389/fmicb.2013.00072.
- Tolar B.B., Powers L.C., Miller W.L., Wallsgrove N.J., Popp B.N. and Hollibaugh J.T. 2016. Ammonia Oxidation in the Ocean Can Be Inhibited by Nanomolar Concentrations of Hydrogen Peroxide. *Frontiers in Marine Science* 3 (237): 1–16. doi:10.3389/fmars.2016.00237.
- Tolar B.B., Wallsgrove N.J., Popp B.N. and Hollibaugh J.T. 2017. Oxidation of Urea-Derived Nitrogen by Thaumarchaeota-Dominated Marine Nitrifying Communities. *Environmental Microbiology* 19 (12): 4838–4850. doi:10.1002/elsc.201200179.
- Tourna M., Stieglmeier M., Spang A., Könneke M., Schintlmeister A., Urich T., Engel M., Schlöter M., Wagner M., Richter A. and Schleper C. 2011. Nitrososphaera Viennensis, an Ammonia Oxidizing Archaeon from Soil. *Proceedings of the National Academy of Sciences of the United States of America* 108 (20): 8420–8425. doi:10.1073/pnas.1013488108/-/DCSupplemental.www.pnas.org/cgi/doi/10.1073/pnas.1013488108.
- Treusch A.H., Leininger S., Kietzin A., Schuster S.C., Klenk H.P. and Schleper C. 2005. Novel Genes for Nitrite Reductase and Amo-Related Proteins Indicate a Role of Uncultivated Mesophilic Crenarchaeota in Nitrogen Cycling. *Environmental Microbiology* 7 (12): 1985–95. doi:10.1111/j.1462-2920.2005.00906.x.
- Tsementzi D., Wu J., Deutsch S., Nath S., Rodriguez-R L.M., Burns A.S., Ranjan P., Sarode N., Malmstrom R.R., Padilla C.C., Stone B.K., Bristow L.A., Larsen M., Glass J.B., Thamdrup B., Woyke T., Konstantinidis K.T. and Stewart F.J. 2016. SAR11 Bacteria Linked to Ocean Anoxia and Nitrogen Loss. *Nature* 536: 179–83. doi:10.1038/nature19068.
- UNEP and WHRC. 2007. *Reactive Nitrogen in the Environment; Too Much or Too Little of a Good Thing*. United Nations Environment Programme and Woods Hole Research Center. http://www.unep.org/pdf/dtie/Reactive_Nitrogen.pdf.
- Vajrala N., Martens-Habbena W., Sayavedra-Soto L. a, Schauer A., Bottomley P.J., Stahl D. a and Arp D.J. 2013. Hydroxylamine as an Intermediate in Ammonia Oxidation by Globally Abundant Marine Archaea. *Proceedings of the National Academy of Sciences of the United States of America* 110 (3): 1006–11. doi:10.1073/pnas.1214272110.
- Valladares A., Montesinos M.L., Herrero A. and Flores E. 2002. An ABC-Type, High-Affinity Urea Permease Identified in Cyanobacteria. *Molecular Microbiology* 43 (3): 703–15. doi:10.1046/j.1365-2958.2002.02778.x.
- van de Graaf A.A., de Bruijn P., Robertson L.A., Jetten M.S.M. and Kuenen J.G. 1997. Metabolic Pathway of Anaerobic Ammonium Oxidation on the Basis of ¹⁵N Studies in a Fluidized Bed Reactor. *Microbiology* 143: 2415–21.
- Van de Vossenberg J., Woebken D., Maalcke W.J., Wessels H.J.C.T., Dutilh B.E., Kartal B., Janssen-Megens E.M., Roeselers G., Yan J., Speth D., Gloerich J., Geerts W., Van der Biezen E., Pluk W., Francoijs K.J., Russ L., Lam P., Malfatti S.A., Tringe S.G., et al. 2013. The Metagenome of the Marine Anammox Bacterium “Candidatus Scalindua Profunda” Illustrates the Versatility of This Globally Important Nitrogen Cycle Bacterium. *Environmental Microbiology* 15 (5): 1275–89. doi:10.1111/j.1462-2920.2012.02774.x.
- van Kessel M.A.H.J., Speth D.R., Albertsen M., Nielsen P.H., Op den Camp H.J.M., Kartal B., Jetten M.S.M. and Lüscher S. 2015. Complete Nitrification by a Single Microorganism. *Nature* 528: 555–59. doi:10.1038/nature16459.
- Venter J.C., Remington K., Heidelberg J.F., Halpern A.L., Rusch D., Eisen J.A., Wu D., Paulsen I., Nelson K.E., Nelson W., Fouts D.E., Levy S., Knap A.H., Lomas M.W., Nealson K., White O., Peterson J., Hoffman J., Parsons R., et al. 2004. Environmental Genome Shotgun Sequencing of the Sargasso Sea. *Science* 304: 66–74. doi:10.1126/science.1093857.
- Wagner M. and Loy A. 2002. Bacterial Community Composition and Function in Sewage Treatment Systems. *Current Opinion in Biotechnology* 13: 218–27. doi:10.1016/S0958-1669(02)00315-4.
- Waksman S.A. 1946. Sergei Nikolaevitch Winogradsky. The Story of a Great Bacteriologist. *Soil Science* 62 (3): 197–226. doi:10.1097/00010694-194609000-00001.
- Ward B.B. 2013. Nitrification. In *Reference Module in Earth Systems and Environmental Sciences*, 1–8. Elsevier. doi:10.1016/B978-0-12-409548-9.00697-7.
- Warington R. 1891. XLVII. - On Nitrification. Part IV. *Journal of the Chemical Society, Transactions* 59: 484–529.
- Watson S.W., Bock E., Valois F.W., Waterbury J.B. and Schlosser U. 1986. Nitrospira Marina Gen. Nov. Sp. Nov.: A Chemolithotrophic Nitrite-Oxidizing Bacterium. *Archives of Microbiology* 144: 1–7. doi:10.1007/BF00454947.

- Watson S.W. and Waterbury J.B. 1971. Characteristics of Two Marine Nitrite Oxidizing Bacteria, *Nitrospina Gracilis* Nov. Gen. Nov. Sp. and *Nitrococcus Mobilis* Nov. Gen. Nov. Sp. *Archives of Microbiology* 77: 203–30.
- Weeks D.L., Eskandari S., Scott D.R. and Sachs G. 2000. A H⁺-Gated Urea Channel: The Link between *Helicobacter Pylori* Urease and Gastric Colonization. *Science* 287: 482–85. doi:10.1126/science.287.5452.482.
- Widner B., Fuchsman C.A., Chang B.X., Rocab G. and Mulholland M.R. 2018a. Utilization of Urea and Cyanate in Waters Overlying and within the Eastern Tropical North Pacific Oxygen Deficient Zone. *FEMS Microbiology Ecology* 94 (10): fiy138. doi:10.1093/femsec/fiy138/5055141.
- Widner B., Mordy C.W. and Mulholland M.R. 2018b. Cyanate Distribution and Uptake above and within the Eastern Tropical South Pacific Oxygen Deficient Zone. *Limnology and Oceanography* 63 (S1): S177–92. doi:10.1002/lno.10730.
- Widner B. and Mulholland M.R. 2017. Cyanate Distribution and Uptake in North Atlantic Coastal Waters. *Limnology and Oceanography* 62 (6): 2538–49. doi:10.1002/lno.10588.
- Widner B., Mulholland M.R. and Mopper K. 2013. Chromatographic Determination of Nanomolar Cyanate Concentrations in Estuarine and Sea Waters by Precolumn Fluorescence Derivatization. *Analytical Chemistry* 85: 6661–66. doi:10.1021/ac400351c.
- Widner B., Mulholland M.R. and Mopper K. 2016. Distribution, Sources, and Sinks of Cyanate in the Coastal North Atlantic Ocean. *Environmental Science & Technology Letters* 3 (8): 297–302. doi:10.1021/acs.estlett.6b00165.
- Winogradsky S. 1890. Recherches Sur Les Organismes de Al Nitrification. *Comptes Rendus de l'Académie Des Sciences* 110: 1013–16.
- Wuchter C., Abbas B., Coolen M.J.L., Herfort L., van Bleijswijk J., Timmers P., Strous M., Teira E., Herndl G.J., Middelburg J.J., Schouten S. and Sinninghe Damsté J.S. 2006. Archaeal Nitrification in the Ocean. *Proceedings of the National Academy of Sciences of the United States of America* 103 (33): 12317–22. doi:10.1073/pnas.0600756103.

Chapter 2

Characterization of the first “*Candidatus Nitrotoga*” isolate reveals metabolic versatility and separate evolution of widespread nitrite-oxidizing bacteria

Katharina Kitzinger^{1,2}, Hanna Koch^{1*}, Sebastian Lücker³, Christopher J. Sedlacek¹, Craig Herbold¹, Jasmin Schwarz¹, Anne Daebeler¹, Anna J. Mueller¹, Michael Lukumbuzya¹, Stefano Romano¹, Nikolaus Leisch², Søren Michael Karst⁴, Rasmus Kirkegaard⁴, Mads Albertsen⁴, Per Halkjær Nielsen⁴, Michael Wagner¹, Holger Daims¹

Author affiliations

¹Division of Microbial Ecology, Department of Microbiology and Ecosystem Science, Research Network Chemistry meets Microbiology, University of Vienna, Vienna, Austria

²Max-Planck-Institute for Marine Microbiology, Bremen, Germany

³Department of Microbiology, Radboud University, Nijmegen, The Netherlands

⁴Center for Microbial Communities, Department of Chemistry and Bioscience, Aalborg University, Aalborg, Denmark

*Present address: Department of Microbiology, Radboud University, Nijmegen, The Netherlands

Correspondence: Holger Daims, daims@microbial-ecology.net

Author contributions

K.K., H.D., H.K. and M.W. designed the study. K.K. enriched and isolated *Ca. Nitrotoga fabula* and maintained it with J.S. S.M.K., R.K. and P.H.N. sequenced the genome. K.K. annotated the genome with S.L., H.K. and H.D. K.K. performed all physiological experiments and data analyses with *Ca. N. fabula*, C.J.S. performed microrespirometry measurements. K.K. performed 16S rRNA gene analyses. A.D., N.L. and S.R. performed electron microscopy. A.D., A.J.M., M.L., H.D., M.A. and C.H. performed analyses of the crenarchaeal enrichment. C.H. and S.L. performed Nxr analyses. K.K. and H.D. wrote the manuscript, with contributions from all co-authors.

Published in mBio 2018, 9 (4) e01186-18

Abstract

Nitrification is a key process of the biogeochemical nitrogen cycle and of biological wastewater treatment. The second step, nitrite oxidation to nitrate, is catalyzed by phylogenetically diverse, chemolithoautotrophic nitrite-oxidizing bacteria (NOB). Uncultured NOB from the genus "*Candidatus Nitrotoga*" are widespread in natural and engineered ecosystems. Knowledge about their biology is sparse, because no genomic information and no pure "*Ca. Nitrotoga*" culture was available. Here we obtained the first "*Ca. Nitrotoga*" isolate from activated sludge. This organism, "*Candidatus Nitrotoga fabula*", prefers higher temperatures (>20°C; optimum 24-28°C) than previous "*Ca. Nitrotoga*" enrichments, which were described as cold-adapted NOB. "*Ca. N. fabula*" also showed an unusually high tolerance to nitrite (activity at 30 mM NO₂⁻) and nitrate (up to 25 mM NO₃⁻). Nitrite oxidation followed Michaelis-Menten kinetics, with $K_{m(\text{app})}$ of ~89 μM nitrite and V_{max} of ~28 μmol nitrite per mg protein per h. Key metabolic pathways of "*Ca. N. fabula*" were reconstructed from the closed genome. "*Ca. N. fabula*" possesses a new type of periplasmic nitrite oxidoreductase belonging to a lineage of mostly uncharacterized proteins. This novel enzyme indicates (i) separate evolution of nitrite oxidation in "*Ca. Nitrotoga*" and other NOB, (ii) the possible existence of phylogenetically diverse, unrecognized NOB, and (iii) together with new metagenomic data, the potential existence of nitrite-oxidizing archaea. For carbon fixation, "*Ca. N. fabula*" uses the Calvin-Benson-Bassham cycle. It also encodes complete pathways for hydrogen and sulfite oxidation, suggesting that alternative energy metabolisms enable "*Ca. N. fabula*" to survive nitrite depletion and colonize new niches.

Importance

Nitrite-oxidizing bacteria (NOB) are major players in the biogeochemical nitrogen cycle and critical for wastewater treatment. However, most NOB remain uncultured and their biology is poorly understood. Here, we obtained the first isolate from the environmentally widespread NOB genus "*Candidatus Nitrotoga*" and performed a detailed physiological and genomic characterization of this organism ("*Candidatus Nitrotoga fabula*"). Differences between key phenotypic properties of "*Ca. N. fabula*" and those of previously enriched "*Ca. Nitrotoga*" members reveal an unexpectedly broad range of physiological adaptations in this genus. Moreover, genes for energy metabolisms outside nitrification suggest that "*Ca. Nitrotoga*" are ecologically more flexible than previously anticipated. The identification of a novel nitrite-oxidizing enzyme in "*Ca. N. fabula*" expands our picture of the evolutionary history of nitrification and might lead to discoveries of novel nitrite oxidizers. Altogether, this study provides urgently needed insights into the biology of understudied but environmentally and biotechnologically important microorganisms.

Introduction

Nitrification, the microbially catalyzed oxidation of ammonia via nitrite to nitrate, is a key process of the natural biogeochemical nitrogen cycle. Nitrification also is critical for the removal of excess nitrogen from sewage in wastewater treatment plants (WWTPs), whereas in agriculture it contributes to the loss of nitrogen from fertilized soils (Prosser 2011). The first step of nitrification – ammonia oxidation to nitrite – is carried out by chemolithoautotrophic ammonia-oxidizing bacteria and archaea, whereas the second step – nitrite oxidation to nitrate – is catalyzed by chemolithoautotrophic nitrite-oxidizing bacteria (NOB).

NOB are the main biological source of nitrate, an important nitrogen source for many plants and microorganisms and an electron acceptor used by many microbes under anoxic conditions. Additionally, NOB have a strong impact on marine carbon cycling (Pachiadaki et al. 2017). Recently, surprising discoveries have been made in NOB-related research, demonstrating alternative energy

metabolisms such as the oxidation of hydrogen, sulfide, formate, and other organic compounds in organisms previously described as obligate nitrifiers (Koch et al. 2014; Koch et al. 2015; Füssel et al. 2017). Furthermore, a novel ‘reciprocal feeding’ interaction of NOB from the genus *Nitrospira* with ammonia oxidizers was described, where the NOB initiate nitrification by releasing ammonia from urea or cyanate (Koch et al. 2015; Palatinszky et al. 2015). Another surprise was the discovery of photolithoautotrophic NOB that use nitrite as an electron donor for anoxygenic photosynthesis (Griffin et al. 2007) and most likely evolved independently of the chemolithoautotrophic NOB (Hemp et al. 2016). For decades, a core paradigm of nitrification research stated that ammonia and nitrite oxidation are always catalyzed by distinct organisms, which cooperate by cross-feeding. This long-standing opinion was contradicted by the discovery of complete nitrifiers (comammox organisms) in the NOB genus *Nitrospira*, which perform both steps of nitrification (Daims et al. 2015; van Kessel et al. 2015). All NOB known until recently belong to the Alpha- and Gammaproteobacteria, the phylum Nitrospirae, or the phylum Nitrospinae (Teske et al. 1994; Ehrich et al. 1995; Lüscher et al. 2013). The known phylogenetic diversity of NOB has been now expanded by the description of several new NOB lineages: the genus *Nitrolancea* in the Chloroflexi (Sorokin et al. 2012), the candidate genus “Nitromaritima” in the Nitrospinae (Ngugi et al. 2016), and the candidate genus “Nitrotoga” in the Betaproteobacteria, family Gallionellaceae (Alawi et al. 2007).

Past research demonstrated that *Nitrospira* are the major NOB in many WWTPs (Juretschko et al. 1998; Daims et al. 2001). However, “*Candidatus (Ca.) Nitrotoga*” have recently been recognized as another widely distributed and sometimes predominant group of NOB in WWTPs (Alawi et al. 2009; Lüscher et al. 2015; Saunders et al. 2016). Other known habitats of “*Ca. Nitrotoga*” include soil, sediment, tap water and recirculation aquaculture biofilms, caves, and subglacial lake ecosystems (Alawi et al. 2007; Chen et al. 2009; Achberger et al. 2016; Hüpeden et al. 2016; Ishii et al. 2017; Kinnunen et al. 2017). Despite their importance, little is known about the microbiology of “*Ca. Nitrotoga*”. The first representative, “*Ca. N. arctica*”, was enriched from Siberian permafrost soil (Alawi et al. 2007). This organism and “*Ca. Nitrotoga*” members enriched from activated sludge (Alawi et al. 2009) or eelgrass sediment (Ishii et al. 2017) are adapted to cold temperatures. Moreover, a slightly acidic pH (5.7 to 6.8) and elevated nitrite loading were reported to favor growth of “*Ca. Nitrotoga*” over *Nitrospira* (Hüpeden et al. 2016; Kinnunen et al. 2017; Ma et al. 2017). In addition, the kinetics of nitrite oxidation were studied using enriched “*Ca. Nitrotoga*” members (Nowka et al. 2014; Ishii et al. 2017). Further characterization of “*Ca. Nitrotoga*”, including the nature of its nitrite-oxidizing enzyme and potential for alternative energy metabolisms, has been hampered by the lack of any pure culture or genome sequence from this genus.

In this study we obtained the first “*Ca. Nitrotoga*” isolate, characterized its key physiological properties, and analyzed its genetic repertoire based on the fully sequenced genome. The new strain, which has been isolated from a municipal WWTP, shows remarkably different physiological adaptations than the previously described “*Ca. Nitrotoga*” enrichments. Phylogenetic analysis of its nitrite oxidoreductase (NXR), the key enzyme for nitrite oxidation, suggests that the evolutionary history of NOB is more complex than previously assumed and indicates that a surprising diversity of yet undiscovered bacterial and archaeal nitrite oxidizers may exist in nature.

Results and Discussion

Isolation of a new “*Ca. Nitrotoga*” species

After inoculation of mineral nitrite medium with nitrifying activated sludge from a municipal WWTP and repeated feeding with nitrite, a nitrite-oxidizing primary enrichment culture was obtained. An initial analysis of the culture by 16S rRNA-targeted fluorescence *in situ* hybridization (FISH) revealed the presence of *Nitrospira*, “*Ca. Nitrotoga*”, and other bacteria. Aliquots of this culture were regularly diluted in fresh nitrite medium and incubated to further enrich the NOB. After the third dilution and transfer step, planktonic “*Ca. Nitrotoga*” cells were still detected by FISH in the culture, whereas *Nitrospira* cells were not found. *Nitrospira* might still have been present in abundances below the detection limit of FISH of approximately 10^4 target cells per ml (Amann et al. 1995). The cause of the prevalence of “*Ca. Nitrotoga*” at this stage of enrichment remains unknown. In addition, this secondary enrichment contained other bacteria that were probably feeding on organic compounds produced by the autotrophic NOB.

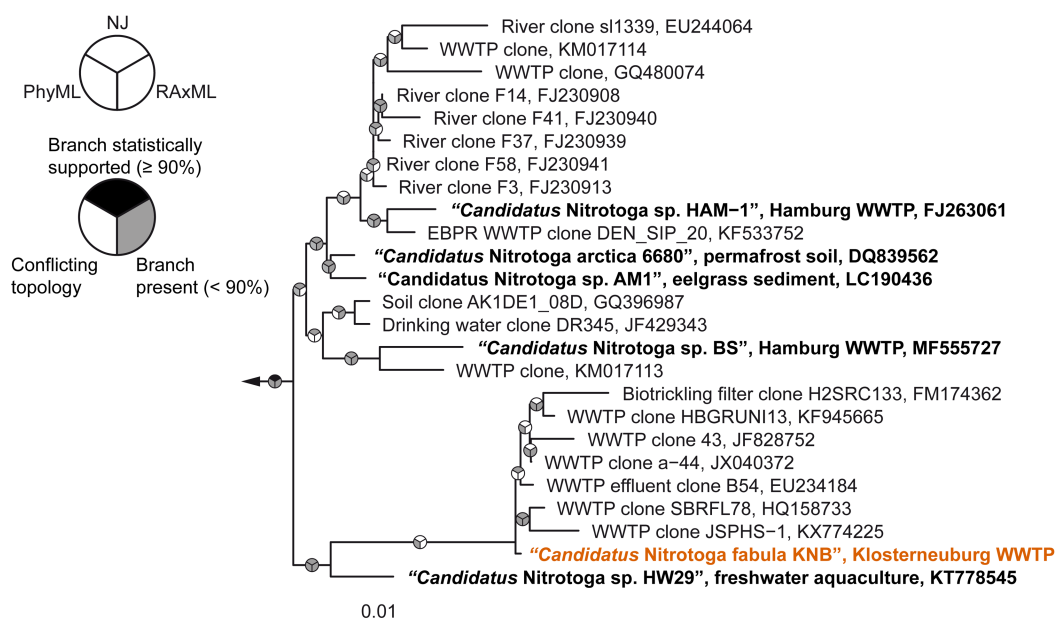


Figure 1 Phylogenetic affiliation of “*Ca. N. fabula*”. The consensus tree, which is based on 16S rRNA gene sequences of cultured and uncultured members of the candidate genus “*Nitrotoga*”, shows the position of the “*Ca. N. fabula*” isolate (highlighted orange) in this genus. Other cultured (enriched) “*Ca. Nitrotoga*” strains are highlighted in boldface. Pie charts indicate statistical support of branches based on maximum likelihood (RAxML; 1,000 bootstrap iterations) and neighbor joining (NJ; 1,000 bootstrap iterations). For PhyML, no bootstrap analysis was performed and grey indicates the presence of a branch. The scale bar indicates 0.01 estimated substitutions per nucleotide.

Since all further attempts to purify “*Ca. Nitrotoga*” in liquid culture were unsuccessful, the capability of this nitrite oxidizer to grow on solid nitrite media was tested. Except for some *Nitrobacter* strains (e.g. Bock et al. 1983) and *Nitrolancea hollandica* (Sorokin et al. 2012), no pure culture of NOB has been grown on solid media. NOB streaked onto plates might be inhibited by ambient oxygen (Spieck & Lipski 2011) or by organics in commonly used solidifying agents (Nowka et al. 2015). Inhibition could also be caused by H_2O_2 that is formed when medium containing agar (or agarose) and phosphate is autoclaved (Tanaka et al. 2014). No growth of “*Ca. Nitrotoga*” was observed after streaking aliquots of the secondary enrichment onto plaque agarose plates, which had been autoclaved in the presence of phosphate, and on media containing noble agar or sieve agarose (with

phosphate added before or after autoclaving). In contrast, small (<1 mm), light brown colonies were obtained after incubation for one month on plaque agarose medium prepared with phosphate addition after autoclaving. Direct Sanger sequencing of 16S rRNA genes PCR-amplified from these colonies confirmed that the colonies consisted of “*Ca. Nitrotoga*” cells. The obtained 16S rRNA gene sequence was identical to that retrieved from subsequent liquid cultures (see below and Figure 1). Thus, selection of a suitable solidifying agent and reduction of H₂O₂ formation in the medium were the key prerequisites for growing “*Ca. Nitrotoga*” on plates. A single colony was then re-streaked onto new plates and cells were finally transferred into liquid nitrite medium. Subsequent purity checks (see Methods) confirmed the absence of any other detectable organism in the culture.

Phylogenetic analysis of 16S rRNA genes revealed a close affiliation of the obtained “*Ca. Nitrotoga*” isolate with all other enriched “*Ca. Nitrotoga*” strains and various environmental sequences (Figure 1). The highest 16S rRNA gene sequence identity shared by the new isolate and a previously enriched “*Ca. Nitrotoga*” member was 98.63% with “*Ca. Nitrotoga* sp. HW29” (Hüpeden et al. 2016). As this value is below the threshold of 98.7 to 99% used to differentiate species (Stackebrandt & Ebers 2006) and the obtained isolate showed distinct physiological properties (see below), we propose this organism represents a separate species within the candidate genus “*Nitrotoga*”.

The new “*Ca. Nitrotoga*” isolate had a peculiar bean-shaped morphology, and the periplasmic space was not enlarged as much as previously described for “*Ca. Nitrotoga*” cells (Alawi et al. 2007; Alawi et al. 2009; Ishii et al. 2017) (Figure 2). Because of the characteristic morphology, we propose the name “*Candidatus Nitrotoga fabula* KNB” (“small bean”, strain designation KNB for the WWTP in Klosterneuburg, Austria) for the new isolate.

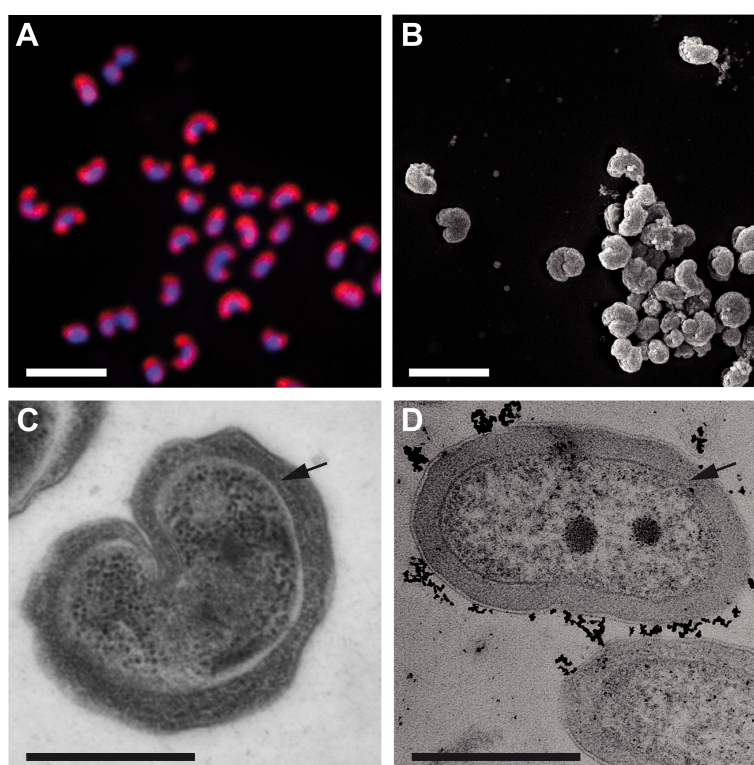


Figure 2 Morphology of “*Ca. N. fabula*”. (A) Pure culture of “*Ca. N. fabula*” visualized by FISH with the “*Ca. Nitrotoga*”-specific probe Ntoga122 (red) and by DAPI staining (blue). Scale bar, 2 μ m. (B) Scanning electron micrograph imaged after chemical fixation (scale bar, 2 μ m). (C and D) Transmission electron micrographs (C: after cryopreservation, D: after chemical fixation; scale bars, 0.5 μ m). Black arrows indicate the periplasmic space.

Physiological characterization of “*Ca. N. fabula*” in comparison to previous “*Ca. Nitrotoga*” enrichments and other NOB

The nitrite-oxidizing activity of “*Ca. N. fabula*” had its temperature optimum at 24 to 28°C and was poor below 20°C (Figure 3A). This preference for elevated temperatures was unexpected, because all characterized enriched “*Ca. Nitrotoga*” members prefer lower temperatures or at least remain active under cold conditions (Table 1). The temperature optimum of “*Ca. N. fabula*” rather resembles that of some NOB in the genus *Nitrospira* also isolated from WWTPs (Nowka et al. 2015). However, it is noteworthy that uncultured “*Ca. Nitrotoga*” in WWTPs showed activity over a broad range of temperatures from 4 to 27°C (Lücker et al. 2015) (Table 1). Thus, “*Ca. Nitrotoga*” members cover a broad temperature range, and not all species are adapted to low temperature as was previously assumed for this genus.

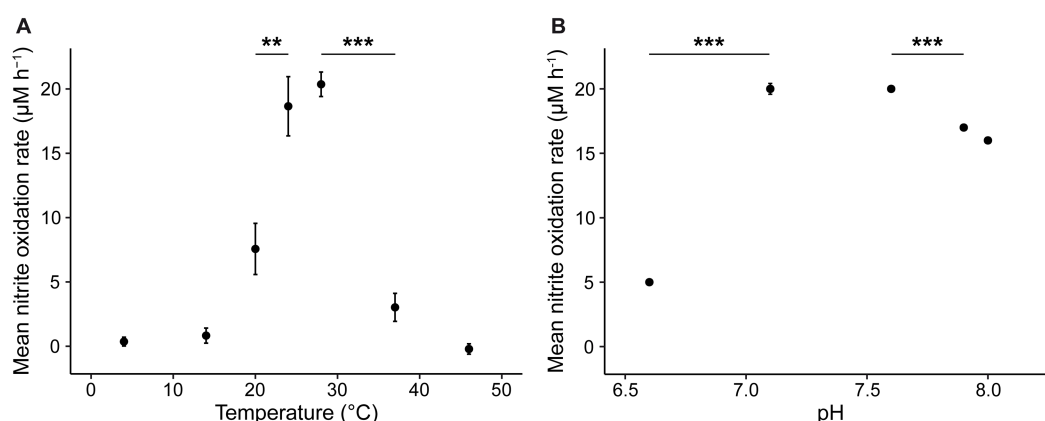


Figure 3 Temperature and pH optima for the nitrite-oxidizing activity of “*Ca. N. fabula*”. (A) Mean nitrite oxidation rates during 48 h of incubation at different temperatures. (B) Mean nitrite oxidation rates during 21 h of incubation at different pH. (A and B) Data points show means, error bars show the standard deviation of three biological replicates. If not visible, error bars are smaller than points. Significance of difference was calculated by Welch’s *t*-test (** $P < 0.01$; *** $P < 0.001$) between data points as indicated by horizontal lines.

The pH optimum of “*Ca. N. fabula*” was between 7.1 and 7.6, and activity decreased at more acidic or alkaline conditions (Figure 3B). Similar to temperature, adaptation to pH varies among “*Ca. Nitrotoga*” members (Table 1). For example, “*Ca. N. sp. HW29*” oxidized nitrite most actively at pH 6.8 and retained as much as 75% of its maximal activity at pH 6.1 (Hüpeden et al. 2016), whereas “*Ca. N. fabula*” lost approximately 75% of its maximal activity already at pH 6.6 (Figure 3B). “*Ca. N. fabula*” showed no lag phase of its nitrite-oxidizing activity even with 30 mM nitrite in the medium (Figure S1A), and thus it tolerated much higher nitrite concentrations than other, enriched “*Ca. Nitrotoga*” members (Table 1). A high tolerance to nitrite was also reported for *Nitrospira defluvii* (maximum 25 mM) (Off et al. 2010) and *Nitrolancea hollandica* (75 mM), two other NOB isolated from activated sludge (Sorokin et al. 2012; Nowka et al. 2015). Little is known about the nitrate tolerance of “*Ca. Nitrotoga*”. Nitrite oxidation by “*Ca. N. fabula*” remained completely inhibited in the presence of >25 mM nitrate even after one year of incubation (Figure S1B).

Nitrite oxidation by “*Ca. N. fabula*” followed Michaelis-Menten kinetics (Figure 4, Figure S2), with a mean apparent half-saturation constant of $K_{m(app)} = 89.3 \pm 3.9 \mu\text{M}$ (s.d.) nitrite. The calculated mean maximum oxidation rate of nitrite (V_{max}) was $27.6 \pm 8.4 \mu\text{mol nitrite (mg protein} \times \text{h)}^{-1}$ (Figure 4, Figure S2). The measured $K_{m(app)}(\text{NO}_2^-)$ of “*Ca. N. fabula*” was higher (but still in the same order of magnitude) than values reported for “*Ca. Nitrotoga*” enrichments from soil and sediment (Table 1). The slightly poorer affinity for nitrite of “*Ca. N. fabula*” may reflect adaptation to different habitats.

However, in enrichment cultures, the accompanying organisms may also respire oxygen or use nitrite (e.g., for denitrification) and thus affect affinity measurements based on respirometry (Nowka et al. 2014) or nitrite consumption (Ishii et al. 2017). In either case, the affinity of the NOB can be overestimated in enrichment cultures. Thus, comparison of results obtained by analyses of an isolate and of enrichment cultures must be interpreted with caution. In comparison to other NOB, the affinity for nitrite of “*Ca. Nitrotoga*” is moderate (Table S1). In particular, *Nitrospira* with a significantly higher affinity (Table S1) may outcompete “*Ca. Nitrotoga*” in oligotrophic habitats and in continuously operated WWTPs (which resemble chemostats) where ambient nitrite concentrations are low.

Altogether, adaptations of NOB in the genus “*Ca. Nitrotoga*” to a broad range of conditions (Table 1) likely reflect the wide distribution of this genus in natural and engineered ecosystems.

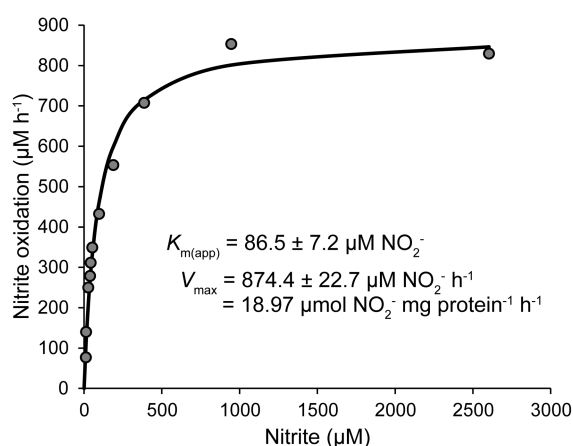


Figure 4 Nitrite oxidation kinetics of “*Ca. N. fabula*”. Nitrite oxidation rates were calculated from microsensor measurements of nitrite-dependent O_2 consumption. The curve indicates the best fit of the data to the Michaelis-Menten kinetic equation. The protein concentration used to calculate V_{max} was 46.1 mg/l. The experiment was performed with biomass concentrated by centrifugation. Data from three additional biological replicates are shown in Figure S2.

Table 1 Physiological characteristics of isolated or enriched NOB in the candidate genus “*Nitrotoga*”. Data for uncultured “*Ca. Nitrotoga*” in activated sludge are listed for comparison.

“ <i>Ca. Nitrotoga</i> ” strain	Temp. optimum (°C)	pH optimum	Nitrite tolerated (mM)	Nitrate tolerated (mM)	$K_{m(app)} NO_2^-$ (µM)
“ <i>Ca. N. fabula</i> KNB” (isolate)	24-28 (poor activity <20)	7.1 to 7.6	Max. concn ND (activity at 1-30)	≤25	89.3 ± 3.9
“ <i>Ca. N. arctica</i> 6680” (enrichment) ^a	10	ND (cultured at 7.4-7.6)	<1.2	ND	58 ± 28
“ <i>Ca. N. sp. HAM-1</i> ” (enrichment) ^b	ND ^f (cultured at 10 and 17)	ND (cultured at 7.4-7.6)	Max. concn ND (cultured at 0.3)	ND	ND
“ <i>Ca. N. sp. AM1</i> ” (enrichment) ^c	16	ND (cultured at 8.0-8.3)	Max. concn ND (cultured at 0.7-2.6)	ND	24.7 ± 9.8
“ <i>Ca. N. sp. HW29</i> ” (enrichment) ^d	22 (40% of max. activity at 10)	6.8	<8	ND	ND
Uncultured “ <i>Ca. Nitrotoga</i> ” in WWTPs ^e	Activity at 4-27	ND	Activity at 0.1-10	ND	ND

^a Data from Alawi et al. (2007), Nowka et al. (2014)

^b Data from Alawi et al. (2009)

^c Data from Ishii et al. (2017)

^d Data from Hüpeden et al. (2016)

^e Data from Lückner et al. (2015)

^f ND = not determined

Genomic characterization of “*Ca. N. fabula*”

The genome of the “*Ca. N. fabula*” isolate was completely reconstructed and closed by Illumina and nanopore sequencing (Table S2 and Figure S3). The chromosome comprises 2,609,426 bp, has an average G+C content of 50.14%, and contains 2,609 coding sequences (CDS). Core metabolic pathways of “*Ca. N. fabula*” were reconstructed from the genomic data (Figure 5 and Table S4). Interestingly, “*Ca. N. fabula*” possesses a plasmid that has a size of 5,404 bp and contains six CDS (Tables S2 and S3). Its average G+C content of 63.55% differs drastically from the chromosome, indicating horizontal acquisition of the plasmid. The high similarity of all six CDS to homologs in Alpha-, Beta- and Gammaproteobacteria (Table S3) suggests a proteobacterial plasmid donor. Plasmids are a rare feature in NOB reported so far only for *Nitrobacter* (Kraft & Bock 1984; Starkenburg et al. 2008). The plasmid of “*Ca. N. fabula*” encodes two hypothetical proteins, a putative transcriptional regulator, a quaternary ammonium compound resistance protein (EmrE), a putative relaxase, and a putative replication initiation protein (Table S3). The latter two likely are involved in plasmid acquisition and replication, respectively. EmrE might be beneficial for life in activated sludge (see below). The plasmid and the capability of “*Ca. N. fabula*” to grow on solid media could facilitate the development of a vector and a transformant selection system for using “*Ca. N. fabula*” as a genetically tractable model nitrite oxidizer. To date, no genetic system has been established for any NOB.

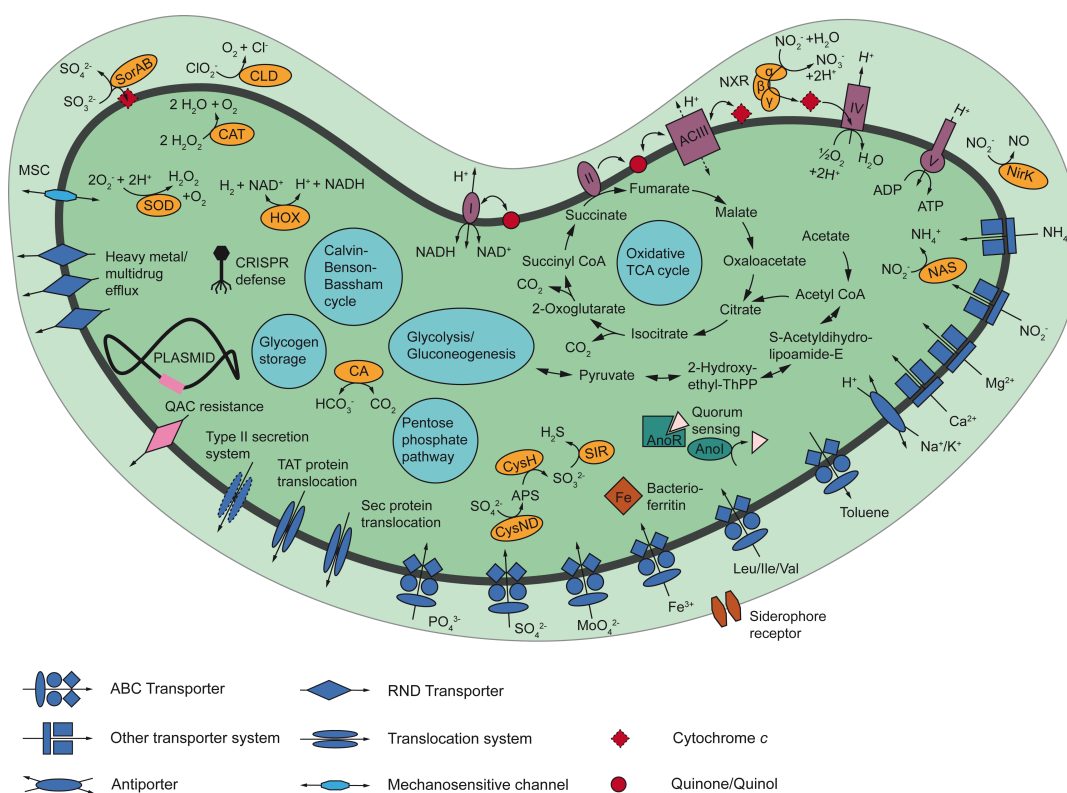


Figure 5 Cell metabolic cartoon constructed from the annotation of the “*Ca. N. fabula*” genome. Enzyme complexes of the electron transport chain are labeled by Roman numerals. Table S4 contains further information on the depicted enzymes and pathways. Abbreviations: ACIII, alternative complex III; Anol/R, acyl-homoserine-lactone synthase/response regulator; CA, carbonic anhydrase; CAT, catalase; CLD, chlorite dismutase; CRISPR, clustered regularly interspaced short palindromic repeats; CysH, adenylylsulfate reductase; CysND, sulfate adenylyltransferase; HOX, bidirectional group 3d [NiFe] hydrogenase; MSC, mechanosensitive channel; NAS, assimilatory nitrite reductase; NirK, nitrite reductase; NXR, nitrite oxidoreductase; QAC, quaternary ammonium compound; SOD, superoxide dismutase; SIR, assimilatory sulfite reductase; Sor, sulfite:cyt. c oxidoreductase; TAT, twin-arginine translocation; TCA cycle, tricarboxylic acid cycle; Sec, secretion.

Nitrite oxidation and nitrite oxidoreductase phylogeny

NXR, the key enzyme for nitrite oxidation, belongs to the type II dimethyl sulfoxide (DMSO) reductase family of molybdopterin cofactor-binding enzymes (Meincke et al. 1992; Lückner et al. 2010). The catalytic alpha subunit (NxrA) of known NXRs contains the Mo cofactor and one Fe-S cluster. It is associated with the beta subunit NxrB, which contains four Fe-S clusters. NxrB likely transfers electrons derived from nitrite to the gamma subunit NxC or directly to the respiratory chain (Lückner et al. 2010). NXR was reported to be a membrane-associated enzyme (Spieck et al. 1996; Spieck et al. 1998; Lückner et al. 2010). The proposed membrane anchor is NxC, which probably binds one or two heme groups and may thus also be involved in electron transfer (Lückner et al. 2010). The three known types of NXR differ in their cellular localization and phylogenetic affiliation (Lückner et al. 2010). In two groups, NxrA and NxrB face the cytoplasmic side of the cell membrane (Spieck et al. 1996; Hemp et al. 2016). These NXRs are closely related to membrane-bound, cytoplasmically oriented nitrate reductases (NAR) (Figure 6). One type is found in *Nitrobacter*, *Nitrococcus*, and *Nitrolancea*, and the second type in the phototrophic NOB *Thiocapsa* KS1 (Meincke et al. 1992; Sorokin et al. 2012; Hemp et al. 2016; Füssel et al. 2017) (Figure 6). In the third group, NxrA and NxrB are oriented towards the periplasmic space. This type occurs in *Nitrospira*, *Nitrospina*, and in anaerobic ammonium oxidizers (anammox organisms) and is phylogenetically distinct from the cytoplasmic NXRs (Spieck et al. 1998; Lückner et al. 2010; Lückner et al. 2013) (Figure 6). In anammox, NXR is localized in the anammoxosome instead of the periplasm (de Almeida et al. 2015).

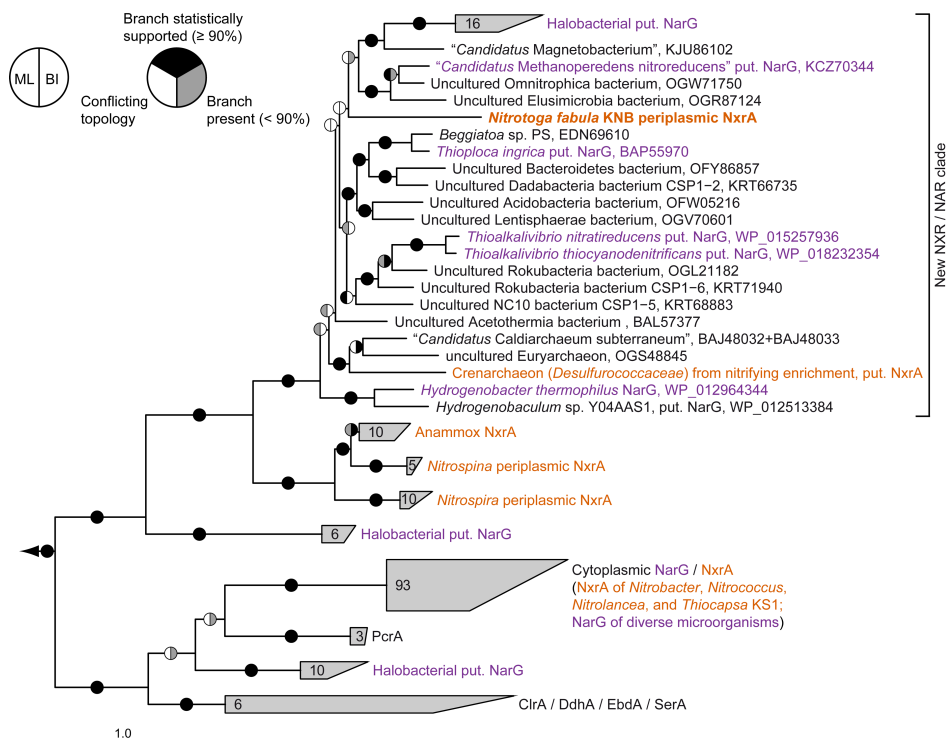


Figure 6 Phylogeny of NxrA from “*Ca. N. fabula*” and related proteins. Consensus tree showing the alpha subunits of selected enzymes from the type II DMSO reductase family. Confirmed and putative (put.) NxrA and NarG proteins are indicated. Organisms or enrichment cultures with an observed nitrite-oxidizing phenotype are highlighted orange, those with an observed nitrate-reducing phenotype are highlighted purple. Pie charts indicate statistical support based on maximum likelihood (ML; 1,000 bootstrap iterations) and Bayesian inference (BI; posterior probability, 10 independent chains). Numbers in wedges indicate the numbers of taxa. The scale bar indicates 1 estimated substitution per residue. Abbreviations not used in the text are ClrA, chlorate reductase; DhA, dimethylsulfide dehydrogenase; EbdA, ethylbenzene dehydrogenase; PcrA, perchlorate reductase; SerA, selenate reductase.

Consistent with its growth on nitrite as the sole energy source and electron donor, “*Ca. N. fabula*” encodes NXR (Figure 5, Figure S3, Table S4). The genome contains two identical loci coding for NxrA, NxrB, a putative NxrC, and a putative chaperone (Figure S3, Table S4). No other *nxr* genes were identified. NxrA and NxrB of “*Ca. N. fabula*” contain the conserved binding sites for the Mo cofactor and the Fe-S clusters found also in the respective homologs of *Nitrospira defluvii* (Lücker et al. 2010) with only few differences. In NxrA, the Mo binding site has the sequence pattern Y-4x-D-11x-QM instead of Y-4x-D-11x-QN as in *N. defluvii*. In NxrB of “*Ca. N. fabula*”, the binding site of Fe-S cluster IV contains cysteine at the position homologous to Asp45 of *N. defluvii* and lacks an insertion of eight residues that is found in *N. defluvii* (Lücker et al. 2010). NxrC shows only low similarity to gamma subunits of other type II DMSO reductase-like enzymes. It contains a predicted heme-binding site but no transmembrane helix, indicating that the NXR of “*Ca. N. fabula*” may be soluble or interacts with another membrane-bound protein, as was also discussed for *Nitrospina gracilis* (Lücker et al. 2013). NxrA contains an N-terminal signal peptide for protein export via the twin-arginine protein translocation mechanism, and NxrC contains an N-terminal signal peptide for translocation via the Sec pathway, suggesting that the NXR of “*Ca. N. fabula*” is located in the periplasmic space (Figure 5). NxrB lacks any translocation signal but may be co-translocated with NxrA as proposed for the periplasmic NXRs of *Nitrospira* and *Nitrospina* (Lücker et al. 2010; Lücker et al. 2013). A periplasmic NXR should be energetically advantageous, because nitrite oxidation outside the cell releases protons into the periplasm and may contribute directly to proton motive force (pmf) (Lücker et al. 2010) (Figure 5). This feature likely helps “*Ca. Nitrotoga*” compete with co-occurring NOB harboring a cytoplasmic NXR.

Intriguingly, phylogenetic analysis of the catalytic NxrA subunit revealed that the NXR of “*Ca. N. fabula*” is not closely related to the other known NXR forms. Instead, it belongs to a distinct “sister clade” of the lineage containing the periplasmic NXRs of *Nitrospira*, *Nitrospina*, and anammox (Figure 6). Some of the proteins affiliated with NxrA of “*Ca. N. fabula*” are catalytic subunits of putative NARs (NarG) from phylogenetically diverse bacteria and archaea, which are known nitrate reducers (Figure 6). Only recently, the enzyme of *Hydrogenobacter thermophilus* has been functionally characterized as a periplasmically oriented, membrane-bound NAR (Kameya et al. 2017). The affiliation of NXR from “*Ca. N. fabula*” with this clade demonstrates that enzymes in this group are capable of nitrite oxidation. Since other NXRs are bidirectional enzymes that oxidize nitrite and also reduce nitrate (Freitag et al. 1987; Koch et al. 2015; Füssel et al. 2017), it is conceivable that also known nitrate-reducing members of this clade could oxidize nitrite for detoxification or even for energy conservation under permissive conditions. An additional requirement for nitrite oxidation would be suitable electron carriers, such as high-potential cytochrome (cyt.) *c*, which accept the electrons derived by NXR from nitrite. To our knowledge, except for “*Ca. N. fabula*”, none of the cultured organisms possessing enzymes in this NXR/NAR clade has systematically been tested for a nitrite-oxidizing phenotype. Moreover, the clade contains proteins from highly diverse, uncultured, and physiologically uncharacterized organisms (Figure 6) that might be novel nitrite oxidizers if they also possess high-potential electron carriers. According to this assumption, nitrite oxidation might occur within the domain Archaea (Figure 6). Recently, we sequenced a joint metagenome from pooled DNA from early-stage nitrifying enrichments, which had been established at 75°C from a hot spring in Iceland (Supplementary text). Nitrite oxidation had been observed in several of these cultures. The only *nxr*-like genes found in the assembly were binned into a metagenome-assembled genome of a crenarchaeon, which was remotely related to the genus *Ignisphaera* (family *Desulfurococcaceae*) (Figure S4). Intriguingly, its putative NxrA fell into the same clade as the NxrA of “*Ca. N. fabula*”. It grouped with the NxrA/NarG of “*Ca. Caldarchaeum subterraneum*” (phylum

“Aigarchaeota”), an uncultured and phenotypically uncharacterized thermophilic archaeon (Figure 6). The absence of unambiguously detectable, canonical NOB from the metagenomic dataset and the presence of archaea possessing a putative NXR is highly conspicuous and deserves further investigation.

Previous analyses suggested that NXR independently evolved at least three times within the type II DMSO reductase family, leading to the aforementioned three types of cytoplasmic and periplasmic NXRs (Lücker et al. 2010; Hemp et al. 2016). The distinct phylogenetic position of the novel NXR of “*Ca. N. fabula*” indicates an even more complex evolutionary history of nitrite oxidation. Functional data for the enzymes in this clade are too sparse to assess whether nitrite oxidation may be an ancestral feature of this lineage, or more likely a secondary adaptation found in “*Ca. Nitrotoga*” (and possibly additional organisms) with the remaining proteins being strict NARs. However, it is remarkable that the clade shares a common ancestor with the *Nitrospira* / *Nitrospina* / anammox enzymes, which exclusively are NXRs (Figure 6). It also remains unclear whether this type of NXR evolved in “*Ca. Nitrotoga*” or was acquired through horizontal gene transfer by an ancestor of this genus.

Central energy and carbon metabolism

In NOB, electrons derived from nitrite are transferred from NXR to cyt. *c* and then to the terminal oxidase (cyt. *c* oxidase; complex IV) for aerobic respiration (Figure 5). The genome of “*Ca. N. fabula*” encodes several *c*-type cytochromes and a predicted high-affinity, proton-pumping heme-copper cyt. *c* oxidase of the *cbb*₃ type (Table S4). The conserved energy is used for ATP synthesis by a canonical F₁F_o ATPase (complex V) (Figure 5 and Table S4). In addition, “*Ca. N. fabula*” possesses a canonical NADH dehydrogenase (complex I) and the complete oxidative tricarboxylic acid cycle, including a four-subunit succinate dehydrogenase complex (complex II) (Figure 5 and Table S4). A canonical quinol:cyt. *c* oxidoreductase (complex III) is lacking, but “*Ca. N. fabula*” encodes an alternative complex III (ACIII) (Refojo et al. 2012) that is highly similar to ACIII of other *Gallionellaceae* members (Emerson et al. 2013). Thus, “*Ca. N. fabula*” possesses a complete electron transport chain for respiration using inorganic low-potential electron donors such as H₂ (see below) or organic compounds. For example, glycogen deposits may serve as an energy source for cell maintenance during starvation (Figure 5 and Table S4). However, “*Ca. N. fabula*” appears to lack genes for the uptake and utilization of formate, pyruvate, and acetate, which can be used as carbon and/or energy sources by several other NOB (Bock 1976; Daims et al. 2001; Ushiki et al. 2013; Koch et al. 2015). A transporter for branched amino acids may enable their use as organic sources of energy, carbon and nitrogen, or directly as protein building blocks (Figure 5). “*Ca. N. fabula*” can also assimilate nitrogen from ammonium and nitrite (Table S4), but in contrast to some other NOB (Koch et al. 2015; Palatinszky et al. 2015) it lacks any known genes for utilizing urea or cyanate.

When nitrite is the sole electron donor, reductants for autotrophic CO₂ fixation must be provided by reverse electron transport. Unlike *Nitrospira*, “*Ca. N. fabula*” lacks multiple copies of complexes I and III that might channel electrons in opposite directions (Lücker et al. 2010; Koch et al. 2015). Thus, we assume that these single complexes of “*Ca. N. fabula*” are bidirectional and consume pmf for reverse electron transport (Figure 5). “*Ca. N. fabula*” encodes the complete Calvin-Benson-Bassham (CBB) cycle for CO₂ fixation, including two divergent copies of the small (37% amino acid identity) and large (56% identity) subunits of type I ribulose-1,5-bisphosphate carboxylase/oxygenase (RuBisCO). Other NOB using the CBB cycle are *Nitrobacter*, *Nitrococcus*, and *Nitrolancea* (Starkenburger et al. 2006; Sorokin et al. 2012; Füssel et al. 2017). In contrast, *Nitrospira* and *Nitrospina* utilize the more oxygen-sensitive reductive TCA cycle (Lücker et al. 2010; Lücker et al. 2013). Hence, “*Ca. Nitrotoga*” might be

more resistant to high dissolved oxygen (DO) concentrations and could have a competitive advantage over *Nitrospira* in strongly aerated activated sludge tanks. Based on its predicted high-affinity terminal oxidase (see above), “*Ca. N. fabula*” could also cope with low-DO conditions that occur, for example, in simultaneously nitrifying and denitrifying bioreactors. This may explain the observed presence of “*Ca. Nitrotoga*” in a low-DO nitrifying bioreactor where it co-occurred with *Nitrospira* (Okabe et al. 1999; Keene et al. 2017; Park & Noguera 2008), which can also oxidize nitrite at low DO concentrations (Okabe et al. 1999; Park & Noguera 2008).

Alternative energy metabolisms

The recent discovery that some *Nitrospira* grow chemolithoautotrophically by aerobic hydrogen oxidation was unexpected, because nitrifiers had been regarded as metabolically restricted organisms whose energy metabolism is intimately linked to the nitrogen cycle (Koch et al. 2014). Interestingly, “*Ca. N. fabula*” harbors a complete set of genes encoding a group 3d NAD-coupled [NiFe] hydrogenase and accessory proteins (Figure S3, Table S4) (Greening et al. 2016). The enzymes in this group are cytosolic bidirectional hydrogenases and can be oxygen tolerant (Vignais & Billoud 2007). The hydrogenase could enable “*Ca. N. fabula*” to use H₂ as an energy source and electron donor for aerobic growth and, if NXR works reversibly, for anaerobic respiration with nitrate as electron acceptor. Both activities were observed for *Nitrospira moscoviensis*, although growth occurred only in oxic incubations (Ehrich et al. 1995; Koch et al. 2014). Hydrogenases occur in various NOB (Koch et al. 2014), and hydrogen oxidation as an alternative energy metabolism has several advantages for these organisms. Firstly, it can help NOB survive nitrite-depleted conditions. Secondly, electrons derived from H₂ can be used for CO₂ fixation without reverse electron transport, saving energy for other cellular functions. Finally, it may enable NOB to colonize niches independent of nitrification. A source of H₂ could be fermenting heterotrophs living nearby in anoxic niches in soils, sediments, biofilms, and flocs (Daims et al. 2016).

“*Ca. N. fabula*” also encodes a periplasmic sulfite:cyt. *c* oxidoreductase (Figure 5, Table S4), which may allow it to use sulfite as energy source and electron donor. Recently, the participation of NOB in sulfur cycling was demonstrated for *Nitrococcus* that oxidized sulfide in the presence of O₂ (Füssel et al. 2017).

Stress response, defense, and cell-cell communication

Contrasting their aerobic metabolism, several NOB and also comammox organisms lack catalase, superoxide dismutase, or both (Lücker et al. 2010; Lücker et al. 2013; Daims et al. 2015). “*Ca. N. fabula*” possesses both enzymes (Figure 5, Table S4) but apparently was nevertheless inhibited by the amount of H₂O₂ formed during the preparation of solid media with phosphate (see above).

Wastewater contains many potentially toxic compounds. Accordingly, the genome of “*Ca. N. fabula*” encodes various resistance and detoxification mechanisms including efflux systems for heavy metals and organic solvents, arsenate reductase, and chlorite dismutase (Figure 5, Table S4). Quaternary ammonium compounds (QAC) are widely used as disinfectants and are ingredients in cosmetics and household products. In addition to gene *emrE* on the plasmid (see above), “*Ca. N. fabula*” has another QAC resistance gene (*sugE*) on the chromosome. QAC resistance is not a common feature of NOB isolated from WWTPs. While the genome of *Nitrospira defluvii* encodes SugE, both *Nitrospira japonica* NJ1 and *Nitrospira* ND1 (Ushiki et al. 2018) lack QAC resistance genes. The sensitivity of NOB to QAC and other harmful compounds has hardly been studied, but it could be an important factor determining the distribution and abundance of different NOB in sewage treatment systems.

“*Ca. N. fabula*” possesses a LuxI/LuxR-type quorum sensing (QS) system that is similar to the Anol/AnoR system of *Acinetobacter nosocomialis* (Oh & Choi 2015) (56% amino acid sequence

identity to Anol, 46% identity to AnoR). QS systems have also been identified in *Nitrobacter* and *Nitrospira* (Ushiki et al. 2018; Mellbye et al. 2017). In *Nitrobacter*, QS has been linked to the production and consumption of nitrogen oxides (Mellbye et al. 2016). Further functions of QS in NOB await investigation, and it will be exciting to see whether QS plays similar or different roles in phylogenetically diverse NOB including “*Ca. Nitrotoga*”.

Description of “*Candidatus Nitrotoga fabula*”

Fabula (L. fem. noun, small bean, referring to the characteristic bean-shaped morphology of the cells).

Cells are Gram-negative short curved rods with a length of approximately 1 μm and width of approximately 0.5 μm . “*Ca. N. fabula*” grows planktonically but forms loose flocs at high cell density. Non-motile. Aerobic chemolithoautotrophic nitrite oxidizer that uses CO_2 as the sole carbon source. Temperature optimum 24-28°C, pH optimum 7.1-7.6. Nitrite oxidation was observed up to 30 mM nitrite (higher concentrations not tested) and below 30 mM nitrate. Grows in mineral liquid and on solid (plaque agarose autoclaved without phosphate) nitrite media. Genome consists of a single chromosome and a plasmid. The G+C content of the DNA is 50.14 mol% (chromosome) and 63.55 mol% (plasmid).

Strain “*Ca. N. fabula* KNB” was isolated from activated sludge of the municipal wastewater treatment plant in Klosterneuburg, Austria. The strain is available from the authors upon request.

Conclusions

The physiological and genomic characterization of the first “*Ca. Nitrotoga*” isolate has revealed potential alternative energy metabolisms and a broader spectrum of physiological adaptations in this genus than previously assumed. Like *Nitrospira*, “*Ca. Nitrotoga*” members can be versatile NOB whose metabolic flexibility may explain their competitive success in dynamic environments such as WWTPs. However, fundamental differences between “*Ca. Nitrotoga*” and *Nitrospira* include the affinity for nitrite (Table S1), as well as the resistance of “*Ca. Nitrotoga*” to higher oxygen levels according to the genetic inventory and growth on plates of “*Ca. N. fabula*”. Previous studies showed that multiple factors, including the concentrations of DO and nitrite, temperature, and pH, influence the community composition of NOB (Schramm et al. 1999; Maixner et al. 2006; Park & Noguera 2008; Alawi et al. 2009; Hüpeden et al. 2016; Keene et al. 2017). Further research is needed to understand which conditions in engineered and natural ecosystems allow the coexistence of “*Ca. Nitrotoga*” with *Nitrospira* or other NOB, and which factors lead to their competitive exclusion. Intriguingly, the phylogenetic affiliation of the novel NXR of “*Ca. Nitrotoga*” with enzymes from uncharacterized microorganisms indicates that the diversity of nitrite oxidizers in nature might be much larger than currently anticipated.

Materials and Methods

Sampling and cultivation conditions

Activated sludge from the combined nitrification/denitrification tank (intermittently aerated, max. DO concentration 2.5 mg/l) of the municipal WWTP Klosterneuburg (Austria) was sampled in January 2014. The sludge was diluted 1:3,000 in mineral medium that was prepared as described elsewhere (Koch et al. 2014) and amended with 3 μg $\text{Na}_2\text{SeO}_3 \times 5\text{H}_2\text{O}$ and 4 μg $\text{Na}_2\text{WO}_4 \times 2\text{H}_2\text{O}$ per liter. Diluted sludge (150 ml) was inoculated in 300 ml Erlenmeyer flasks that were loosely closed with aluminum caps, supplied with 1 mM NaNO_2 , and incubated at room temperature in darkness and without agitation. Nitrite consumption was regularly monitored by using nitrite/nitrate test stripes

(Merckoquant, Merck). Upon depletion of nitrite, the cultures were fed with 1 mM NaNO₂. Aliquots of the enrichments were sub-cultured into fresh medium (dilution factor 1:200) in intervals of 3 to 8 weeks. After the second transfer, the cultures were kept in 100 ml borosilicate bottles filled with 40 ml medium and closed with plastic lids.

Solid mineral nitrite media were prepared with 1% (wt/vol) noble agar (Difco, item no. 214220), sieve 3:1 agarose (Biozym, item no. 850091), or plaque agarose (Biozym, item no. 840100). The pH of the media was adjusted to 7.8 either by adding KH₂PO₄ prior to the addition of solidifying agent and autoclaving or by adding sterile filtered KH₂PO₄ of pH 8 after autoclaving. Aliquots (5 to 10 µl) of 1:100 diluted culture were streaked onto the solid media and incubated at room temperature in darkness for several weeks. Grown colonies were re-streaked onto solid medium, and single colonies were finally inoculated into liquid mineral medium. Culture aliquots were cryopreserved in mineral medium containing 10% (vol/vol) DMSO (Vekeman et al. 2013).

Assessment of culture purity

The NOB community composition in liquid enrichment cultures was monitored by rRNA-targeted FISH after cell fixation in formalin according to standard protocols (Daims et al. 2005). The oligonucleotide probes applied were Ntspa662 specific for the genus *Nitrospira* (Daims et al. 2001), Ntoga122 specific for the candidate genus “*Nitrotoga*” (Lücker et al. 2015), probes EUB338-I to III that detect most bacteria (Amann et al. 1990; Daims et al. 1999), and NON338 as control for nonspecific probe binding (Wallner et al. 1993). Probes were 5′ and 3′ double-labeled with the fluorochromes Fluos, Cy3 and Cy5 and used in combination with the unlabeled competitor oligonucleotides of Ntspa662 and Ntoga122, respectively (Daims et al. 2001; Lücker et al. 2015). FISH was combined with nonspecific fluorescent labeling of all cells by DAPI. Fluorescence micrographs were recorded using an epifluorescence microscope (Zeiss Axio Imager M2 with AxioCam 506 Mono). The purity of the “*Ca. N. fabula*” isolate was assessed by (i) FISH and DAPI staining as described above; (ii) inoculation of Luria Bertani medium, which was diluted 1:10 in mineral medium, to test for heterotrophic contaminants; and (iii) PCR screening of the culture using the primers 8F and 1492R that target the bacterial 16S rRNA gene (Juretschko et al. 1998; Loy et al. 2002). After purification (QIAquick PCR purification kit, Qiagen), the PCR products were Sanger sequenced (Microsynth, Austria) without cloning. The purity of the isolate was also confirmed by Illumina sequencing (see below) and by the absence of cells with a divergent morphology in electron micrographs (for a detailed description of sample preparation for electron microscopy, see Text S1).

Physiological experiments

Cells from pre-grown liquid cultures of “*Ca. N. fabula*” were collected by centrifugation (8,200×g, 20 min, 20°C). The supernatant was discarded, and the cells resuspended in fresh mineral medium without nitrite. This procedure was repeated until no nitrite and nitrate was detectable in the supernatant. The cells were finally resuspended in fresh mineral medium and served as an inoculum for physiological experiments. All experiments were carried out in biological triplicates. To quantify the nitrite-oxidizing activity, nitrite and nitrate concentrations were measured photometrically as described elsewhere (Miranda et al. 2001; García-Robledo et al. 2014). At each time point, samples (0.5 ml) of the incubated cultures were taken, cells were removed by centrifugation (20,100×g, 10 min, 4°C), and the supernatant was stored at -20°C until chemical measurements were performed. To determine the temperature optimum for activity of “*Ca. N. fabula*”, 100 ml borosilicate glass bottles containing 40 ml medium supplemented with 1 mM NaNO₂ were pre-incubated at the tested temperatures (4 to 46°C). After inoculation with washed cells (see above), the bottles were incubated at the respective temperatures and the nitrite and nitrate concentrations were quantified after 48 h

as described above. To determine the pH optimum for activity of “*Ca. N. fabula*”, mineral medium was supplemented with 5 mM (final concentration) sterile-filtered HEPES (Sigma Aldrich) after autoclaving. The pH was adjusted to 6.6, 7.1, 7.6, 7.9, and 8.1 by adding 1 N NaOH and remained stable throughout the experiment. Samples for nitrite and nitrate concentration measurements were taken during three days of incubation at 28°C.

To determine the nitrite and nitrate tolerance, “*Ca. N. fabula*” cells were incubated in media containing 1 to 30 mM nitrite or 15 to 50 mM nitrate, respectively, at the optimal temperature (28°C). The media containing nitrate were also supplemented with 1 mM nitrite as substrate. Nitrite oxidation was then monitored for up to six weeks (nitrite tolerance) and up to one year (nitrate tolerance).

The nitrite oxidation kinetics of “*Ca. N. fabula*” were inferred from instantaneous oxygen uptake measurements in four independent experiments as previously described (Kits et al. 2017). Nitrite uptake rates were calculated from the measured oxygen uptake rates, and Michaelis-Menten plots of nitrite uptake rates versus nitrite concentration were obtained by fitting a Michaelis-Menten model to the data. Kinetic constants were estimated by nonlinear least squares regression. For a detailed description of the approach, see Text S1.

DNA extraction, genome sequencing, and genome annotation

Cells were collected from a liquid “*Ca. N. fabula*” culture, which had been inoculated from a single colony, by centrifugation (8,200×g, 20 min, 20°C) and frozen at -20°C. Total DNA was extracted according to (Angel et al. 2012) with bead beating for cell disruption at 4 m s⁻¹. The genome of “*Ca. N. fabula*” was sequenced and closed by applying a combination of Illumina and Nanopore technologies (for details of genome sequencing and assembly, please refer to Text S1). The reconstructed genome of “*Ca. N. fabula*” was uploaded to the MicroScope platform (Vallenet et al. 2017) for automatic annotation and manual annotation refinement of selected metabolic pathways (Lücker et al. 2010).

Phylogenetic analyses

Representative full-length 16S rRNA gene sequences classified as “*Ca. Nitrotoga*” in the SILVA Ref NR 99 database (release 132, 13th December 2017) (Pruesse et al. 2007) and the 20 top BLASTn hits (>95% alignment coverage, >98% identity) to the 16S rRNA gene sequence of “*Ca. N. fabula*” were used to calculate phylogenetic trees. The 16S rRNA gene sequences of cultured *Gallionella* species, and environmental sequences clustering between “*Ca. Nitrotoga*” and *Gallionella*, were used as outgroup. Sequences were aligned using SINA (Pruesse et al. 2012); the length of analyzed sequences was between 1,361 and 1,528 bp. Trees were calculated using the neighbor joining implementation in ARB (Ludwig et al. 2004) (Jukes Cantor substitution model; 1,000 bootstrap iterations) and maximum likelihood algorithms implemented in PhyML (Guindon & Gascuel 2003) and RAxML (Stamatakis 2014) (GAMMA model of rate heterogeneity and GTR substitution model; 1,000 bootstrap iterations). A consensus tree was reconstructed using ARB and branching patterns were compared manually between all calculated trees. NxrA/NarG protein sequences were aligned using mafft-linsi v.7.312 (Katoh & Standley 2013) and trimmed using Trimal v1.4.rev15 (Capella-Gutiérrez et al. 2009) with option -automated1. The resulting alignment consisting of 1,206 columns was used to calculate trees in IQ-TREE v1.6.2 (Nguyen et al. 2015) and PhyloBayes v4.1b (Lartillot et al. 2009). IQ-TREE calculations included model prediction by ModelFinder (Kalyaanamoorthy et al. 2017), which identified the best-fit model to be LG+R8, and support values for bipartitions were calculated using UFboot2 (Hoang et al. 2017). PhyloBayes calculations were carried out with 10 independent chains of 5,000 generations using the CAT-GTR model; 2,000 generations of each chain were discarded as

burn-in, and the remainder were subsampled every third tree and pooled together for calculation of posterior probabilities.

Accession numbers

The genome sequence of “*Ca. N. fabula*” has been deposited in the European Nucleotide Archive (ENA) under the project PRJEB26077. The metagenome-assembled genome sequence of the *Desulfurococcaceae*-related crenarchaeon from the thermophilic enrichment has been deposited at NCBI GenBank under the project PRJNA461265, accession QFWU00000000.

Acknowledgements

Daniela Gruber and Norbert Cyran from the Core Facility of Cell Imaging and Ultrastructure Research at the University of Vienna are gratefully acknowledged for help with electron microscopy. We thank A. Giguere and K. D. Kits for assistance with microrespirometry, Andreas Richter for providing samples used to inoculate thermophilic enrichments, and A. Galushko for helpful discussions. We are grateful to M. Ücker for technical assistance. This study was supported by the Austrian Science Fund (FWF) projects P25231-B21, P27319-B21, 30570-B29, and W 1257 to H.D., FWF project T938-B32 to A.D., the European Research Council Advanced Grant Nitrification Reloaded (NITRICARE) to M.W., a research grant (15510) from VILLUM FONDEN to M.A., the Danish Research Council for Independent Research (DFF) grant 4005-00369 to P.H.N., the Volkswagen Foundation VW-Vorab grant ZN3112 to H.K., the Netherlands Organization for Scientific Research (NWO) grant 863.14.019 to S.L., and the Max Planck Society (N.L.).

References

- Achberger A.M., Christner B.C., Michaud A.B., Priscu J.C., Skidmore M.L., Vick-Majors T.J. and WISSARD Science Team. 2016. Microbial Community Structure of Subglacial Lake Whillans, West Antarctica. *Frontiers in Microbiology* 7 (1457): 1–13. doi:10.3389/fmicb.2016.01457.
- Alawi M., Lipski A., Sanders T., Pfeiffer E.M. and Spieck E. 2007. Cultivation of a Novel Cold-Adapted Nitrite Oxidizing Betaproteobacterium from the Siberian Arctic. *The ISME Journal* 1 (3): 256–64. doi:10.1038/ismej.2007.34.
- Alawi M., Off S., Kaya M. and Spieck E. 2009. Temperature Influences the Population Structure of Nitrite-Oxidizing Bacteria in Activated Sludge. *Environmental Microbiology Reports* 1 (3): 184–90. doi:10.1111/j.1758-2229.2009.00029.x.
- Amann R.I., Binder B.J., Olson R.J., Chisholm S.W., Devereux R. and Stahl D. a. 1990. Combination of 16S rRNA-Targeted Oligonucleotide Probes with Flow Cytometry for Analyzing Mixed Microbial Populations. *Applied and Environmental Microbiology* 56 (6): 1919–25.
- Amann R.I., Ludwig W. and Schleifer K.H. 1995. Phylogenetic Identification and In Situ Detection of Individual Microbial Cells Without Cultivation. *Microbiological Reviews* 59 (1): 143–69.
- Angel R., Claus P. and Conrad R. 2012. Methanogenic Archaea Are Globally Ubiquitous in Aerated Soils and Become Active under Wet Anoxic Conditions. *The ISME Journal* 6 (4). Nature Publishing Group: 847–62. doi:10.1038/ismej.2011.141.
- Bock E. 1976. Growth of Nitrobacter in Presence of Organic Matter II. Chemoorganotrophic Growth of Nitrobacter Agilis. *Archives Of Microbiology* 108: 305–12. doi:10.1007/bf00454857.
- Bock E., Sundermeyer-Klinger H. and Stackebrandt E. 1983. New Facultative Lithoautotrophic Nitrite-Oxidizing Bacteria. *Archives of Microbiology* 136: 281–84. doi:10.1007/BF00425217.
- Capella-Gutiérrez S., Silla-Martínez J.M. and Gabaldón T. 2009. TrimAl: A Tool for Automated Alignment Trimming in Large-Scale Phylogenetic Analyses. *Bioinformatics* 25 (15): 1972–73. doi:10.1093/bioinformatics/btp348.
- Chen Y., Wu L., Boden R., Hillebrand A., Kumaresan D., Moussard H., Baciu M., Lu Y. and Murrell J.C. 2009. Life without Light: Microbial Diversity and Evidence of Sulfur- and Ammonium-Based Chemolithotrophy in Mobile Cave. *The ISME Journal* 3: 1093–1104. doi:10.1038/ismej.2009.57.
- Daims H., Brühl A., Amann R., Schleifer K.-H. and Wagner M. 1999. The Domain-Specific Probe EUB338 Is Insufficient for the Detection of All Bacteria: Development and Evaluation of a More Comprehensive Probe Set. *Systematic and Applied Microbiology* 22 (September): 434–44. doi:10.1016/S0723-2020(99)80053-8.
- Daims H., Lebedeva E. V., Pjevac P., Han P., Herbold C., Albertsen M., Jehmlich N., Palatinszky M., Vierheilig J., Bulaev A., Kirkegaard R.H., von Bergen M., Rattei T., Bendinger B., Nielsen P.H. and Wagner M. 2015. Complete Nitrification by Nitrospira Bacteria. *Nature* 528 (7583): 504–9. doi:10.1038/nature16461.
- Daims H., Lückner S. and Wagner M. 2016. A New Perspective on Microbes Formerly Known as Nitrite-Oxidizing Bacteria. *Trends in Microbiology* 24 (9): 699–712. doi:10.1016/j.tim.2016.05.004.
- Daims H., Nielsen J., Nielsen P.H., Schleifer K.-H. and Wagner M. 2001. In Situ Characterization of Nitrospira-Like Nitrite-Oxidizing Bacteria Active in Wastewater Treatment Plants. *Applied and Environmental Microbiology* 67 (11): 5273–84. doi:10.1128/AEM.67.11.5273.
- Daims H., Stoecker K. and Wagner M. 2005. Fluorescence in Situ Hybridization for the Detection of Prokaryotes. In *Molecular Microbial Ecology*, edited by AM Osborn and Cindy J Smith, 213–39. Abington: Bios-Garland.
- de Almeida N.M., Neumann S., Mesman R.J., Ferousi C., Keltjens J.T., Jetten M.S.M., Kartal B. and van Niftrik L. 2015. Immunogold Localization of Key Metabolic Enzymes in the Anammoxosome and on the Tubule-Like Structures of Kuenenia stuttgartiensis. *Journal of Bacteriology* 197 (14): 2432–41. doi:10.1128/jb.00186-15.
- Ehrich S., Behrens D., Lebedeva E., Ludwig W. and Bock E. 1995. A New Obligately Chemolithoautotrophic, Nitrite-Oxidizing Bacterium, Nitrospira moscoviensis Sp. Nov. and Its Phylogenetic Relationship. *Archives of Microbiology* 164: 16–23.
- Emerson D., Field E.K., Chertkov O., Davenport K.W., Goodwin L., Munk C., Nolan M. and Woyke T. 2013. Comparative Genomics of Freshwater Fe-Oxidizing Bacteria: Implications for Physiology, Ecology, and Systematics. *Frontiers in Microbiology* 4: 1–17. doi:10.3389/fmicb.2013.00254.
- Freitag A., Rudert M. and Bock E. 1987. Growth of Nitrobacter by Dissimilatory Nitrate Reduction. *FEMS Microbiology Letters* 48: 105–9. doi:10.1111/j.1574-6968.1987.tb02524.x.

- Füssel J., Lücker S., Yilmaz P., Nowka B., van Kessel M.A.H.J., Bourceau P., Hach P.F., Littmann S., Berg J., Spieck E., Daims H., Kuypers M.M.M. and Lam P. 2017. Adaptability as the Key to Success for the Ubiquitous Marine Nitrite Oxidizer Nitrococcus. *Science Advances* 3: 1–9. doi:10.1126/sciadv.1700807.
- García-Robledo E., Corzo A. and Papaspyrou S. 2014. A Fast and Direct Spectrophotometric Method for the Sequential Determination of Nitrate and Nitrite at Low Concentrations in Small Volumes. *Marine Chemistry* 162: 30–36. doi:10.1016/j.marchem.2014.03.002.
- Greening C., Biswas A., Carere C.R., Jackson C.J., Taylor M.C., Stott M.B., Cook G.M. and Morales S.E. 2016. Genomic and Metagenomic Surveys of Hydrogenase Distribution Indicate H₂ Is a Widely Utilised Energy Source for Microbial Growth and Survival. *The ISME Journal* 10: 761–77. doi:10.1038/ismej.2015.153.
- Griffin B.M., Schott J. and Schink B. 2007. Nitrite, an Electron Donor for Anoxygenic Photosynthesis. *Science* 316: 1870. doi:10.1126/science.1139478.
- Guindon S. and Gascuel O. 2003. A Simple, Fast, and Accurate Algorithm to Estimate Large Phylogenies by Maximum Likelihood. *Systematic Biology* 52 (5): 696–704. doi:10.1080/10635150390235520.
- Hemp J., Lücker S., Schott J., Pace L.A., Johnson J.E., Schink B., Daims H. and Fischer W.W. 2016. Genomics of a Phototrophic Nitrite Oxidizer: Insights into the Evolution of Photosynthesis and Nitrification. *The ISME Journal* 10: 1–10. doi:10.1038/ismej.2016.56.
- Hoang D.T., Chernomor O., von Haeseler A., Minh B.Q. and Vinh L.S. 2017. UFBoot2: Improving the Ultrafast Bootstrap Approximation. *Molecular Biology and Evolution* 35 (2): 518–22. doi:10.5281/zenodo.854445.
- Hüpeden J., Wegen S., Off S., Lücker S., Bedarf Y., Daims H., Kühn C. and Spieck E. 2016. Relative Abundance of Nitrotoga Spp. in a Biofilter of a Cold-Freshwater Aquaculture Plant Appears to Be Stimulated by Slightly Acidic pH. *Applied and Environmental Microbiology* 82: 1838–45. doi:10.1128/AEM.03163-15.
- Ishii K., Fujitani H., Soh K., Nakagawa T., Takahashi R. and Tsuneda S. 2017. Enrichment and Physiological Characterization of a Cold-Adapted Nitrite-Oxidizing Nitrotoga Sp. from an Eelgrass Sediment. *Applied and Environmental Microbiology* 83: e00549-17. doi:10.1128/aem.00549-17.
- Juretschko S., Timmermann G., Schmid M., Schleifer K.H., Pommerening-Röser A., Koops H.P. and Wagner M. 1998. Combined Molecular and Conventional Analyses of Nitrifying Bacterium Diversity in Activated Sludge: Nitrosococcus Mobilis and Nitrospira-Like Bacteria as Dominant Populations. *Applied and Environmental Microbiology* 64 (8): 3042–51.
- Kalyaanamoorthy S., Minh B.Q., Wong T.K.F., Von Haeseler A. and Jermin L.S. 2017. ModelFinder: Fast Model Selection for Accurate Phylogenetic Estimates. *Nature Methods* 14 (6): 587–89. doi:10.1038/nmeth.4285.
- Kameya M., Kanbe H., Igarashi Y., Arai H. and Ishii M. 2017. Nitrate Reductases in Hydrogenobacter Thermophilus with Evolutionarily Ancient Features: Distinctive Localization and Electron Transfer. *Molecular Microbiology* 106 (1): 129–41. doi:10.1111/mmi.13756.
- Katoh K. and Standley D.M. 2013. MAFFT Multiple Sequence Alignment Software Version 7: Improvements in Performance and Usability. *Molecular Biology and Evolution* 30 (4): 772–80. doi:10.1093/molbev/mst010.
- Keene N.A., Reusser S.R., Scarborough M.J., Grooms A.L., Seib M., Domingo J.S. and Noguera D.R. 2017. Pilot Plant Demonstration of Stable and Efficient High Rate Biological Nutrient Removal with Low Dissolved Oxygen Conditions. *Water Research* 121: 72–85.
- Kinnunen M., Gülay A., Albrechtsen H.J., Dechesne A. and Smets B.F. 2017. Nitrotoga Is Selected over Nitrospira in Newly Assembled Biofilm Communities from a Tap Water Source Community at Increased Nitrite Loading. *Environmental Microbiology* 19 (7): 2785–93. doi:10.1111/1462-2920.13792.
- Kits D.K., Sedlacek C.J., Lebedeva E. V., Han P., Bulaev A., Pjevac P., Daebeler A., Romano S., Albertsen M., Stein L.Y., Daims H. and Wagner M. 2017. Kinetic Analysis of a Complete Nitrifier Reveals an Oligotrophic Lifestyle. *Nature* 549: 269–72. doi:10.1038/nature23679.
- Koch H., Galushko A., Albertsen M., Schintlmeister A., Gruber-Dorninger C., Lücker S., Pelletier E., Le Paslier D., Spieck E., Richter A., Nielsen P.H., Wagner M. and Daims H. 2014. Growth of Nitrite-Oxidizing Bacteria by Aerobic Hydrogen Oxidation. *Science* 345 (6200): 761–63.
- Koch H., Lücker S., Albertsen M., Kitzinger K., Herbold C., Spieck E., Nielsen P.H., Wagner M. and Daims H. 2015. Expanded Metabolic Versatility of Ubiquitous Nitrite-Oxidizing Bacteria from the Genus Nitrospira. *Proceedings of the National Academy of Sciences of the United States of America* 112 (36): 11371–76. doi:10.1073/pnas.1506533112.
- Kraft I. and Bock E. 1984. Plasmids in Nitrobacter. *Archives of Microbiology* 140: 79–82.

- Lartillot N., Lepage T. and Blanquart S. 2009. PhyloBayes 3: A Bayesian Software Package for Phylogenetic Reconstruction and Molecular Dating. *Bioinformatics* 25 (17): 2286–88. doi:10.1093/bioinformatics/btp368.
- Loy A., Lehner A., Lee N., Adamczyk J., Meier H., Ernst J., Schleifer K.-H. and Wagner M. 2002. Oligonucleotide Microarray for 16S rRNA Gene-Based Detection of All Recognized Lineages of Sulfate-Reducing Prokaryotes in the Environment. *Applied and Environmental Microbiology* 68 (10): 5064–81. doi:10.1128/AEM.68.10.5064-5081.2002.
- Lücker S., Nowka B., Rattei T., Spieck E. and Daims H. 2013. The Genome of Nitrospina Gracilis Illuminates the Metabolism and Evolution of the Major Marine Nitrite Oxidizer. *Frontiers in Microbiology* 4 (27): 1–19. doi:10.3389/fmicb.2013.00027.
- Lücker S., Schwarz J., Gruber-Dorninger C., Spieck E., Wagner M. and Daims H. 2015. Nitrotoga-like Bacteria Are Previously Unrecognized Key Nitrite Oxidizers in Full-Scale Wastewater Treatment Plants. *The ISME Journal* 9: 708–20. doi:10.1038/ismej.2014.158.
- Lücker S., Wagner M., Maixner F., Pelletier E., Koch H., Vacherie B., Rattei T., Sinninghe Damsté J.S., Spieck E., Le Paslier D. and Daims H. 2010. A Nitrospira Metagenome Illuminates the Physiology and Evolution of Globally Important Nitrite-Oxidizing Bacteria. *Proceedings of the National Academy of Sciences of the United States of America* 107 (30): 13479–84. doi:10.1073/pnas.1003860107.
- Ludwig W., Strunk O., Westram R., Richter L., Meier H., Yadhukumar A., Buchner A., Lai T., Steppi S., Jobb G., Förster W., Brettske I., Gerber S., Ginhart A.W., Gross O., Grumann S., Hermann S., Jost R., König A., et al. 2004. ARB: A Software Environment for Sequence Data. *Nucleic Acids Research* 32 (4): 1363–71. doi:10.1093/nar/gkh293.
- Ma B., Yang L., Wang Q., Yuan Z., Wang Y. and Peng Y. 2017. Inactivation and Adaptation of Ammonia-Oxidizing Bacteria and Nitrite-Oxidizing Bacteria When Exposed to Free Nitrous Acid. *Bioresource Technology* 245: 1266–70. doi:10.1016/j.biortech.2017.08.074.
- Maixner F., Noguera D.R.D., Anneser B., Stoecker K., Wegl G., Wagner M. and Daims H. 2006. Nitrite Concentration Influences the Population Structure of Nitrospira-like Bacteria. *Environmental Microbiology* 8 (8): 1487–95. doi:10.1111/j.1462-2920.2006.01033.x.
- Meincke M., Bock E., Kastrau D. and Kroneck P.M.H. 1992. Nitrite Oxidoreductase from Nitrobacter Hamburgensis: Redox Centers and Their Catalytic Role. *Archives of Microbiology* 158: 127–31. doi:10.1007/BF00245215.
- Mellbye B.L., Giguere A.T., Bottomley P.J. and Sayavedra-Soto L.A. 2016. Quorum Quenching of Nitrobacter Winogradskyi Suggests That Quorum Sensing Regulates Fluxes of Nitrogen Oxide(s) during Nitrification. *MBio* 7 (5): e01753-16. doi:10.1128/mBio.01753-16.
- Mellbye B.L., Spieck E., Bottomley P.J. and Sayavedra-Soto L.A. 2017. Acyl-Homoserine Lactone Production in Nitrifying Bacteria of the Genera Nitrosospira, Nitrobacter, and Nitrospira Identified via a Survey of Putative Quorum-Sensing Genes. *Applied and Environmental Microbiology* 83: e01540-17.
- Miranda K.M., Espey M.G. and Wink D.A. 2001. A Rapid, Simple Spectrophotometric Method for Simultaneous Detection of Nitrate and Nitrite. *Nitric Oxide: Biology and Chemistry* 5 (1): 62–71. doi:10.1006/niox.2000.0319.
- Ngugi D.K., Blom J., Stepanauskas R. and Stingl U. 2016. Diversification and Niche Adaptations of Nitrospina-like Bacteria in the Polyextreme Interfaces of Red Sea Brines. *The ISME Journal* 10: 1383–99. doi:10.1038/ismej.2015.214.
- Nguyen L.T., Schmidt H.A., Von Haeseler A. and Minh B.Q. 2015. IQ-TREE: A Fast and Effective Stochastic Algorithm for Estimating Maximum-Likelihood Phylogenies. *Molecular Biology and Evolution* 32 (1): 268–74. doi:10.1093/molbev/msu300.
- Nowka B., Daims H. and Spieck E. 2014. Comparative Oxidation Kinetics of Nitrite-Oxidizing Bacteria: Nitrite Availability as Key Factor for Niche Differentiation. *Applied and Environmental Microbiology* 81 (2): 745–53. doi:10.1128/AEM.02734-14.
- Nowka B., Off S., Daims H. and Spieck E. 2015. Improved Isolation Strategies Allowed the Phenotypic Differentiation of Two Nitrospira Strains from Widespread Phylogenetic Lineages. *FEMS Microbiology Ecology* 91 (3).
- Off S., Alawi M. and Spieck E. 2010. Enrichment and Physiological Characterization of a Novel Nitrospira-Like Bacterium Obtained From a Marine Sponge. *Applied and Environmental Microbiology* 76 (14): 4640–46. doi:10.1128/AEM.00320-10.

- Oh M.H. and Choi C.H. 2015. Role of LuxIR Homologue AnolR in *Acinetobacter Nosocomialis* and the Effect of Virstatin on the Expression of AnolR Gene. *Journal of Microbiology and Biotechnology* 25 (8): 1390–1400. doi:10.4014/jmb.1504.04069.
- Okabe S., Satoh H. and Watanabe Y. 1999. In Situ Analysis of Nitrifying Biofilms as Determined by in Situ Hybridization and the Use of Microelectrodes. *Applied and Environmental Microbiology* 65 (7): 3182–91. <http://www.pubmedcentral.nih.gov/articlerender.fcgi?artid=91473&tool=pmcentrez&rendertype=abstract>.
- Pachiadaki M.G., Sintés E., Bergauer K., Brown J.M., Record N.R., Swan B.K., Mathyer M.E., Hallam S.J., Lopez-García P., Takaki Y., Nunoura T., Woyke T., Herndl G.J. and Stepanauskas R. 2017. Major Role of Nitrite-Oxidizing Bacteria in Dark Ocean Carbon Fixation. *Science* 358: 1046–51. doi:10.1126/science.aan8260.
- Palatinszky M., Herbold C., Jehmlich N., Pogoda M., Han P., Bergen M. Von, Lagkouvardos I., Karst S.M., Galushko A., Koch H., Berry D., Daims H. and Wagner M. 2015. Cyanate as an Energy Source for Nitrifiers. *Nature* 524: 105–8. doi:10.1038/nature14856.
- Park H.D. and Noguera D.R. 2008. Nitrospira Community Composition in Nitrifying Reactors Operated with Two Different Dissolved Oxygen Levels. *Journal of Microbiology and Biotechnology* 18 (8): 1470–74.
- Prosser J.I. 2011. Soil Nitrifiers and Nitrification. In *Nitrification*, edited by Bess B Ward, Daniel J Arp, and Martin G Klotz, 347–83. Washington: ASM Press, Washington DC. doi:10.1128/9781555817145.
- Pruesse E., Peplies J. and Glöckner F.O. 2012. SINA: Accurate High-Throughput Multiple Sequence Alignment of Ribosomal RNA Genes. *Bioinformatics* 28 (14): 1823–29. doi:10.1093/bioinformatics/bts252.
- Pruesse E., Quast C., Knittel K., Fuchs B.M., Ludwig W., Peplies J. and Glöckner F.O. 2007. SILVA: A Comprehensive Online Resource for Quality Checked and Aligned Ribosomal RNA Sequence Data Compatible with ARB. *Nucleic Acids Research* 35 (21): 7188–96. doi:10.1093/nar/gkm864.
- Refojo P.N., Teixeira M. and Pereira M.M. 2012. The Alternative Complex III: Properties and Possible Mechanisms for Electron Transfer and Energy Conservation. *Biochimica et Biophysica Acta - Bioenergetics* 1817: 1852–59. doi:10.1016/j.bbabi.2012.05.003.
- Saunders A.M., Albertsen M., Vollesen J. and Nielsen P.H. 2016. The Activated Sludge Ecosystem Contains a Core Community of Abundant Organisms. *The ISME Journal* 10 (1): 11–20. doi:10.1038/ismej.2015.117.
- Schramm A., De Beer D., Van Den Heuvel J.C., Ottengraf S. and Amann R. 1999. Microscale Distribution of Populations and Activities of Nitrospira and Nitrospira Spp. along a Macroscale Gradient in a Nitrifying Bioreactor: Quantification by in Situ Hybridization and the Use of Microsensors. *Applied and Environmental Microbiology* 65 (8): 3690–96.
- Sorokin D.Y., Lückner S., Vejmekova D., Kostrikina N. a, Kleerebezem R., Rijpstra W.I.C., Damsté J.S.S., Le Paslier D., Muyzer G., Wagner M., van Loosdrecht M.C.M. and Daims H. 2012. Nitrification Expanded: Discovery, Physiology and Genomics of a Nitrite-Oxidizing Bacterium from the Phylum Chloroflexi. *The ISME Journal* 6: 2245–56. doi:10.1038/ismej.2012.70.
- Spieck E., Aamand J., Bartosch S. and Bock E. 1996. Immunocytochemical Detection and Location of the Membrane-Bound Nitrite Oxidoreductase in Cells of Nitrobacter and Nitrospira. *FEMS Microbiology Letters* 139: 71–76. doi:10.1016/0378-1097(96)00123-1.
- Spieck E., Ehrlich S., Aamand J. and Bock E. 1998. Isolation and Immunocytochemical Location of the Nitrite-Oxidizing System in Nitrospira Moscoviensis. *Archives of Microbiology* 169: 225–30. doi:10.1007/s002030050565.
- Spieck E. and Lipski A. 2011. Cultivation, Growth Physiology, and Chemotaxonomy of Nitrite-Oxidizing Bacteria. In *Methods in Enzymology*, edited by Martin G. Klotz, 1st ed., 486:109–30. Elsevier Inc. doi:10.1016/B978-0-12-381294-0.00005-5.
- Stackebrandt E. and Ebers J. 2006. Taxonomic Parameters Revisited: Tarnished Gold Standards. *Microbiology Today* 33: 152–55.
- Stamatakis A. 2014. RAxML Version 8: A Tool for Phylogenetic Analysis and Post-Analysis of Large Phylogenies. *Bioinformatics* 30 (9): 1312–13. doi:10.1093/bioinformatics/btu033.
- Starkenburger S.R., Chain P.S.G., Sayavedra-Soto L. a, Hauser L., Land M.L., Larimer F.W., Malfatti S. a, Klotz M.G., Bottomley P.J., Arp D.J. and Hickey W.J. 2006. Genome Sequence of the Chemolithoautotrophic Nitrite-Oxidizing Bacterium *Nitrobacter Winogradskyi* Nb-255. *Applied and Environmental Microbiology* 72 (3): 2050–63. doi:10.1128/AEM.72.3.2050.
- Starkenburger S.R., Larimer F.W., Stein L.Y., Klotz M.G., Chain P.S.G., Sayavedra-Soto L. a, Poret-Peterson A.T., Gentry M.E., Arp D.J., Ward B. and Bottomley P.J. 2008. Complete Genome Sequence of Nitrobacter

- Hamburgensis X14 and Comparative Genomic Analysis of Species within the Genus Nitrobacter. *Applied and Environmental Microbiology* 74 (9): 2852–63. doi:10.1128/AEM.02311-07.
- Tanaka T., Kawasaki K., Daimon S., Kitagawa W., Yamamoto K., Tamaki H., Tanaka M., Nakatsu C.H. and Kamagata Y. 2014. A Hidden Pitfall in Agar Media Preparation Undermines Cultivability of Microorganisms. *Applied and Environmental Microbiology* 80 (24): 7659–66. doi:10.1128/AEM.02741-14.
- Teske A., Alm E., Regan J.M., Toze S., Rittmann B.E. and Stahl D.A. 1994. Evolutionary Relationships among Ammonia- and Nitrite-Oxidizing Bacteria. *Journal of Bacteriology* 176 (21): 6623–30.
- Ushiki N., Fujitani H., Aoi Y. and Tsuneda S. 2013. Isolation of Nitrospira Belonging to Sublineage II from a Wastewater Treatment Plant. *Microbes and Environments* 28 (3): 346–53. doi:10.1264/jsme2.ME13042.
- Ushiki N., Fujitani H., Shimada Y., Morohoshi T., Sekiguchi Y. and Tsuneda S. 2018. Genomic Analysis of Two Phylogenetically Distinct Nitrospira Species Reveals Their Genomic Plasticity and Functional Diversity. *Frontiers in Microbiology* 8 (2637): 1–12. doi:10.3389/fmicb.2017.02637.
- Vallenet D., Calteau A., Cruveiller S., Gachet M., Lajus A., Josso A., Mercier J., Renaux A., Rollin J., Rouy Z., Roche D., Scarpelli C. and Medigue C. 2017. MicroScope in 2017: An Expanding and Evolving Integrated Resource for Community Expertise of Microbial Genomes. *Nucleic Acids Research* 45 (Database issue): D517–28. doi:10.1093/nar/gkw1101.
- van Kessel M.A.H.J., Speth D.R., Albertsen M., Nielsen P.H., Op den Camp H.J.M., Kartal B., Jetten M.S.M. and Lücker S. 2015. Complete Nitrification by a Single Microorganism. *Nature* 528: 555–59. doi:10.1038/nature16459.
- Vekeman B., Hoefman S., De Vos P., Spieck E. and Heylen K. 2013. A Generally Applicable Cryopreservation Method for Nitrite-Oxidizing Bacteria. *Systematic and Applied Microbiology* 36: 579–84. doi:10.1016/j.syapm.2013.07.002.
- Vignais P.M. and Billoud B. 2007. Occurrence, Classification, and Biological Function of Hydrogenases: An Overview. *Chemical Reviews* 107: 4206–72. doi:10.1021/cr050196r.
- Wallner G., Amann R. and Beisker W. 1993. Optimizing Fluorescent in Situ Hybridization with rRNA-Targeted Oligonucleotide Probes for Flow Cytometric Identification of Microorganisms. *Cytometry* 14: 136–43. doi:10.1002/cyto.990140205.

Supplementary information

Supplementary text

Electron microscopy

Scanning electron microscopy was performed as described previously (Daebeler et al. 2018) with the following modifications. Sterile poly-L-lysine coated slides were submerged in an actively growing “*Ca. N. fabula*” culture for 3 days before fixation of attached cells. All fixatives were diluted in, and all washing steps were performed with, cacodylate buffer (25 mM sodium cacodylate, 0.7 mM MgCl₂, pH 7.0) mimicking medium osmolarity. For transmission electron microscopy following chemical fixation, 300 ml of a late exponential phase “*Ca. N. fabula*” culture was fixed by adding glutaraldehyde (2.5% vol/vol final concentration) and harvested by centrifugation (9,000×g, 15 min). Cells were embedded in 1% (wt/vol) plaque agarose (Biozym) in cacodylate buffer, cut into 1 mm-sized blocks and post-fixed with a 1% (wt/vol) OsO₄ solution in cacodylate buffer for 1 h. Fixed cells were washed three times in cacodylate buffer, dehydrated in 30 to 100% (vol/vol) ethanol, washed twice in propylene oxide, and infiltrated with increasing concentrations of low viscosity resin in propylene oxide. For polymerization, the resin blocks were incubated at 60°C for one week. Ultra-thin sections (70 nm) were cut from the resin blocks (Ultracut S, Leica) with a glass knife. Sections were placed on copper grid mesh holders and post-stained with gadolinium triacetate and lead citrate before visualization with a Libra120 transmission electron microscope (Zeiss). For transmission electron microscopy following high pressure freezing, concentrated live culture was mixed with 2% agarose in a 3 mm aluminum sample holder and immediately high pressure frozen with an HPM 100 (Leica). Samples were transferred onto frozen acetone containing 1% (wt/vol) OsO₄ and processed using the super quick freeze-substitution method (McDonald and Webb 2011). After reaching room temperature, the samples were washed three times with acetone and two times with ethanol, and were infiltrated sequentially using centrifugation (McDonald 2014) in 2 ml tubes with 25, 50, 75 and 25 2× 100% LR-White resin (Agar Scientific). The samples were placed on top of the resin and centrifuged for 30 s at 2,000×g in each step. After the second pure resin step, samples were transferred into fresh resin in gelatin capsules and polymerized at 60°C for 1 h (Bowling and Vaughn 2008). Ultra-thin (70 nm) sections were cut with an Ultracut UC7 (Leica) and mounted on formvar coated slot grids (Agar Scientific). Sections were contrasted with 0.5% aqueous uranyl acetate (Science Services) for 20 min and with 2% Reynold's lead citrate for 6 min before imaging with a Quanta FEG 250 scanning electron microscope (FEI) equipped with a STEM detector.

Nitrite oxidation kinetic measurements

Nitrite oxidation kinetics of “*Ca. N. fabula*” were inferred from instantaneous oxygen uptake measurements in four independent experiments as previously described (Kits et al. 2017). Biomass of “*Ca. N. fabula*” was sampled upon substrate depletion (early stationary phase), which was predictable to 2-3 hours. Oxygen uptake measurements were done using a microrespiration (MR) system submerged in a recirculating water bath (28°C) (Martens-Habbena et al. 2009; Martens-Habbena and Stahl 2011). All measurements were performed utilizing 2 ml glass MR chambers equipped with an MR injection lid, a glass coated stir bar, a PA 2000 picoammeter, and an OX-MR oxygen microsensor with a 500 µm tip diameter (Unisense). Before the experiments, the OX-MR microsensor was polarized continuously for at least one week (Martens-Habbena et al. 2009; Martens-Habbena and Stahl 2011).

Culture biomass, either concentrated (10× by centrifugation at 6000×g, 5 min, 20°C) or un-concentrated, was incubated for a minimum of 30 min in the recirculating water bath before transfer to an MR chamber. MR chambers with glass coated stir bars were filled headspace-free with “*Ca. N. fabula*” culture. Once immersed in the recirculating water bath, stirring (350 r.p.m.) was started. The OX-MR microsensor was inserted into the MR chamber and equilibrated (1 to 2 h). Stable sensor signal drift was measured for at least 10 min prior the initial injection of nitrite using Hamilton syringes. Multiple nitrite injection oxygen uptake measurement traces were performed. Nitrite additions started from low concentrations and moved toward high concentrations (the injections led to different start concentrations of nitrite in the MR chambers). Once the nitrite oxidation rate was stable for 2-5 minutes, another injection was performed. The rate of oxygen uptake was measured after each individual injection of nitrite (Kits et al. 2017). The endogenous rate of oxygen consumption was subtracted from the measured rates at the different nitrite concentrations. Dissolved oxygen (DO) was not a limiting factor in the experiments. The DO concentration in the MR chambers was 200-220 μM at the beginning and 15-160 μM at the end of the experiments. After the experiments, MR chamber contents were immediately frozen for chemical and protein analysis. Nitrite and nitrate concentrations were measured to confirm the total injected nitrite concentration and oxidation to nitrate. Total protein content per MR chamber was determined using the Pierce bicinchoninic acid (BCA) Protein Assay Kit (Thermo Scientific) “Enhanced Test-tube Procedure” after cell lysis (Bacterial Protein Extraction Reagent, Thermo Scientific). The kinetic constants $K_{m(app)}$ and V_{max} of “*Ca. N. fabula*” were estimated from multiple nitrite injection oxygen uptake measurements. Nitrite uptake rates were calculated from the measured oxygen uptake rates, according to a nitrite to oxygen uptake stoichiometry of 2:1 for NOB. Michaelis-Menten plots of nitrite uptake rates versus nitrite concentration were obtained by fitting a Michaelis-Menten model to the data. A nonlinear least squares regression analysis was used to estimate both $K_{m(app)}$ and V_{max} of “*Ca. N. fabula*” (Kemmer and Keller 2010).

“*Ca. N. fabula*” genome sequencing and assembly

Illumina sequencing libraries were prepared using the Nextera DNA library prep kit (Illumina Inc.) following the manufacturer’s recommendations and paired-end sequenced (2×300 bp) on a MiSeq using a MiSeq Reagent kit v3 (Illumina) following the manufacturer’s recommendations. In addition, Nanopore library preparation was done using the Nanopore sequencing kit (SQK-MAP006, Oxford Nanopore), following the manufacturers recommendations (v. MN006_1124_revF_14Aug2015). The library was sequenced using the MinION Mk1 device (Oxford Nanopore) with the MinKnow software (v. 0.50.2.15). Base calling was carried out using Metrichor and the 2D base calling workflow (Rev. 1.62). Illumina read quality and adaptor trimming (trim limit: 0.01, no ambiguous bases, min length: 55 bp), *de novo* assembly (word size: 21, bubble size: 186, min length: 500 bp), and read mapping (default settings except length fraction: 0.95 and similarity fraction: 0.95) were performed in CLC Genomics Workbench v. 8.5.1. The Illumina *de novo* assembly was checked for contamination and completeness using the mmgenome workflow (<http://madsalbertsen.github.io/mmgenome/>). Afterwards, the Illumina *de novo* assembly was manually scaffolded with nanopore data (mapping reads to scaffolds ends). Gaps were polished by recruiting Illumina reads mapping to the nanopore reads and performing local gap reassembly with the Illumina reads (read mapping and *de novo* assembly settings were the same as above except read similarity fraction: 0.85).

Enrichment and metagenomic analysis of thermophilic nitrifiers

Biofilm was sampled from a hot spring (77°C, pH ~6) in Grændalur valley, Iceland (N 64° 2' 0", W 21° 11' 43"). To enrich nitrifying organisms, approximately 0.1 g of the biofilm sample was added to 40 ml sterile mineral medium, which had been prepared according to Koch et al. (2015). The medium was modified by the addition of 3 µM Na₂WO₄·2H₂O (instead of Na₂MoO₄, which was not added), 3.4 nM Na₂SeO₃·5H₂O, and 0.5 mM filter-sterilized NH₄Cl. The culture was incubated at 75°C and without agitation in 100 ml glass bottles in darkness. The ammonium, nitrite, and nitrate content was checked weekly by using Nessler's reagent (Sigma–Aldrich) and nitrite/nitrate test stripes (Merckoquant, Merck). Ammonium (0.5 mM NH₄Cl) was replenished when completely consumed. The pH was monitored with pH test stripes (Macherey-Nagel) and kept between 6 and 7 by titration with NaHCO₃. Aliquots of the ammonia- and nitrite-oxidizing enrichment were transferred into bottles containing fresh medium when 5 to 8 mM of ammonium had been consumed. By this approach, several subcultures were established from the same primary enrichment.

For the extraction of genomic DNA, biomass from several bottles was pooled, collected by centrifugation (4,500×g, 20 min, 20°C), and stored at -20°C until further processing. The biomass was then freeze-thawed three times before total nucleic acids were extracted by bead beating for 40 s with speed setting 6.0 in the presence of phosphate buffer, 10% (w/v) SDS, and phenol as described elsewhere (Angel et al. 2012). Between the addition of phosphate buffer and the addition of SDS and phenol, a 30 min incubation with 2 µl of proteinase K (10 mg/ml) at 37°C and shaking (200 r.p.m.) was added. In total 41.34 ng of DNA was sheared by ultrasonication for 40 s, using Covaris SonoLite v. 2.07. Sequencing was performed at the next generation sequencing unit of the Vienna Biocenter Core Facilities (www.vbcf.ac.at) using an Illumina HiSeq 2500 instrument to generate paired end (2×125 bp) reads. Paired end reads were 3' end-trimmed using a q-score of 15 and minimum length of 50 nucleotides. Quality-trimmed reads were assembled using Metaspades v. 3.11.1 (Nurk et al. 2017). Assembly coverage was determined by mapping quality-trimmed reads with bwa v. 0.7.16a (Li and Durbin 2009). Metabat v. 2.12.1 (Kang et al. 2015) was used to bin metagenome-assembled genomes (MAGs) using tetranucleotide frequency and coverage. CheckM v. 1.0.7 (Parks et al. 2015) was used to assess MAG completeness and contamination. MAGs were automatically annotated by using an in-house modified version of prokka (Seemann 2014), which uses a local copy of the NCBI non redundant protein database (NCBI nr) for blast searches and reports for each predicted gene product the best blast hit, sequence identity to this hit, and query and subject alignment coverage values.

Annotation of *nxr* genes

The *nxr* genes of "*Ca. N. fabula*", and the putative *nxr* genes of the *Desulfurococcaceae* related crenarchaeon, were identified (i) by screening the automated annotations for predicted *nxr/nar*-like genes, and (ii) by blast searching the genomic datasets for members of the type II DMSO reductase family with similarity to known NXR and NAR alpha, beta, and gamma subunits. Phylogenetic analysis (Figure 6 in the main text) confirmed the affiliation of the predicted alpha subunits with (putative) NARs of nitrate-reducing organisms. In the case of "*Ca. N. fabula*", a detailed sequence comparison to the validated NXR of *Nitrospira defluvii* confirmed the presence of the conserved, cofactor-binding residues in the alpha and beta subunits (see main text). The identified *nxr/nar*-like genes were annotated as *nxr* ("*Ca. N. fabula*") or putative *nxr* (*Desulfurococcaceae*-related crenarchaeon) based on the nitrite oxidizing phenotype of the "*Ca. N. fabula*" isolate and of the nitrifying thermophilic enrichment culture, respectively.

Supplementary references

- Angel, R., Claus, P., & Conrad, R. (2012). Methanogenic archaea are globally ubiquitous in aerated soils and become active under wet anoxic conditions. *The ISME Journal*, *6*(4), 847–862. doi:10.1038/ismej.2011.141
- Bowling, A. J., & Vaughn, K. C. (2008). A simple technique to minimize heat damage to specimens during thermal polymerization of LR White in plastic and gelatin capsules. *Journal of Microscopy*, *231*, 186–189.
- Daebeler, A., Herbold, C. W., Vierheilig, J., Sedlacek, C. J., Pjevac, P., Albertsen, M., et al. (2018). Cultivation and Genomic Analysis of “Candidatus Nitrosocaldus islandicus,” an Obligately Thermophilic, Ammonia-Oxidizing Thaumarchaeon from a Hot Spring Biofilm in Graendalur Valley, Iceland. *Frontiers in Microbiology*, *9*, 1–16. doi:10.3389/fmicb.2018.00193
- Kang, D. D., Froula, J., Egan, R., & Wang, Z. (2015). MetaBAT, an efficient tool for accurately reconstructing single genomes from complex microbial communities. *PeerJ*, *3*, e1165. doi:10.7717/peerj.1165
- Kemmer, G., & Keller, S. (2010). Nonlinear least-squares data fitting in Excel spreadsheets. *Nature Protocols*, *5*(2), 267–281. doi:10.1038/nprot.2009.182
- Kits, D. K., Sedlacek, C. J., Lebedeva, E. V., Han, P., Bulaev, A., Pjevac, P., et al. (2017). Kinetic analysis of a complete nitrifier reveals an oligotrophic lifestyle. *Nature*, *549*, 269–272. doi:10.1038/nature23679
- Koch, H., Lückner, S., Albertsen, M., Kitzinger, K., Herbold, C., Spieck, E., et al. (2015). Expanded metabolic versatility of ubiquitous nitrite-oxidizing bacteria from the genus Nitrospira. *Proceedings of the National Academy of Sciences of the United States of America*, *112*(36), 11371–11376. doi:10.1073/pnas.1506533112
- Li, H., & Durbin, R. (2009). Fast and accurate long-read alignment with Burrows-Wheeler transform. *Bioinformatics*, *25*(14), 1754–1760. doi:10.1093/bioinformatics/btp698
- Martens-Habbena, W., Berube, P. M., Urakawa, H., de la Torre, J. R., & Stahl, D. A. (2009). Ammonia oxidation kinetics determine niche separation of nitrifying Archaea and Bacteria. *Nature*, *461*, 976–979. doi:10.1038/nature08465
- Martens-Habbena, W., & Stahl, D. A. (2011). Nitrogen metabolism and kinetics of ammonia-oxidizing archaea. In *Methods in Enzymology* (1st ed., Vol. 496, pp. 465–487). doi:10.1016/B978-0-12-386489-5.00019-1
- McDonald, K L, & Webb, R. I. (2011). Freeze substitution in 3 hours or less. *Journal of Microscopy*, *243*(3), 227–233. doi:10.1111/j.1365-2818.2011.03526.x
- McDonald, Kent L. (2014). Rapid Embedding Methods into Epoxy and LR White Resins for Morphological and Immunological Analysis of Cryofixed Biological Specimens. *Microscopy and Microanalysis*, *20*, 152–163.
- Nurk, S., Meleshko, D., Korobeynikov, A., & Pevzner, P. A. (2017). MetaSPAdes: A new versatile metagenomic assembler. *Genome Research*, *27*, 824–834. doi:10.1101/gr.213959.116
- Parks, D. H., Imelfort, M., Skennerton, C. T., Hugenholtz, P., & Tyson, G. W. (2015). CheckM: Assessing the quality of microbial genomes recovered from isolates, single cells, and metagenomes. *Genome Research*, *25*(7), 1043–1055. doi:10.1101/gr.186072.114
- Seemann, T. (2014). Prokka: Rapid prokaryotic genome annotation. *Bioinformatics*, *30*(14), 2068–2069. doi:10.1093/bioinformatics/btu153

Supplementary figures

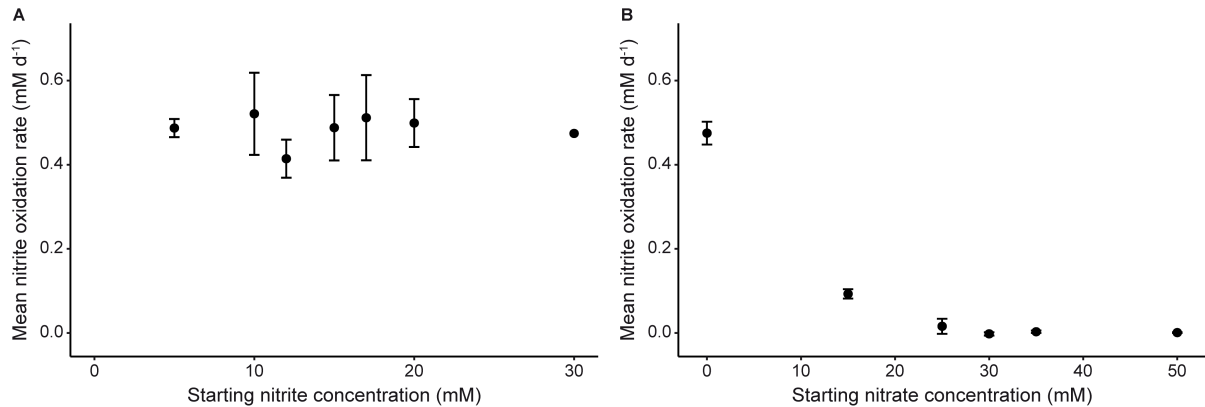


Figure S1 Tolerance of “*Ca. N. fabula*” to nitrite and nitrate. (A) Mean nitrite oxidation rates with different starting concentrations of nitrite in the medium. The rates were calculated for 7.2 days of incubation. (B) Mean nitrite oxidation rates with different starting concentrations of nitrate in the medium. The rates were calculated between the start of the experiment and depletion of nitrite for setups containing initially 0 or 15 mM nitrate (2.1 and 10.9 days, respectively) and for 13 days of incubation for all other setups. In experiments with starting nitrate concentrations >25 mM, nitrite was not depleted after one year of incubation. (A and B) Data points show means, error bars show the standard deviation of three biological replicates (only a single replicate in panel A for 30 mM nitrite). If not visible, error bars are smaller than points.

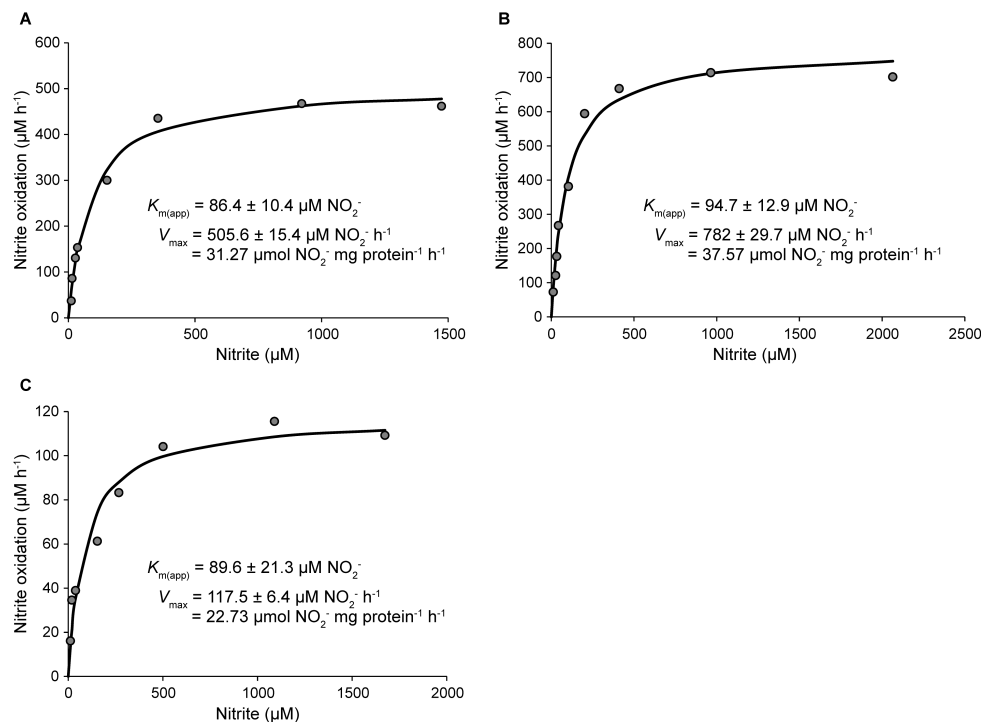


Figure S2 Nitrite oxidation kinetics of “*Ca. N. fabula*”. (A-C) Nitrite oxidation rates were calculated from microsensor measurements of nitrite-dependent O₂ consumption. The curves indicate the best fit of the data to the Michaelis-Menten kinetic equation. The protein concentrations used to calculate V_{max} were (A) 16.17 mg/l, (B) 20.82 mg/l, and (C) 5.17 mg/l. Experiments were performed with concentrated (panels A and B) or unconcentrated biomass (panel C). Results for three biological replicates are shown here; a fourth biological replicate is shown in Figure 4 in the main text.

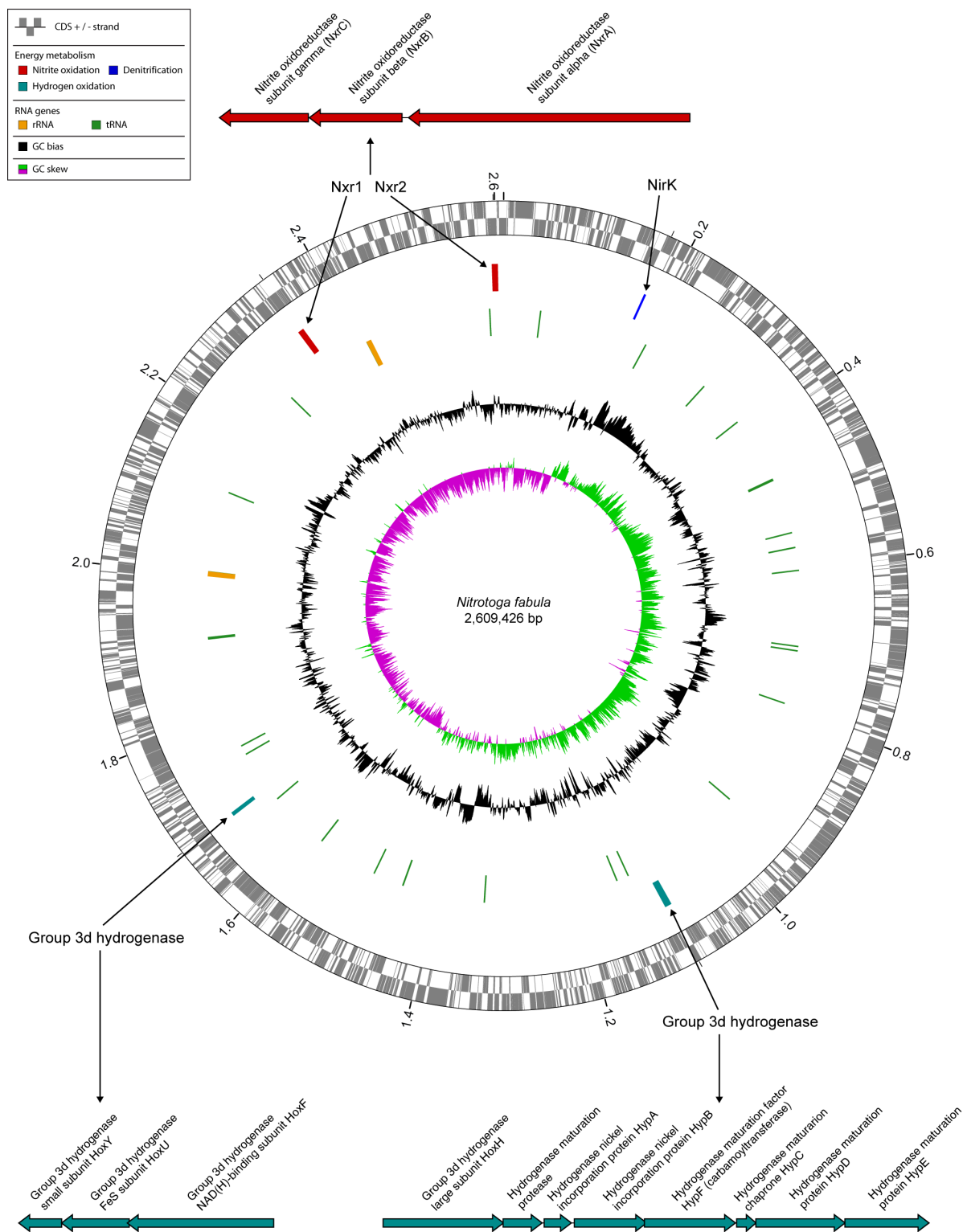


Figure S3 Circular representation of the “*Ca. N. fabula*” chromosome. Predicted coding sequences (CDS; rings 1+2), genes of enzymes involved in nitrite oxidation, hydrogen oxidation, and denitrification (ring 3), RNA genes (ring 4), and local nucleotide composition measures (rings 5+6) are shown. Very short features were enlarged to enhance visibility. Clustered genes, such as several transfer RNA genes, may appear as one line owing to space limitations. The tick interval is 0.2 Mbp. Genes at loci coding for NXR and hydrogenase, and the predicted functions of the respective gene products, are also shown. NirK, Cu-dependent nitrite reductase.

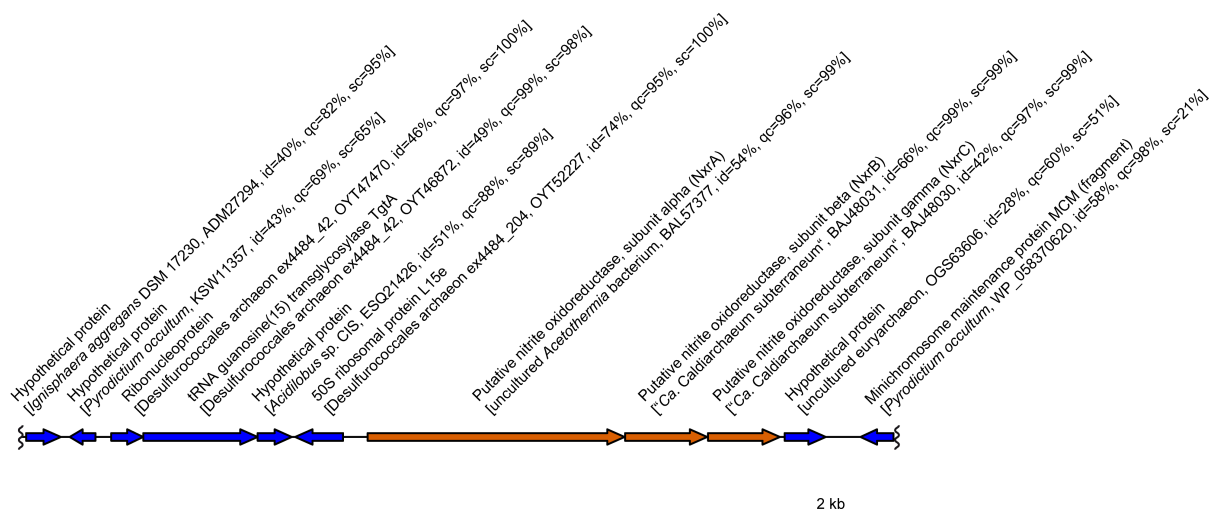


Figure S4 Metagenomic contig from a crenarchaeal sequence bin, which represents a member of the family *Desulfurococcaceae* remotely related to the genus *Ignisphaera*. The contig was retrieved from a metagenomic dataset, which had been produced from pooled genomic DNA from thermophilic (75°C) nitrifying enrichments (Supplementary Text). No other sequence bin in the metagenomic dataset contained *nxr*-like genes. The predicted gene product of *nxrA* is affiliated with the same phylogenetic clade as the NxrA of “*Ca. N. fabula*” in the type II DMSO reductase family (see Figure 6 in the main text). The putative *nxr* genes are highlighted orange, the flanking archaeal genes are shown in blue. Wiggly lines indicate the ends of the contig. Best BLASTP hits (NCBI nr) for each gene are indicated in brackets together with sequence identity (id), alignment coverage of the query (=contig) sequence (qc), and alignment coverage of the subject (=database) sequence (sc) in per cent. Genes and noncoding regions are drawn to scale.

Supplementary tables

Table S1 Kinetic constants of nitrite oxidation of NOB isolates and “*Ca. Nitrotoga*” enrichments.

Organism	$K_{m(\text{app})}$ ($\mu\text{M NO}_2^-$)	V_{max} ($\mu\text{mol NO}_2^-$ $\text{mg protein}^{-1} \text{h}^{-1}$)	V_{max} (fmol NO_2^- $\text{cell}^{-1} \text{h}^{-1}$)	Reference
<i>Nitrotoga fabula</i> KNB (isolate, WWTP)	89	28	ND ^b	This study
“ <i>Ca. Nitrotoga arctica</i> ” (enrichment, arctic soil)	58	26	ND	1
“ <i>Ca. Nitrotoga sp. AM1</i> ” (enrichment, eelgrass sediment)	25	ND	6.1	2
<i>Nitrospira defluvii</i> (isolate, WWTP)	9	48	ND	1
<i>Nitrospira lenta</i> BS10 (isolate, WWTP)	27	20	ND	1
<i>Nitrospira sp.</i> ND1 (isolate, WWTP)	6	45	ND	3
<i>Nitrospira japonica</i> NJ1 (isolate, WWTP)	10	31	ND	3
<i>Nitrospira moscoviensis</i> (isolate, corroded iron pipe)	9	18	ND	1
<i>Nitrospira marina</i> Ecomares 2.1 (isolate, marine aquaculture biofilter)	54	21	ND	4
<i>Nitrospira inopinata</i> (isolate, hot groundwater) ^a	449	17	ND	5
<i>Nitrobacter hamburgensis</i> (isolate, soil)	540 - 1,370	ND	1 - 3.3	6
<i>Nitrobacter hamburgensis</i> (isolate, soil)	544	64	ND	1
<i>Nitrobacter winogradskyi</i> (isolate, soil)	36 - 260	ND	1.9 - 3.7	6
<i>Nitrobacter winogradskyi</i> (isolate, soil)	309	78	ND	1
<i>Nitrobacter vulgaris</i> (isolate, sewage)	49	164	ND	1
<i>Nitrobacter sp.</i> 311 (isolate, ocean surface water)	28	95	ND	4
<i>Nitrolancea hollandica</i> Lb (isolate, WWTP)	1,000	ND	ND	7
<i>Nitrococcus mobilis</i> 231 (isolate, ocean surface water)	120	141	ND	4
<i>Nitrospina watsonii</i> 347 (isolate, Black Sea)	19	37	ND	4

a *N. inopinata* is a complete ammonia oxidizer (comammox organism)

b ND=not determined.

1 Data from Nowka et al. (2014)

2 Data from Ishii et al. (2017)

3 Data from Ushiki et al. (2017)

4 Data from Jacob et al. (2017)

5 Data from Kits et al. (2017)

6 Data from Both et al. (1992)

7 Data from Sorokin et al. (2012)

Table S2 Overview of key features of the “*Ca. N. fabula* KNB” genome.

	Chromosome	Plasmid
Genome size	2,609,426 bp	5,404 bp
Average G+C content	50.14%	63.55%
Number of genomic objects [CDS, fragment CDS, (r,t)RNA]	2,664	6
Number of coding sequences (CDS)	2,609	6
rRNA operons	2	0
tRNA genes	42	0
Coding density	84.98%	62.71%
Repeated regions	5.04%	0

Chromosome clusters of orthologous groups (COG) automated classification		
Functional category	CDS	CDS (%)
D Cell cycle control, cell division, chromosome partitioning	38	1.46
M Cell wall/membrane/envelope biogenesis	174	6.69
N Cell motility	14	0.54
O Posttranslational modification, protein turnover, chaperones	126	4.84
T Signal transduction mechanisms	65	2.50
U Intracellular trafficking, secretion, and vesicular transport	60	2.31
V Defense mechanisms	36	1.38
A RNA processing and modification	1	0.04
J Translation, ribosomal structure and biogenesis	151	5.81
K Transcription	100	3.85
L Replication, recombination and repair	170	6.54
C Energy production and conversion	125	4.81
E Amino acid transport and metabolism	154	5.92
F Nucleotide transport and metabolism	57	2.19
G Carbohydrate transport and metabolism	87	3.35
H Coenzyme transport and metabolism	106	4.08
I Lipid transport and metabolism	49	1.88
P Inorganic ion transport and metabolism	130	5.00
Q Secondary metabolites biosynthesis, transport and catabolism	38	1.46

Table S3 Proteins encoded by the plasmid of “*Ca. N. fabula* KNB” and their closest homologs in the TrEMBL, Swiss-Prot, and NCBI nr databases.

Plasmid Gene	Predicted function	Database	Best hit, accession no.	Best hit, identity (%)	Best hit, predicted function	Best hit, organism
NITFABP_0001	Protein of unknown function	TrEMBL	A0A0F3GCT4	69	Uncharacterized protein	<i>Pseudomonas pseudoalcaligenes</i>
		Swiss-Prot	P20085	49	Mobilization protein MobL	<i>Acidithiobacillus ferrooxidans</i>
		nr	XP_012260969	99	uncharacterized protein LOC105688902	<i>Athalia rosae</i> ^a
NITFABP_0002	Putative protein involved in initiation of plasmid replication	TrEMBL	A0A1I3FIQ5	83	Initiator Replication protein	<i>Paracoccus aminovorans</i>
		Swiss-Prot	P17492	29	Replication protein	<i>Neisseria gonorrhoeae</i>
		nr	XP_012260970	100	uncharacterized protein LOC105688903	<i>Athalia rosae</i> ^a
NITFABP_0003	Conserved protein of unknown function	TrEMBL	A0A212B9I4	71	Uncharacterized protein	<i>Pseudomonas</i> sp. A46
		Swiss-Prot	No hit			
		nr	WP_088193532	71	hypothetical protein	<i>Pseudomonas</i> sp. A46
NITFABP_0004	Putative transcriptional regulator, TetR family	TrEMBL	A7KK53	100	Putative transcriptional regulator	<i>Delftia acidovorans</i>
		Swiss-Prot	P39897	34	HTH-type transcriptional regulator MtrR	<i>Neisseria gonorrhoeae</i>
		nr	WP_043008328	100	TetR/AcrR family transcriptional regulator	<i>Comamonas testosteronii</i>
NITFABP_0005	Quaternary ammonium compound-resistance protein EmrE	TrEMBL	A7TX95	100	Small multidrug resistance protein	<i>Delftia tsuruhatensis</i>
		Swiss-Prot	Q9X2N9	59	Quaternary ammonium compound-resistance protein QacF	<i>Klebsiella aerogenes</i>
		nr	WP_043008326	100	quaternary ammonium compound efflux SMR transporter QacF	<i>Comamonas testosteronii</i>
NITFABP_0006	Putative Mobilization protein, MobS-like	TrEMBL	A0A238DWW0	84	Uncharacterized protein	<i>Thiomonas</i> sp. X19
		Swiss-Prot	P20086	51	Mobilization protein MobS	<i>Acidithiobacillus ferrooxidans</i>
		nr	ART89884	70	hypothetical protein	uncultured bacterium

Table S4 Proteins of “*Ca. N. fabula*” with predicted functions in key metabolic pathways, and genes of “*Ca. N. fabula*” coding for rRNAs or tRNAs. Proteins with an amino acid identity $\geq 35\%$ (over at least 80% of the sequence lengths) to characterized proteins in the SwissProt or TrEMBL databases were annotated as homologous to proteins with a known function. Proteins with an amino acid identity $\geq 25\%$ (over at least 80% of the sequence lengths) to characterized proteins or signatures in the aforementioned databases were annotated as putative homologs of the respective database entries.

Central Carbon Metabolism						
Pathway	Identifier	Type	Begin	End	Gene	Product
C-fixation	NITFAB_0176	CDS	159745	160809	<i>fdx</i>	Fructose-1,6-bisphosphate aldolase, class II
C-fixation	NITFAB_0177	CDS	160899	162338	<i>pykA</i>	Pyruvate kinase
C-fixation	NITFAB_0178	CDS	162355	163539	<i>pgk</i>	Phosphoglycerate kinase
C-fixation	NITFAB_0179	CDS	163617	164612	<i>gapA</i>	Glyceraldehyde-3-phosphate dehydrogenase A
C-fixation	NITFAB_0181	CDS	165202	167217	<i>tktA</i>	Transketolase 1, thiamin-binding
C-fixation	NITFAB_0347	CDS	350588	353368	<i>ppc</i>	Phosphoenolpyruvate carboxylase
C-fixation	NITFAB_0411	CDS	418433	419437	<i>fbp</i>	Fructose-1,6-bisphosphatase class I
C-fixation	NITFAB_0432	CDS	441142	442029	<i>cbpP</i>	Phosphoribulokinase
C-fixation	NITFAB_1072	CDS	1103461	1105800	<i>cbpO</i>	von Willebrand factor type A
C-fixation	NITFAB_1073	CDS	1105873	1106688	<i>cbpQ</i>	CbpQ
C-fixation	NITFAB_1074	CDS	1106824	1107180	<i>cbpS1</i>	Ribulose bisphosphate carboxylase/oxygenase small chain
C-fixation	NITFAB_1075	CDS	1107243	1108664	<i>cbpL1</i>	Ribulose bisphosphate carboxylase/oxygenase large chain
C-fixation	NITFAB_1105	CDS	1141097	1141852	<i>tpiA</i>	Triosephosphate isomerase
C-fixation	NITFAB_1227	CDS	1242715	1243149	<i>cbpS2</i>	Ribulose bisphosphate carboxylase/oxygenase small chain
C-fixation	NITFAB_1228	CDS	1243171	1244646	<i>cbpL2</i>	Ribulose bisphosphate carboxylase/oxygenase large chain
C-fixation	NITFAB_1234	CDS	1251630	1254005	<i>xpkA</i>	Xylulose-5-phosphate phosphoketolase
C-fixation	NITFAB_1933	CDS	1931517	1932245	<i>rpe</i>	Ribulose-phosphate 3-epimerase
C-fixation	NITFAB_2483	CDS	2497131	2497790	<i>rpiA</i>	Ribose 5-phosphate isomerase, constitutive
Glycogen formation/degradation	NITFAB_0535	CDS	533427	534872	<i>glgA</i>	Glycogen synthase
Glycogen formation/degradation	NITFAB_0599	CDS	592567	593943	<i>pgm</i>	Phosphoglucomutase
Glycogen formation/degradation	NITFAB_2047	CDS	2053431	2054711	<i>glgC</i>	glucose-1-phosphate adenylyltransferase
Glycogen formation/degradation	NITFAB_2048	CDS	2054819	2057017	<i>glgB</i>	1,4-alpha-glucan branching enzyme
Glycogen formation/degradation	NITFAB_2215	CDS	2227727	2229445		Putative Phosphorylase
Glycolysis/Gluconeogenesis	NITFAB_0176	CDS	159745	160809	<i>fdx</i>	Fructose-1,6-bisphosphate aldolase, class II
Glycolysis/Gluconeogenesis	NITFAB_0177	CDS	160899	162338	<i>pykA</i>	Pyruvate kinase
Glycolysis/Gluconeogenesis	NITFAB_0178	CDS	162355	163539	<i>pgk</i>	Phosphoglycerate kinase
Glycolysis/Gluconeogenesis	NITFAB_0179	CDS	163617	164612	<i>gapA</i>	Glyceraldehyde-3-phosphate dehydrogenase A
Glycolysis/Gluconeogenesis	NITFAB_0411	CDS	418433	419437	<i>fbp</i>	Fructose-1,6-bisphosphatase class I
Glycolysis/Gluconeogenesis	NITFAB_0599	CDS	592567	593943	<i>pgm</i>	Phosphoglucomutase

Glycolysis/Gluconeogenesis	NITFAB_0652	CDS	652423	653409	<i>glk</i>	Glucokinase
Glycolysis/Gluconeogenesis	NITFAB_1105	CDS	1141097	1141852	<i>tpiA</i>	Triosephosphate isomerase
Glycolysis/Gluconeogenesis	NITFAB_1993	CDS	1995346	1996629	<i>eno</i>	enolase
Glycolysis/Gluconeogenesis	NITFAB_2049	CDS	2057251	2058894	<i>pgi</i>	glucosephosphate isomerase
Glycolysis/Gluconeogenesis	NITFAB_2281	CDS	2292994	2294520	<i>gpmI</i>	phosphoglycerat mutase, cofactor-independent
Glycolysis/Gluconeogenesis	NITFAB_2363	CDS	2367922	2369181		putative Pyrophosphate-fructose 6-phosphate 1-phosphotransferase
Glyoxylate Shunt	NITFAB_0625	CDS	618890	619543	<i>gph2</i>	Phosphoglycolate phosphatase
Glyoxylate Shunt	NITFAB_0676	CDS	687556	689046	<i>glcD</i>	Glycolate oxidase GlcD subunit, FAD-linked
Glyoxylate Shunt	NITFAB_0677	CDS	689046	690110	<i>glcE</i>	Glycolate oxidase FAD binding GlcE subunit
Glyoxylate Shunt	NITFAB_0678	CDS	690118	691335	<i>glcF</i>	glycolate oxidase iron-sulfur GlcF subunit
Glyoxylate Shunt	NITFAB_2021	CDS	2026998	2027972	<i>mcl</i>	Maly-CoA lyase
Glyoxylate Shunt	NITFAB_2022	CDS	2027982	2029160	<i>mtkA</i>	Probable Malate--CoA ligase, subunit beta
Glyoxylate Shunt	NITFAB_2023	CDS	2029182	2030054	<i>sucD</i>	Probable Malate--CoA ligase, alpha subunit
Glyoxylate Shunt	NITFAB_2118	CDS	2126338	2127354	<i>mdh</i>	Malate dehydrogenase
Pentose-phosphate pathway	NITFAB_0176	CDS	159745	160809	<i>fdx</i>	Fructose-1,6-bisphosphate aldolase, class II
Pentose-phosphate pathway	NITFAB_0181	CDS	165202	167217	<i>tktA</i>	Transketolase, thiamin-binding
Pentose-phosphate pathway	NITFAB_0411	CDS	418433	419437	<i>fbp</i>	Fructose-1,6-bisphosphatase class I
Pentose-phosphate pathway	NITFAB_0549	CDS	549127	550080	<i>prs</i>	ribose-phosphate pyrophosphokinase (Phosphoribosyl pyrophosphate syntetase)
Pentose-phosphate pathway	NITFAB_0599	CDS	592567	593943	<i>pgm</i>	Phosphoglucomutase
Pentose-phosphate pathway	NITFAB_0788	CDS	813734	814645		putative 6-phosphogluconate dehydrogenase
Pentose-phosphate pathway	NITFAB_1234	CDS	1251630	1254005	<i>xpkA</i>	Xylulose-5-phosphate phosphoketolase
Pentose-phosphate pathway	NITFAB_2044	CDS	2048141	2048860		putative 6-phosphogluconolactonase
Pentose-phosphate pathway	NITFAB_2049	CDS	2057251	2058894	<i>pgi</i>	glucosephosphate isomerase
Pentose-phosphate pathway	NITFAB_2453	CDS	2465032	2465793	<i>rpe</i>	D-ribulose-5-phosphate 3-epimerase
Pentose-phosphate pathway	NITFAB_2473	CDS	2486672	2487757		putative Transaldolase
Pentose-phosphate pathway	NITFAB_2474	CDS	2487861	2489324	<i>zwf</i>	Glucose-6-phosphate 1-dehydrogenase
Pentose-phosphate pathway	NITFAB_2483	CDS	2497131	2497790	<i>rpiA</i>	Ribose 5-phosphate isomerase, constitutive
TCA Cycle	NITFAB_0684	CDS	698060	698434	<i>sdhC</i>	Succinate dehydrogenase, cytochrome b556 subunit
TCA Cycle	NITFAB_0685	CDS	698428	698802	<i>sdhD</i>	Succinate dehydrogenase, hydrophobic membrane anchor protein
TCA Cycle	NITFAB_0686	CDS	698802	700565	<i>sdhA</i>	Succinate dehydrogenase, flavoprotein subunit
TCA Cycle	NITFAB_0687	CDS	700925	701620	<i>sdhB</i>	Succinate dehydrogenase, iron-sulfur subunit
TCA Cycle	NITFAB_0689	CDS	701857	703200	<i>gltA</i>	Citrate synthase
TCA Cycle	NITFAB_0690	CDS	703316	706222	<i>sucA</i>	2-oxoglutarate dehydrogenase, E1 component
TCA Cycle	NITFAB_0691	CDS	706240	707400	<i>sucB</i>	2-oxoglutarate dehydrogenase, dihydrolipoyllysine-residue succinyltransferase (E2) component
TCA Cycle	NITFAB_0692	CDS	707529	708953	<i>lpdG</i>	2-oxo-acid dehydrogenase, dihydroliipoamide dehydrogenase (E3) component

TCA Cycle	NITFAB_1259	CDS	1283730	1284977	<i>icd</i>	isocitrate dehydrogenase
TCA Cycle	NITFAB_1443	CDS	1484837	1486219	<i>fumC</i>	fumarate hydratase (fumarase C), aerobic Class II
TCA Cycle	NITFAB_2118	CDS	2126338	2127354	<i>mdh</i>	Malate dehydrogenase
TCA Cycle	NITFAB_2202	CDS	2216587	2217468	<i>sucD</i>	Succinyl-CoA ligase [ADP-forming], subunit alpha
TCA Cycle	NITFAB_2203	CDS	2217456	2218634	<i>sucC</i>	Succinyl-CoA ligase [ADP-forming] subunit beta
TCA Cycle	NITFAB_2306	CDS	2313435	2316161	<i>acnA</i>	aconitate hydratase 1
TCA Cycle	NITFAB_2386	CDS	2393636	2395429	<i>lpaA</i>	2-oxo-acid dehydrogenase complex, Dihydropyrimidine dehydrogenase (E3) component
Hydrogen Metabolism						
Pathway	Label	Type	Begin	End	Gene	Product
Hydrogen Metabolism	NITFAB_0289	CDS	287290	287868	<i>hupE</i>	Hydrogenase/urease accessory protein HupE/UreI
Hydrogen Metabolism	NITFAB_1062	CDS	1092550	1094052	<i>hoxH</i>	[NiFe] NAD-reducing hydrogenase, large subunit HoxH
Hydrogen Metabolism	NITFAB_1063	CDS	1094046	1094534	<i>hoxW</i>	Hydrogenase maturation protease
Hydrogen Metabolism	NITFAB_1064	CDS	1094558	1094899	<i>hypA</i>	Hydrogenase nickel incorporation protein HypA
Hydrogen Metabolism	NITFAB_1065	CDS	1094936	1095838	<i>hypB</i>	Hydrogenase nickel incorporation protein HypB
Hydrogen Metabolism	NITFAB_1066	CDS	1095810	1096946	<i>hypF</i>	Carbamoyltransferase HypF (fragment)
Hydrogen Metabolism	NITFAB_1067	CDS	1096960	1097202	<i>hypC</i>	Hydrogenase expression/formation protein HypC
Hydrogen Metabolism	NITFAB_1068	CDS	1097199	1098314	<i>hypD</i>	Hydrogenase expression/formation protein HypD
Hydrogen Metabolism	NITFAB_1069	CDS	1098311	1099360	<i>hypE</i>	Hydrogenase maturation protein HypE
Hydrogen Metabolism	NITFAB_1663	CDS	1683318	1683854	<i>hoxY</i>	[NiFe] NAD-reducing hydrogenase, small subunit HoxY
Hydrogen Metabolism	NITFAB_1664	CDS	1683851	1684696	<i>hoxU</i>	[NiFe] NAD-reducing hydrogenase, subunit HoxU
Hydrogen Metabolism	NITFAB_1665	CDS	1684672	1686498	<i>hoxF</i>	[NiFe] NAD-reducing hydrogenase, subunit HoxF
Miscellaneous						
Pathway	Label	Type	Begin	End	Gene	Product
Amino Acid Transport	NITFAB_1244	CDS	1265623	1268685		putative Amino acid ABC transporter, permease protein, 3-TM region, His/Glu/Gln/Arg/opine family
Amino Acid Transport	NITFAB_1245	CDS	1268682	1269785		putative ABC-type polar amino acid transport system, ATPase component
Arsenic Resistance	NITFAB_1123	CDS	1150900	1151916		Transcriptional regulator, ArsR family
Arsenic Resistance	NITFAB_1500	CDS	1547297	1547692	<i>arsC</i>	arsenate reductase
Arsenic Resistance	NITFAB_1579	CDS	1615184	1615585		Transcriptional regulator, ArsR family
Arsenic Resistance	NITFAB_2149	CDS	2162629	2162961		putative Transcriptional regulator, ArsR family
Arsenic Resistance	NITFAB_2150	CDS	2162958	2163725		putative NADPH-dependent FMN reductase, Arsenical resistance protein
Arsenic Resistance	NITFAB_2151	CDS	2163722	2164228		putative Arsenate reductase
Arsenic Resistance	NITFAB_2217	CDS	2230354	2230785		putative Transcriptional regulator, ArsR family
Branched AA Transport	NITFAB_0006	CDS	5844	7028	<i>livK</i>	leucine/isoleucine/valine transporter subunit; periplasmic-binding component of ABC superfamily
Branched AA Transport	NITFAB_0007	CDS	7088	8011	<i>livH</i>	leucine/isoleucine/valine transporter subunit; membrane component of ABC superfamily

Branched AA Transport	NITFAB_0008	CDS	7995	9107	<i>livM</i>	leucine/isoleucine/valine transporter subunit; membrane component of ABC superfamily
Branched AA Transport	NITFAB_0009	CDS	9113	9922	<i>livG</i>	leucine/isoleucine/valine transporter subunit; ATP-binding component of ABC superfamily
Branched AA Transport	NITFAB_0010	CDS	9962	10690	<i>livF</i>	leucine/isoleucine/valine transporter subunit; ATP-binding component of ABC superfamily
Calcium Transport	NITFAB_0651	CDS	649611	652247	<i>tcaB</i>	Calcium-transporting ATPase
Calcium Transport	NITFAB_1239	CDS	1260412	1261389		putative Sodium/potassium/calcium antiporter CaxA
Carbonic Anhydrases	NITFAB_0956	CDS	995979	996668	<i>cynT1</i>	Carbonic anhydrase
Carbonic Anhydrases	NITFAB_1300	CDS	1326582	1327205	<i>cynT2</i>	Carbonic anhydrase
Carbonic Anhydrases	NITFAB_1418	CDS	1463115	1463750		putative Carbonic anhydrase
Catalase	NITFAB_1016	CDS	1046232	1048457	<i>kafG</i>	catalase/hydroperoxidase HPI(I)
Catalase	NITFAB_1541	CDS	1584179	1586377	<i>kafG</i>	catalase/hydroperoxidase HPI(I)
Catalase	NITFAB_1652	CDS	1667427	1669601	<i>kafG</i>	catalase/hydroperoxidase HPI(I)
Chlorite Dismutase	NITFAB_1630	CDS	1651185	1652057	<i>clid</i>	Chlorite dismutase
Chlorite Dismutase	NITFAB_2070	CDS	2082825	2083667	<i>clid</i>	Chlorite dismutase
Co/Zn/Cd Export	NITFAB_1397	CDS	1438159	1441356	<i>czcA</i>	Cobalt-zinc-cadmium resistance protein CzcA (Cation efflux system protein CzcA)
Co/Zn/Cd Export	NITFAB_1398	CDS	1441377	1442879	<i>czcB</i>	Cobalt-zinc-cadmium resistance protein CzcB
Co/Zn/Cd Export	NITFAB_1399	CDS	1442917	1444209	<i>czcC</i>	Cobalt-zinc-cadmium resistance protein CzcC
CRISPR/CAS	NITFAB_1828	CDS	1819684	1820550		putative CRISPR-associated RAMP protein, Cmr4 family
CRISPR/CAS	NITFAB_2256	CDS	2265092	2265397		putative CRISPR-associated endonuclease Cas2
CRISPR/CAS	NITFAB_2257	CDS	2265425	2266354		putative CRISPR-associated endonuclease Cas1
CRISPR/CAS	NITFAB_2258	CDS	2266360	2268777		putative CRISPR-associated endonuclease, cas9
Cytochrome c biogenesis	NITFAB_0081	CDS	70926	72869	<i>ccmF</i>	heme lyase, CcmF subunit
Cytochrome c biogenesis	NITFAB_0082	CDS	72881	73408	<i>ccmG</i>	periplasmic thioredoxin of cytochrome c-type biogenesis
Cytochrome c biogenesis	NITFAB_0083	CDS	73398	73892	<i>ccmH</i>	Cytochrome C biogenesis protein
Cytochrome c biogenesis	NITFAB_0084	CDS	73889	75145		putative Cytochrome c-type biogenesis protein
Cytochrome c biogenesis	NITFAB_0203	CDS	193708	194415		putative DsbA-like protein
Cytochrome c biogenesis	NITFAB_0437	CDS	447234	449078	<i>dsbD</i>	Thiol:disulfide interchange protein DsbD
Cytochrome c biogenesis	NITFAB_2312	CDS	2320186	2320662	<i>ccmE</i>	heme chaperone
Cytochrome c biogenesis	NITFAB_2313	CDS	2320786	2320950		putative Heme exporter protein CcmD (fragment)
Cytochrome c biogenesis	NITFAB_2314	CDS	2320947	2321624	<i>ccmC</i>	heme exporter subunit; membrane component of ABC superfamily
Cytochrome c biogenesis	NITFAB_2315	CDS	2321716	2322399	<i>ccmB</i>	heme exporter subunit; membrane component of ABC superfamily
Cytochrome c biogenesis	NITFAB_2316	CDS	2322396	2323010	<i>ccmA</i>	heme exporter subunit; ATP-binding component of ABC superfamily
Cytochrome c biogenesis	NITFAB_2519	CDS	2533438	2533950		putative Disulfide bond formation protein B DsbB
Cytochromes	NITFAB_0005	CDS	4899	5273		putative Cytochrome c class I
Cytochromes	NITFAB_0057	CDS	49810	50406		putative monohaem cytochrome c

Cytochromes	NITFAB_0058	CDS	50531	51310			Dihaem cytochrome c
Cytochromes	NITFAB_0187	CDS	175579	176259			Dihaem cytochrome c
Cytochromes	NITFAB_0188	CDS	176249	176599			Monohaem cytochrome c
Cytochromes	NITFAB_0192	CDS	178774	179205			putative Monohaem cytochrome c
Cytochromes	NITFAB_1009	CDS	1042294	1042614			putative Cytochrome c class I
Cytochromes	NITFAB_1049	CDS	1077880	1078497			putative Cytochrome b
Cytochromes	NITFAB_1656	CDS	1670809	1672320			putative Multahaem cytochrome c
Cytochromes	NITFAB_1911	CDS	1906967	1907455		<i>cybB</i>	Cytochrome b561
Cytochromes	NITFAB_2103	CDS	2111941	2112516			putative cytochrome c
Cytochromes	NITFAB_2210	CDS	2223161	2223841			putative Cytochrome c-551
Cytochromes	NITFAB_2356	CDS	2360153	2361046			putative Cytochrome c family protein
FeS Cluster Assembly	NITFAB_2525	CDS	2537721	2538206		<i>sufU</i>	FeS cluster assembly SUF system, sulfur-transfer protein SufU
FeS Cluster Assembly	NITFAB_2527	CDS	2539462	2540769		<i>sufD</i>	FeS cluster assembly SUF system , protein SufD
FeS Cluster Assembly	NITFAB_2528	CDS	2540766	2541557		<i>sufC</i>	FeS cluster assembly SUF system, ATPase SufC
FeS Cluster Assembly	NITFAB_2529	CDS	2541554	2542990		<i>sufB</i>	FeS cluster assembly SUF system, protein SufB
FeS Cluster Assembly	NITFAB_2530	CDS	2543076	2543435		<i>sufA</i>	FeS cluster assembly SUF system, protein SufA
Iron Metabolism	NITFAB_1367	CDS	1404069	1405892			putative siderophore biosynthesis protein
Iron Metabolism	NITFAB_1371	CDS	1408682	1410799			putative TonB-dependent siderophore receptor
Iron Metabolism	NITFAB_1391	CDS	1429456	1429860			putative ferric reductase (fragment)
Iron Metabolism	NITFAB_1392	CDS	1429820	1430251			putative ferric reductase (fragment)
Iron Metabolism	NITFAB_1393	CDS	1430369	1430788			putative Ferric reductase domain (fragment)
Iron Metabolism	NITFAB_1692	CDS	1708850	1709389			putative Bacterioferritin
Iron Metabolism	NITFAB_1876	CDS	1855863	1858343			putative TonB-dependent siderophore receptor
Iron Metabolism	NITFAB_1999	CDS	2005271	2006299			putative Ferric iron ABC transporter, iron-binding protein
Iron Metabolism	NITFAB_2000	CDS	2006309	2007955			putative Iron ABC transporter permease protein
Iron Metabolism	NITFAB_2001	CDS	2008056	2009126			putative Fe(3+)-transporting ATPase
Iron Metabolism	NITFAB_2003	CDS	2009256	2009681		<i>fur</i>	DNA-binding transcriptional dual regulator of siderophore biosynthesis and transport
Iron Metabolism	NITFAB_2056	CDS	2066098	2068296			putative TonB-dependent receptor
Iron Metabolism	NITFAB_2086	CDS	2098496	2098960		<i>bfr</i>	bacterioferritin, iron storage and detoxification protein
Magnesium Transport	NITFAB_0324	CDS	325549	326814			putative magnesium/nickel/cobalt transporter (fragment)
Magnesium Transport	NITFAB_0408	CDS	411945	414539		<i>mgtA</i>	Magnesium-transporting ATPase, P-type 1
Magnesium Transport	NITFAB_2346	CDS	2350309	2351763			putative Magnesium transporter
Mechanosensitive Channel	NITFAB_0994	CDS	1027439	1027843		<i>mscL</i>	mechanosensitive channel
Molybdenum Transport	NITFAB_2422	CDS	2430033	2431103		<i>modC</i>	Molybdenum import ATP-binding protein ModC
Molybdenum Transport	NITFAB_2423	CDS	2431100	2431804		<i>modB</i>	Molybdenum transport system permease protein ModB
Molybdenum Transport	NITFAB_2424	CDS	2431819	2432595			putative Molybdenum ABC transporter, periplasmic molybdenum-binding protein ModA

Monovalent Cation/Proton Antiporter	NITFAB_1283	CDS	1307823	1309199	<i>nhaA</i>	Na(+)/H(+) antiporter NhaA
Monovalent Cation/Proton Antiporter	NITFAB_2132	CDS	2146579	2149503	<i>mnpAB</i>	monovalent cation/H(+) antiporter subunit A/B
Monovalent Cation/Proton Antiporter	NITFAB_2133	CDS	2149503	2149850	<i>mnpC</i>	monovalent cation/H(+) antiporter subunit C
Monovalent Cation/Proton Antiporter	NITFAB_2134	CDS	2149906	2151522	<i>mnpD</i>	proton transporter component of monovalent cation/H+ antiporter subunit D
Monovalent Cation/Proton Antiporter	NITFAB_2135	CDS	2151474	2151716		protein of unknown function
Monovalent Cation/Proton Antiporter	NITFAB_2136	CDS	2151519	2152007		putative monovalent cation/H(+) antiporter subunit E
Monovalent Cation/Proton Antiporter	NITFAB_2137	CDS	2152004	2152285	<i>mnpF</i>	monovalent cation/H(+) antiporter subunit F
Monovalent Cation/Proton Antiporter	NITFAB_2138	CDS	2152282	2152593	<i>mnpG</i>	monovalent cation/H(+) antiporter subunit G
Peroxidase	NITFAB_1212	CDS	1229745	1230830		putative Cytochrome c peroxidase (<i>ccp</i>)
Peroxidase	NITFAB_1373	CDS	1412079	1413359		putative Di-heme cytochrome c peroxidase
Peroxidase	NITFAB_1903	CDS	1893290	1894333	<i>ccpA</i>	Cytochrome c551 peroxidase
Phosphate Transport	NITFAB_0743	CDS	765491	766264	<i>pstB1</i>	phosphate transporter subunit; ATP-binding component of ABC superfamily
Phosphate Transport	NITFAB_0744	CDS	766277	767122	<i>pstA1</i>	phosphate transporter subunit; membrane component of ABC superfamily
Phosphate Transport	NITFAB_0745	CDS	767125	768087	<i>pstC1</i>	phosphate transporter subunit; membrane component of ABC superfamily
Phosphate Transport	NITFAB_0746	CDS	768211	769260	<i>pstS1</i>	phosphate transporter subunit; periplasmic-binding component of ABC superfamily
Phosphate Transport	NITFAB_0967	CDS	1005708	1006757	<i>pstS2</i>	phosphate transporter subunit; periplasmic-binding component of ABC superfamily
Phosphate Transport	NITFAB_1051	CDS	1080264	1081037	<i>pstB2</i>	high-affinity phosphate transport protein (ABC superfamily, <i>atp_bind</i>)
Phosphate Transport	NITFAB_1052	CDS	1081050	1081895	<i>pstA2</i>	phosphate transporter subunit; membrane component of ABC superfamily
Phosphate Transport	NITFAB_1053	CDS	1081898	1082860	<i>pstC2</i>	phosphate transporter subunit; membrane component of ABC superfamily
Phosphate Transport	NITFAB_1054	CDS	1082984	1084033	<i>pstS3</i>	phosphate transporter subunit; periplasmic-binding component of ABC superfamily
Phosphate Transport	NITFAB_2482	CDS	2496355	2497062	<i>phoU</i>	negative regulator of PhoR/PhoB two-component regulator
Potassium Transport	NITFAB_1894	CDS	1881154	1883025	<i>kup</i>	potassium transporter
Quaternary Ammonium Compound resistance	NITFAB_1750	CDS	1754843	1755163	<i>sugE</i>	Quaternary ammonium compound-resistance protein SugE
Quaternary Ammonium Compound resistance	NITFAB_p0005	CDS	3780	4112	<i>emrE</i>	Quaternary ammonium compound-resistance protein EmrE
Quorum Sensing	NITFAB_1168	CDS	1181820	1182377	<i>anol</i>	Acyl-homoserine-lactone synthase
Quorum Sensing	NITFAB_2191	CDS	2206256	2206843	<i>anol</i>	Acyl-homoserine-lactone synthase
Quorum Sensing	NITFAB_2193	CDS	2207440	2208222	<i>anoR</i>	Transcriptional activator protein AnoR
RND family Heavy metal/cation/multidrug Efflux	NITFAB_0193	CDS	179386	180711		putative Cation efflux system, membrane fusion protein
RND family Heavy metal/cation/multidrug Efflux	NITFAB_0194	CDS	180708	183818	<i>cusA</i>	Cation efflux system protein CusA

RND family Heavy metal/cation/multidrug Efflux	NITFAB_0537	CDS	535178	536479		putative Outer membrane efflux protein, cusC-like
RND family Heavy metal/cation/multidrug Efflux	NITFAB_0538	CDS	536476	537627		putative Efflux transporter, RND family, MFP subunit
RND family Heavy metal/cation/multidrug Efflux	NITFAB_0539	CDS	537629	540727	<i>cusA2</i>	Cation efflux system protein
RND family Heavy metal/cation/multidrug Efflux	NITFAB_1570	CDS	1604686	1607775		putative Cation efflux system protein CzcA
RND family Heavy metal/cation/multidrug Efflux	NITFAB_1571	CDS	1607785	1609026		putative Efflux transporter, RND family, MFP subunit
RND family Heavy metal/cation/multidrug Efflux	NITFAB_1572	CDS	1609028	1610380		putative Outer membrane efflux protein
RND family Heavy metal/cation/multidrug Efflux	NITFAB_1586	CDS	1618626	1621790	<i>cusA3</i>	copper/silver efflux system, membrane component
RND family Heavy metal/cation/multidrug Efflux	NITFAB_1587	CDS	1621787	1623397		putative Cation efflux system protein CusB
RND family Heavy metal/cation/multidrug Efflux	NITFAB_1588	CDS	1623394	1624737		putative outer membrane silver resistance, three components proton antiporter efflux system SilC
RND family Heavy metal/cation/multidrug Efflux	NITFAB_1602	CDS	1631892	1633019		putative RND efflux pump, membrane fusion protein, similar to AcrA family
RND family Heavy metal/cation/multidrug Efflux	NITFAB_1603	CDS	1633016	1636099		putative RND efflux pump, similar to multidrug efflux transporter AcrB
RND family Heavy metal/cation/multidrug Efflux	NITFAB_1757	CDS	1760980	1764081		putative Heavy metal efflux pump
RND family Heavy metal/cation/multidrug Efflux	NITFAB_1864	CDS	1847929	1848708		putative Zinc transporter
RND family Heavy metal/cation/multidrug Efflux	NITFAB_1968	CDS	1964135	1965367	<i>mdtA</i>	multidrug efflux system, subunit A
RND family Heavy metal/cation/multidrug Efflux	NITFAB_1969	CDS	1965364	1968453	<i>mdtB</i>	multidrug efflux system, subunit B
RND family Heavy metal/cation/multidrug Efflux	NITFAB_1970	CDS	1968476	1971583	<i>mdtC</i>	multidrug efflux system, subunit C
RND family Heavy metal/cation/multidrug Efflux	NITFAB_2005	CDS	2010740	2012266		putative RND efflux system, outer membrane lipoprotein, NodT family
RND family Heavy metal/cation/multidrug Efflux	NITFAB_2006	CDS	2012244	2015381	<i>acrB</i>	multidrug efflux system protein
RND family Heavy metal/cation/multidrug Efflux	NITFAB_2007	CDS	2015390	2016550	<i>acrE</i>	RND efflux pump, membrane fusion protein
Sec Pathway	NITFAB_0271	CDS	265750	268467	<i>secA</i>	Preprotein translocase subunit SecA, ATPase

Sec Pathway	NITFAB_0463	CDS	471358	471702	<i>secE</i>	Preprotein translocase, subunit SecE
Sec Pathway	NITFAB_0497	CDS	497006	498337	<i>secY</i>	Preprotein translocase, membrane subunit SecY
Sec Pathway	NITFAB_0943	CDS	984982	985785	<i>lepB</i>	leader peptidase (signal peptidase I)
Sec Pathway	NITFAB_1106	CDS	1141882	1142232	<i>secG</i>	Preprotein translocase, membrane subunit SecG
Sec Pathway	NITFAB_1253	CDS	1275506	1275961	<i>lspA</i>	prolipoprotein signal peptidase (signal peptidase II)
Sec Pathway	NITFAB_1761	CDS	1768203	1769132	<i>secF</i>	Protein-export membrane protein SecF
Sec Pathway	NITFAB_1762	CDS	1769168	1770979	<i>secD</i>	Protein-export membrane protein SecD
Sec Pathway	NITFAB_1763	CDS	1770989	1771312	<i>yajC</i>	Preprotein translocase, subunit YajC
Sec Pathway	NITFAB_2081	CDS	2093522	2094580	<i>ftsY</i>	Signal recognition particle receptor FtsY
Sec Pathway	NITFAB_2288	CDS	2300518	2300997	<i>secB</i>	protein export chaperone
Sec Pathway	NITFAB_2354	CDS	2356946	2358298	<i>ffh</i>	Signal Recognition Particle (SRP) component with 4.5S RNA (ffs)
Superoxide dismutase	NITFAB_0901	CDS	937741	938319	<i>sodB</i>	superoxide dismutase (Fe)
Superoxide dismutase	NITFAB_1655	CDS	1670177	1670785		putative superoxide dismutase (copper/zinc)
TAT secretion	NITFAB_2544	CDS	2555372	2556127	<i>tatC</i>	Sec-independent protein translocase protein TatC
TAT secretion	NITFAB_2545	CDS	2556127	2556855		putative Sec-independent protein translocase protein TatB
TAT secretion	NITFAB_2546	CDS	2556871	2557101	<i>tatA</i>	Sec-independent protein translocase protein Tata
Toluene transport (export)	NITFAB_0135	CDS	119077	119886	<i>yrbF</i>	toluene transporter subunit: ATP-binding component of ABC superfamily
Toluene transport (export)	NITFAB_0136	CDS	119877	120671	<i>yrbE</i>	toluene transporter subunit: membrane component of ABC superfamily
Toluene transport (export)	NITFAB_0137	CDS	120674	121135	<i>yrbD</i>	toluene transporter subunit: membrane component of ABC superfamily
Toluene transport (export)	NITFAB_0138	CDS	121167	121808		putative ABC-type toluene transporter, auxiliary component
Toluene transport (export)	NITFAB_0140	CDS	122124	123029	<i>yadG</i>	putative transporter subunit: ATP-binding component of ABC superfamily
Toluene transport (export)	NITFAB_0141	CDS	123037	123792		putative transporter subunit: membrane component of ABC superfamily
Ubiquinone Synthesis	NITFAB_0124	CDS	108342	109499	<i>ubiF</i>	Ubiquinone biosynthesis hydroxylase, UbiH/UbiF/VisC/COQ6 family
Ubiquinone Synthesis	NITFAB_0128	CDS	112688	114151	<i>ubiD</i>	3-octaprenyl-4-hydroxybenzoate decarboxylase
Ubiquinone Synthesis	NITFAB_0233	CDS	225742	226899	<i>ubiH</i>	2-octaprenyl-6-methoxyphenol hydroxylase, FAD/NAD(P)-binding
Ubiquinone Synthesis	NITFAB_0325	CDS	326861	327718	<i>ubiA</i>	p-hydroxybenzoate octaprenyltransferase
Ubiquinone Synthesis	NITFAB_0326	CDS	327715	328335	<i>ubiC</i>	putative chorismate pyruvate-lyase ubiC
Ubiquinone Synthesis	NITFAB_0412	CDS	419530	421050	<i>ubiB</i>	2-octaprenylphenol hydroxylase
Ubiquinone Synthesis	NITFAB_0415	CDS	422717	423451	<i>ubiE</i>	bifunctional 2-octaprenyl-6-methoxy-1,4-benzoquinone methylase and S-adenosylmethionine:2-DMK methyltransferase
Ubiquinone Synthesis	NITFAB_0626	CDS	619536	620231	<i>ubiG</i>	3-demethylubiquinone-9 3-O-methyltransferase and 2-octaprenyl-6-hydroxy phenol methylase
Nitrogen Metabolism						
Pathway	Label	Type	Begin	End	Gene	Product
Ammonium Transporter	NITFAB_1755	CDS	1758819	1760042		putative Ammonium transporter
Nitrite Assimilation	NITFAB_1038	CDS	1067122	1069557	<i>nasD</i>	Assimilatory Nitrite reductase, NAD(P)H dependent, large subunit
Nitrite Assimilation	NITFAB_1039	CDS	1069570	1069893	<i>nasE</i>	Assimilatory Nitrite reductase, NAD(P)H dependent, small subunit
Nitrite Oxidation	NITFAB_2341	CDS	2341774	2342514		putative nitrite oxidoreductase assembly chaperone protein

Nitrite Oxidation	NITFAB_2342	CDS	2342583	2343692			putative nitrite oxidoreductase, gamma subunit
Nitrite Oxidation	NITFAB_2343	CDS	2343703	2344860	<i>nxrB1</i>		Nitrite oxidoreductase, beta subunit
Nitrite Oxidation	NITFAB_2344	CDS	2344941	2348450	<i>nxrA1</i>		Nitrite oxidoreductase, alpha subunit
Nitrite Oxidation	NITFAB_2593	CDS	2594871	2595611			putative nitrite oxidoreductase assembly chaperone protein
Nitrite Oxidation	NITFAB_2594	CDS	2595680	2596789			putative nitrite oxidoreductase, gamma subunit
Nitrite Oxidation	NITFAB_2595	CDS	2596800	2597957	<i>nxrB2</i>		Nitrite oxidoreductase, beta subunit
Nitrite Oxidation	NITFAB_2596	CDS	2598038	2601547	<i>nxrA2</i>		Nitrite oxidoreductase, alpha subunit
Nitrite Reduction	NITFAB_0189	CDS	176679	177623	<i>nirK</i>		Copper-containing nitrite reductase (NO-forming)
Nitrite Transporter	NITFAB_1230	CDS	1246759	1247571			putative Formate/nitrite transporter
Respiratory Chain							
Pathway	Label	Type	Begin	End	Gene	Product	
Alternative Complex III (ACIII)	NITFAB_0001	CDS	356	2566		putative Menaquinol oxidoreductase complex ACIII, molybdopterin-binding subunit ActB1	
Alternative Complex III (ACIII)	NITFAB_0002	CDS	2610	3215		putative Menaquinol oxidoreductase complex ACIII, cytochrome c subunit ActA	
Alternative Complex III (ACIII)	NITFAB_2604	CDS	2605395	2606408		putative Menaquinol oxidoreductase complex ACIII, membrane subunit ActF	
Alternative Complex III (ACIII)	NITFAB_2605	CDS	2606422	2606961		putative Menaquinol oxidoreductase complex ACIII, monohaem cytochrome c subunit ActE	
Alternative Complex III (ACIII)	NITFAB_2606	CDS	2606958	2607485		putative Menaquinol oxidoreductase complex ACIII, DUF3341 subunit ActD	
Alternative Complex III (ACIII)	NITFAB_2607	CDS	2607485	2608849		putative Menaquinol oxidoreductase complex ACIII, menaquinol-binding membrane protein subunit ActC	
Alternative Complex III (ACIII)	NITFAB_2608	CDS	2608924	2609424		putative Menaquinol oxidoreductase complex ACIII, iron-sulfur cluster-binding subunit ActB2 (C-terminal fragment)	
Alternative Complex III (ACIII)	NITFAB_CDS2R	CDS	2	262		putative Menaquinol oxidoreductase complex ACIII, iron-sulfur cluster-binding subunit ActB2 (N-terminal fragment)	
Complex I	NITFAB_1772	CDS	1777637	1779088	<i>nuoN</i>	NADH-quinone oxidoreductase subunit N	
Complex I	NITFAB_1773	CDS	1779111	1780595	<i>nuoM</i>	NADH-quinone oxidoreductase subunit M	
Complex I	NITFAB_1774	CDS	1780626	1782647	<i>nuoL</i>	NADH-quinone oxidoreductase subunit L	
Complex I	NITFAB_1775	CDS	1782654	1782965	<i>nuoK</i>	NADH-quinone oxidoreductase subunit K	
Complex I	NITFAB_1776	CDS	1783114	1783734	<i>nuoJ</i>	NADH-quinone oxidoreductase subunit J	
Complex I	NITFAB_1777	CDS	1783902	1784390	<i>nuoI</i>	NADH-quinone oxidoreductase subunit I	
Complex I	NITFAB_1778	CDS	1784410	1785450	<i>nuoH</i>	NADH:ubiquinone oxidoreductase, subunit H	
Complex I	NITFAB_1779	CDS	1785447	1787825	<i>nuoG</i>	NADH-quinone oxidoreductase, subunit G	
Complex I	NITFAB_1780	CDS	1787840	1789111	<i>nuoF</i>	NADH:ubiquinone oxidoreductase, subunit F	
Complex I	NITFAB_1781	CDS	1789108	1789587	<i>nuoE</i>	NADH-quinone oxidoreductase, subunit E	
Complex I	NITFAB_1782	CDS	1789695	1790948	<i>nuoD</i>	NADH-quinone oxidoreductase subunit D	
Complex I	NITFAB_1783	CDS	1791054	1791695	<i>nuoC</i>	NADH-quinone oxidoreductase subunit C	

Complex I	NITFAB_1784	CDS	1791751	1792227	<i>nuoB</i>	NADH-quinone oxidoreductase subunit B
Complex I	NITFAB_1785	CDS	1792218	1792574	<i>nuoA</i>	NADH-quinone oxidoreductase subunit A
Complex II	NITFAB_0684	CDS	698060	698434	<i>sdhC</i>	Succinate dehydrogenase, cytochrome b556 subunit
Complex II	NITFAB_0685	CDS	698428	698802	<i>sdhD</i>	Succinate dehydrogenase, hydrophobic membrane anchor protein
Complex II	NITFAB_0686	CDS	698802	700565	<i>sdhA</i>	Succinate dehydrogenase, flavoprotein subunit
Complex II	NITFAB_0687	CDS	700925	701620	<i>sdhB</i>	Succinate dehydrogenase, iron-sulfur subunit
Complex IV	NITFAB_0046	CDS	42673	43638	<i>ccoO</i>	Cbb3-type cytochrome oxidase, cytochrome c subunit
Complex IV	NITFAB_0047	CDS	43674	45083	<i>ccoN</i>	Cbb3-type cytochrome oxidase, subunit I
Complex IV	NITFAB_0056	CDS	49317	49829		putative Cbb3-type cytochrome oxidase-like protein
Complex V	NITFAB_0146	CDS	128827	129255	<i>atpC</i>	F1 sector of membrane-bound ATP synthase, epsilon subunit
Complex V	NITFAB_0147	CDS	129304	130725	<i>atpD</i>	F1 sector of membrane-bound ATP synthase, beta subunit
Complex V	NITFAB_0148	CDS	130927	131796	<i>atpG</i>	F1 sector of membrane-bound ATP synthase, gamma subunit
Complex V	NITFAB_0149	CDS	131812	133353	<i>atpA</i>	F1 sector of membrane-bound ATP synthase, alpha subunit
Complex V	NITFAB_0150	CDS	133385	133918	<i>atpH</i>	F1 sector of membrane-bound ATP synthase, delta subunit
Complex V	NITFAB_0151	CDS	133924	134394	<i>atpF</i>	F0 sector of membrane-bound ATP synthase, subunit b
Complex V	NITFAB_0152	CDS	134429	134671	<i>atpE</i>	F0 sector of membrane-bound ATP synthase, subunit c
Complex V	NITFAB_0153	CDS	134730	135590	<i>atpB</i>	F0 sector of membrane-bound ATP synthase, subunit a
Complex V	NITFAB_0154	CDS	135587	135952		putative ATP synthase, subunit I
RNAs						
Pathway	Label	Type	Begin	End	Gene	Product
rRNA	NITFAB_16s_rRNA_1	rRNA	2414812	2416339		ribosomal RNA, 16s_rRNA
rRNA	NITFAB_16s_rRNA_2	rRNA	2002980	2004507		ribosomal RNA, 16s_rRNA
rRNA	NITFAB_23s_rRNA_1	rRNA	2411340	2414224		ribosomal RNA, 23s_rRNA
rRNA	NITFAB_23s_rRNA_2	rRNA	1999508	2002392		ribosomal RNA, 23s_rRNA
rRNA	NITFAB_5s_rRNA_1	rRNA	2411105	2411216		ribosomal RNA, 5s_rRNA
rRNA	NITFAB_5s_rRNA_2	rRNA	1999273	1999384		ribosomal RNA, 5s_rRNA
tRNA	NITFAB_tmRNA6	tmRNA	1843652	1844020		tmRNA
tRNA	NITFAB_tRNA1	tRNA	51890	51966		Arg tRNA
tRNA	NITFAB_tRNA10	tRNA	602524	602600		Met tRNA
tRNA	NITFAB_tRNA11	tRNA	709368	709452		Leu tRNA
tRNA	NITFAB_tRNA12	tRNA	715552	715627		Val tRNA
tRNA	NITFAB_tRNA13	tRNA	715639	715715		Asp tRNA
tRNA	NITFAB_tRNA14	tRNA	791095	791170		Arg tRNA
tRNA	NITFAB_tRNA15	tRNA	946270	946359		Ser tRNA
tRNA	NITFAB_tRNA16	tRNA	1142253	1142337		Leu tRNA
tRNA	NITFAB_tRNA17	tRNA	1331693	1331785		Ser tRNA
tRNA	NITFAB_tRNA18	tRNA	1331812	1331888		Arg tRNA
tRNA	NITFAB_tRNA19	tRNA	1448189	1448264		Gly tRNA

tRNA	NITFAB_tRNA2	tRNA	375633	375708		Phe tRNA
tRNA	NITFAB_tRNA20	tRNA	1448322	1448395		Cys tRNA
tRNA	NITFAB_tRNA21	tRNA	1448457	1448533		Pro tRNA
tRNA	NITFAB_tRNA22	tRNA	1491971	1492046		Lys tRNA
tRNA	NITFAB_tRNA23	tRNA	1740015	1740103		Leu tRNA
tRNA	NITFAB_tRNA24	tRNA	1753309	1753393		Leu tRNA
tRNA	NITFAB_tRNA25	tRNA	1912389	1912464		Ala tRNA
tRNA	NITFAB_tRNA26	tRNA	1912488	1912563		Glu tRNA
tRNA	NITFAB_tRNA27	tRNA	2589815	2589890		Thr tRNA
tRNA	NITFAB_tRNA28	tRNA	2414608	2414684		Ile tRNA
tRNA	NITFAB_tRNA29	tRNA	2414527	2414602		Ala tRNA
tRNA	NITFAB_tRNA3	tRNA	469563	469647		Tyr tRNA
tRNA	NITFAB_tRNA30	tRNA	2410795	2410881		Leu tRNA
tRNA	NITFAB_tRNA31	tRNA	2279241	2279332		Ser tRNA
tRNA	NITFAB_tRNA32	tRNA	2119279	2119369		Ser tRNA
tRNA	NITFAB_tRNA33	tRNA	2004741	2004817		Met tRNA
tRNA	NITFAB_tRNA34	tRNA	2002776	2002852		Ile tRNA
tRNA	NITFAB_tRNA35	tRNA	2002695	2002770		Ala tRNA
tRNA	NITFAB_tRNA36	tRNA	1910664	1910740		Val tRNA
tRNA	NITFAB_tRNA37	tRNA	1663771	1663847		Pro tRNA
tRNA	NITFAB_tRNA38	tRNA	1578123	1578199		Arg tRNA
tRNA	NITFAB_tRNA39	tRNA	1578018	1578093		His tRNA
tRNA	NITFAB_tRNA4	tRNA	469756	469829		Gly tRNA
tRNA	NITFAB_tRNA40	tRNA	1125124	1125199		Asn tRNA
tRNA	NITFAB_tRNA41	tRNA	307277	307353		Met tRNA
tRNA	NITFAB_tRNA42	tRNA	207082	207155		Gly tRNA
tRNA	NITFAB_tRNA5	tRNA	469840	469914		Thr tRNA
tRNA	NITFAB_tRNA6	tRNA	471249	471324		Trp tRNA
tRNA	NITFAB_tRNA7	tRNA	548995	549069		Gln tRNA
tRNA	NITFAB_tRNA8	tRNA	570123	570198		Lys tRNA
tRNA	NITFAB_tRNA9	tRNA	570257	570332		Thr tRNA
Sulfur Metabolism						
Pathway	Label	Type	Begin	End	Gene	Product
Sulfate Import	NITFAB_1675	CDS	1693177	1694232	<i>cysA</i>	sulfate/thiosulfate import ATP-binding protein CysA
Sulfate Import	NITFAB_1676	CDS	1694229	1695110	<i>cysW</i>	sulfate import protein (ABC superfamily, membrane subunit)
Sulfate Import	NITFAB_1677	CDS	1695107	1695937	<i>cysT</i>	sulfate transport protein (ABC superfamily, membrane subunit)
Sulfate Import	NITFAB_1685	CDS	1699887	1700900	<i>sbp</i>	sulfate transporter subunit; periplasmic-binding component of ABC superfamily

Sulfur Assimilation	NITFAB_0850	CDS	880756	882501	<i>sir</i>	assimilatory sulfite reductase (ferredoxin)
Sulfur Assimilation	NITFAB_0852	CDS	883006	883731	<i>cysH</i>	adenylsulfate reductase, thioredoxin dependent
Sulfur Assimilation	NITFAB_0854	CDS	883841	884746	<i>cysD</i>	sulfate adenyltransferase, subunit 2
Sulfur Assimilation	NITFAB_0855	CDS	884749	886002	<i>cysN</i>	sulfate adenyltransferase, subunit 1
Sulfur Assimilation	NITFAB_2037	CDS	2042834	2043718	<i>cysK1</i>	cysteine synthase A, O-acetylserine sulfhydrylase A subunit
Sulfur Assimilation	NITFAB_2043	CDS	2047067	2047954	<i>cysM</i>	cysteine synthase B, O-acetylserine sulfhydrylase B subunit
Sulfur Assimilation	NITFAB_2345	CDS	2348995	2349924	<i>cysK2</i>	cysteine synthase A, O-acetylserine sulfhydrylase A subunit
Sulfite Oxidoreductase	NITFAB_0978	CDS	1012389	1013624	<i>sorA</i>	sulfite:cytochrome c oxidoreductase, subunit A
Sulfite Oxidoreductase	NITFAB_0979	CDS	1013634	1014266	<i>sorB</i>	sulfite:cytochrome c oxidoreductase, subunit B
Prophage						
Pathway	Label	Type	Begin	End	Gene	Product
Predicted functional Prophage	NITFAB_1795	CDS	1796778	1798265		protein of unknown function
Predicted functional Prophage	NITFAB_1796	CDS	1798344	1799444		protein of unknown function
Predicted functional Prophage	NITFAB_1799	CDS	1800230	1802245		membrane protein of unknown function
Predicted functional Prophage	NITFAB_1800	CDS	1802289	1802540		conserved protein of unknown function
Predicted functional Prophage	NITFAB_1801	CDS	1802609	1802917		conserved protein of unknown function
Predicted functional Prophage	NITFAB_1802	CDS	1803010	1803666		putative phage tail protein
Predicted functional Prophage	NITFAB_1806	CDS	1804599	1805543		conserved protein of unknown function
Predicted functional Prophage	NITFAB_1807	CDS	1805555	1805893		putative Phage-related exported protein
Predicted functional Prophage	NITFAB_1808	CDS	1805895	1807187		ClpP class periplasmic serine protease
Predicted functional Prophage	NITFAB_1809	CDS	1807184	1808887		Phage portal protein, lambda family
Predicted functional Prophage	NITFAB_1810	CDS	1808841	1809068		conserved protein of unknown function
Predicted functional Prophage	NITFAB_1811	CDS	1809206	1809511		conserved protein of unknown function
Predicted functional Prophage	NITFAB_1812	CDS	1809504	1809791		conserved protein of unknown function
Predicted functional Prophage	NITFAB_1817	CDS	1811974	1813905		Phage terminase GpA
Predicted functional Prophage	NITFAB_1818	CDS	1813871	1814251		protein of unknown function
Predicted functional Prophage	NITFAB_1820	CDS	1814617	1815180		protein of unknown function
Predicted functional Prophage	NITFAB_1824	CDS	1816266	1816547		conserved membrane protein of unknown function
Predicted functional Prophage	NITFAB_1825	CDS	1816544	1817140		protein of unknown function
Predicted functional Prophage	NITFAB_1827	CDS	1817688	1819391		exported protein of unknown function

Predicted functional Prophage	NITFAB_1832	CDS	1823121	1823621	Uncharacterized endonuclease
Predicted functional Prophage	NITFAB_1835	CDS	1824390	1825679	DNA modification methylase
Predicted functional Prophage	NITFAB_1838	CDS	1826613	1826876	conserved protein of unknown function
Predicted functional Prophage	NITFAB_1840	CDS	1827241	1827798	protein of unknown function
Predicted functional Prophage	NITFAB_1843	CDS	1828936	1831212	DNA primase/helicase, phage-associated
Predicted functional Prophage	NITFAB_1845	CDS	1831477	1831788	conserved protein of unknown function
Predicted functional Prophage	NITFAB_1846	CDS	1832045	1832278	conserved protein of unknown function
Predicted functional Prophage	NITFAB_1848	CDS	1832959	1833237	conserved protein of unknown function

Chapter 3

Cyanate and Urea are Substrates for Nitrification by Thaumarchaeota in the Marine Environment

Katharina Kitzi^{1,2}, Cory C. Padilla³, Hannah K. Marchant^{1*}, Philipp F. Hach¹, Craig W. Herbold², Abiel T. Kidane¹, Martin Kö⁴, Sten Littmann¹, Maria Mooshammer², Jutta Niggemann⁵, Sandra Petrov⁴, Andreas Richter², Frank J. Stewart³, Michael Wagner², Marcel M. M. Kuypers¹, Laura A. Bristow^{1,6}

Author affiliations

¹ Max Planck Institute for Marine Microbiology, Celsiusstrasse 1, 28359 Bremen, Germany

² Department of Microbiology and Ecosystem Science, University of Vienna, Althanstrasse 14, 1090 Vienna, Austria

³ School of Biological Sciences, Georgia Institute of Technology, 311 Ferst Drive, Atlanta GA 30332-0230, USA

⁴ Marine Archaea Group, MARUM – Center for Marine Environmental Sciences & Department of Geosciences, University of Bremen, 28359 Bremen, Germany

⁵ Research Group for Marine Geochemistry (ICBM-MPI Bridging Group), Institute for Chemistry and Biology of the Marine Environment, Carl von Ossietzky University Oldenburg, Carl-von-Ossietzky-Strasse 9-11, 26129 Oldenburg, Germany

⁶ Present address: Department of Biology and Nordic Center for Earth Evolution (NordCEE), University of Southern Denmark, Odense, Denmark

Correspondence: Hannah K. Marchant, hmarchan@mpi-bremen.de

Author Contributions

L.A.B., K.K., H.K.M., M.M.M.K. and M.W. designed the study. K.K., L.A.B. and H.K.M. performed experiments, S.L. and A.K. ran nanoSIMS analyses. K.K., L.A.B., H.K.M. and P.H. analyzed samples and data. C.C.P. sampled for and performed molecular analyses with contribution from C.W.H. and F.J.S. Cyanate concentrations were measured by M.M. and A.R., TDN was analyzed by J.N. Cultures were provided by S.P. and M.K. The manuscript was written by K.K., L.A.B. and H.K.M., with contributions from all co-authors.

Published in Nature Microbiology 2019, 4, 234–243

Abstract

Ammonia-oxidizing archaea of the phylum Thaumarchaeota are among the most abundant marine microorganisms (Francis et al. 2005). These organisms thrive in the oceans despite ammonium being present at low nanomolar concentrations (Martens-Habbena et al. 2009; Horak et al. 2013). Some Thaumarchaeota isolates have been shown to utilize urea and cyanate as energy and N-sources through intracellular conversion to ammonium (Qin et al. 2014; Bayer et al. 2016; Palatinszky et al. 2015). Yet, it is unclear whether patterns observed in culture extend to marine Thaumarchaeota, and whether Thaumarchaeota in the ocean directly utilize urea and cyanate or rely on co-occurring microorganisms to break these substrates down to ammonium. Urea utilization has been reported for marine ammonia-oxidizing communities (Alonso-Saez et al. 2012; Connelly et al. 2014; Tolar et al. 2017; Santoro et al. 2017), but no evidence of cyanate utilization exists for marine ammonia oxidizers. Here, we demonstrate that in the Gulf of Mexico, Thaumarchaeota use urea and cyanate both directly and indirectly as energy and N-sources. We observed substantial and linear rates of nitrite production from urea and cyanate additions, which often persisted even when ammonium was added to micromolar concentrations. Furthermore, single cell analysis revealed that the Thaumarchaeota incorporated ammonium-, urea- and cyanate-derived N at significantly higher rates than most other microorganisms. Yet, no cyanases were detected in thaumarchaeal genomic data from the Gulf of Mexico. Therefore, we tested cyanate utilization in *Nitrosopumilus maritimus*, which also lacks a canonical cyanase, and showed that cyanate was oxidized to nitrite. Our findings demonstrate that marine Thaumarchaeota can use urea and cyanate as both an energy and N-source. Based on these results we hypothesize that urea and cyanate are substrates for ammonia-oxidizing Thaumarchaeota throughout the ocean.

Main text

Nitrification, the stepwise oxidation of ammonia to nitrate, plays a key role linking the most reduced and oxidized species of the nitrogen (N) cycle. In marine systems, the first step of nitrification, ammonia oxidation, is predominantly carried out by ammonia-oxidizing archaea (AOA) belonging to the phylum Thaumarchaeota (Francis et al. 2005; Wuchter et al. 2006). Marine Thaumarchaeota have generally been considered to be metabolically restricted organisms that use ammonia as a substrate for energy generation. However, dissolved organic N (DON, here defined as N-compounds containing at least one C atom) can provide additional substrates for ammonia oxidizers via intracellular conversion of DON to ammonium. The simple DON-compounds urea and cyanate are present ubiquitously in marine systems (Sipler & Bronk 2015; Tolar et al. 2017; Widner et al. 2016; Widner & Mulholland 2017; Widner et al. 2018). From the limited set of measurements available, urea concentrations appear to be of the same order of magnitude as ammonium concentrations, while cyanate concentrations are generally less than 30 % of ammonium (Supplementary Figure 1) (Antia et al. 1991; Sipler & Bronk 2015; Widner et al. 2016; Widner & Mulholland 2017; Widner et al. 2018). Urea is an intracellular metabolite and component of nitrogenous waste from both prokaryotes and eukaryotes and is released during remineralization of organic matter (Antia et al. 1991; Sipler & Bronk 2015), while sources of cyanate include urea, cyanide, and thiocyanate decomposition and photoproduction (Dirnhuber & Schütz 1948; Widner et al. 2016). Some marine Thaumarchaeota cultures have been shown to encode a urease (e.g. Bayer et al. 2016; Qin et al. 2014), and there is evidence that marine thaumarchaeal communities use urea as an alternative energy source (Alonso-Saez et al. 2012; Connelly et al. 2014; Tolar et al. 2017; Santoro et al. 2017). To date however, only one Thaumarchaeon, the terrestrial *Nitrososphaera gargensis*, has been shown to encode a cyanase, which seems to have been acquired via lateral gene transfer (Palatinszky et al. 2015). Cyanate

utilization by nitrifiers has not been investigated so far in the marine environment, even though ammonia oxidation has been hypothesized to be a main factor shaping cyanate concentration profiles (Widner et al. 2016; Widner & Mulholland 2017).

The continental shelves are regions with high ammonia oxidation rates, which sustain the nutrient turnover that drives disproportionately high primary production in these regions, which despite their small surface area, account for 20 to 30 % of total marine primary productivity (Liu et al. 2010). We aimed to assess whether Thaumarchaeota supplement their ammonia requirement in the continental shelf waters of the Gulf of Mexico by utilizing urea and cyanate. Furthermore, we investigated whether the Thaumarchaeota were directly utilizing urea and cyanate, or whether they were relying on co-occurring microorganisms to break down these substrates to ammonium and therefore utilizing them indirectly. During a cruise in 2016 to the GoM, bottom waters were hypoxic ($< 63 \mu\text{mol kg}^{-1}$ dissolved oxygen) due to summertime eutrophic conditions, which recur yearly (Rabalais et al. 2001) (Figure 1a and Supplementary Figure 2). Ammonium, urea, and cyanate were present at variable concentrations in the water column along the entire east-west sampling transect and were generally highest in the hypoxic bottom waters. The median ammonium, urea and cyanate concentrations were 320 nM, 69 nM and 11.5 nM, respectively. The ratios of these three N-compounds fell in the range observed across other shelf regions (Figure 1b and Supplementary Figure 1, 3) (Antia et al. 1991; Sipler & Bronk 2015; Tolar et al. 2017; Widner et al. 2016; Widner & Mulholland 2017; Widner et al. 2018). The median concentration of total DON was 12,100 nM (Supplementary Figure 3), similar to previous measurements in the GoM and other shelf regions (Sipler & Bronk 2015). These compounds could therefore all potentially serve as energy and N-sources for microorganisms in the GoM.

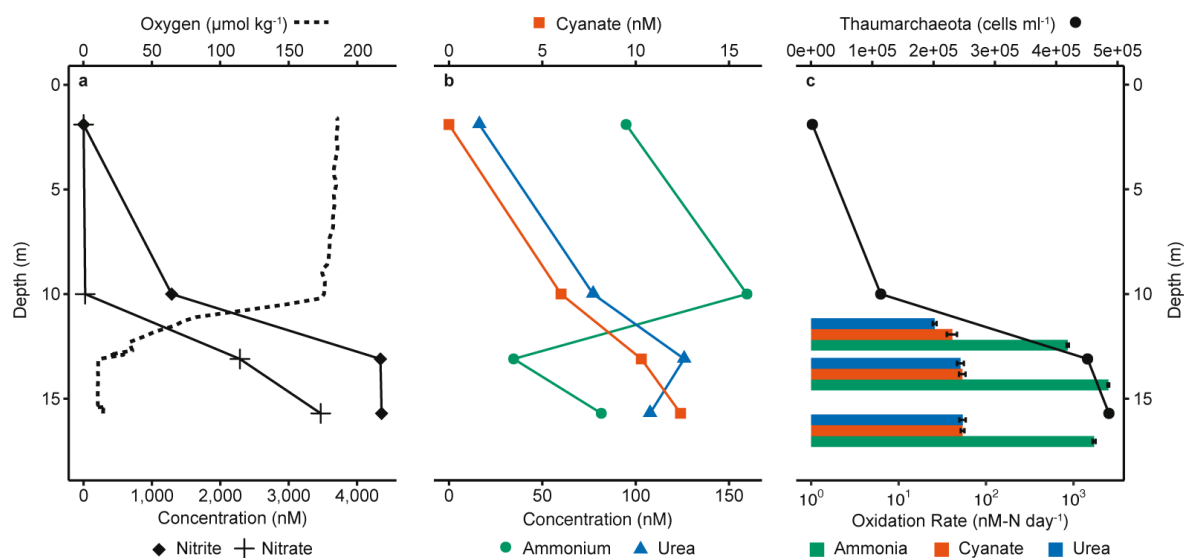


Figure 1 Depth distribution of nutrient and oxygen concentrations, Thaumarchaeota cell counts and oxidation rates from Station 2. a) Nitrite, nitrate and oxygen concentrations. b) Ammonium, urea and cyanate concentrations. c) Thaumarchaeota depth distribution based on CARD-FISH counts and measured ammonia and urea- and cyanate-derived oxidation rates (without added ^{14}N -ammonium), calculated from slopes across all time points and triplicate incubations. Oxidation rates are depicted on a log-axis. Rate experiments were carried out at 12 m, 14 m and 16.5 m. Error bars for rates represent standard errors of slopes calculated across all biological triplicates and all timepoints. All rates were significant (see Supplementary Table 1). Thaumarchaeota abundance was determined from CARD-FISH counts (n for DAPI-stained / Thaumarchaeota cells = 9,247 / 7; 13,296 / 389; 17,253 / 1,541; 16,770 / 1,660 from 1.7 m, 10.1 m, 13.0 m and 15.7 m depth, respectively). Data from an additional 2 stations are shown in Figure 2 d-f and Supplementary Figure 3, 4 and 8.

Thaumarchaeota have previously been identified as the dominant ammonia oxidizers in the GoM (Tolar et al. 2013; Bristow et al. 2015); this was also the case in summer 2016, when Thaumarchaeota cell counts (determined by CARD-FISH) were up to 4.9×10^5 cells ml⁻¹, approximately 10 % of total cell counts (Figure 1c, Supplementary Figure 4, Supplementary Discussion). 16S rRNA gene amplicon sequencing confirmed that Thaumarchaeota were the only detectable ammonia oxidizers in the GoM, with reads clustering primarily into one operational taxonomic unit (OTU, 97% sequence similarity cluster). This OTU was closely related to *Nitrosopumilus sp.*, which previous 16S-based approaches have revealed to be a dominant ammonia oxidizer in continental shelf waters (Woebken et al. 2007; Galand et al. 2010; Liu et al. 2018, Supplementary Figure 5). Using metagenomic sequencing, we generated six Thaumarchaeota metagenome-assembled genomes (MAGs). Four of these were more than 90% complete, with the most abundant MAGs branching confidently with *Nitrosopumilus sp.* and *Nitrosomarinus sp.* in a phylogenetic analysis based on 34 single-copy marker genes (Supplementary Figure 6, Supplementary Table 2). Furthermore, five of the MAGs contained *amoA*, the gene encoding the structural subunit of ammonia monooxygenase (see Supplementary Table 2). We also investigated *amoA* transcription; all *amoA* transcripts retrieved from metatranscriptomes were phylogenetically affiliated with Thaumarchaeota and also clustered with the obtained MAGs (Supplementary Figure 7).

The use of ammonia, urea and cyanate as energy sources was investigated using ¹⁵N¹³C-tracer incubations at three depths and three stations. Upon addition of ¹⁵N-ammonium, we observed linear production of ¹⁵N-nitrite over time in the dark under *in situ* oxygen and temperature conditions. Ammonia oxidation rates ranged between 80 – 2,500 nM-N d⁻¹ (Figure 1c, Figure 2, Supplementary Figure 8), comparable to rates previously measured in the region (Carini et al. 2010; Bristow et al. 2015) and in other shelf and oxygen-depleted systems (Ward 2008; Lam et al. 2009; Tolar et al. 2017). Although all of the measured rates are potential rates due to the addition of ¹⁵N-tracers, the short length of the incubations (< 24h) and the linearity of the rates from the beginning indicate that the ammonia oxidizers were active *in situ*. Moreover, rates showed a strong positive correlation with *in situ* nitrite concentrations (Figure 2d), indicating that ammonia oxidation is a major determinant of nitrite concentration in the GoM.

Significant and linear production of ¹⁵N-nitrite was also observed after addition of ¹⁵N¹³C-urea or ¹⁵N¹³C-cyanate. The maximum rates measured were similar for both compounds (up to 54 nM-N d⁻¹), although rates varied between stations and depths (Figure 1c and Figure 2, Supplementary Figure 8). The measured urea-derived oxidation rates are in the range of those previously reported from the marine environment (see Supplementary Discussion for per cell rates) (Tolar et al. 2017; Santoro et al. 2017). Until now there were no nitrifier-associated cyanate-derived oxidation rates from the marine environment. Urea- and cyanate-derived oxidation rates constituted up to 7% and 10%, respectively, of the measured ammonia oxidation rates (Figure 1c, and Figure 2, Supplementary Figure 8) and showed a strong positive correlation with ammonia oxidation rates (Figure 2e, 2f).

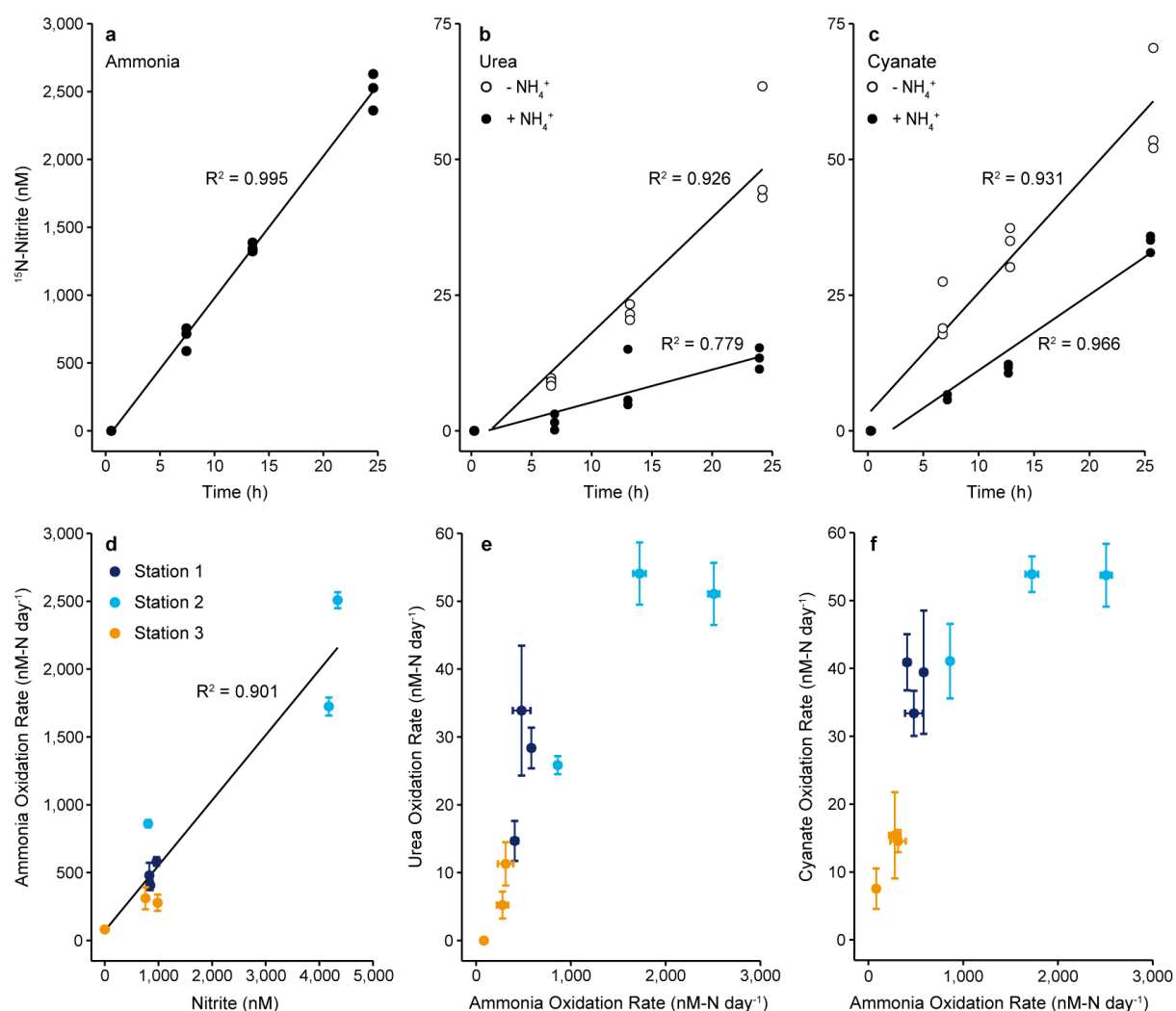


Figure 2 Production of ^{15}N -nitrite over time and correlations between rates obtained from various substrate additions. Upper panels: ^{15}N -nitrite concentration over time after addition of a) ^{15}N -ammonium, b) ^{15}N -urea, and c) ^{15}N -cyanate without (open circles) and with (filled circles) added ^{14}N -ammonium (5 μM) at Station 2, 14 m depth. Data points represent biological triplicates. Lower panels: Correlations between d) ammonia oxidation rate and *in situ* nitrite concentration, e) ammonia oxidation rate and urea-derived oxidation rate, and f) ammonia oxidation rate and cyanate-derived oxidation rate (from incubations without added ^{14}N -ammonium). Black lines in panels a) – d) are linear regressions, R^2 was calculated based on Pearson Correlations, and was significant in all analyses (a-c), one-sided t-test; a) $t = 42.66$, $\text{DF} = 10$, $p = 1.20 \times 10^{-13}$, b) $t = 11.184$, $\text{DF} = 10$, $p = 5.65 \times 10^{-7}$ and $t = 5.931$, $\text{DF} = 10$, $p = 1.45 \times 10^{-4}$ for urea without and with added ammonium, respectively, c) $t = 11.634$, $\text{DF} = 10$, $p = 3.91 \times 10^{-7}$ and $t = 16.935$, $\text{DF} = 10$, $p = 1.08 \times 10^{-8}$ for cyanate without and with added ammonium, respectively, d) two-sided t-test; $t = 8.002$, $\text{DF} = 7$, $p = 9.10 \times 10^{-5}$. For panels e) and f), Spearman rank correlations were calculated and were significant for both e) $S = 10$, $\rho = 0.917$, $p = 0.001$ and f) $S = 10$, $\rho = 0.917$, $p = 0.001$. Error bars in panels (d-f) represent standard errors of slopes calculated across all biological triplicates and all timepoints.

In principle, the production of ^{15}N -nitrite from additions of $^{15}\text{N}^{13}\text{C}$ -urea or $^{15}\text{N}^{13}\text{C}$ -cyanate could indicate both direct and indirect utilization of these substrates by Thaumarchaeota. Indirect utilization could result from either abiotic or biotic breakdown of urea and cyanate. In water, abiotic urea and cyanate breakdown to ammonium and carbon dioxide can occur through a temperature and pH dependent process (Dirnhuber & Schütz 1948; Palatinszky et al. 2015; see Supplementary Discussion) and the resulting ammonium can subsequently be used by microorganisms. The measured abiotic breakdown rates of urea to ammonium were insignificant in GoM seawater, and

cyanate breakdown was minor (Supplementary Table 3 and Supplementary Discussion). Alternatively, other microorganisms might intracellularly break down urea or cyanate to carbon dioxide and ammonium (biotic breakdown), which is subsequently released to the environment and used by Thaumarchaeota. Such cross-feeding has been demonstrated in co-culture experiments with urea- and cyanate-degrading nitrite oxidizers and ammonia-oxidizing bacteria (Palatinszky et al. 2015; Koch et al. 2015). In our experiments, breakdown of urea and cyanate would progressively increase the amount of ^{15}N in the extracellular ammonium pool, which would lead to exponential production of ^{15}N -nitrite from ammonia oxidation over time in the case of indirect utilization.

We quantified how much of the observed nitrite production could be assigned to direct substrate utilization by Thaumarchaeota or to the breakdown of urea and cyanate into the extracellular ammonium pool by biotic or abiotic breakdown (indirect utilization). We ran parallel incubations which were identical except for the addition of a large ^{14}N -ammonium pool (ammonium pool incubations). These were intended to reduce the likelihood that ^{15}N -ammonium formed from biotic or abiotic breakdown of urea or cyanate, would be oxidized to ^{15}N -nitrite by Thaumarchaeota. In the ammonium pool incubations, the rates of ^{15}N -nitrite production were still linear, although they were lower than those in the incubations without added ^{14}N -ammonium (Figure 2b, 2c, Supplementary Figure 9). We could observe the production of ^{15}N -ammonium in the ammonium pool incubations, some of which was still oxidized to ^{15}N -nitrite, due to the high ammonia oxidation rates (indirect utilization). However, by quantifying the amount of ^{14}N and ^{15}N -ammonium at each time point and combining this with the known ammonia oxidation rates, we were able to calculate the proportion of ^{15}N -nitrite production that could have stemmed from indirect utilization of ^{15}N -urea or ^{15}N -cyanate. Thereby, we were able to quantify the direct utilization rates and can confidently show that there were significant rates of ^{15}N -nitrite production as a result of direct utilization (up to 9.9 nM d^{-1} , Supplementary Table 3, Supplementary Figure 10). These rates are likely to be underestimations, as it is possible that the Thaumarchaeota utilized less urea and cyanate in response to the large ammonium addition in the ammonium pool incubations.

We used nanoSIMS to determine the incorporation of ammonium, urea and cyanate into Thaumarchaeota cells in the GoM, which enabled us to gain insights into metabolic heterogeneity within the Thaumarchaeota community at a single cell level. All measured Thaumarchaeota cells ($n=58$) incorporated ^{15}N from ammonium (average $14.4 \text{ amol-N cell}^{-1} \text{ d}^{-1}$) and ^{13}C from bicarbonate (average $19.8 \text{ amol-C cell}^{-1} \text{ d}^{-1}$) and were significantly more enriched than the surrounding microorganisms (Figure 3, Mann-Whitney U test, $p < 0.01$). Thaumarchaeota also assimilated ^{15}N from urea (29 of 30 measured cells) and cyanate (all measured cells, $n=47$). Rates of N assimilation from urea and cyanate were up to two orders of magnitude lower (average $0.72 \text{ amol-N cell}^{-1} \text{ d}^{-1}$ urea and $0.64 \text{ amol-N cell}^{-1} \text{ d}^{-1}$ cyanate) than rates of N-assimilation from ammonium, but significantly higher than those of surrounding cells (Figure 3, Mann-Whitney U test, $p < 0.01$). Average bulk rates of assimilation by Thaumarchaeota in the GoM were 6.0 nM-N d^{-1} for ammonium, 0.3 nM-N d^{-1} for urea and 0.3 nM-N d^{-1} for cyanate. Thaumarchaeota assimilation of ^{15}N from urea was more heterogeneous than from ammonium and cyanate, with some cells showing a distinctly higher enrichment of ^{15}N from urea compared to others (Figure 3, Supplementary Figure 11). We could not detect any ^{13}C -incorporation from additions of $^{15}\text{N}^{13}\text{C}$ -urea or $^{15}\text{N}^{13}\text{C}$ -cyanate. This is likely due to a combination of the small amount of ^{13}C - CO_2 produced from urea and cyanate degradation and strong dilution by the 2 mM ambient dissolved inorganic carbon (DIC). Although this nanoSIMS analysis cannot distinguish between direct and indirect assimilation, the data show that most Thaumarchaeota cells were active and metabolically versatile, using urea and cyanate as additional N-sources.

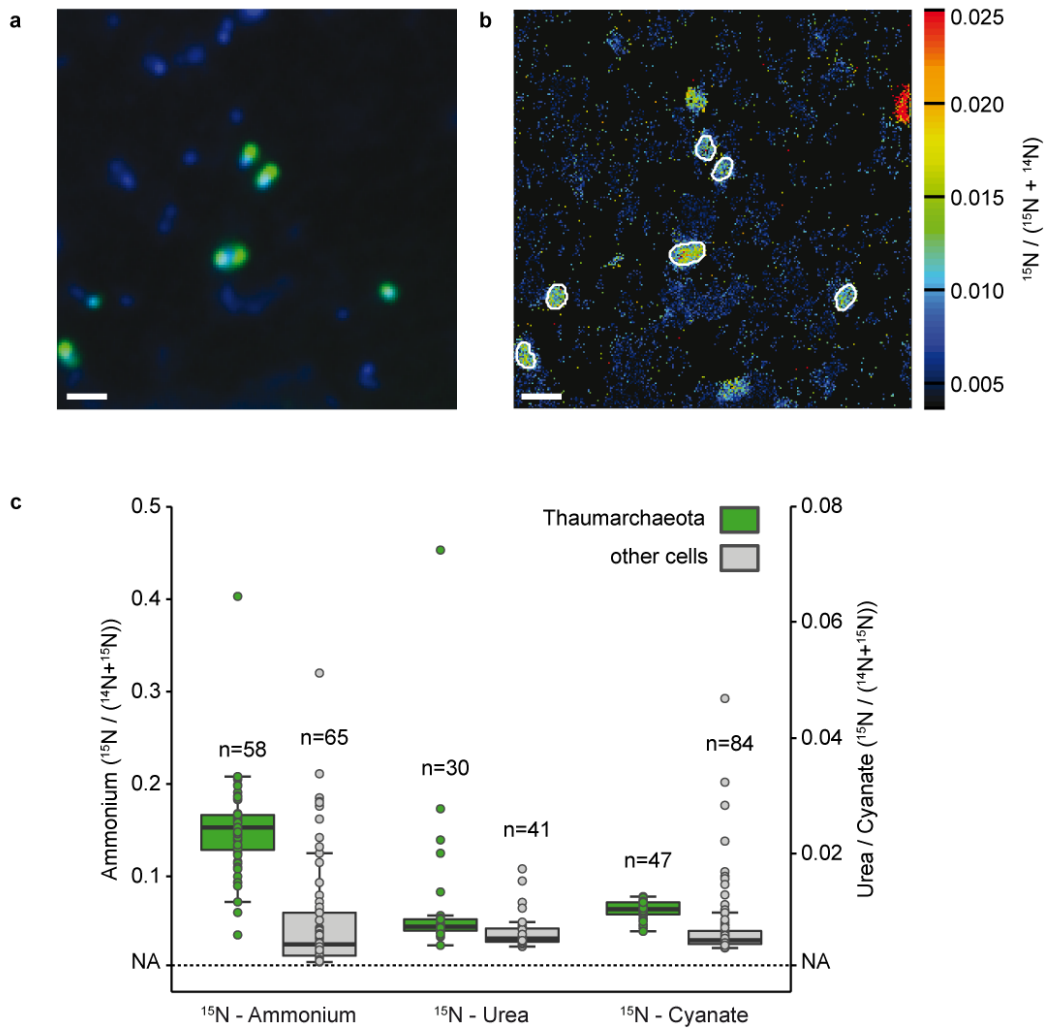


Figure 3 Thaumarchaeota single cell ammonium, urea and cyanate uptake determined by nanoSIMS at Station 2, 14m depth. a) Representative CARD-FISH image of Thaumarchaeota (green; counterstained by DAPI, blue) with a specific probe (Thaum726). b) corresponding nanoSIMS image of $^{15}\text{N}/(^{14}\text{N}+^{15}\text{N})$ enrichment after addition of ^{15}N -cyanate. Thaumarchaeota are marked by white outlines. Scale bar is 1 μm . In total, 9, 6 and 8 fields of view were analyzed by nanoSIMS for the ^{15}N -cyanate, ^{15}N -ammonium and ^{15}N -urea treatment. c) $^{15}\text{N}/(^{14}\text{N}+^{15}\text{N})$ enrichment of Thaumarchaeota (green) and non-targeted cells (grey) after incubation with ^{15}N -ammonium (left), ^{15}N -urea (middle, without added ^{14}N -ammonium) or ^{15}N -cyanate (right, without added ^{14}N -ammonium). Note the different scales for ^{15}N -ammonium and ^{15}N -urea and ^{15}N -cyanate, respectively. Number of cells analyzed per category is indicated above each boxplot. Boxplots depict the 25 – 75 % quantile range, with the center line depicting the median (50% quantile); whiskers encompass data points within $1.5 \times$ the interquartile range. NA is the natural abundance $^{15}\text{N}/(^{14}\text{N}+^{15}\text{N})$ value (0.0037). Four non-Thaumarchaeota cell values in the ^{15}N -urea treatment are not depicted and have $^{15}\text{N}/(^{14}\text{N}+^{15}\text{N})$ values of 0.326, 0.095, 0.118 and 0.139, these cells were included in all calculations. More ammonium was assimilated than urea and cyanate by the Thaumarchaeota, and the Thaumarchaeota assimilated significantly more ^{15}N compared to surrounding cells in all treatments (one-sided Mann-Whitney U Test, $U = 3348.5$, $p = 6.19 \times 10^{-14}$; $U = 873$, $p = 0.001$; $U = 3409$, $p = 2.91 \times 10^{-12}$ for ammonium, urea and cyanate, respectively).

Using the nanoSIMS results, we calculated single cell N-based growth rates for Thaumarchaeota of 0.23 ± 0.012 (SE) d^{-1} for ammonium, similar to previous measurements in marine systems ($0.21 - 0.47 \text{ d}^{-1}$, Alonso-Saez et al. 2012; Herndl et al. 2005) and in enrichments or pure cultures (Wuchter et al. 2006; Qin et al. 2014). This ammonium growth was supplemented by urea- and cyanate-based growth (0.011 ± 0.0035 (SE) d^{-1} and 0.009 ± 0.0003 (SE) d^{-1} , respectively). Interestingly, ^{13}C -DIC-based

growth rates were about 6-fold lower than ammonium-based growth rates (0.04 ± 0.005 (SE) d^{-1}). This could be an artifact due to the small size of the Thaumarchaeota (see methods) or could indicate that Thaumarchaeota in the GoM did not meet all of their C-demand from autotrophic C-fixation. However, more work is required to resolve this. The single cell uptake and growth rates provide further evidence that Thaumarchaeota in the GoM have the capability to use N from urea and cyanate, directly or indirectly, in addition to ammonium, however, they seem to do so at lower rates compared to when using ammonium.

To examine how Thaumarchaeota in the GoM might be utilizing urea and cyanate, we screened both the metagenome assemblies and the Thaumarchaeota MAGs for ureases (*ureC*) and cyanases (*cynS*), the enzymes responsible for intracellular breakdown of urea and cyanate to ammonia, respectively. Detected *ureC* sequences were very diverse (Supplementary Figure 12), with 10.2 % associated with *Thaumarchaeota*. Based on the recovery of thaumarchaeal *ureC* versus thaumarchaeal 16S rRNA genes and *amoA* genes, we estimated that approximately 10-15% of Thaumarchaeota cells contain a urease, which is similar to the ratio reported previously for coastal Georgia (Tolar et al. 2017). Of the metagenomic *ureC* identified, 1.1% could be assigned to GoM MAG1 (putatively assigned to the genus *Nitrosopelagicus*, Figure 4a and Supplementary Figure 6) while others were related to the genus *Nitrosopumilus* (Supplementary Figure 12) but did not bin into one of the six almost complete MAGs. These ureases were similar to those identified in coastal Georgia (Tolar et al. 2017), many of which were related to *Nitrosopumilus sediminis* strain AR2. The transcribed ureases were also diverse, with 5.9 % of *ureC* transcripts associated with Thaumarchaeota and clustering either with GoM MAG1 or *Nitrosopumilus* related *ureC* sequences (Supplementary File 1-6). Metagenomic analyses therefore indicated that only a sub-population of Thaumarchaeota in the GoM have known ureases, consistent with the single-cell observation that some Thaumarchaeota cells assimilated significantly more N from urea than others (Figure 3, Supplementary Figure 11).

We could not assign any meta-omics *cynS* sequences to *Thaumarchaeota*, and no sequences related to cyanases were detected in the Thaumarchaeota MAGs (Supplementary Figure 13). To reconcile this result with the indications that cyanate was utilized directly in the GoM, we examined cyanate utilization in four cultures of *Nitrosopumilus maritimus* SCM1. Identifiable cyanases are absent from the genome of *Nitrosopumilus maritimus* SCM1, and from the genomes available for other marine Thaumarchaeota (Figure 4a). However, when we incubated *Nitrosopumilus maritimus* with $^{15}N^{13}C$ -cyanate, we observed production of ^{15}N -nitrite. This production occurred at much higher rates than could be accounted for by abiotic breakdown of cyanate to ammonium (Figure 4b). Interestingly, we observed linear ^{15}N -ammonium production in all four cultures, which was far above the abiotic breakdown rate. When this production rate was taken into account in a modelling approach similar to that used above, it appears that almost all of the cyanate utilized by the Thaumarchaeota cultures could have entered the extracellular ammonium pool prior to oxidation (Supplementary Figure 14). This could suggest that cyanate breakdown by Thaumarchaeota occurs extracellularly, or that there was equilibration between intra- and extracellular ammonium pools (see Supplementary Discussion). These results indicate that *Nitrosopumilus maritimus* is capable of utilizing cyanate, even though it does not have a canonical cyanase. Currently, the biochemical pathway involved in cyanate utilization is unclear.

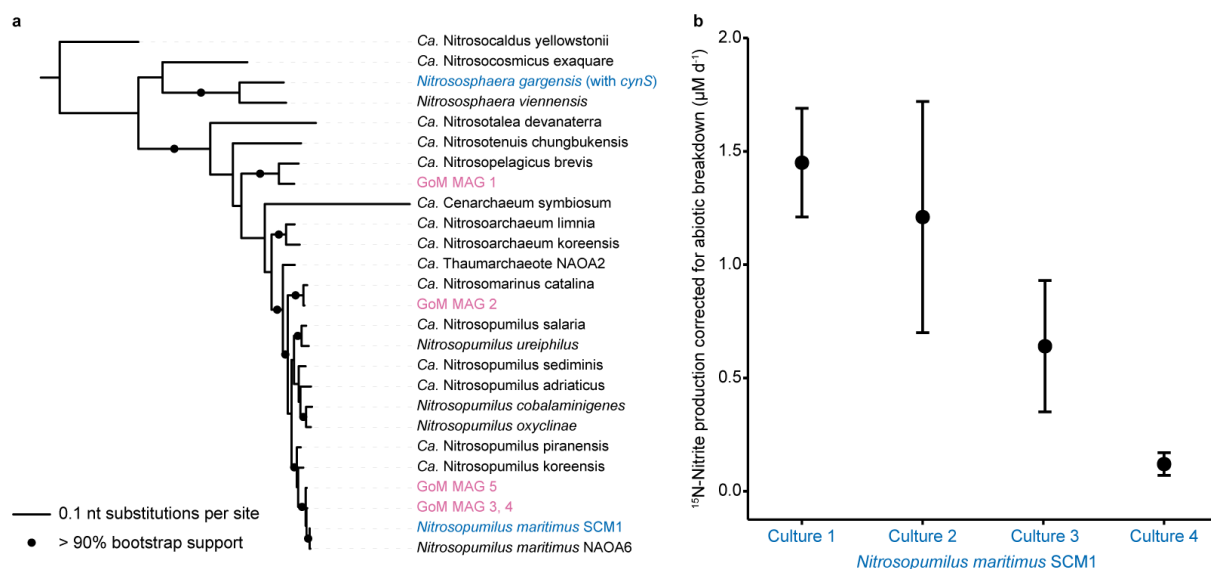


Figure 4 *amoA* based phylogeny of Thaumarchaeota MAGs recovered in this study and cyanate utilization by the marine Thaumarchaeon *Nitrosopumilus maritimus*. a) Phylogenetic placement of the *amoA* sequences from Gulf of Mexico metagenome assembled genomes (GoM MAGs, magenta) and Thaumarchaeota cultures that are able to utilize cyanate (blue). *N. gargensis* is the only Thaumarchaeon that encodes a known cyanase. Reference Thaumarchaeota *amoA* sequences are shown in black. Tree was constructed using IQ-TREE (Nguyen et al. 2015) with automated model selection from near full-length *amoA* sequences and confidence was assessed with ultrafast bootstrapping (1,000 iterations). The scale bar represents nt substitutions per site, bootstrap support values >90% are depicted. b) ^{15}N -nitrite production rate by the marine Thaumarchaeon *N. maritimus* SCM1 incubated with ^{15}N -cyanate and a ^{14}N -ammonium pool, corrected for abiotic breakdown of cyanate to ammonium in the culture medium. Error bars are the standard errors of the slope across all time points of one biological replicate. Rates were calculated based on linear regressions (one-sided t-test, $t = 6.13$, $DF = 2$, $p = 0.012$; $t = 2.38$, $DF = 2$, $p = 0.070$; $t = 2.22$, $DF = 2$, $p = 0.078$; $t = 3.72$, $DF = 2$, $p = 0.033$, for culture 1, 2, 3 and 4, respectively). When data were fitted with an exponential regression, p was < 0.001 for all four cultures. Differences in rates between biological replicates correlate with the different starting biomass in each culture.

Until recently, marine Thaumarchaeota were considered to be metabolically restricted organisms that only use ammonia as a substrate for energy conservation (Tolar et al. 2017; Santoro et al. 2017). Here we show that in the GoM, Thaumarchaeota can use urea and cyanate to supplement their N- and energy requirements. The presence and transcription of urease in a sub-population of the Thaumarchaeota, combined with the single cell uptake data and rate determinations, suggest that part of the Thaumarchaeota community directly utilize urea as a substrate. Similar evidence was obtained for cyanate utilization; however, we could not detect Thaumarchaeota cyanases. In fact, no known marine Thaumarchaeota have an identifiable cyanase. Yet, we show that *Nitrosopumilus maritimus*, which is closely related to GoM Thaumarchaeota, can oxidize cyanate to nitrite. This indicates that cyanate can be utilized by marine Thaumarchaeota from distinct geographical regions, even when known cyanases cannot be detected. Considering that the GoM has ratios of cyanate, urea and ammonium typical of shelf regions (Supplementary Figure 1, Sipler & Bronk 2015; Tolar et al. 2017; Widner et al. 2016; Widner & Mulholland 2017; Widner et al. 2018) and a thaumarchaeal community representative of continental shelves (Woebken et al. 2007; Galand et al. 2010; Liu et al. 2018), the use of urea and cyanate to supplement N-requirements could be a widespread trait. In the oligotrophic gyres where ratios of DON to ammonium are higher relative to the shelf seas (Antia et al. 1991), we hypothesize that urea and cyanate are also important substrates for ammonia oxidizers.

Materials and Methods

Sampling

Sampling took place on the Louisiana Shelf in the northern Gulf of Mexico aboard the *R/V Pelican*, cruise PE17-02, from July 23rd to August 1st, 2016, spanning a west-east transect from 92°48'4" W to 90°18'7" W. Seawater was collected in 20 L Niskin bottles on a rosette equipped with a CTD and SBE 43 oxygen sensor. Nutrient profiles spanning the water column (surface water to water-sediment interface at max. 19 m) were determined at nine stations. Process rate measurements, molecular and FISH analyses were carried out at three of the nine stations (Supplementary Figure 2).

Nutrient analyses

Ammonium concentrations were measured in unfiltered seawater samples to avoid sample contamination by the filtration process (Supplementary Discussion and Supplementary Figure 15). For all other nutrient measurements, seawater was prefiltered using 0.22 µm PES syringe filters (Millex, Millipore, Supplementary Discussion and Supplementary Figure 15). Ammonium concentrations were measured fluorometrically by the orthophthaldialdehyde method (limit of detection (LOD) 10 nM in a 1 cm cuvette) (Holmes et al. 1999). Nitrite (LOD 50 nM in a 1 cm cuvette) and urea (LOD 30 nM in a 10 cm cuvette) concentrations were measured photometrically onboard using the Griess and diacetylmonoxime methods respectively (Grasshoff et al. 1999; Mulvenna & Savidge 1992). Samples for cyanate concentration measurements (LOD 1.5 nM) were derivatized onboard and stored at -20°C until return to the laboratory, where samples were stored at -80°C until analysis using high performance liquid chromatography (Dionex, ICS-3000 system coupled to fluorescence detector, Thermo Scientific, Dionex Ultimate 3000) (Widner et al. 2013). Samples for nitrate measurements (LOD 50 nM) were stored at -20°C and concentrations were determined upon return with a chemiluminescence NO/NO_x analyzer after reduction to NO with acidic vanadium (II) chloride (Braman & Hendrix 1989). Samples for total dissolved nitrogen (TDN) concentrations were filtered through pre-combusted GF/F filters (Whatman) in HCl-cleaned filter holders by gravity filtration from Niskin bottles, acidified with HCl and subsequently stored at 4°C in the dark until measurement by chemiluminescence (Shimadzu TOC-VCPh) (Seidel et al. 2017). Dissolved organic nitrogen (DON) was calculated by subtraction of measured ammonium, nitrite and nitrate concentrations.

Process rate experiments

Process rate measurements were carried out as described in Bristow *et al.* (2015) and were determined at three stations at three depths in and below the oxycline (Supplementary Figure 2, 8). Water was sampled directly from the Niskin bottle into 250 ml serum bottles, which were sealed bubble-free with deoxygenated butyl rubber stoppers (De Brabandere et al. 2012). Bottles were stored at *in situ* temperature (28°C) in the dark until the start of the experiments (< 7 h after sampling). Exposure to natural light during sampling was minimized and all further handling took place under red light to prevent assimilation by phytoplankton.

For each amendment and depth, tracer was added to triplicate serum bottles. Amendments were designed to test for ammonia (¹⁵NH₄⁺), urea (¹⁵N¹³C-urea)- and cyanate (¹⁵N¹³C-cyanate)-derived oxidation rates (Supplementary Table 5) and were made as 5 µM additions. Additionally, in ammonia oxidation experiments, 200 µM ¹³C-bicarbonate (DIC) was added. Abiotic breakdown of urea and cyanate to ammonium was determined upon return, using sterile filtered bottom water from Station 1, and its potential contribution to the observed oxidation rates was calculated (see Supplementary Discussion). To further test the contribution of biotic and abiotic breakdown of urea

and cyanate and subsequent use of the resulting extracellular ^{15}N -ammonium by ammonia oxidizers, additional ammonium pool incubations with a ^{14}N -ammonium amendment (5 μM) were performed to dilute any extracellular ^{15}N -ammonium formed (see Supplementary Discussion).

$^{15}\text{N}^{13}\text{C}$ -tracer solutions and ^{14}N -pools (Supplementary Table 5) were added using gas tight syringes (Hamilton). Pre-weighed aliquots of $^{15}\text{N}^{13}\text{C}$ -tracers were dissolved in sterile filtered seawater just before the start of every experiment to minimize abiotic breakdown. After tracer amendments and subsequent gentle shaking for approximately 10 seconds, a volume of 40 ml was removed and replaced with helium (He). The headspaces were then flushed with He twice, before adding pure oxygen according to Garcia and Gordon (1992) to match *in situ* oxygen concentrations. Triplicate serum bottles per depth contained optode spots (Firesting, Pyroscience), enabling us to monitor oxygen concentrations, which remained within 20% of *in situ* concentrations throughout the experiment. The removed 40 ml were sterile filtered (0.22 μm , PES, Q-Max, Frisette ApS) and stored at -20°C as time zero samples. The amended ^{15}N -tracer concentrations were determined by concentration measurements and subtraction of *in situ* values. For determination of ^{13}C -DIC labeling percentage, unfiltered samples were filled bubble-free into exetainers (Labco, UK) and preserved with saturated mercury(II) chloride solution (50 μl per 6 ml sample). After sampling, serum bottles were incubated in a recirculated water bath at *in situ* temperature (28°C), in the dark. After 6 h, 12 h and 24h, 20 ml of seawater was sampled and replaced with He. Samples were sterile filtered and frozen. Serum bottle headspaces were flushed with He twice and oxygen was added to match *in situ* concentrations as before. After 24 h, the remaining seawater of triplicates was combined, and 20 ml were fixed and filtered onto 0.22 μm GTTP filters for FISH and 0.22 μm gold sputtered GTTP filters for nanoSIMS, respectively.

^{15}N -rate measurements and determination of ^{13}C -DIC labeling percentage

Ammonia, urea- and cyanate-derived oxidation rates were determined from ^{15}N -nitrite increase over time. Nitrite was converted to N_2 with sulfamic acid (Füssel et al. 2012) and $^{29}\text{N}_2$ was measured by gas-chromatography isotope ratio mass spectrometry (GC-IRMS) on a customized TraceGas coupled to a multicollector IsoPrime100 (Manchester, UK). Abiotic breakdown rates of $^{15}\text{N}^{13}\text{C}$ -urea and $^{15}\text{N}^{13}\text{C}$ -cyanate to ^{15}N -ammonium were measured according to Zhang *et al.* (2007), combining hypobromite oxidation of ammonium to nitrite and subsequent neutralization by HCl before reduction to N_2 by sulfamic acid (see section below). All rates were inferred from the slopes of linear regressions across all time points and replicates and were corrected for initial ^{15}N -labeling percentage. Only slopes that were significantly different from zero are reported ($p < 0.05$, one-sided Student t-test). Non-significant regressions are reported as not detected rates. Initial ^{13}C -DIC labeling percentages were determined after acidification (Torres et al. 2005) by $^{13}\text{C}\text{-CO}_2/^{12}\text{C}\text{-CO}_2$ measurements using cavity ring-down spectroscopy (G2201-i coupled to a Liaison A0301, Picarro Inc., Santa Clara, USA, connected to an AutoMate Prep Device, Bushnell, USA).

Hypobromite conversions for ^{15}N -ammonium measurement in cyanate and urea samples

^{15}N -ammonium concentrations in samples containing $^{15}\text{N}^{13}\text{C}$ -urea and $^{15}\text{N}^{13}\text{C}$ -cyanate were determined following a modified protocol from Zhang *et al.* (2007) where ammonium was oxidized to nitrite by hypobromite, and subsequently converted to N_2 by sulfamic acid (Füssel et al. 2012). This method minimizes concurrent conversion of urea and cyanate (see below). After hypobromite conversion and sodium arsenite addition, the sample pH must be set to pH 8-9 by addition of 6 N HCl. This step is crucial because a too acidic pH results in spontaneous oxidation of nitrite to nitrate and a too basic pH interferes with the subsequent reduction of nitrite to N_2 by sulfamic acid (Granger & Sigman 2009). After sulfamic acid conversion of nitrite to N_2 , $^{29}\text{N}_2$ was measured on a customized

TraceGas Isotope Ratio Mass Spectrometer (TraceGas IRMS) coupled to a multicollector IsoPrime100 (Manchester, UK). Detection limits were estimated from the median of the standard error of the slope, multiplied by the t value for $p = 0.05$.

We did not remove the ^{15}N -nitrite prior to hypobromite conversion, and therefore measured combined ^{15}N -ammonium + ^{15}N -nitrite. Prior nitrite removal was omitted because this requires a sulfamic acid conversion, which is carried out at low pH. Low pH leads to increased abiotic decay of cyanate to ammonium (Palatinszky et al. 2015), which impedes subsequent accurate ^{15}N -ammonium measurement. To obtain ^{15}N -ammonium values, we measured ^{15}N -nitrite (following the method of Füssel *et al.* 2012) in a separate sample aliquot and subtracted the obtained ^{15}N -nitrite values from the combined ^{15}N -ammonium + ^{15}N -nitrite values.

For all hypobromite conversions, freshly prepared $^{15}\text{N}^{13}\text{C}$ -urea and $^{15}\text{N}^{13}\text{C}$ -cyanate standards were converted concurrently. Across conversions, only minor proportions of $^{15}\text{N}^{13}\text{C}$ -urea-N ($0.42\% \pm 0.06\%$) and $^{15}\text{N}^{13}\text{C}$ -cyanate-N ($0.14\% \pm 0.03\%$) were converted to $^{29}\text{N}_2$. This $^{29}\text{N}_2$ can either stem from a minor ^{15}N -ammonium contamination of the stocks, or from direct conversion of $^{15}\text{N}^{13}\text{C}$ -urea and $^{15}\text{N}^{13}\text{C}$ -cyanate during the hypobromite protocol. While we did not detect ammonium based on concentration measurements in $^{15}\text{N}^{13}\text{C}$ -urea stocks, we did detect a minor ammonium contamination in $^{15}\text{N}^{13}\text{C}$ -cyanate stocks, corresponding to the $^{29}\text{N}_2$ measured in hypobromite conversions of cyanate standards. Therefore, we assume that the $^{29}\text{N}_2$ detected in hypobromite conversions of $^{15}\text{N}^{13}\text{C}$ -urea does not represent actual ammonium contamination but rather direct conversion of $^{15}\text{N}^{13}\text{C}$ -urea. As the labeling percentage within our experiments did not vary across time points, the direct conversion of $^{15}\text{N}^{13}\text{C}$ -urea was simply accounted for by using the slope of change in $^{29}\text{N}_2$ concentration with time to calculate the rate. However, if the labeling percentage were to change across time points, each time point would need to be corrected individually for this direct conversion, before a rate could be calculated. In contrast, $^{29}\text{N}_2$ detected in hypobromite conversions of $^{15}\text{N}^{13}\text{C}$ -cyanate is likely due to a small ^{15}N -ammonium contamination of the $^{15}\text{N}^{13}\text{C}$ -potassium cyanate salt.

Additionally, we found that some $^{15}\text{N}^{13}\text{C}$ -urea was also converted to $^{30}\text{N}_2$ during hypobromite conversions. To test if hypobromite combines the amide groups of one and the same or two different urea molecules, hypobromite conversions of equimolar ($5 \mu\text{M}$) concentrations of $^{15}\text{N}^{13}\text{C}$ -urea and $^{14}\text{N}^{12}\text{C}$ -urea were performed. We detected no increase in $^{29}\text{N}_2$ in these samples, indicating that hypobromite combines the two amide groups of a single urea molecule. Therefore, we recommend that if analysis of $^{30}\text{N}_2$ after hypobromite conversions on samples containing ^{15}N -urea is required, the sample can be stripped of $^{30}\text{N}_2$ before sulfamic acid conversion by prolonged bubbling of the sample liquid with He.

DNA and RNA analyses

Nucleic acid extraction

Seawater for molecular analyses was collected from the same casts and depths as seawater for process rate measurements. For each sample, a peristaltic pump was used to directly filter 1L of seawater onto $0.22 \mu\text{m}$ cartridge filters (Sterivex™, Millipore). An upstream prefilter was not used, thereby avoiding potential bias in taxon representation due to prefilter clogging (Padilla et al. 2015). Replicate cartridges for DNA analysis (16S rRNA gene sequencing and metagenomics) were filled with lysis buffer (50 mM Tris-HCl, 40 mM EDTA, 0.73 M sucrose) and stored at -20°C . Replicates for RNA analysis (metatranscriptomics) were filled with RNA stabilizing buffer (25 mM sodium citrate, 10 mM EDTA, 5.3 M ammonium sulfate, pH 5.2), flash frozen in liquid nitrogen, and stored at -80°C .

DNA was extracted from Sterivex cartridges using a phenol:chloroform protocol, as described previously (Padilla et al. 2016). Cells were lysed by adding lysozyme (2 mg in $50 \mu\text{l}$ of lysis buffer per

filter) directly to the cartridges, sealing the cartridges, and incubating for 45 min at 37°C. Proteinase K (1 mg in 100 µL lysis buffer, 100 µl 20% SDS) was added, and the cartridges were resealed and incubated for 2 hours at 55°C. The lysate was removed, and DNA was extracted once with phenol:chloroform:isoamyl alcohol (25:24:1) and once with chloroform:isoamyl alcohol (24:1) and then concentrated by spin dialysis using Ultra-4 (100 kDa, Amicon) centrifugal filters.

RNA was extracted from cartridges using a modification of the *mirVana*[™] miRNA Isolation kit (Ambion) (Frias-Lopez et al. 2008). Cartridges were thawed on ice, RNA stabilizing buffer was then expelled and discarded, and cells were lysed by adding Lysis buffer and miRNA Homogenate Additive (Ambion) directly to the cartridges. Following vortexing and incubation on ice (10 min), lysates were transferred to RNAase-free tubes and processed through an acid-phenol:chloroform extraction according to the kit protocol. The TURBO DNA-free[™] kit (Ambion) was used to remove DNA, and the extract was purified using the RNeasy MinElute Cleanup Kit (Qiagen).

16S rRNA gene sequencing and analysis

The proportional abundances of microbial taxa were assessed at all experimental depths and stations using 16S rRNA gene amplicon sequencing, following an established pipeline (e.g. Padilla et al. 2015; Padilla et al. 2016). Briefly, amplicons were generated by PCR using equal amounts of DNA template (1 ng), Platinum[®] PCR SuperMix (Life Technologies), and primers F515 and R806 encompassing the V4 region of the 16S rRNA gene (Caporaso et al. 2011). Despite a mismatch in the 515F primer to most Thaumarchaeota, the 16S rRNA gene of this group is recovered in PCR assays using this primer (Parada et al. 2016). This is in line with *in-silico* coverage tests (test-prime, arb-silva) allowing for 1 mismatch overall, but 0 mismatches for at least 5 bases at the 3' end of the primer, suggesting an estimated recovery of 95% of known marine Thaumarchaeota (Nitrosopumilales and Marine benthic group1). This indicates that the Thaumarchaeota in the Gulf of Mexico were well covered despite a mismatch in the forward primer (see Supplementary Discussion). Both forward and reverse primers were barcoded and appended with Illumina-specific adapters. Thermal cycling involved: denaturation at 94°C (3 min), followed by 30 cycles of denaturation at 94°C (45 sec), primer annealing at 55°C (45 sec) and primer extension at 72°C (90 sec), followed by extension at 72°C for 10 min. Amplicons were analyzed by gel electrophoresis to verify size (~400 bp) and purified using Diffinity RapidTip2 pipette tips (Diffinity Genomics, NY). Amplicons from different samples were pooled at equal concentrations and sequenced on an Illumina MiSeq using a 500-cycle Nano kit.

Barcoded sequences were de-multiplexed, trimmed (length cutoff 100 nt), and filtered to remove low quality reads (average Phred score < 25) using Trim Galore! (http://www.bioinformatics.babraham.ac.uk/projects/trim_galore/). Paired-end reads were merged using FLASH (Magoč & Salzberg 2011), with a minimum average length of 250 nt for each read, minimum average length of 300 nt for paired read fragments, and maximum allowable fragment standard deviation of 30 nt. The number of trimmed and merged reads per sample ranged from 11,842 – 21,970. Chimeric sequences were detected by reference-based searches using USEARCH (Edgar 2010) and removed from the sequence pools. Operational Taxonomic Units (OTUs) were defined by clustering at 97% sequence identity using open-reference picking with the UCLUST algorithm (Edgar 2010) in QIIME1 (Caporaso et al. 2010). The average number of sequences assigned per OTU was 836 (range 646 – 1,138). Taxonomy was assigned to OTUs using the Greengenes database (DeSantis et al. 2006). Singleton sequences and sequences affiliated with mitochondria and chloroplasts were removed from any further analysis. Proportional abundances of orders constituting >0.5% of the community were calculated after rarefaction based on the sample with the lowest number of reads (11,842 reads).

OTUs identified as Thaumarchaeota were analyzed further to assess the diversity and abundance of the ammonia-oxidizing community. The Thaumarchaeota sequences, which constituted the only known ammonia oxidizers in the dataset, were analyzed by placement into a reference phylogeny composed of near full-length reference Thaumarchaeota 16S rRNA sequences compiled from the ribosomal database project (RDP). To identify additional sequences for inclusion in the reference phylogeny, all Thaumarchaeota OTU sequences were queried against the NCBI non-redundant database via BLASTN. Top matching sequences and 16S rRNA sequences of cultured representatives were sorted by size and near-full sequences ($\geq 1,300$ nt), including both RDP and BLASTN matches ($n=32$), were aligned with MUSCLE (Edgar 2004) and then used to generate a phylogenetic tree (Supplementary Figure 5) in RAxML (Stamatakis 2006) via maximum likelihood estimation with the “GTRGAMMA” model and rapid bootstrapping (1,000 iterations). Short sequences consisting of both the Thaumarchaeota OTU amplicon sequences and non-full length top matches ($< 1,300$ nt, identified via BLASTN) were placed into the phylogenetic tree using the Evolutionary Placement Algorithm (EPA) (Berger et al. 2011). The resulting tree was visualized in FigTree v1.4.3 (<http://tree.bio.ed.ac.uk/software/figtree/>).

Metagenome sequencing, assembly and binning

Metagenomic libraries were constructed using NEBNext® UltraTM II FS DNA Library Prep Kit for Illumina, creating average fragment sizes of 550 bp. Samples were sequenced on one lane of an Illumina HiSeq using 2x250 bp cycle kit at Georgia Tech’s High-Throughput DNA Sequencing core facility.

Paired-end Illumina reads were pre-processed with `bbduk` (BBMap - Bushnell B. - sourceforge.net/projects/bbmap/) to remove adapters and residual phiX sequences. Reads were further quality-filtered with `bbduk` (`ktrim=r k=21 mink=11 hdist=2 minlen=149 qtrim=r trimq=15`). Quality-filtered reads were assembled with `Metaspades` (`-k 21,33,55,77,99,127`) (Nurk et al. 2017). `BBMap` (BBMap - Bushnell B. - sourceforge.net/projects/bbmap/) was used to map each individual read set to each assembly to assist in differential-coverage genome binning. Large (> 2 kb) scaffolds were clustered into Metagenome-Assembled Genomes (MAGs) by oligonucleotide frequency ($k=4$) and read coverage using `Maxbin2` (Wu et al. 2015) and `Metabat2` (Kang et al. 2015). Redundant bins were subsequently dereplicated and evaluated using `dRep` (Olm et al. 2017) with a completeness cutoff of 40%, contamination cutoff of 10% and minimum genome size of 200kb. Thaumarchaeal genomes were identified using a phylogenetic tree calculated using `FastTree2` (Price et al. 2010) based on an automated alignment generated by `CheckM` (Parks et al. 2015) and containing sequences from the dereplicated MAGs and known Thaumarchaeota. Metagenome sequencing statistics and information on dereplicated thaumarchaeal MAGs are listed in Supplementary Table 6 and 2, respectively.

MAG phylogenetic reconstruction

A concatenated alignment of 34 universal single-copy marker genes was generated using `CheckM` for published Thaumarchaeota and thaumarchaeal MAGs as well as representative Bathyarchaeota and Aigarchaeota (as outgroups). Phylogenetic reconstruction was carried out using `IQ-TREE` (Nguyen et al. 2015) with automated model selection and confidence was assessed with ultrafast bootstrapping (1,000 iterations).

Metatranscriptome sequencing

Community RNA (metatranscriptome) from Station 2, where the measured oxidation rates were highest, was analyzed for evidence of ammonium, urea, and cyanate utilization. To enrich for mRNA,

ribosomal RNA (rRNA) was depleted from total RNA using the Ribo-Zero™ rRNA Removal Kit for bacteria (Epicentre). mRNA-enriched total RNA was converted to cDNA and prepared for sequencing using the ScriptSeq™ v2 RNA-Seq Library preparation kit (Epicentre) and sequenced on an Illumina MiSeq using a 600 cycle kit. Metatranscriptomes were separated into ribosomal and non-ribosomal partitions using SortMeRNA (Kopylova et al. 2012). Metatranscriptome sequencing statistics are listed in Supplementary Table 7.

Single-gene phylogenetic reconstruction

Small subunit rRNA sequences from metagenomes were identified in metagenomic assemblies using nhmmer against rfam databases for small subunit rRNAs (RFAM: RF00177, RF01959, RF01960), requiring at least 300 nucleotides to match the model. Sequences were classified using the RDPclassifier (Wang et al. 2007) as implemented in Mothur.

Prodigal (Hyatt et al. 2010) was used to generate gene predictions from each metagenomic assembly, using the metagenome option (-p meta). Assemblies were screened for marker genes of ammonium, urea, and cyanate utilization: ammonia monooxygenase subunit alpha (*amoA*), urease subunit alpha (*ureC*), and cyanate lyase/hydratase (*cynS*), respectively. hmmsearch (Eddy 2011), which identifies protein sequences based on pfam hmm models, was used to identify genes of interest (archaeal *amoA* (PF12942.2); *cynS* (PF02560.9) and *ureC* (PF00449.15)), with the requirement that the protein sequence and hmm model align over at least 70% of the length of the model and that the reverse search of the identified protein sequence against the pfam database returned the target model as the best hit. Metagenome encoded genes of interest were used as queries against the NCBI non-redundant (nr) protein database (as of March, 2018) using default settings and the hits were filtered to remove sequences with less than 50% sequence coverage of the query gene. Hits were then clustered at 90% identity using Usearch (Edgar 2010) and added to custom *amoA* nucleotide, UreC amino acid, and CynS amino acid sequence databases. The CynS database was previously compiled (Palatinszky et al. 2015). The *amoA* and UreC databases were compiled from Pfam entries (Finn et al. 2016). Metagenomic-encoded *amoA*, UreC and CynS sequences were added to the custom databases and aligned with mafft-linsi (Kato et al. 2002) and trimmed using trimal -automated1 (Capella-Gutiérrez et al. 2009). Phylogenetic reconstruction was calculated with IQ-TREE (Nguyen et al. 2015) with automated model selection and confidence assessed with ultrafast bootstrapping (1,000 iterations). Resulting trees were visualized using ITOL (Letunic & Bork 2016).

Metagenomic and metatranscriptomic reads were used to quantify *amoA*, *ureC* and *cynS* in these datasets. mRNA reads were screened by BLASTX against the datasets assembled for phylogenetic analysis (see above). Positive BLASTX matches were defined by a bit score ≥ 50 and amino acid identity $\geq 40\%$. Reads were added to alignments used for calculating phylogeny of each gene of interest using the --add-fragments option in mafft and placed into single gene trees using the evolutionary placement algorithm (Berger et al. 2011). Fragments per kilobase per million reads (FPKM) values were calculated based on the number of read pairs for which one or both reads placed into a specified location in the tree, divided by the average gene length in the reference alignment (in kb) divided by the number of total metagenomic read pairs or ribosomal-RNA free metatranscriptomic read pairs (in millions). Gene lengths for the target genes are as follows: *amoA* (593 nt), *ureC* (1,477 nt), *cynS* (462 nt).

The percentage of *ureC*-containing Thaumarchaeota was estimated for each metagenomic dataset using a method similar to that of Tolar *et al.* and Santoro *et al.* (Tolar et al. 2017; Santoro et al. 2017), which involved comparing the FPKM for urease genes (FPKM_{*ureC*}) classified as thaumarchaeal *ureC* and the FPKM for thaumarchaeal *amoA* (FPKM_{*amoA*}) and SSU (16S rRNA genes, FPKM_{SSU}) genes, under

the assumption that *amoA* and SSU were universally present in all Thaumarchaeota as single copy genes. The percentage of *ureC* Thaumarchaeota was then calculated as $FPKM_{ureC} / FPKM_{amoA}$ and/or as $FPKM_{ureC} / FPKM_{SSU}$.

Thaumarchaeota quantification by CARD-FISH

For Thaumarchaeota quantification, seawater samples were fixed with 1% paraformaldehyde (PFA, without methanol, EMS) for 12 to 24 h at 4°C before filtration (< 400 mbar) onto 0.22 µm GTTP filters (Millipore) and washing with sterile filtered seawater. Filters were stored frozen at -20°C. Thaumarchaeota abundances were determined by CARD-FISH following Perenthaler *et al.* (2004) using the horseradish peroxidase (HRP) labeled probe Thaum726 (GCTTTCATCCCTCACCGTC, for probe specifications see below and Supplementary Table 8) and unlabeled competitor probes (Thaum726_compA: GCTTTCGTCCCTCACCGTC, Thaum726_compB: GCTTTCATCCCTCACTGTC) (Beam 2015; Sauder *et al.* 2017). For CARD-FISH, cells were immobilized on the filters by embedding in 0.2% low gelling agarose and endogenous peroxidases were inactivated by incubation in 0.01 M HCl for 10 min. Cells were permeabilized by HCl (0.1 M HCl for 1 min) and lysozyme (10 mg ml⁻¹ in 50 mM EDTA and 100 mM Tris-HCl at 37°C for 1 h). Filter pieces were hybridized with HRP probes and the respective competitor probes at 25% formamide concentration at 46°C for up to 3.5 h. After a 5 min washing step at 48°C and HRP probe equilibration in 1x PBS for 15 min, signal amplification was done with OregonGreen488 labeled tyramides at 48°C for 15 to 30 min. Before enumeration on an epifluorescence microscope (Axioplan 2, Zeiss), cells were counterstained with DAPI (10 µg ml⁻¹, 5 min at room temperature). For each CARD-FISH experiment, positive controls using probes EUB338 I-III (Amann *et al.* 1990; Daims *et al.* 1999) and negative controls with the probe NonEUB (Wallner *et al.* 1993) on separate filter pieces were included to exclude non-specific binding of oligonucleotides or insufficient inactivation of endogenous peroxidases.

The probe used for CARD-FISH (Thaum726) targeted all recovered GoM Thaumarchaeota OTUs except for three, which together made up only 0.07% of all Thaumarchaeota 16S rRNA gene reads. Thaum726 also targeted all Thaumarchaeota 16S rRNA gene fragments obtained by metagenomics that had sequence information at the probe binding site. Furthermore, Thaum726 targets 94.6% of Nitrosopumilales Thaumarchaeota (Marine Group 1, sequences included in ARB Silva database SSURef_NR99_128_SILVA_07_09_16, Supplementary Table 8). To ensure specificity to Thaumarchaeota for our samples, Thaum726 was also screened for non-target matches against the entire retrieved GoM 16S rRNA gene amplicon dataset. We found that it targeted only one non-target Crenarchaeota OTU present only at Station 1, 16m depth with a relative abundance of 0.01%. It is therefore unlikely that we under- or overestimated Thaumarchaeota present in the GoM due to mismatches in the probe binding site in Thaumarchaeota, or probe binding to non-target organisms.

nanoSIMS Analyses and Calculation of Single Cell Growth and N-uptake Rates

For nanoSIMS analyses, unfixed seawater samples were gently filtered (< 100 mbar) onto gold sputtered 0.22 µm GTTP filters (Millipore), and subsequently fixed in 3% PFA (in sterile filtered seawater) for 30 min at room temperature, washed twice in sterile filtered seawater and then stored at -20°C until CARD-FISH and nanoSIMS. CARD-FISH targeting Thaumarchaeota was done without embedding filters in agarose. After counterstaining with DAPI, regions of interest were marked on a laser microdissection microscope (6000 B, Leica) and images of CARD-FISH signals were acquired on an epifluorescence microscope (Axioplan 2, Zeiss).

Single cell ¹⁵N- and ¹³C-uptake from ¹⁵N-ammonium and ¹³C-bicarbonate, ¹⁵N¹³C-urea and ¹⁵N¹³C-cyanate were determined for Station 2, 14m depth, using a nanoSIMS 50L (CAMECA), as previously described (Martínez-Pérez *et al.* 2016). Instrument precision for detection of ¹⁵N/¹⁴N and ¹³C/¹²C

isotope ratios was monitored daily on Graphite Planchet and regularly on caffeine standards. Due to the small size of Thaumarchaeota (< 1 μm), samples were only briefly (10 s) pre-sputtered with a Cs^+ beam (~300 pA) before measurement. Measurements were done on a field size of $10 \times 10 \mu\text{m}$ or $15 \times 15 \mu\text{m}$, with a dwelling time of 2 ms per pixel and 256×256 pixel resolution over 40 planes. Analysis of the acquired data was performed using the Look@NanoSIMS software package (Polerecky et al. 2012) as previously described (Martínez-Pérez et al. 2016). Ratios of $^{15}\text{N}/(^{15}\text{N}+^{14}\text{N})$ and $^{13}\text{C}/(^{13}\text{C}+^{12}\text{C})$ of Thaumarchaeota and non-Thaumarchaeota cells were used for calculation of growth rates only when the overall enrichment Poisson error across all planes of a given cell was < 5%. The variability in $^{15}\text{N}/(^{15}\text{N}+^{14}\text{N})$ ratios across measured Thaumarchaeota and non-Thaumarchaeota cells was calculated following Svedén *et al.* (2015) (see section below).

Single cell growth rates were calculated as previously described (Martínez-Pérez et al. 2016), where cell ^{15}N - and ^{13}C -atom% excess was calculated by subtracting natural abundance $^{15}\text{N}/(^{15}\text{N}+^{14}\text{N})$ and $^{13}\text{C}/(^{13}\text{C}+^{12}\text{C})$ values (0.37% and 1.11%, respectively). To be conservative in our calculations, we did not take the isotopic dilution of $^{15}\text{N}/(^{15}\text{N}+^{14}\text{N})$ and $^{13}\text{C}/(^{13}\text{C}+^{12}\text{C})$ ratios due to CARD-FISH into account (Musat et al. 2012; Woebken et al. 2015) (see section below). For calculation of per-cell N-uptake rates, an average carbon content of 9 fg-C per Thaumarchaeota cell (Berg et al. 2015) and a C:N ratio following Redfield (C:N = 6.625:1) were assumed, resulting in an average N-content of 1.36 fg-N per Thaumarchaeota cell. N-uptake rates were calculated by:

$$\text{N-UptakeRate} [\text{fg-N cell}^{-1} \text{d}^{-1}] = (^{15}\text{Nat}\%_{\text{excess}_{\text{cell}}}) / (^{15}\text{Nat}\%_{\text{excess}_{\text{label}}}) \times \text{fgN}_{\text{cell}} \times 1/\text{time} \quad (1)$$

$$\text{N-UptakeRate} [\text{amol-N cell}^{-1} \text{d}^{-1}] = \text{N-UptakeRate} [\text{fg-N cell}^{-1} \text{d}^{-1}] / 14 \times 10^3 \quad (2)$$

where $^{15}\text{Nat}\%_{\text{excess}_{\text{cell}}}$ and $^{15}\text{Nat}\%_{\text{excess}_{\text{label}}}$ are ^{15}N -atom% of a given measured cell and of the ^{15}N -enriched seawater during the incubation after subtraction of natural abundance ^{15}N -atom% (0.37%), fgN_{cell} is the assumed N-content per cell, and time is the incubation time in days (Krupke et al. 2015).

Analysis of $^{15}\text{N}/(^{14}\text{N}+^{15}\text{N})$ ratio variability and isotopic dilution due to CARD-FISH

To test if sufficient cells have been measured by nanoSIMS, we calculated the mean and standard error for randomly subsampled ROIs according to Svedén *et al.* (2015), who propose that the error of randomly subsampled ROIs of one population should be < 10%. Our analysis showed that the standard error for Thaumarchaeota $^{15}\text{N}/(^{14}\text{N}+^{15}\text{N})$ ratios was < 10% after random subsampling of 5 and 3 cells respectively, for ammonium and cyanate incubations (Supplementary Figure 11). This indicates a highly homogenous ^{15}N -uptake by the measured Thaumarchaeota population. However, the spread in $^{15}\text{N}/(^{14}\text{N}+^{15}\text{N})$ ratios was much larger for Thaumarchaeota in the urea incubation (20%, Supplementary Figure 11). This could be either due to too few measured cells, or, alternatively, due to the presence of several Thaumarchaeota subpopulations, which have different activities on urea. The latter is in line with the presence of urease in only approximately 10-15% of the Thaumarchaeota based on metagenomics (see main text), indicating that the spread in $^{15}\text{N}/(^{14}\text{N}+^{15}\text{N})$ ratios in the urea treatment is an inherent feature of the Thaumarchaeota community. The spread in $^{15}\text{N}/(^{14}\text{N}+^{15}\text{N})$ ratios was higher in all treatments for non-Thaumarchaeota than for Thaumarchaeota, likely due to the diversity of microorganisms and their physiology in this class.

CARD-FISH has previously been shown to introduce isotopic dilution of both target and, to a lesser extent, non-target cells (Musat et al. 2012; Woebken et al. 2015). The extent of isotopic dilution is affected by growth stage and hypothesized to also depend on washing steps and the CARD-FISH protocol used. We have not accounted for isotopic dilution of Thaumarchaeota cells due to CARD-FISH in our experiments to be conservative, as the isotopic dilution effect for complex environmental

samples is still not well constrained. Thaumarchaeota are therefore likely to be even higher enriched in ^{15}N and ^{13}C compared to other cells than reported, and *in situ* growth rates may have been underestimated.

Cyanate oxidation by cultures of *Nitrosopumilus maritimus*

Experiments were carried out to assess cyanate use by four cultures of the marine Thaumarchaeon *N. maritimus* SCM1 (Könneke et al. 2005). All cultures were inoculated in 100 ml synthetic Crenarchaeota medium (Martens-Habbena et al. 2009) containing 1 mM NH_4Cl . Cultures were incubated in the dark at 28°C without shaking. After consumption of >0.7 mM NH_4^+ , cultures were amended with freshly prepared, sterile filtered (0.2 μm) 200 μM $^{14}\text{N}\text{-NH}_4^+$ and 40 μM $^{13}\text{C}^{15}\text{N}$ -cyanate. At the time of tracer addition, cell numbers were 1.11×10^8 , 1.35×10^8 , 7.89×10^7 and 9.42×10^7 cells ml^{-1} in culture 1, 2, 3 and 4, respectively. At each time point (0, 3, 6 and 12 h), 20 ml samples were taken under sterile conditions, sterile filtered and stored at -80°C until concentration analysis (cyanate, ammonium, nitrite), and GC-IRMS (^{15}N -ammonium and ^{15}N -nitrite) measurements. The purity of cultures was confirmed at the end of the experiment using CARD-FISH (probe Thaum726 and DAPI staining), as described above. Abiotic breakdown of cyanate was assessed in sterile filtered media and a further experiment assessed the breakdown of cyanate in the culture supernatant of *N. maritimus* SCM1 after growth on 1 mM ammonium (supernatant controls, see Supplementary Discussion). The contribution of abiotic cyanate breakdown to the observed cyanate-derived oxidation rates in the *N. maritimus* cultures was calculated analogously to field experiments (Supplementary Discussion).

Data Availability

All sequence data and thaumarchaeal MAGs generated in this study are deposited in NCBI under BioProject number: PRJNA397176. Metatranscriptomes are deposited under BioSample numbers SAMN07461123-SAMN07461125; 16S amplicon sequencing under SAMN07461114-SAMN07461122; metagenomes under SAMN10227777-SAMN10227781, and MAGs under SAMN10233969 – SAMN10233974. Accession numbers of sequences used for tree calculations (16S rRNA gene, *amoA*, *UreC*, *CynS*, and genome sequences) are given in Supplementary Table 9. CTD data, measured nutrient concentrations, process rates, Thaumarchaeota relative abundance based on 16S rRNA gene amplicon sequencing and Thaumarchaeota specific CARD-FISH counts are given in Supplementary Table 10.

Acknowledgements

The authors thank the captain and crew of the *R/V Pelican* PE17-02 cruise. The authors are grateful to G. Klockgether, D. Tienken, I. Ulber, L. Seidl, W. Neweshey, N. Alrubeay, M. Philippi and D.J. Parris for technical support; G. Lavik, J. Milucka, W. Mohr, N. Lehnen and S. Ahmerkamp for fruitful discussions. This research was funded by the Max-Planck-Society, the European Research Council Advanced Grant project NITRICARE 294343 (to M.W) and the National Science Foundation grants 1558916 and 1564559 (to F.J.S.)

References

- Alonso-Saez L., Waller A.S., Mende D.R., Bakker K., Farnelid H., Yager P.L., Lovejoy C., Tremblay J.-E., Potvin M., Heinrich F., Estrada M., Riemann L., Bork P., Pedros-Alio C. and Bertilsson S. 2012. Role for Urea in Nitrification by Polar Marine Archaea. *Proceedings of the National Academy of Sciences of the United States of America* 109 (44): 17989–94. doi:10.1073/pnas.1201914109.
- Amann R.I., Binder B.J., Olson R.J., Chisholm S.W., Devereux R. and Stahl D. a. 1990. Combination of 16S RRNA-Targeted Oligonucleotide Probes with Flow Cytometry for Analyzing Mixed Microbial Populations. *Applied and Environmental Microbiology* 56 (6): 1919–25.
- Antia N.J., Harrison P.J. and Oliveira L. 1991. The Role of Dissolved Organic Nitrogen in Phytoplankton Nutrition, Cell Biology and Ecology. *Phycologia* 30 (1): 1–89. doi:10.2216/i0031-8884-30-1-1.1.
- Bayer B., Vojvoda J., Offre P., Alves R.J.E., Elisabeth N.H., Garcia J. AL, Volland J.-M., Srivastava A., Schleper C. and Herndl G.J. 2016. Physiological and Genomic Characterization of Two Novel Marine Thaumarchaeal Strains Indicates Niche Differentiation. *The ISME Journal* 10. Nature Publishing Group: 1051–63. doi:10.1038/ismej.2015.200.
- Beam J.P. 2015. Geobiological Interactions of Archaeal Populations in Acidic Geothermal Springs of Yellowstone National Park, WY, USA. Montana State University.
- Berg C., Listmann L., Vandieken V., Vogts A. and Jürgens K. 2015. Chemoautotrophic Growth of Ammonia-Oxidizing Thaumarchaeota Enriched from a Pelagic Redox Gradient in the Baltic Sea. *Frontiers in Microbiology* 5: 1–10. doi:10.3389/fmicb.2014.00786.
- Berger S.A., Krompass D. and Stamatakis A. 2011. Performance, Accuracy, and Web Server for Evolutionary Placement of Short Sequence Reads under Maximum Likelihood. *Systematic Biology* 60 (3): 291–302. doi:10.1093/sysbio/syr010.
- Braman R.S. and Hendrix S.A. 1989. Nanogram Nitrite and Nitrate Determination in Environmental and Biological Materials by Vanadium(III) Reduction with Chemiluminescence Detection. *Analytical Chemistry* 61: 2715–18. doi:10.1021/ac00199a007.
- Bristow L.A., Sarode N., Cartee J., Caro-Quintero A., Thamdrup B. and Stewart F.J. 2015. Biogeochemical and Metagenomic Analysis of Nitrite Accumulation in the Gulf of Mexico Hypoxic Zone. *Limnology and Oceanography* 60 (5): 1733–50. doi:10.1002/lno.10130.
- Capella-Gutiérrez S., Silla-Martínez J.M. and Gabaldón T. 2009. TrimAl: A Tool for Automated Alignment Trimming in Large-Scale Phylogenetic Analyses. *Bioinformatics* 25 (15): 1972–73. doi:10.1093/bioinformatics/btp348.
- Caporaso J.G., Kuczynski J., Stombaugh J., Bittinger K., Bushman F.D., Costello E.K., Fierer N., Gonzales Peña A., Goodrich J.K., Gordon J.I., Huttley G.A., Kelley S.T., Knights D., Koenig J.E., Ley R.E., Lozupone C.A., McDonald D., Muegge B.D., Pirrung M., et al. 2010. QIIME Allows Analysis of High-Throughput Community Sequencing Data. *Nature Methods* 7 (5). Nature Publishing Group: 335–336. doi:10.1038/nmeth.f.303.QIIME.
- Caporaso J.G., Lauber C.L., Walters W.A., Berg-Lyons D., Lozupone C.A., Turnbaugh P.J., Fierer N. and Knight R. 2011. Global Patterns of 16S RRNA Diversity at a Depth of Millions of Sequences per Sample. *Proceedings of the National Academy of Sciences of the United States of America* 108 (suppl. 1): 4516–22. doi:10.1073/pnas.1000080107.
- Carini S.A., McCarthy M.J. and Gardner W.S. 2010. An Isotope Dilution Method to Measure Nitrification Rates in the Northern Gulf of Mexico and Other Eutrophic Waters. *Continental Shelf Research* 30. Elsevier: 1795–1801. doi:10.1016/j.csr.2010.08.001.
- Connelly T.L., Baer S.E., Cooper J.T., Bronk D.A. and Wawrik B. 2014. Urea Uptake and Carbon Fixation by Marine Pelagic Bacteria and Archaea During the Arctic Summer and Winter Seasons. *Applied and Environmental Microbiology* 80 (19): 6013–22. doi:10.1128/AEM.01431-14.
- Daims H., Brühl A., Amann R., Schleifer K.-H. and Wagner M. 1999. The Domain-Specific Probe EUB338 Is Insufficient for the Detection of All Bacteria: Development and Evaluation of a More Comprehensive Probe Set. *Systematic and Applied Microbiology* 22 (September): 434–44. doi:10.1016/S0723-2020(99)80053-8.
- De Brabandere L., L. B.T., Revsbech N.P. and Foadi R. 2012. A Critical Assessment of the Occurrence and Extend of Oxygen Contamination during Anaerobic Incubations Utilizing Commercially Available Vials. *Journal of Microbiological Methods* 88 (1): 147–154. doi:doi:10.1016/j.mimet.2011.11.001.
- DeSantis T.Z., Hugenholtz P., Larsen N., Rojas M., Brodie E.L., Keller K., Huber T., Dalevi D., Hu P. and Andersen G.L. 2006. Greengenes, a Chimera-Checked 16S RRNA Gene Database and Workbench Compatible with ARB. *Applied and Environmental Microbiology* 72 (7): 5069–72. doi:10.1128/AEM.03006-05.

- Dirnhuber P. and Schütz F. 1948. The Isomeric Transformation of Urea into Ammonium Cyanate in Aqueous Solutions. *Biochemical Journal* 42 (4): 628–32.
- Eddy S.R. 2011. Accelerated Profile HMM Searches. *PLoS Computational Biology* 7 (10): e1002195. doi:10.1371/journal.pcbi.1002195.
- Edgar R.C. 2004. MUSCLE: Multiple Sequence Alignment with High Accuracy and High Throughput. *Nucleic Acids Research* 32 (5): 1792–97. doi:10.1093/nar/gkh340.
- Edgar R.C. 2010. Search and Clustering Orders of Magnitude Faster than BLAST. *Bioinformatics* 26 (19): 2460–61. doi:10.1093/bioinformatics/btq461.
- Finn R.D., Coghill P., Eberhardt R.Y., Eddy S.R., Mistry J., Mitchell A.L., Potter S.C., Punta M., Qureshi M., Sangrador-Vegas A., Salazar G.A., Tate J. and Bateman A. 2016. The Pfam Protein Families Database: Towards a More Sustainable Future. *Nucleic Acids Research* 44 (Database issue): D279–85. doi:10.1093/nar/gkv1344.
- Francis C.A., Roberts K.J., Beman J.M., Santoro A.E. and Oakley B.B. 2005. Ubiquity and Diversity of Ammonia-Oxidizing Archaea in Water Columns and Sediments of the Ocean. *Proceedings of the National Academy of Sciences of the United States of America* 102 (41): 14683–88. doi:10.1073/pnas.0506625102.
- Frias-Lopez J., Shi Y., Tyson G.W., Coleman M.L., Schuster S.C., Chisholm S.W. and DeLong E.F. 2008. Microbial Community Gene Expression in Ocean Surface Waters. *Proceedings of the National Academy of Sciences of the United States of America* 105 (10): 3805–10. doi:10.1073/pnas.0708897105.
- Füssel J., Lam P., Lavik G., Jensen M.M., Holtappels M., Günter M. and Kuypers M.M.M. 2012. Nitrite Oxidation in the Namibian Oxygen Minimum Zone. *The ISME Journal* 6: 1200–1209. doi:10.1038/ismej.2011.178.
- Galand P.E., Gutiérrez-Provecho C., Massana R., Gasol J.M. and Casamayor E.O. 2010. Inter-Annual Recurrence of Archaeal Assemblages in the Coastal NW Mediterranean Sea (Blanes Bay Microbial Observatory). *Limnology and Oceanography* 55 (5): 2117–25. doi:10.4319/lo.2010.55.5.2117.
- Garcia H.E. and Gordon L.I. 1992. Oxygen Solubility in Seawater: Better Fitting Equations. *Limnology and Oceanography* 37 (6): 1307–12. doi:10.2307/2837876.
- Granger J. and Sigman D.M. 2009. Removal of Nitrite with Sulfamic Acid for Nitrate N and O Isotope Analysis with the Denitrifier Method. *Rapid Communications in Mass Spectrometry* 23: 3753–62. doi:10.1002/rcm.4307.
- Grasshoff K., Kremling K. and Ehrhardt M. 1999. *Methods of Seawater Analysis*. Edited by K Grasshoff, K Kremling, and M Ehrhardt. 3rd editio. Wiley-VCH. doi:10.1016/0304-4203(78)90045-2.
- Herndl G.J., Reinthaler T., Teira E., Aken H. Van, Veth C., Pernthaler A. and Pernthaler J. 2005. Contribution of Archaea to Total Prokaryotic Production in the Deep Atlantic Ocean. *Applied and Environmental Microbiology* 71 (5): 2303–9. doi:10.1128/AEM.71.5.2303.
- Holmes R.M., Aminot A., Kérouel R., Hooker B.A. and Peterson B.J. 1999. A Simple and Precise Method for Measuring Ammonium in Marine and Freshwater Ecosystems. *Canadian Journal of Fisheries and Aquatic Sciences* 56: 1801–8.
- Horak R.E.A., Qin W., Schauer A.J., Armbrust E.V., Ingalls A.E., Moffett J.W., Stahl D.A. and Devol A.H. 2013. Ammonia Oxidation Kinetics and Temperature Sensitivity of a Natural Marine Community Dominated by Archaea. *The ISME Journal* 7: 2023–33. doi:10.1038/ismej.2013.75.
- Hyatt D., Chen G.-L.L., LoCascio P.F., Land M.L., Larimer F.W. and Hauser L.J. 2010. Prodigal: Prokaryotic Gene Recognition and Translation Initiation Site Identification. *BMC Bioinformatics* 11 (119): 1–11. doi:10.1186/1471-2105-11-119.
- Kang D.D., Froula J., Egan R. and Wang Z. 2015. MetaBAT, an Efficient Tool for Accurately Reconstructing Single Genomes from Complex Microbial Communities. *PeerJ* 3: e1165. doi:10.7717/peerj.1165.
- Katoh K., Misawa K., Kuma K. and Miyata T. 2002. MAFFT: A Novel Method for Rapid Multiple Sequence Alignment Based on Fast Fourier Transform. *Nucleic Acids Research* 30 (14): 3059–66. doi:10.1093/nar/gkf436.
- Koch H., Lüscher S., Albertsen M., Kitzinger K., Herbold C., Spieck E., Nielsen P.H., Wagner M. and Daims H. 2015. Expanded Metabolic Versatility of Ubiquitous Nitrite-Oxidizing Bacteria from the Genus *Nitrospira*. *Proceedings of the National Academy of Sciences of the United States of America* 112 (36): 11371–76. doi:10.1073/pnas.1506533112.
- Könneke M., Bernhard A.E., de la Torre J.R., Walker C.B., Waterbury J.B. and Stahl D.A. 2005. Isolation of an Autotrophic Ammonia-Oxidizing Marine Archaeon. *Nature* 437: 543–46. doi:10.1038/nature03911.

- Kopylova E., Noé L. and Touzet H. 2012. SortMeRNA: Fast and Accurate Filtering of Ribosomal RNAs in Metatranscriptomic Data. *Bioinformatics* 28 (24): 3211–17. doi:10.1093/bioinformatics/bts611.
- Krupke A., Mohr W., LaRoche J., Fuchs B.M., Amann R.I. and Kuypers M.M.M. 2015. The Effect of Nutrients on Carbon and Nitrogen Fixation by the UCYN-A – Haptophyte Symbiosis. *The ISME Journal* 9: 1635–47. doi:10.1038/ismej.2014.253.
- Lam P., Lavik G., Jensen M.M., van de Vossenberg J., Schmid M., Woebken D., Gutiérrez D., Amann R., Jetten M.S.M. and Kuypers M.M.M. 2009. Revising the Nitrogen Cycle in the Peruvian Oxygen Minimum Zone. *Proceedings of the National Academy of Sciences of the United States of America* 106 (12): 4752–57. doi:10.1073/pnas.0812444106.
- Letunic I. and Bork P. 2016. Interactive Tree of Life (ITOL) v3: An Online Tool for the Display and Annotation of Phylogenetic and Other Trees. *Nucleic Acids Research* 44 (W1): W242–45. doi:10.1093/nar/gkw290.
- Liu K.-K., Atkinson L., Quiñones R. and Talaue-McManus L. 2010. *Carbon and Nutrient Fluxes in Continental Margins - A Global Synthesis. Carbon and Nutrient Fluxes in Continental Margins*. Springer. doi:10.1007/978-3-540-92735-8.
- Liu Q., Tolar B.B., Ross M.J., Cheek J.B., Sweeney C.M., Wallsgrove N.J., Popp B.N. and Hollibaugh J.T. 2018. Light and Temperature Control the Seasonal Distribution of Thaumarchaeota in the South Atlantic Bight. *The ISME Journal* 12: 1473–85. doi:10.1038/s41396-018-0066-4.
- Magoč T. and Salzberg S.L. 2011. FLASH: Fast Length Adjustment of Short Reads to Improve Genome Assemblies. *Bioinformatics* 27 (21): 2957–63. doi:10.1093/bioinformatics/btr507.
- Martens-Habbena W., Berube P.M., Urakawa H., de la Torre J.R. and Stahl D.A. 2009. Ammonia Oxidation Kinetics Determine Niche Separation of Nitrifying Archaea and Bacteria. *Nature* 461: 976–79. doi:10.1038/nature08465.
- Martínez-Pérez C., Mohr W., Löscher C.R., Dekaezemacker J., Littmann S., Yilmaz P., Lehnen N., Fuchs B.M., Lavik G., Schmitz R.A., LaRoche J. and Kuypers M.M.M. 2016. The Small Unicellular Diazotrophic Symbiont, UCYN-A, Is a Key Player in the Marine Nitrogen Cycle. *Nature Microbiology* 1 (11): 1–7. doi:10.1038/nmicrobiol.2016.163.
- Mulvenna P.F. and Savidge G. 1992. A Modified Manual Method for the Determination of Urea in Seawater Using Diacetylmonoxime Reagent. *Estuarine, Coastal and Shelf Science* 34: 429–38. doi:10.1016/S0272-7714(05)80115-5.
- Musat N., Foster R., Vagner T., Adam B. and Kuypers M.M.M. 2012. Detecting Metabolic Activities in Single Cells, with Emphasis on NanoSIMS. *FEMS Microbiology Reviews* 36: 486–511. doi:10.1111/j.1574-6976.2011.00303.x.
- Nguyen L.T., Schmidt H.A., Von Haeseler A. and Minh B.Q. 2015. IQ-TREE: A Fast and Effective Stochastic Algorithm for Estimating Maximum-Likelihood Phylogenies. *Molecular Biology and Evolution* 32 (1): 268–74. doi:10.1093/molbev/msu300.
- Nurk S., Meleshko D., Korobeynikov A. and Pevzner P.A. 2017. MetaSPAdes: A New Versatile Metagenomic Assembler. *Genome Research* 27: 824–34. doi:10.1101/gr.213959.116.
- Olm M.R., Brown C.T., Brooks B. and Banfield J.F. 2017. DRep: A Tool for Fast and Accurate Genomic Comparisons That Enables Improved Genome Recovery from Metagenomes through de-Replication. *ISME Journal* 11: 2864–68. doi:10.1038/ismej.2017.126.
- Padilla C.C., Bristow L.A., Sarode N., Garcia-Robledo E., Gómez Ramírez E., Benson C.R., Bourbonnais A., Altabet M.A., Girguis P.R., Thamdrup B. and Stewart F.J. 2016. NC10 Bacteria in Marine Oxygen Minimum Zones. *The ISME Journal* 10: 2067–71. doi:10.1038/ismej.2015.262.
- Padilla C.C., Ganesh S., Gantt S., Huhman A., Parris D.J., Sarode N. and Stewart F.J. 2015. Standard Filtration Practices May Significantly Distort Planktonic Microbial Diversity Estimates. *Frontiers in Microbiology* 6 (547): 1–10. doi:10.3389/fmicb.2015.00547.
- Palatinszky M., Herbold C., Jehmlich N., Pogoda M., Han P., Bergen M. Von, Lagkouvardos I., Karst S.M., Galushko A., Koch H., Berry D., Daims H. and Wagner M. 2015. Cyanate as an Energy Source for Nitrifiers. *Nature* 524: 105–8. doi:10.1038/nature14856.
- Parada A.E., Needham D.M. and Fuhrman J.A. 2016. Every Base Matters: Assessing Small Subunit rRNA Primers for Marine Microbiomes with Mock Communities, Time Series and Global Field Samples. *Environmental Microbiology* 18 (5): 1403–14. doi:10.1111/1462-2920.13023.

- Parks D.H., Imelfort M., Skennerton C.T., Hugenholtz P. and Tyson G.W. 2015. CheckM: Assessing the Quality of Microbial Genomes Recovered from Isolates, Single Cells, and Metagenomes. *Genome Research* 25 (7): 1043–55. doi:10.1101/gr.186072.114.
- Pernthaler A., Pernthaler J. and Amann R. 2004. Sensitive Multi-Color Fluorescence in Situ Hybridization for the Identification of Environmental Microorganisms. In *Molecular Microbial Ecology Manual*, edited by G. Kowalchuk, F. J. de Bruijn, Ian M. Head, A. D. L. Akkermans, and J. D. van Elsas, 2nd ed., 711–26. Dordrecht, Boston, London: Kluwer Academic Publishers. doi:10.1007/978-1-4020-2177-0_311.
- Polerecky L., Adam B., Milucka J., Musat N., Vagner T. and Kuypers M.M.M. 2012. Look@NanoSIMS - a Tool for the Analysis of NanoSIMS Data in Environmental Microbiology. *Environmental Microbiology* 14 (4): 1009–23. doi:10.1111/j.1462-2920.2011.02681.x.
- Price M.N., Dehal P.S. and Arkin A.P. 2010. FastTree 2 - Approximately Maximum-Likelihood Trees for Large Alignments. *PLoS ONE* 5 (3): e9490. doi:10.1371/journal.pone.0009490.
- Qin W., Amin S.A., Martens-Habbena W., Walker C.B., Urakawa H., Devol A.H., Ingalls A.E., Moffett J.W., Armbrust E.V. and Stahl D.A. 2014. Marine Ammonia-Oxidizing Archaeal Isolates Display Obligate Mixotrophy and Wide Ecotypic Variation. *Proceedings of the National Academy of Sciences of the United States of America* 111 (34): 12504–9. doi:10.1073/pnas.1324115111.
- Rabalais N.N., Turner R.E. and Wiseman W.J. 2001. Hypoxia in the Gulf of Mexico. *Journal of Environment Quality* 30: 320–29. doi:10.2134/jeq2001.302320x.
- Santoro A.E., Saito M.A., Goepfert T.J., Lamborg C.H., Dupont C.L. and Ditullio G.R. 2017. Thaumarchaeal Ecotype Distributions across the Equatorial Pacific Ocean and Their Potential Roles in Nitrification and Sinking Flux Attenuation. *Limnology and Oceanography* 62: 1984–2003. doi:10.1002/lno.10547.
- Sauder L.A., Albertsen M., Engel K., Schwarz J., Nielsen P.H., Wagner M. and Neufeld J.D. 2017. Cultivation and Characterization of Candidatus Nitrosocosmicus Exaquare, an Ammonia-Oxidizing Archaeon from a Municipal Wastewater Treatment System. *The ISME Journal* 11 (5): 1142–57. doi:10.1038/ismej.2016.192.
- Seidel M., Manecki M., Herlemann D.P.R., Deutsch B., Schulz-Bull D., Jürgens K. and Dittmar T. 2017. Composition and Transformation of Dissolved Organic Matter in the Baltic Sea. *Frontiers in Earth Science* 5 (31): 1–20. doi:10.3389/feart.2017.00031.
- Sipler R.E. and Bronk D.A. 2015. Dynamics of Dissolved Organic Nitrogen. In *Biogeochemistry of Marine Dissolved Organic Matter: Second Edition*, edited by Dennis A. Hansell and Craig A. Carlson, Second Edi, 127–232. ACADEMIC PRESS, INC. doi:10.1016/B978-0-12-405940-5.00004-2.
- Stamatakis A. 2006. RAxML-VI-HPC: Maximum Likelihood-Based Phylogenetic Analyses with Thousands of Taxa and Mixed Models. *Bioinformatics* 22 (21): 2688–90. doi:10.1093/bioinformatics/btl446.
- Svedén J.B., Adam B., Walve J., Nahar N., Musat N., Lavik G., Whitehouse M.J., Kuypers M.M.M. and Ploug H. 2015. High Cell-Specific Rates of Nitrogen and Carbon Fixation by the Cyanobacterium Aphanizomenon Sp. at Low Temperatures in the Baltic Sea. *FEMS Microbiology Ecology* 91 (12): 1–10. doi:10.1093/femsec/fiv131.
- Tolar B.B., King G.M. and Hollibaugh J.T. 2013. An Analysis of Thaumarchaeota Populations from the Northern Gulf of Mexico. *Frontiers in Microbiology* 4 (72): 1–36. doi:10.3389/fmicb.2013.00072.
- Tolar B.B., Wallsgrrove N.J., Popp B.N. and Hollibaugh J.T. 2017. Oxidation of Urea-Derived Nitrogen by Thaumarchaeota-Dominated Marine Nitrifying Communities. *Environmental Microbiology* 19 (12): 4838–4850. doi:10.1002/elsc.201200179.
- Torres M.E., Mix A.C. and Rugh W.D. 2005. Precise $\Delta^{13}\text{C}$ Analysis of Dissolved Inorganic Carbon in Natural Waters Using Automated Headspace Sampling and Continuous-Flow Mass Spectrometry. *Limnology and Oceanography: Methods* 3: 349–60. doi:10.4319/lom.2005.3.349.
- Wallner G., Amann R. and Beisker W. 1993. Optimizing Fluorescent in Situ Hybridization with rRNA-Targeted Oligonucleotide Probes for Flow Cytometric Identification of Microorganisms. *Cytometry* 14: 136–43. doi:10.1002/cyto.990140205.
- Wang Q., Garrity G.M., Tiedje J.M. and Cole J.R. 2007. Naïve Bayesian Classifier for Rapid Assignment of rRNA Sequences into the New Bacterial Taxonomy. *Applied and Environmental Microbiology* 73 (16): 5261–67. doi:10.1128/AEM.00062-07.
- Ward B.B. 2008. Nitrification in Marine Systems. In *Nitrogen in the Marine Environment*, edited by Douglas G Capone, Deborah A Bronk, Margaret R Mulholland, and Edward J Carpenter, 2nd ed., 199–261. Elsevier Inc. doi:10.1016/B978-0-12-372522-6.00005-0.

- Widner B., Mordy C.W. and Mulholland M.R. 2018. Cyanate Distribution and Uptake above and within the Eastern Tropical South Pacific Oxygen Deficient Zone. *Limnology and Oceanography* 63 (S1): S177–92. doi:10.1002/lno.10730.
- Widner B. and Mulholland M.R. 2017. Cyanate Distribution and Uptake in North Atlantic Coastal Waters. *Limnology and Oceanography* 62 (6): 2538–49. doi:10.1002/lno.10588.
- Widner B., Mulholland M.R. and Mopper K. 2013. Chromatographic Determination of Nanomolar Cyanate Concentrations in Estuarine and Sea Waters by Precolumn Fluorescence Derivatization. *Analytical Chemistry* 85: 6661–66. doi:10.1021/ac400351c.
- Widner B., Mulholland M.R. and Mopper K. 2016. Distribution, Sources, and Sinks of Cyanate in the Coastal North Atlantic Ocean. *Environmental Science & Technology Letters* 3 (8): 297–302. doi:10.1021/acs.estlett.6b00165.
- Woebken D., Burow L.C., Behnam F., Mayali X., Schintlmeister A., Fleming E.D., Prufert-Bebout L., Singer S.W., Cortés A.L., Hoehler T.M., Pett-Ridge J., Spormann A.M., Wagner M., Weber P.K. and Bebout B.M. 2015. Revisiting N₂ Fixation in Guerrero Negro Intertidal Microbial Mats with a Functional Single-Cell Approach. *The ISME Journal* 9: 485–96. doi:10.1038/ismej.2014.144.
- Woebken D., Fuchs B.M., Kuypers M.M.M. and Amann R. 2007. Potential Interactions of Particle-Associated Anammox Bacteria with Bacterial and Archaeal Partners in the Namibian Upwelling System. *Applied and Environmental Microbiology* 73 (14): 4648–57. doi:10.1128/AEM.02774-06.
- Wu Y.W., Simmons B.A. and Singer S.W. 2015. MaxBin 2.0: An Automated Binning Algorithm to Recover Genomes from Multiple Metagenomic Datasets. *Bioinformatics* 32 (4): 605–7. doi:10.1093/bioinformatics/btv638.
- Wuchter C., Abbas B., Coolen M.J.L., Herfort L., van Bleijswijk J., Timmers P., Strous M., Teira E., Herndl G.J., Middelburg J.J., Schouten S. and Sinninghe Damsté J.S. 2006. Archaeal Nitrification in the Ocean. *Proceedings of the National Academy of Sciences of the United States of America* 103 (33): 12317–22. doi:10.1073/pnas.0600756103.
- Zhang L., Altabet M.A., Wu T. and Hadas O. 2007. Sensitive Measurement of NH₄⁺ 15N/14N ($\Delta^{15}\text{NH}_4^+$) at Natural Abundance Levels in Fresh and Saltwaters. *Analytical Chemistry* 79: 5589–95.

Supplementary information

Supplementary text

Comparison of Thaumarchaeota CARD-FISH, amplicon and metagenomic abundances

Thaumarchaeota relative abundances determined by specific CARD-FISH counts and staining of all cells by DAPI were approximately 50% lower than Thaumarchaeota relative abundances based on 16S rRNA gene amplicon sequencing (Supplementary Figure 4), an opposing pattern to that observed by Mincer *et al.* (2007). Unlike amplicon relative abundances, metagenomic relative Thaumarchaeota abundances based on read fragment mapping to the obtained Thaumarchaeota MAGs were in the same range as relative CARD-FISH abundances but were correlated with the relative abundances obtained by amplicon sequencing (Supplementary Figure 4).

Thaumarchaeota genomes usually contain a single copy (operon) of rRNA genes (see overviews in Bayer *et al.* 2016; Stieglmeier *et al.* 2014), therefore, abundances based on 16S rRNA gene amplicon sequencing, metagenomics and CARD-FISH should be similar. The discrepancy observed between relative abundances of Thaumarchaeota CARD-FISH, metagenomics and amplicon sequencing could be due to primer/PCR biases, actively replicating cells (and thus multiple chromosome copies per cell), low ribosome content and insufficient cell permeabilization, or cell lysis during the CARD-FISH procedure.

While the CARD-FISH probe used was unlikely to miss a large fraction of Thaumarchaeota, the forward primer used for amplicon sequencing (Caporaso *et al.* 2011) shows a mismatch to most Thaumarchaeota (Parada *et al.* 2016). Despite this, environmental Thaumarchaeota appear to be well covered with this primer pair (Parada *et al.* 2016). We have assessed the Thaumarchaeota coverage by the used primers *in-silico* using the arb-silva test-prime online tool. Allowing for 1 mismatch over the entire primer length, but 0 mismatches for at least 5 bases at the 3' end as suggested in the test-prime documentation on arb-silva for realistic simulation of PCR behavior, the used primer pair targets 95% of marine Thaumarchaeota (Nitrosopumilales and Marine benthic group1), indicating that the Thaumarchaeota in the Gulf of Mexico were well covered despite a mismatch in the forward primer. Furthermore, all retrieved Thaumarchaeota 16S rRNA sequence fragments from the GoM metagenomes, where information for the primer binding sites is available, were also targeted when using the realistic PCR simulation scenario. These sequences also show a mismatch to the forward primer and are perfectly matched by the reverse primer 806R. Ultimately, the cause for the discrepancies in Thaumarchaeota relative abundances between different methods is unknown.

Per cell oxidation rates

CARD-FISH cell counts and ammonia oxidation rates were combined to calculate Thaumarchaeota per-cell ammonia oxidation rates. Assuming that the entire Thaumarchaeota community was actively oxidizing ammonia, per cell rates were between 0.9 – 30.8 fmol-N cell⁻¹ d⁻¹ which are in the same range reported for marine Thaumarchaeota pure cultures (Martens-Habbena *et al.* 2009; Qin *et al.* 2014) and in most studies of marine systems dominated by Thaumarchaeota (Wuchter *et al.* 2006; Santoro *et al.* 2010; Tolar *et al.* 2017). As we have assumed the entire community was active, these rates might be underestimates as there is evidence to suggest that not all ammonia oxidizers are active in natural communities (Smith *et al.* 2014). There are fewer examples of per cell urea-derived

oxidation rates available, and none so far for cyanate. We observed per-cell urea-derived oxidation rates ranging from below detection to $0.93 \text{ fmol-N cell}^{-1} \text{ d}^{-1}$, at the lower end of those reported by Tolar *et al.* (2017), and per-cell cyanate-derived oxidation rates ranged from $0.05 - 1.52 \text{ fmol-N cell}^{-1} \text{ d}^{-1}$.

Contribution of abiotic breakdown of urea and cyanate to the observed oxidation rates

As both urea and cyanate can undergo abiotic decay to ammonium (Dirnhuber & Schütz 1948), we measured the extent of abiotic breakdown of $^{15}\text{N}^{13}\text{C}$ -urea and $^{15}\text{N}^{13}\text{C}$ -cyanate to ^{15}N -ammonium and modeled its potential contribution to the observed oxidation rates in incubations with added ^{14}N -ammonium (ammonium pool incubations).

The amount of ^{15}N -nitrite which can stem from abiotic breakdown of $^{15}\text{N}^{13}\text{C}$ -urea or $^{15}\text{N}^{13}\text{C}$ -cyanate to ^{15}N -ammonium and subsequent ammonium oxidation depends on (I) the abiotic breakdown rates of $^{15}\text{N}^{13}\text{C}$ -urea or $^{15}\text{N}^{13}\text{C}$ -cyanate to ^{15}N -ammonium, (II) the regeneration rate of ammonium, (III) the ammonia oxidation rate to nitrite, (IV) the size of the ammonium pool and (V) the amount of added $^{15}\text{N}^{13}\text{C}$ -urea or $^{15}\text{N}^{13}\text{C}$ -cyanate.

Ammonia oxidation rates (III) were obtained from ^{15}N -ammonium incubations. The exact concentrations of added (IV) ^{14}N -ammonium (V) $^{15}\text{N}^{13}\text{C}$ -urea or $^{15}\text{N}^{13}\text{C}$ -cyanate were obtained from concentration measurements at time zero of the ammonium pool incubation experiments. Below, we detail how the abiotic breakdown rates and the ammonium regeneration rates were determined and how these five parameters were used to model the contribution of abiotic urea and cyanate breakdown to the observed nitrite production rates.

(I) Abiotic breakdown rates of $^{15}\text{N}^{13}\text{C}$ -urea and $^{15}\text{N}^{13}\text{C}$ -cyanate to ^{15}N -ammonium

We determined the abiotic breakdown rates of $^{15}\text{N}^{13}\text{C}$ -urea and $^{15}\text{N}^{13}\text{C}$ -cyanate to ^{15}N -ammonium in bottom water taken from one sampling location (Station 1) at two different oxygen concentrations. To determine abiotic breakdown rates of $^{15}\text{N}^{13}\text{C}$ -urea and $^{15}\text{N}^{13}\text{C}$ -cyanate to ^{15}N -ammonium, bottom water was sterile filtered ($0.22 \mu\text{m}$, Nalgene Fast-Flow filtration unit) onboard. Upon return to a land-based laboratory, seawater was again sterile filtered and bubbled with helium to decrease oxygen concentrations. 250 ml HCl-cleaned serum bottles were filled bubble-free. All further handling was done as in ammonium pool incubations in the field (see Methods and Supplementary Table 5).

Triplicate serum bottles for urea and cyanate were amended with $2.5 \mu\text{M}$ or $25 \mu\text{M}$ oxygen, mimicking typical oxygen concentrations in the GoM. Additional serum bottles containing oxygen sensor spots were used for monitoring oxygen concentration. Sampling was performed as described in the main text, but the filtered samples were immediately processed for analysis. ^{15}N -ammonium was measured at all time points. Moreover, to test for possible abiotic oxidation of urea or cyanate to nitrite, ^{15}N -nitrite concentrations were measured at time zero and the final time point.

For $^{15}\text{N}^{13}\text{C}$ -urea, we detected neither abiotic breakdown to ^{15}N -ammonium nor abiotic oxidation to ^{15}N -nitrite under the tested conditions. Therefore, we did not include any parameters for abiotic urea breakdown when modelling direct vs indirect urea utilization by Thaumarchaeota. The measured abiotic $^{15}\text{N}^{13}\text{C}$ -cyanate decay to ^{15}N -ammonium was linear and highly reproducible between replicates, with $9.4 \pm 0.17 \text{ nM d}^{-1}$ per μM cyanate, independent of the oxygen concentration. We did not observe abiotic oxidation of $^{15}\text{N}^{13}\text{C}$ -cyanate to ^{15}N -nitrite.

We do not expect the abiotic breakdown rate of urea and cyanate to differ between stations and depths, as these rates are determined by salinity, pH, temperature and seawater composition (Lister 1954; Taillades *et al.* 2001; Kamennaya *et al.* 2008). These factors did not differ significantly between depths or stations.

(II) Ammonium regeneration rate

Ammonium regeneration rates (AR) were determined from ammonia oxidation experiments (¹⁵N-ammonium addition) using the ¹⁵N-pool dilution approach (Kirkham & Bartholomew 1954; Kirkham & Bartholomew 1955). Regeneration rates were calculated between adjacent time points (0h and 6h, 6h and 12h, and 12h and 24h, respectively), according to Equation 1 (Kirkham & Bartholomew 1954; Kirkham & Bartholomew 1955; Inselsbacher et al. 2007). Parameters are given in Supplementary Table 11.

$$AR = (A_t - A_{t-1})/T * (\ln(AAPE_{t-1}/AAPE_t))/\ln(A_t/A_{t-1}) \quad \text{Equation (1)}$$

Ammonium regeneration rate (AR) values were averaged across triplicates and time points per depth. Total ammonium concentration at each time point (A_t) was determined fluorometrically (Holmes et al. 1999). ¹⁵N-content of the ammonium pool was assessed by conversion to N₂ by alkaline hypobromite (Warembourg 1993) and subsequent analysis of ²⁹N₂ and ³⁰N₂ by TraceGas-IRMS. ¹⁵N-atom% excess above ¹⁵N-natural abundance (>0.37 %) of the ammonium pool (AAPE) for each time point was then calculated according to:

$$AAPE = {}^{15}\text{N-NH}_4^+ / (\text{NH}_4^+_{\text{total}}) * 100 - 0.37 \quad \text{Equation (2)}$$

Ammonium regeneration rates ranged between 170 – 1,550 nM d⁻¹, depending on the depth investigated, which is in the lower range of ammonium regeneration rates measured previously in the Northern GoM (Gardner et al. 1993; Bode & Dortch 1996; Gardner et al. 1997).

Modeling the contribution of abiotic cyanate breakdown to observed oxidation rates

The expected amount of ¹⁵N in the nitrite pool above ¹⁵N-natural abundance (> 0.37 atom%) over 24 h (NAPE_{t=24}) stemming from abiotic breakdown of cyanate to ammonium and subsequent ammonia oxidation was calculated in 1 h increments (T) as follows (see Supplementary Table 12):

$$\text{NAPE}_t = \text{sum}(\text{NAPE}_{T(0-t)}) \quad \text{Equation (3)}$$

Where

$$\text{NAPE}_T = \text{AO}_{15\text{NT}} - \text{AO}_T / 100 * 0.37 \quad \text{Equation (4)}$$

$$\text{AO}_{15\text{NT}} = \text{AO}_T / 100 * \text{A}\%_{15\text{Nt}} \quad \text{Equation (5)}$$

$$\text{A}\%_{15\text{Nt}} = \text{A}_{15\text{Nt}} / (\text{A}_t) \quad \text{Equation (6)}$$

$$\text{A}_{15\text{Nt}} = \text{A}_{15\text{Nt-1}} - \text{AO}_{15\text{NT}} + \text{AI}_{15\text{NT}} \quad \text{Equation (7)}$$

$$\text{A}_t = \text{A}_{t-1} - \text{AO}_T + \text{AI}_T \quad \text{Equation (8)}$$

Briefly, the amount of ¹⁵N-nitrite appearing in the nitrite pool as a result of abiotic breakdown during each time interval was calculated by determining the labelling percentage of the ammonium pool (which is controlled by ammonium regeneration and cyanate breakdown rates) and then calculating how much of this ¹⁵N-ammonium is oxidized to ¹⁵N-nitrite (taking into account the ammonia oxidation rate).

To account for the input parameter variability (equations above and Supplementary Table 12), and their effect on the contribution of abiotic cyanate breakdown to the measured oxidation rates, we calculated minimum and maximum expected ¹⁵N in the nitrite pool.

We calculated minimum expected ^{15}N in the nitrite pool from abiotic breakdown using average values minus standard deviation (SD) for $^{15}\text{N}^{13}\text{C}$ -cyanate concentration and ammonia oxidation rate, and average values plus SD for ammonium regeneration rate and initial ammonium pool size. This combination of low cyanate concentration, low ammonia oxidation rate, high ammonium regeneration rate and large initial ammonium pool size gives the lowest rate, as any ^{15}N -ammonium from cyanate breakdown would be strongly diluted into the ambient ^{14}N -ammonium pool and additionally, lower ammonia oxidation would result in less ^{15}N -ammonium oxidation to ^{15}N -nitrite. Vice versa, the maximum expected ^{15}N in the nitrite pool from abiotic breakdown was calculated using average values plus SD for ammonia oxidation rate and $^{15}\text{N}^{13}\text{C}$ -cyanate concentration, and average values minus SD for ammonium regeneration rate and initial ammonium pool size.

We also accounted for the putative initial ^{15}N -ammonium contamination of $^{15}\text{N}^{13}\text{C}$ -cyanate (see main text section on Hypobromite conversions for ^{15}N -ammonium measurement in cyanate and urea samples) in our calculations by adding it to the natural abundance ^{15}N in the ammonium pool at time zero.

Indirect cyanate oxidation rates due to abiotic breakdown

For each time point, minimum and maximum ^{15}N above natural abundance in the nitrite pool (NAPE_t) resulting from abiotic breakdown was subtracted from measured ^{15}N -nitrite in ammonium pool incubations with ^{15}N -cyanate. The resulting corrected cyanate-derived oxidation rates were still significant and linear (Supplementary Figure 10, Supplementary Table 4) and constituted between 30% and 61% of the uncorrected rates in ammonium pool incubations at Station 2, depending on the depth investigated and the lower/upper bounds of the parameters used in the model. These results strongly indicate there is biological oxidation of cyanate to nitrite that cannot be accounted for by abiotic decay of $^{15}\text{N}^{13}\text{C}$ -cyanate to ^{15}N -ammonium and oxidation of the resulting ^{15}N -ammonium to ^{15}N -nitrite.

Contribution of biotic breakdown of urea and cyanate to the observed oxidation rates

In addition to abiotic breakdown, urea and cyanate can also be biotically degraded to ammonium by non-Thaumarchaeota cells. Part of the resulting ammonium could be released from cells to the environment and then be oxidized to nitrite by Thaumarchaeota. Similar to the contribution of abiotic breakdown, the amount of ^{15}N -nitrite stemming from biotic degradation of urea or cyanate to ammonium and subsequent ammonia oxidation depends on (I) the biotic degradation rate of $^{15}\text{N}^{13}\text{C}$ -urea or $^{15}\text{N}^{13}\text{C}$ -cyanate to ^{15}N -ammonium (analogous to abiotic breakdown rate above), (II) the regeneration rate of ammonium, (III) the ammonia oxidation rate to nitrite, and (IV) the size of the ammonium pool.

To model how much nitrite production was the result of biotic degradation of urea and cyanate, the same equations were used as those above. Unfortunately, the measurement of ^{15}N -ammonium in ammonium pool incubations with ^{15}N -cyanate was not possible due to inappropriate sample storage, which caused cyanate breakdown to ammonium in all samples. However, we could determine biotic degradation of $^{15}\text{N}^{13}\text{C}$ -urea to ^{15}N -ammonium in ammonium pool incubations with ^{15}N -urea at Station 2. Therefore, we used the values calculated for biotic urea breakdown to estimate indirect and direct cyanate utilization rates.

The biotic breakdown rate was calculated from ammonium pool incubations with ^{15}N -urea. We measured the production of ^{15}N -ammonium at rates ranging from 12 – 25 nM d⁻¹. However, this rate alone does not represent the biotic urea breakdown rate, as ammonia oxidation would have converted some of the produced ^{15}N -ammonium into ^{15}N -nitrite. Therefore, to determine the

absolute urea breakdown in the ammonium pool incubations, we used the model developed above to estimate how much ^{15}N -ammonium derived from biotic breakdown was oxidized further to nitrite. To achieve this, the breakdown rate of urea in the model was changed iteratively until the modeled ^{15}N -ammonium excess at each time point best corresponded to what was measured in the ammonium pool experiments with ^{15}N -urea. As the model included the ammonia oxidation rates, we could therefore determine the ^{15}N -nitrite excess that was a result of urea breakdown to ammonia and subsequent oxidation.

As described above, we accounted for the input parameter variability. We calculated minimum expected ^{15}N in the nitrite pool from biotic breakdown using average values minus SD for ammonia oxidation rate and average values plus SD for ammonium regeneration rate and initial ammonium pool size. To calculate maximum expected ^{15}N in the nitrite pool from biotic breakdown, we used average values plus SD for ammonia oxidation rate and average values minus SD for ammonium regeneration rate and initial ammonium pool size.

Modeled biotic urea breakdown rates at Station 2 ranged from 15 to 34 nM-N d^{-1} (7.5 – 17 nM urea) depending on the depth investigated and the lower/upper bounds of the parameters used for the model. These modeled values are similar to maximum urea breakdown rates measured by Cho & Azam (1995) in the Southern California Bight.

Direct urea and cyanate utilization rates

Direct urea oxidation rates were calculated by subtracting the ^{15}N -nitrite concentration (NAPet) that occurred at each time point as a result of biotic urea breakdown (abiotic rates were below detection) from the total ^{15}N -nitrite production measured in the ammonium pool incubations. The remaining ^{15}N -nitrite production was still linear over time and rates calculated from this production were still significant (Supplementary Figure 10). The direct urea oxidation rates were around 50 % of the total measured ^{15}N -nitrite production rates, depending on the depth investigated and the lower/upper bounds of the parameters used for the model. These results strongly indicate that Thaumarchaeota directly use urea as an energy source via intracellular conversion to ammonium.

Direct cyanate oxidation rates were calculated by subtracting the ^{15}N -nitrite concentration (NAPet) that could have been produced at each time point as a result of abiotic cyanate breakdown and biotic breakdown (taken from urea experiment) from the total ^{15}N -nitrite production measured in the ammonium pool incubations (Supplementary Table 3). The remaining ^{15}N -nitrite, which represents the corrected cyanate-derived oxidation rates were still significant at a number of depths, which strongly supports that cyanate is directly used by GoM Thaumarchaeota.

To estimate the detection limits for direct urea and cyanate utilization rates, the median of the standard error of the slope for single replicates (for which the calculated direct rate was significant) was multiplied by the t value for $p = 0.05$. This was done separately for urea and cyanate incubations and resulted in estimated detection limits of 2.2 nM d^{-1} and 2.6 nM d^{-1} for ammonium pool incubations with urea and cyanate, respectively. Nevertheless, at 12m depth, station 2, we were still able to observe direct urea utilization rates between 1.2 to 1.6 $\text{nM NO}_2^- \text{d}^{-1}$, which were significantly different from zero, highlighting that the detection limits in this case are only an estimate.

Our results show that ammonium pool incubations to differentiate between direct and indirect use of urea and cyanate by Thaumarchaeota are vital to draw correct conclusions from tracer incubations.

Controls to assess cyanate breakdown in *Nitrosopumilus maritimus* cultures

Control experiments were carried out to test for 1) abiotic breakdown of cyanate in the medium (abiotic controls) and 2) breakdown of cyanate in the culture supernatant of *N. maritimus* after growth on 1 mM ammonium (supernatant controls). In the culture experiments, the oxidation of 1 mM ammonium caused the pH of the medium to drop from 7.6 to 7.2 and led to the production of 1mM NO_2^- . Both of these factors can influence cyanate breakdown, therefore, medium for abiotic controls was titrated to 7.2 with HCl prior to the addition of tracer and amended with 1mM $^{14}\text{N-NaNO}_2^-$.

For supernatant controls, *N. maritimus* was inoculated as described in the methods and allowed to consume 0.9 mM ammonium, after which cells were gently removed using a hand-operated vacuum pump (<5 mbar, 0.2 μm Nalgene Fast-Flow filtration unit). Subsequently, both the abiotic and supernatant controls were amended with 200 μM $^{14}\text{N-NH}_4^+$ and 40 μM $^{13}\text{C}^{15}\text{N}$ -cyanate and were incubated and sampled as described in the methods section.

The contribution of abiotic cyanate breakdown to the observed cyanate-derived oxidation rates in the *N. maritimus* cultures was calculated analogously to field experiments. The expected amount of ^{15}N in the nitrite pool stemming from abiotic decay of cyanate to ammonium and subsequent ammonia oxidation was calculated over 12 h as described above (Supplementary Discussion Modeling the contribution of abiotic cyanate breakdown to observed oxidation rates), in this case however, ammonium regeneration was not accounted for.

Additionally, we calculated the expected amount of ^{15}N in the nitrite pool assuming that all ^{15}N -nitrite produced in biotic incubations first was released into the extracellular ammonium pool and subsequently oxidized to nitrite. This was done by using the production rate of ^{15}N -ammonium + ^{15}N -nitrite in biotic incubations (after subtraction of abiotic cyanate decay to ammonium) as input parameters for $\text{Al}_{15\text{NT}}$ and Al_T in Equation 7 and 8.

Abiotic breakdown of ^{15}N -cyanate to ammonium in sterile filtered media (adjusted to pH 7.2) occurred at a rate of 34.4 nM of NH_4^+ per 1 μM of cyanate added per day in the presence of 200 μM ammonium and 1 mM nitrite. This is 3.7x higher than cyanate breakdown in GoM seawater, which is likely due to the differences in pH and salt composition between medium and natural seawater.

When the cultures were incubated with $^{15}\text{N}^{13}\text{C}$ -cyanate and a large (ca. 200 μM) ^{14}N -ammonium pool, the production of ^{15}N -nitrite was significantly higher than could be explained by abiotic breakdown of cyanate to ammonium in the medium (main text, Figure 4b, Supplementary Figure 14). However, ^{15}N -nitrite production was not linear, with a lag at the start of the experiment, while we detected linear production of ^{15}N -ammonium (Supplementary Figure 14). When we modeled the expected ^{15}N -nitrite production assuming that all cyanate first enters the extracellular ammonium pool as ^{15}N -ammonium before oxidation to nitrite, the modeled rate was similar to the measured ^{15}N -nitrite production rate (Supplementary Figure 14). This could indicate that either the breakdown of cyanate occurs extracellularly, by soluble compounds or enzymes secreted by the AOA during growth, or, if cyanate breakdown occurs intracellularly, that there is a rapid equilibration between the intracellular and extracellular ammonium pools.

We assessed the possible extracellular component of cyanate breakdown by the AOA in supernatant controls. Cyanate breakdown rates measured in the supernatant controls were around 50 % of the rates measured in the culture incubations, indicating that part of the cyanate breakdown might occur due to extracellular compounds, for example promiscuous enzymes with activity on cyanate, or secreted metabolites which catalyze the breakdown of cyanate to ammonium. However, we cannot exclude that intracellular components may have been released via cell lysis during the low-pressure

filtration. Regardless of the mechanism, these experiments show that *Nitrosopumilus maritimus*, which lacks a known cyanase can use cyanate as an energy source at higher rates than can be explained by abiotic breakdown.

Urea, Ammonium and Cyanate Contamination from Syringe Filters

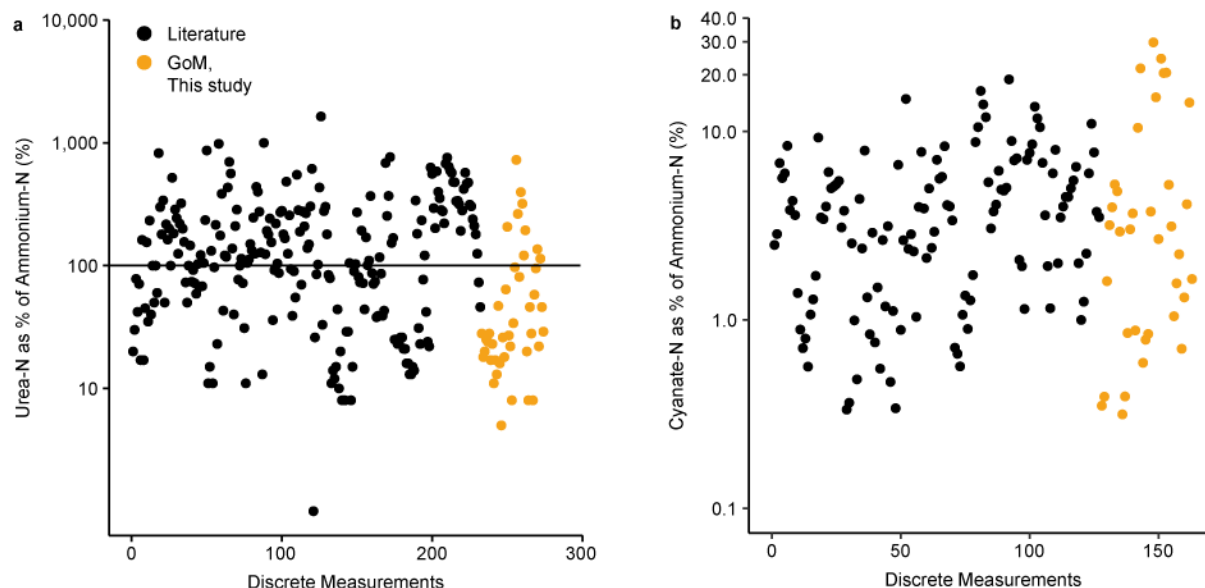
Two syringe filter types were tested for contamination with urea and ammonium, 0.22 μm PES (Millex, Millipore) and 0.20 μm CA syringe filters (Minisart, Supelco). North Sea seawater was amended with two urea (100 and 1,000 nM addition) and ammonium concentrations (80 and 160 nM addition) and additionally tested without amendments. 20 ml of seawater were filtered in triplicate through the two types of syringe filters, once directly, and once after pre-rinsing the filter by filtration of 10 ml ultrapure water. Ammonium and urea concentrations were measured in unfiltered and filtered samples. While urea contamination from the two filter types was generally low and did not vary between filters pre-rinsed with ultrapure water and filters directly used for seawater filtration, high ammonium contamination was observed for CA filters, especially when filters were not pre-rinsed with ultrapure water (Supplementary Figure 15). These results indicate that the choice of filter material and filter type (as PES filters from other suppliers result in different contamination patterns), is crucial for nutrient measurements. Especially for ammonium concentration measurements, pre-filtration is problematic, and measurements should be performed using unfiltered seawater samples. Cyanate contamination was tested for 0.22 μm PES syringe filters (Millex, Millipore) only and was below the detection limit.

Supplementary references

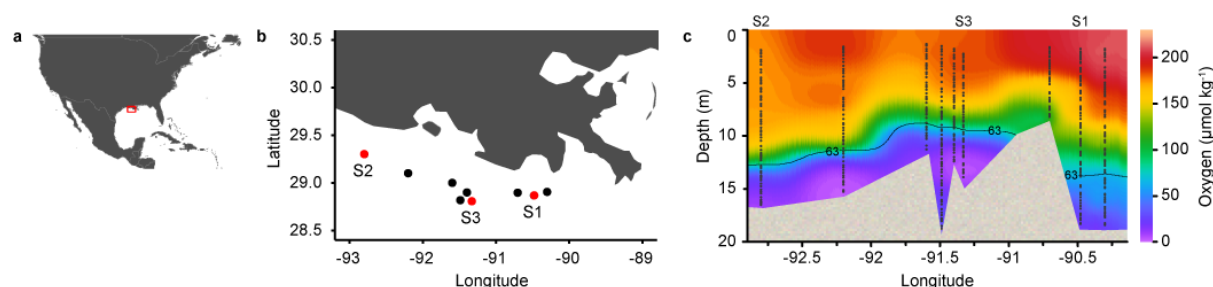
- Bayer B., Vojvoda J., Offre P., Alves R.J.E., Elisabeth N.H., Garcia J. AL, Volland J.-M., Srivastava A., Schleper C. and Herndl G.J. 2016. Physiological and Genomic Characterization of Two Novel Marine Thaumarchaeal Strains Indicates Niche Differentiation. *The ISME Journal* 10. Nature Publishing Group: 1051–63. doi:10.1038/ismej.2015.200.
- Bode A. and Dortch Q. 1996. Uptake and Regeneration of Inorganic Nitrogen in Coastal Waters Influenced by the Mississippi River: Spatial and Seasonal Variations. *Journal of Plankton Research* 18 (12): 2251–68.
- Butler E.I., Knox S. and Liddicoat M.I. 1979. The Relationship between Inorganic and Organic Nutrients in Seawater. *Journal of the Marine Biological Association of the United Kingdom* 59. Max-Planck-Institut fuer Marine Mikrobiologie: 239–50.
- Caporaso J.G., Lauber C.L., Walters W.A., Berg-Lyons D., Lozupone C.A., Turnbaugh P.J., Fierer N. and Knight R. 2011. Global Patterns of 16S RRNA Diversity at a Depth of Millions of Sequences per Sample. *Proceedings of the National Academy of Sciences of the United States of America* 108 (suppl. 1): 4516–22. doi:10.1073/pnas.1000080107.
- Cho B.C. and Azam F. 1995. Urea Decomposition by Bacteria in the Southern California Bight and Its Implications for the Mesopelagic Nitrogen Cycle. *Marine Ecology Progress Series* 122: 21–26. doi:10.3354/meps122021.
- Dirnhuber P. and Schütz F. 1948. The Isomeric Transformation of Urea into Ammonium Cyanate in Aqueous Solutions. *Biochemical Journal* 42 (4): 628–32.
- Gardner W.S., Cavaletto J.F., Cotner J.B. and Johnson J.R. 1997. Effects of Natural Light on Nitrogen Cycling Rates in the Mississippi River Plume. *Limnology and Oceanography* 42 (2): 273–81.
- Gardner W.S., Jr. J.B.C. and Herche L.R. 1993. Chromatographic Measurement of Nitrogen Mineralization Rates in Marine Coastal Waters with ¹⁵N. *Marine Ecology Progress Series* 93: 65–73.
- Holmes R.M., Aminot A., Kérouel R., Hooker B.A. and Peterson B.J. 1999. A Simple and Precise Method for Measuring Ammonium in Marine and Freshwater Ecosystems. *Canadian Journal of Fisheries and Aquatic Sciences* 56: 1801–8.
- Inselsbacher E., Cambui C.A., Richter A., Stange C.F., Mercier H. and Wanek W. 2007. Microbial Activities and Foliar Uptake of Nitrogen in the Epiphytic Bromeliad *Vriesea Gigantea*. *New Phytologist* 175: 311–20. doi:10.1111/j.1469-8137.2007.02098.x.
- Kamennaya N.A., Chernihovsky M. and Post A.F. 2008. The Cyanate Utilization Capacity of Marine Unicellular Cyanobacteria. *Limnology and Oceanography* 53 (6): 2485–94. doi:10.4319/lo.2008.53.6.2485.
- Kirkham D. and Bartholomew W. V. 1954. Equations for Following Nutrient Transformations in Soil, Utilizing Tracer Data. *Soil Science Society of America Journal* 18: 33–34.
- Kirkham D. and Bartholomew W. V. 1955. Equations for Following Nutrient Transformations in Soil, Utilizing Tracer Data II. *Soil Science Society of America Journal* 19: 189–92. doi:10.2136/sssaj1954.03615995001800010009x.
- Lister M.W. 1954. Some Observations on Cyanic Acid and Cyanates. *Canadian Journal of Chemistry* 33 (2): 426–40.
- Liu Q., Tolar B.B., Ross M.J., Cheek J.B., Sweeney C.M., Wallsgrove N.J., Popp B.N. and Hollibaugh J.T. 2018. Light and Temperature Control the Seasonal Distribution of Thaumarchaeota in the South Atlantic Bight. *The ISME Journal* 12: 1473–85. doi:10.1038/s41396-018-0066-4.
- Martens-Habbena W., Berube P.M., Urakawa H., de la Torre J.R. and Stahl D.A. 2009. Ammonia Oxidation Kinetics Determine Niche Separation of Nitrifying Archaea and Bacteria. *Nature* 461: 976–79. doi:10.1038/nature08465.
- McCarthy J.J. 1972. The Uptake of Urea by Natural Populations of Marine Phytoplankton. *Limnology and Oceanography* 17 (5): 738–48.
- McCarthy J.J. and Kamykowski D. 1972. Urea and Other Nitrogenous Nutrients in La Jolla Bay during February, March, and April 1970. *Fishery Bulletin* 70 (4): 1261–74.
- Mincer T.J., Church M.J., Taylor L.T., Preston C., Karl D.M. and DeLong E.F. 2007. Quantitative Distribution of Presumptive Archaeal and Bacterial Nitrifiers in Monterey Bay and the North Pacific Subtropical Gyre. *Environmental Microbiology* 9 (5): 1162–75. doi:10.1111/j.1462-2920.2007.01239.x.

- Mitamura O. and Saijo Y. 1975. Decomposition of Urea Associated with Photosynthesis of Phytoplankton in Coastal Waters. *Marine Biology* 30 (1): 67–72. doi:10.1007/BF00393754.
- Newell B.S. 1967. The Determination of Ammonia in Sea Water. *Journal of the Marine Biological Association of the United Kingdom* 47: 271–80. doi:doi.org/10.1017/S0025315400056381.
- Nguyen L.T., Schmidt H.A., Von Haeseler A. and Minh B.Q. 2015. IQ-TREE: A Fast and Effective Stochastic Algorithm for Estimating Maximum-Likelihood Phylogenies. *Molecular Biology and Evolution* 32 (1): 268–74. doi:10.1093/molbev/msu300.
- Parada A.E., Needham D.M. and Fuhrman J.A. 2016. Every Base Matters: Assessing Small Subunit rRNA Primers for Marine Microbiomes with Mock Communities, Time Series and Global Field Samples. *Environmental Microbiology* 18 (5): 1403–14. doi:10.1111/1462-2920.13023.
- Qin W., Amin S.A., Martens-Habbenha W., Walker C.B., Urakawa H., Devol A.H., Ingalls A.E., Moffett J.W., Armbrust E.V. and Stahl D.A. 2014. Marine Ammonia-Oxidizing Archaeal Isolates Display Obligate Mixotrophy and Wide Ecotypic Variation. *Proceedings of the National Academy of Sciences of the United States of America* 111 (34): 12504–9. doi:10.1073/pnas.1324115111.
- Santoro A.E., Casciotti K.L. and Francis C.A. 2010. Activity, Abundance and Diversity of Nitrifying Archaea and Bacteria in the Central California Current. *Environmental Microbiology* 12 (7): 1989–2006. doi:10.1111/j.1462-2920.2010.02205.x.
- Savidge G. and Hutley H.T. 1977. Rates of Remineralization and Assimilation of Urea by Fractionated Plankton Populations in Coastal Waters. *Journal of Experimental Marine Biology and Ecology* 28: 1–16. doi:10.1016/0022-0981(77)90058-2.
- Schlitzer R. 2016. Ocean Data View.
- Smith J.M., Casciotti K.L., Chavez F.P. and Francis C. a. 2014. Differential Contributions of Archaeal Ammonia Oxidizer Ecotypes to Nitrification in Coastal Surface Waters. *The ISME Journal* 8: 1704–14. doi:10.1038/ismej.2014.11.
- Stieglmeier M., Alves R.J.E. and Schleper C. 2014. The Phylum Thaumarchaeota. In *The Prokaryotes: Other Major Lineages of Bacteria and The Archaea*, 347–62. Springer. doi:10.1007/978-3-642-38954-2.
- Taillades J., Boiteau L., Beuzelin I., Lagrille O., Biron J.-P., Vayaboury W., Vandenabeele-Trambouze O., Giani O. and Commeyras A. 2001. A PH-Dependent Cyanate Reactivity Model: Application to Preparative N-Carbamoylation of Amino Acids. *Journal of the Chemical Society, Perkin Transactions 2* 7: 1247–54. doi:10.1039/b005856o.
- Tolar B.B., Wallsgrove N.J., Popp B.N. and Hollibaugh J.T. 2017. Oxidation of Urea-Derived Nitrogen by Thaumarchaeota-Dominated Marine Nitrifying Communities. *Environmental Microbiology* 19 (12): 4838–4850. doi:10.1002/elsc.201200179.
- Turley C.M. 1986. Urea Uptake by Phytoplankton at Different Fronts and Associated Stratified and Mixed Waters on the European Shelf. *British Phycological Journal* 21 (2): 225–38. doi:10.1080/00071618600650271.
- Warembourg F.R. 1993. Nitrogen Fixation in Soil and Plant Systems. In *Nitrogen Isotope Techniques*, edited by Roger Knowles and Henry Blackburn, 1st editio, 127–56. San Diego: ACADEMIC PRESS, INC. doi:10.1016/B978-0-08-092407-6.50010-9.
- Widner B., Mordy C.W. and Mulholland M.R. 2018. Cyanate Distribution and Uptake above and within the Eastern Tropical South Pacific Oxygen Deficient Zone. *Limnology and Oceanography* 63 (S1): S177–92. doi:10.1002/lno.10730.
- Widner B. and Mulholland M.R. 2017. Cyanate Distribution and Uptake in North Atlantic Coastal Waters. *Limnology and Oceanography* 62 (6): 2538–49. doi:10.1002/lno.10588.
- Widner B., Mulholland M.R. and Mopper K. 2016. Distribution, Sources, and Sinks of Cyanate in the Coastal North Atlantic Ocean. *Environmental Science & Technology Letters* 3 (8): 297–302. doi:10.1021/acs.estlett.6b00165.
- Wuchter C., Abbas B., Coolen M.J.L., Herfort L., van Bleijswijk J., Timmers P., Strous M., Teira E., Herndl G.J., Middelburg J.J., Schouten S. and Sinninghe Damsté J.S. 2006. Archaeal Nitrification in the Ocean. *Proceedings of the National Academy of Sciences of the United States of America* 103 (33): 12317–22. doi:10.1073/pnas.0600756103.

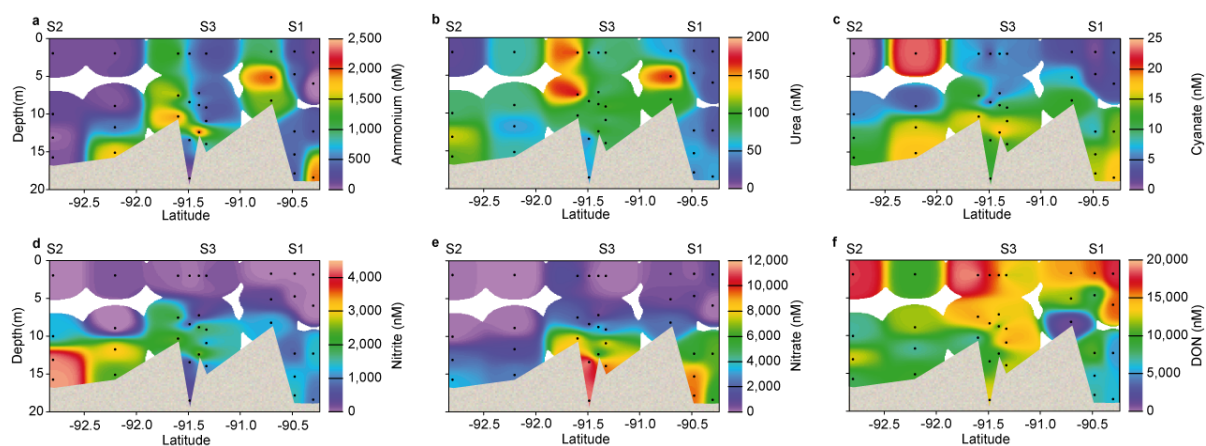
Supplementary figures



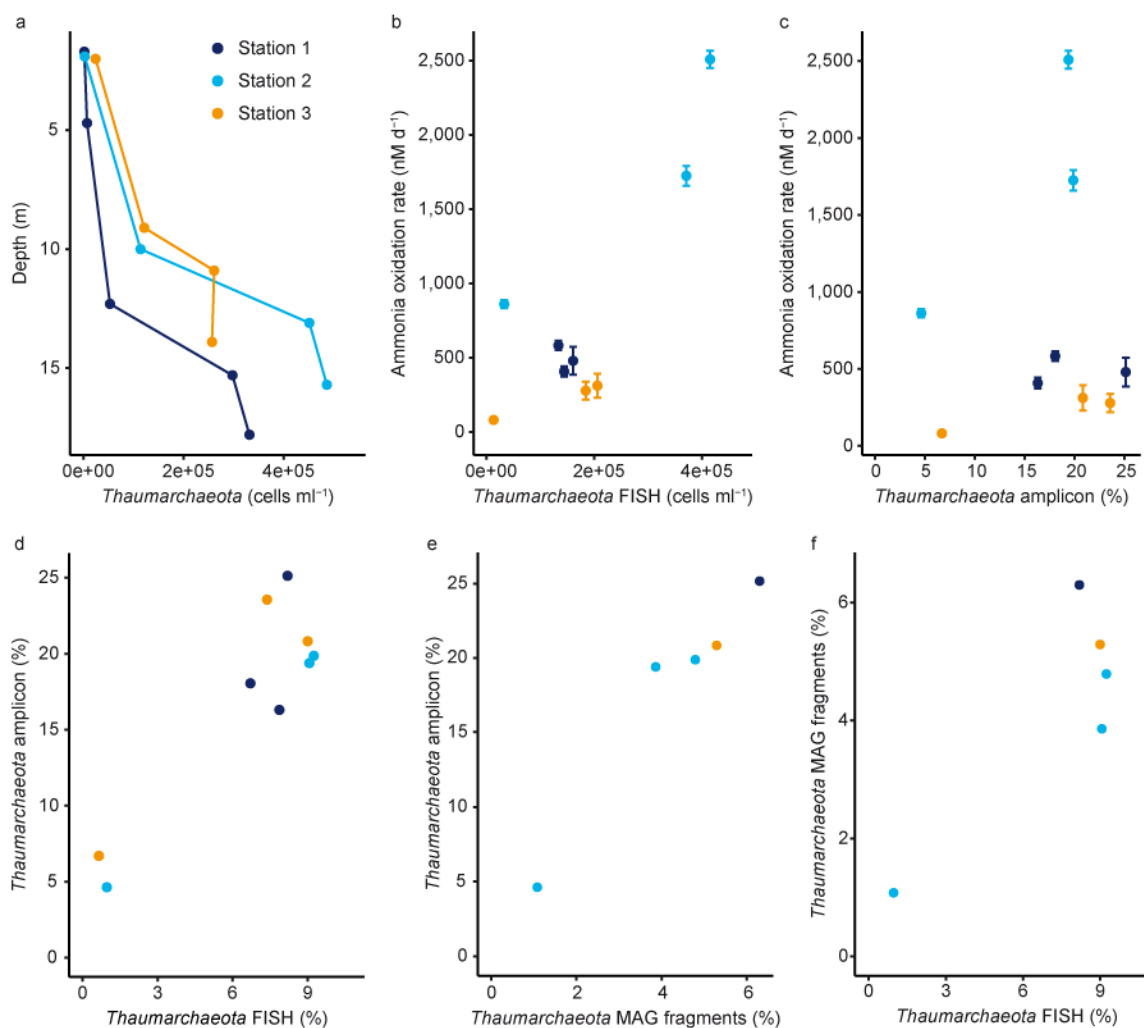
Supplementary Figure 1 Concentrations of urea (a) and cyanate (b) depicted as percentages of ammonium in continental shelf waters. Urea concentrations were converted to nmol N for the comparison (i.e. 1 mol of urea contains 2 mol of N). Literature values are depicted in black, values for the GoM obtained in this study in orange. Each data point represents one discrete sample for which both urea and ammonium (a) or cyanate and ammonium (b) were determined. It should be noted that less data are available for cyanate, furthermore the detection limits of ammonium and cyanate differ by two orders of magnitude (10 - 40 nM ammonium, 0.4 nM cyanate). Studies shown on the x-axis in a) are 1-38 Newell (1967); 39-48 Turley (1986); 49-74 McCarthy (1972); 75-80 McCarthy & Kamykowski (1972); 81-90 Mitamura & Saijo (1975); 91-99 Savidge & Hutley (1977); 100-113 Butler *et al.* (1979); 114-128 Tolar *et al.* (2017); 129-232 Liu *et al.* (2018). Studies included in b) are 1-28 Widner *et al.* (2016); 29-108 Widner & Mulholland (2017); 109-127 Widner *et al.* (2018).



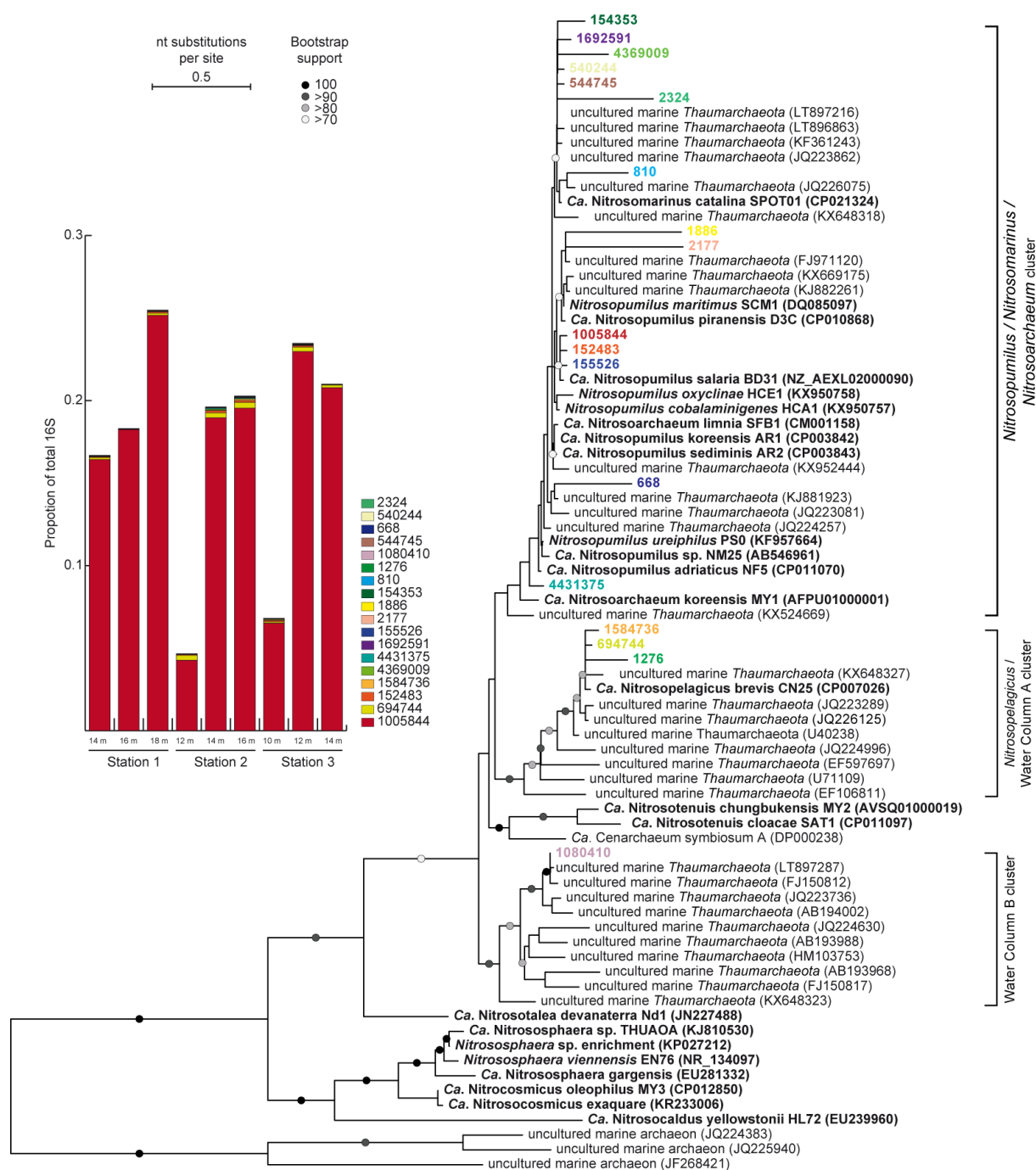
Supplementary Figure 2 Overview of sampling transect and oxygen concentration profiles in the GoM. a) Sampling location is marked by a red square. b) Station locations, with red dots (S1 – S3) marking experimental stations and black dots marking additional stations for oxygen and nutrient profiles. c) Oxygen concentrations across the sampling transect (with shaded area indicating the seafloor). The 63 $\mu\text{mol kg}^{-1}$ contour marks the onset of hypoxic conditions. Plot was generated using Ocean Data View (Schlitzer 2016).



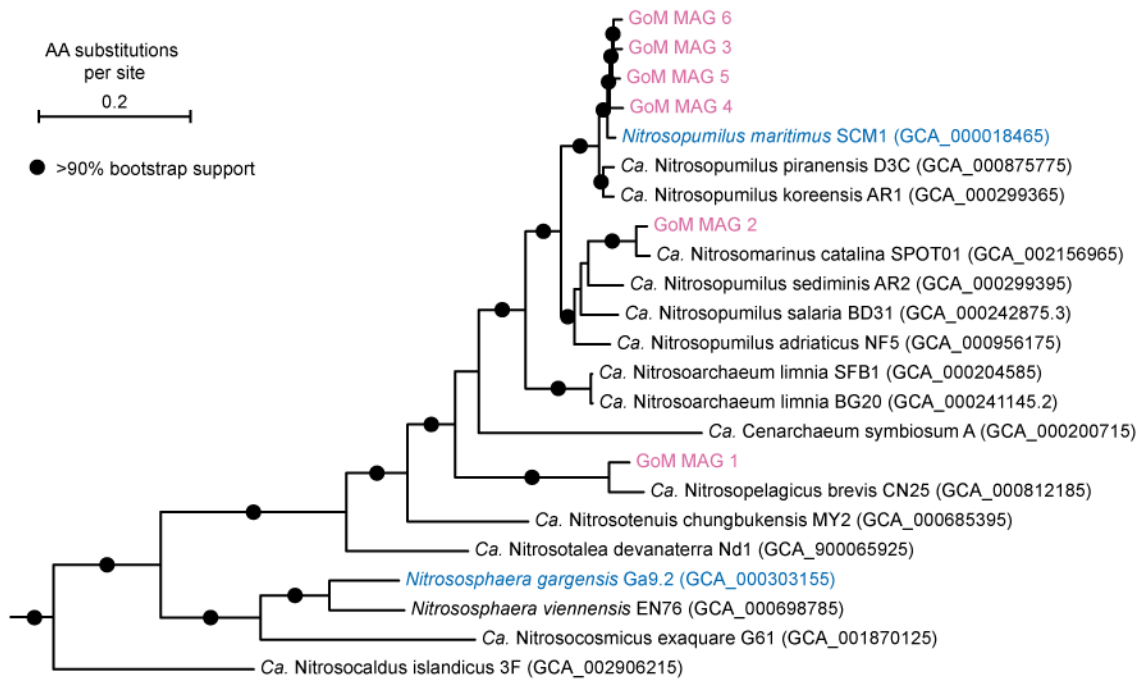
Supplementary Figure 3 Nutrient profiles across the sampling transect (with shaded area indicating the seafloor). a) Ammonium, b) urea, c) cyanate, d) nitrite e) nitrate and f) DON concentrations. Black dots mark locations of nutrient measurements. S1 – S3 mark the position of experimental stations. Plots were generated using Ocean Data View (Schlitzer 2016).



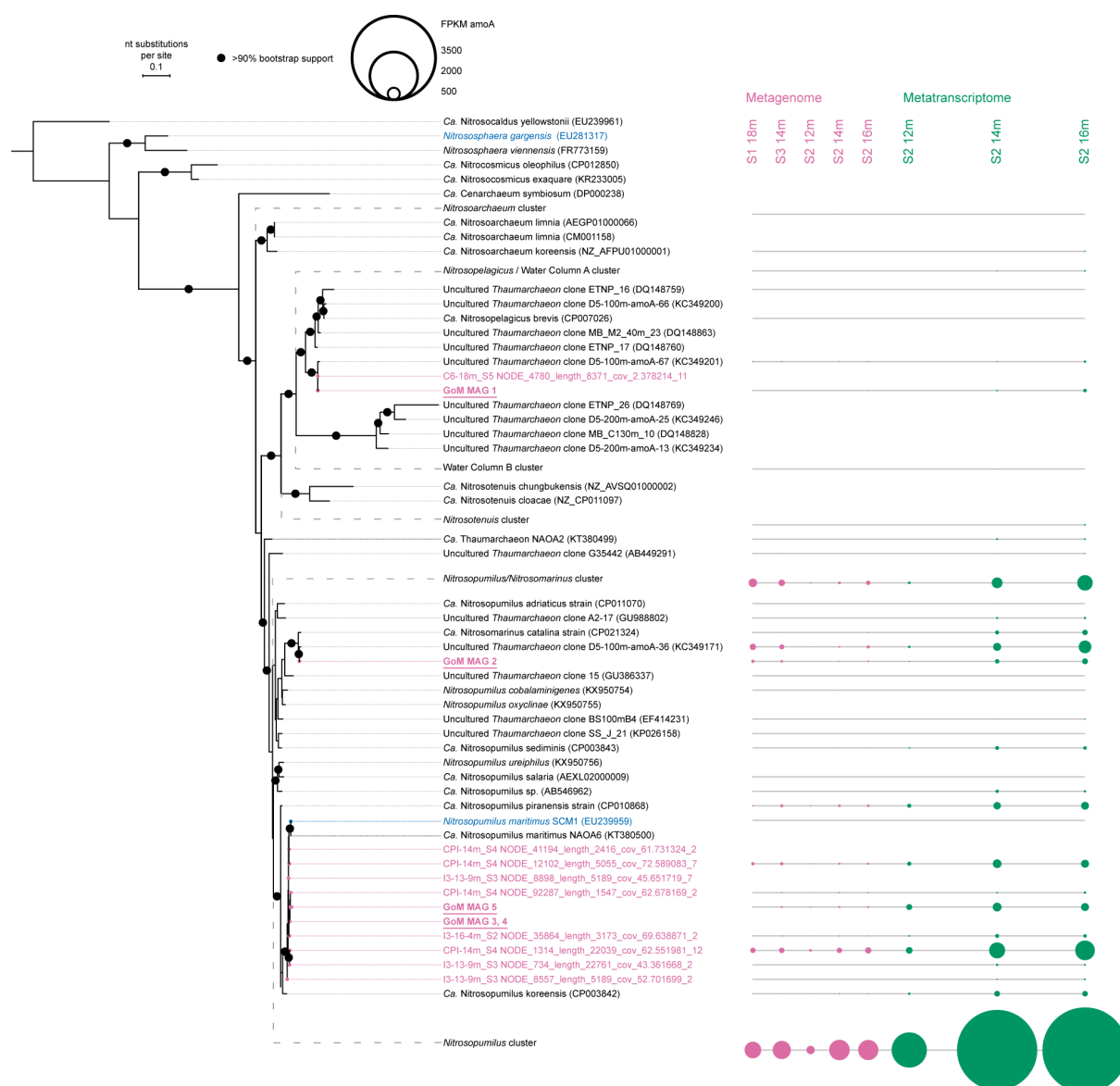
Supplementary Figure 4 Thaumarchaeota abundances a) Thaumarchaeota abundance depth profiles across all experimental stations, determined by CARD-FISH. b) Correlation between Thaumarchaeota abundance in experimental samples (based on CARD-FISH counts) and ammonia oxidation rate. c) Correlation between relative Thaumarchaeota abundance (based on amplicon sequencing data) and ammonia oxidation rate. d) Correlation between relative Thaumarchaeota abundance from specific CARD-FISH counts and amplicon sequencing data. e) Correlation between relative Thaumarchaeota abundance from Thaumarchaeota MAG relative FPKM abundance and amplicon sequencing data. A breakdown of MAG coverage per site is shown in Supplementary Table 2. f) Correlation between relative Thaumarchaeota abundance from specific CARD-FISH counts and Thaumarchaeota MAG relative FPKM abundance. No significant correlations (Spearman rank correlation) were found for b) $S = 8$, $\rho = 0.45$, $p = 0.230$, c) $S = 32$, $\rho = -0.08$, $p = 0.843$, d) $S = 50$, $\rho = 0.58$, $p = 0.108$, f) $S = 18$, $\rho = 0.1$, $p = 0.950$. Significant correlation (Pearson correlation coefficient) was found for e) $t = 7.7$, $DF = 3$, $p = 0.005$, $R^2 = 0.976$. Error bars for rates represent the standard error of slopes across biological triplicates and all time points. *Thaumarchaeota* abundance was determined from CARD-FISH counts. For panel a), n for DAPI-stained / *Thaumarchaeota* cells was 9,039 / 6; 13,902 / 24; 8,915 / 203; 12,409 / 1,143; 10,042 / 1,132 at Station 1 for 1.7 m, 4.8 m, 12.1 m, 15.4 m and 18.0 m, respectively; $n = 9,247 / 7$; 13,296 / 389; 17,253 / 1,541; 16,770 / 1,660 at Station 2 for 1.7 m, 10.1 m, 13.0 m and 15.7 m, respectively; $n = 8,874 / 82$; 10,047 / 725; 7,642 / 780; 7,126 / 767 at Station 3 for 2.0 m, 9.1 m, 10.9 m and 14.1 m, respectively. In panels b), d) and f), n for DAPI-stained / *Thaumarchaeota* cells was = 6,306 / 493; 6,484 / 457; 6,223 / 481 at Station 1 for 14.0 m, 16.1 m and 18.2 m, respectively; $n = 9,486 / 99$; 14,304 / 1,240; 12,406 / 1,109 at Station 2 for 11.9 m, 13.9 m and 16.4 m, respectively; and $n = 5,774 / 46$; 8,206 / 630; 9,586 / 888 at Station 3 for 9.9 m, 11.8 m and 14.0 m, respectively.



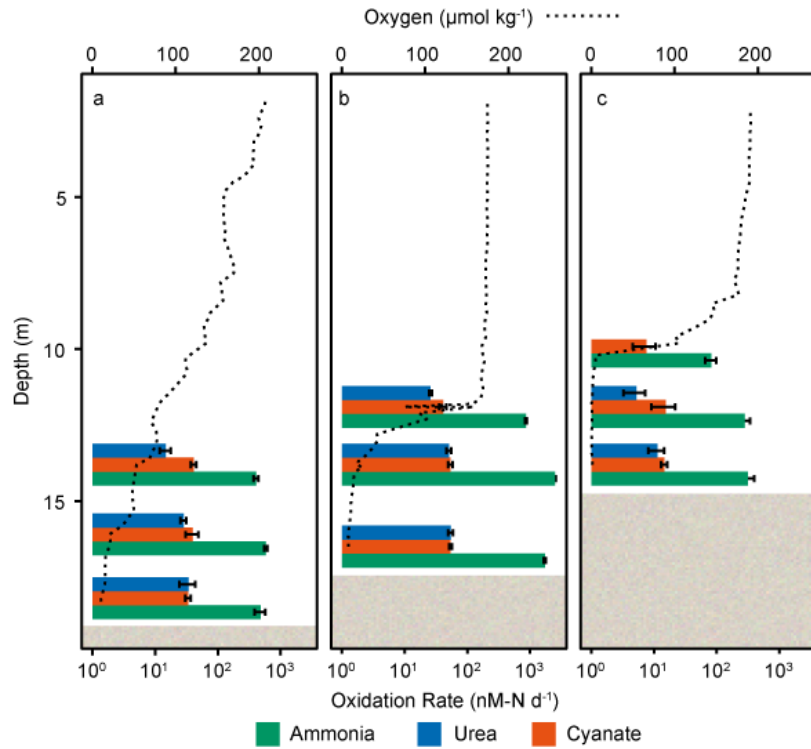
Supplementary Figure 5 Phylogenetic affiliation of Thaumarchaeota 16S rRNA gene reads obtained from the GoM samples. Phylogenetic maximum likelihood tree of Thaumarchaeota-affiliated OTUs (97% similarity clustering). Colored labels are OTUs from this study. Black labels are reference sequences. Enrichment and pure culture representatives are in bold. The tree was made using RAXML EPA. The core phylogeny was generated from an alignment of near full-length 16S rRNA gene (≥ 1300 nt) sequences and estimated via maximum likelihood using the “GTRGAMMA” model in RAXML with 1000 bootstrap iterations. Short sequences (< 1300 nt) were placed into the tree using the RAXML EPA function. The scale bar represents substitutions per site and bootstrap support values >70 are displayed. Insert middle left shows abundance of different Thaumarchaeota OTUs, represented as a proportion of all obtained 16S rRNA gene amplicons. All stations and depths were dominated by a single OTU (1005844).



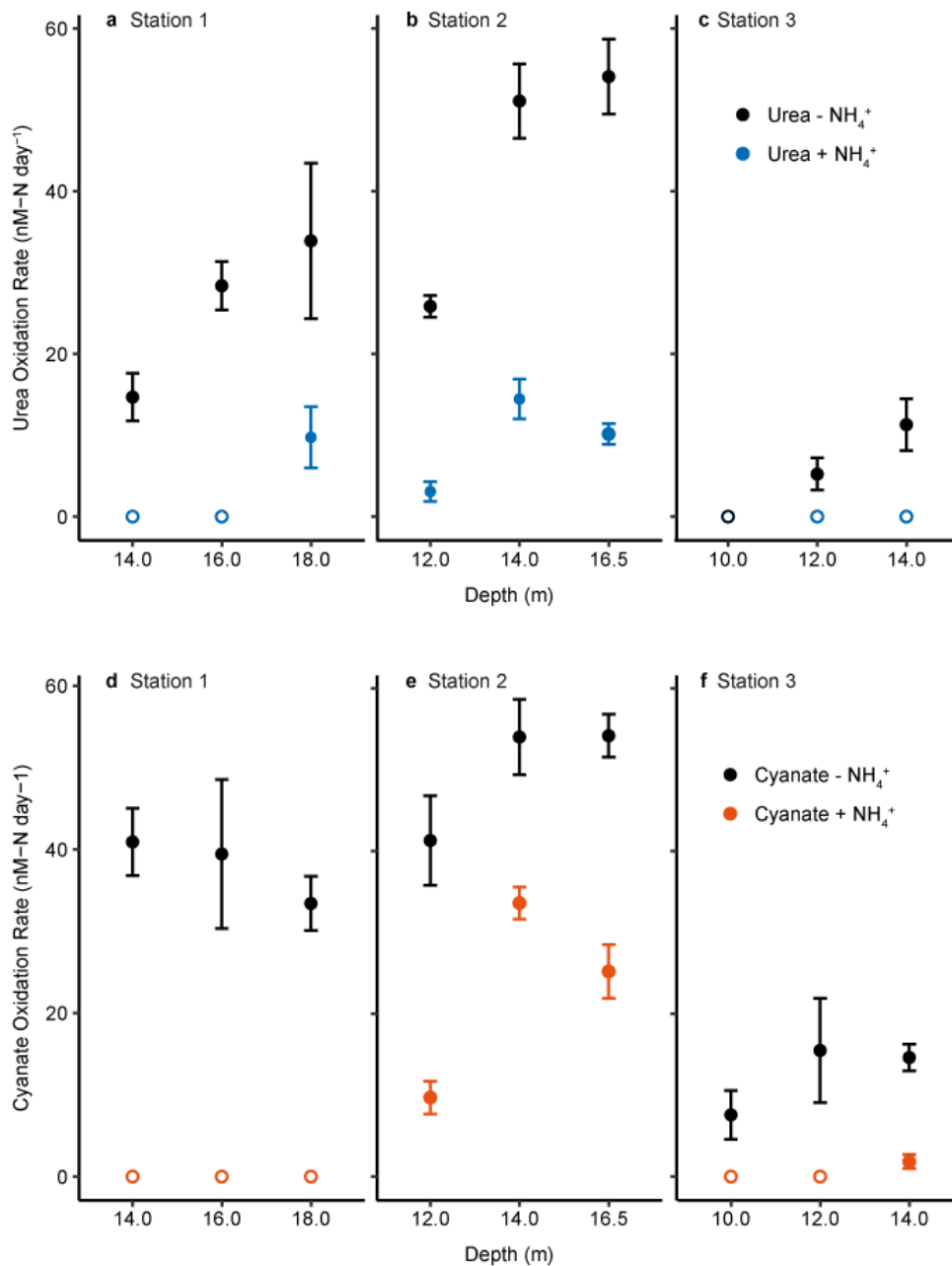
Supplementary Figure 6 Thaumarchaeota genome tree based on 34 universal concatenated marker genes. Thaumarchaeal GoM metagenome assembled genomes (GoM MAGs) are depicted in magenta, Thaumarchaeota cultures that are able to utilize cyanate are depicted in blue. Aigarchaeota and Bathyarchaeota genomes were used as an outgroup. Concatenated alignment was created using CheckM, tree was calculated using IQ-TREE (Nguyen et al. 2015) with automated model selection. Confidence was assessed with ultrafast bootstrapping (1,000 iterations). Scale bar represents amino acid substitutions per site, and bootstrap values > 90 are displayed.



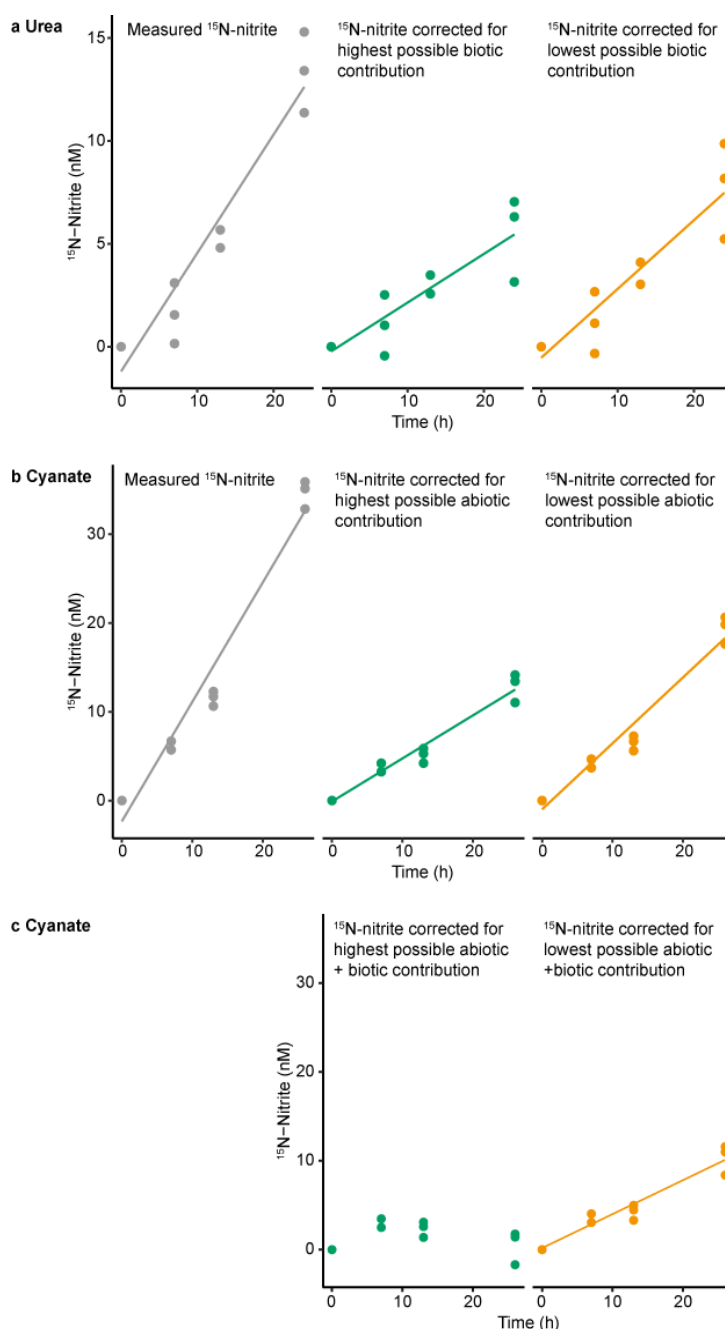
Supplementary Figure 7 *amoA* phylogenetic affiliation and abundance obtained from GoM metagenomics and metatranscriptomics. Assembled *amoA* sequences obtained from GoM metagenomic data are indicated in magenta, *amoA* sequences present in Thaumarchaeota GoM MAGs are in bold and underlined. Blue branches indicate Thaumarchaeota cultures tested for cyanate use. Black branches are Thaumarchaeota reference *amoA* nucleotide (nt) sequences. GoM metagenomic and metatranscriptomic read fragments were mapped onto the alignment and are shown next to the respective branch as magenta and green circles for metagenomics and metatranscriptomics, respectively. Read fragments mapping to internal nodes were grouped together for closely related sequences and are indicated by dashed lines. The most abundant *amoA* sequences were closely related to *Nitrosopumilus maritimus* SCM1. Tree was constructed using IQ-TREE (Nguyen et al. 2015) with automated model selection from near full-length *amoA* sequences and confidence was assessed with ultrafast bootstrapping (1,000 iterations). Metagenomic and metatranscriptomic *amoA* read fragments were fit into the core alignment using the short fragment add option in mafft. The resulting alignment was used to place short sequences into the core phylogeny using EPA. The scale bar represents nt substitutions per site, and bootstrap values > 90 are displayed.



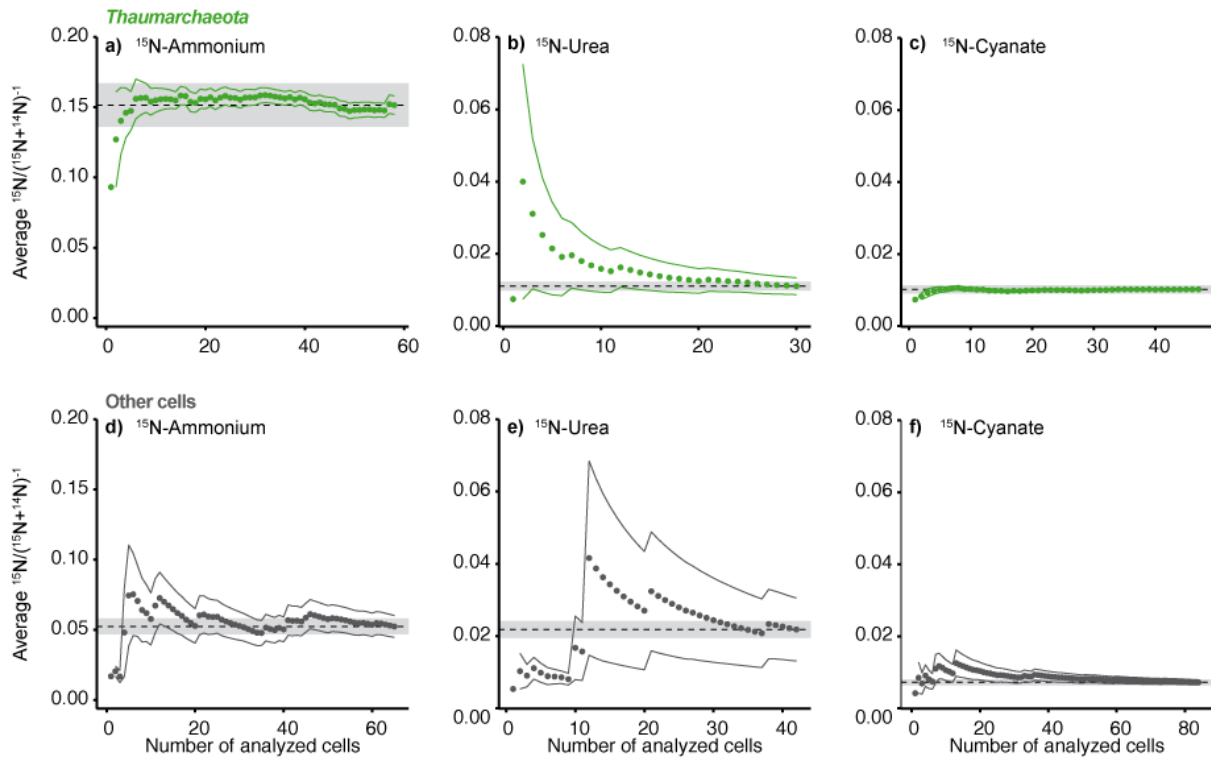
Supplementary Figure 8 Ammonia, urea- and cyanate-derived oxidation rates across experimental stations. a) Station 1, b) Station 2, c) Station 3. Dashed black line represents oxygen concentration. Green bars represent ammonia oxidation rates. Blue and red bars represent urea- and cyanate-derived oxidation rates, respectively. Oxidation rates are depicted on a log-scale. Error bars represent standard error of slopes calculated across biological triplicates and all time points. All rates were significant (see Supplementary Table 1). Brown shading indicates the sediment. Urea- and cyanate-derived oxidation rates are from incubations without added ^{14}N -ammonium.



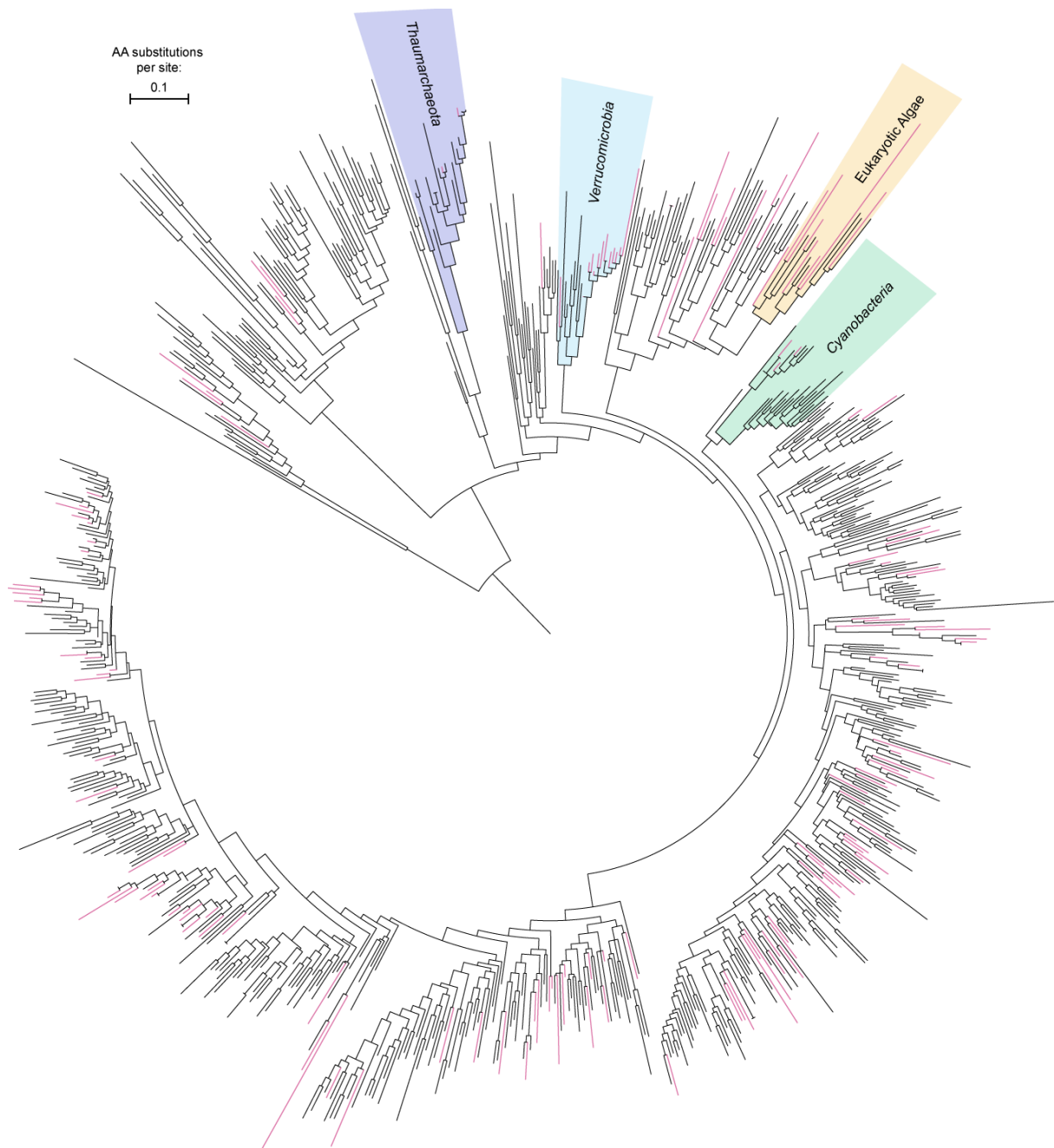
Supplementary Figure 9 Urea (a – c) and cyanate-derived oxidation rates (d – f) at all experimental stations. Black circles show rates without added ¹⁴N-ammonium, colored circles show rates with 5 μM added ¹⁴N-ammonium (ammonium pool incubations). Significant rates are depicted as filled circles (see Supplementary Table 1), non-significant rates as open circles. Error bars represent standard errors of slopes calculated across biological triplicates and all time points.



Supplementary Figure 10 Measured ^{15}N -nitrite production in the ammonium pool incubations and the ^{15}N -nitrite production that could have stemmed from direct urea or cyanate utilization depending on the amount of abiotic and biotic breakdown (Station 2, 14m depth). a) ^{15}N -nitrite production from urea (left panel) corrected for the highest possible biotic breakdown (middle panel) and the lowest possible biotic breakdown (right panel). Abiotic rates of urea breakdown were below detection. b) ^{15}N -nitrite production from cyanate (left panel) corrected for the highest possible abiotic breakdown (middle panel) and the lowest possible abiotic breakdown (right panel). In c) we show the same data as in b, but have also incorporated the biotic breakdown rates which were calculated from the urea data. See text for further details including how the highest and lowest breakdown values were determined. Rates were calculated as linear regressions across biological triplicates and all time points (one-sided t-test, panel a) left / middle / right: $t = 5.93 / 5.76 / 7.09$, $DF = 10 / 10 / 10$, $p = 7.23 \times 10^{-5} / 9.11 \times 10^{-5} / 1.67 \times 10^{-5}$; panel b) left / middle / right: $t = 16.96 / 14.46 / 14.97$, $DF = 10 / 10 / 10$, $p = 5.35 \times 10^{-9} / 2.48 \times 10^{-8} / 1.78 \times 10^{-8}$; panel c) middle / right: $t = 0.18 / 11.20$, $DF = 10 / 10$, $p = 0.430 / 2.80 \times 10^{-7}$). Similar results were obtained for two additional depths at Station 2 (see Supplementary Table 3).



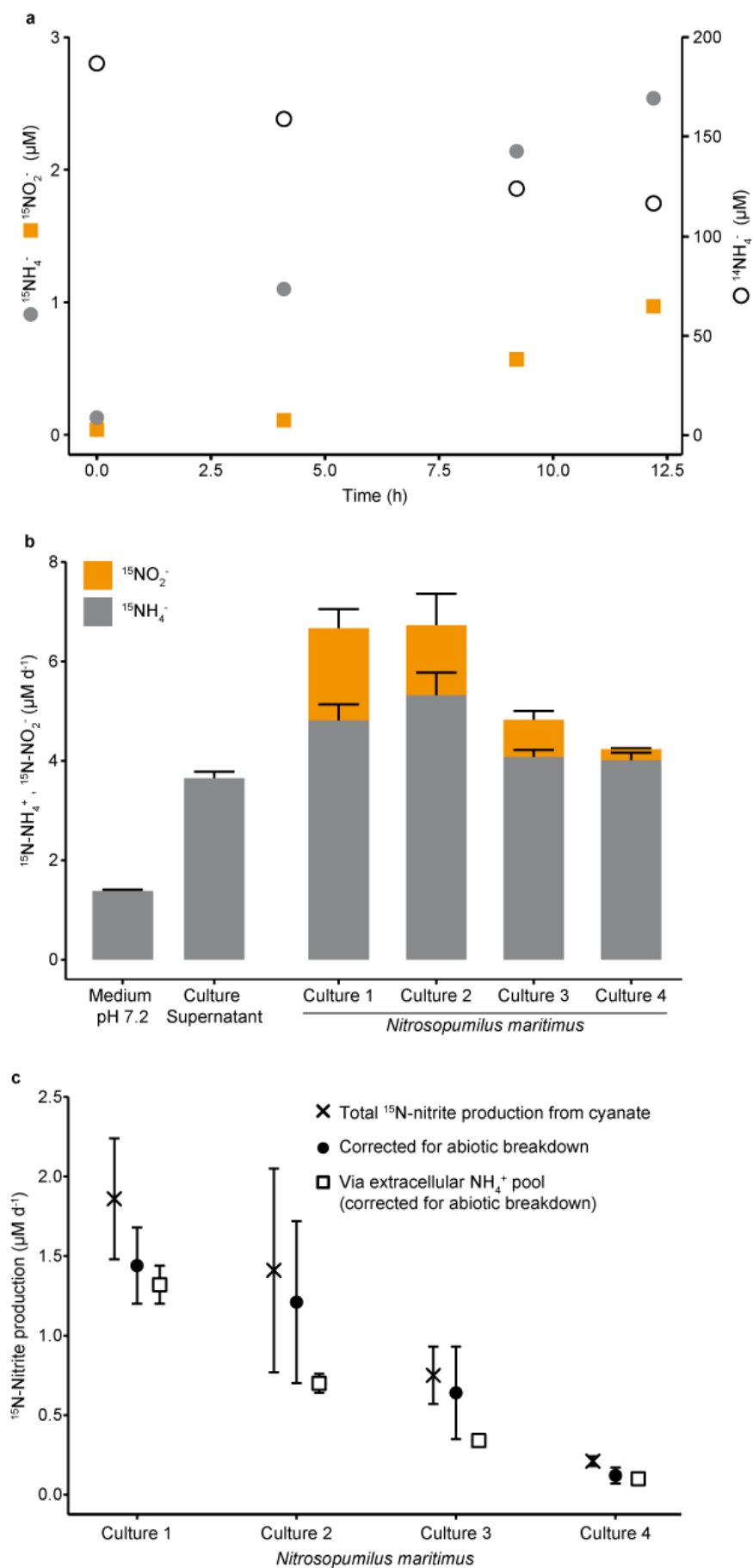
Supplementary Figure 11 Enrichment statistics of Thaumarchaeota cells (green) and other cells (dark grey) analyzed by nanoSIMS. Dots and solid lines represent the means and standard errors of $^{15}\text{N}/(^{15}\text{N}+^{14}\text{N})$ ratios calculated across randomly subsampled cells. The black dashed line represents the mean across all cells, the light grey area $\pm 10\%$ of the mean. Note the different scales for ^{15}N -ammonium and ^{15}N -urea and ^{15}N -cyanate. Standard errors for Thaumarchaeota were $< 10\%$ after analysis of 5 and 3 cells in ammonium and cyanate incubations, respectively, indicating a highly homogenous Thaumarchaeota population, where all Thaumarchaeota cells are capable of ammonium and cyanate utilization. The variability was larger for Thaumarchaeota in the urea incubation (20% error), because there appeared to be a Thaumarchaeota subpopulation that was capable of direct urea utilization. This was also seen from the metagenomic data, which indicated that only 10-15% of the Thaumarchaeota have a *ureC*. Therefore, the 20% error reflects Thaumarchaeota population heterogeneity, which is in line with the presence of ureases in only some of the cultivated marine Thaumarchaeota. The spread for other cells (d-f) was higher in all treatments, likely due to the phylogenetic and physiological diversity of the other diverse microorganisms in this class. The total number of analyzed cells was a) $n = 58$, b) $n = 30$, c) $n = 47$, d) $n = 65$, e) $n = 41$, f) $n = 84$.



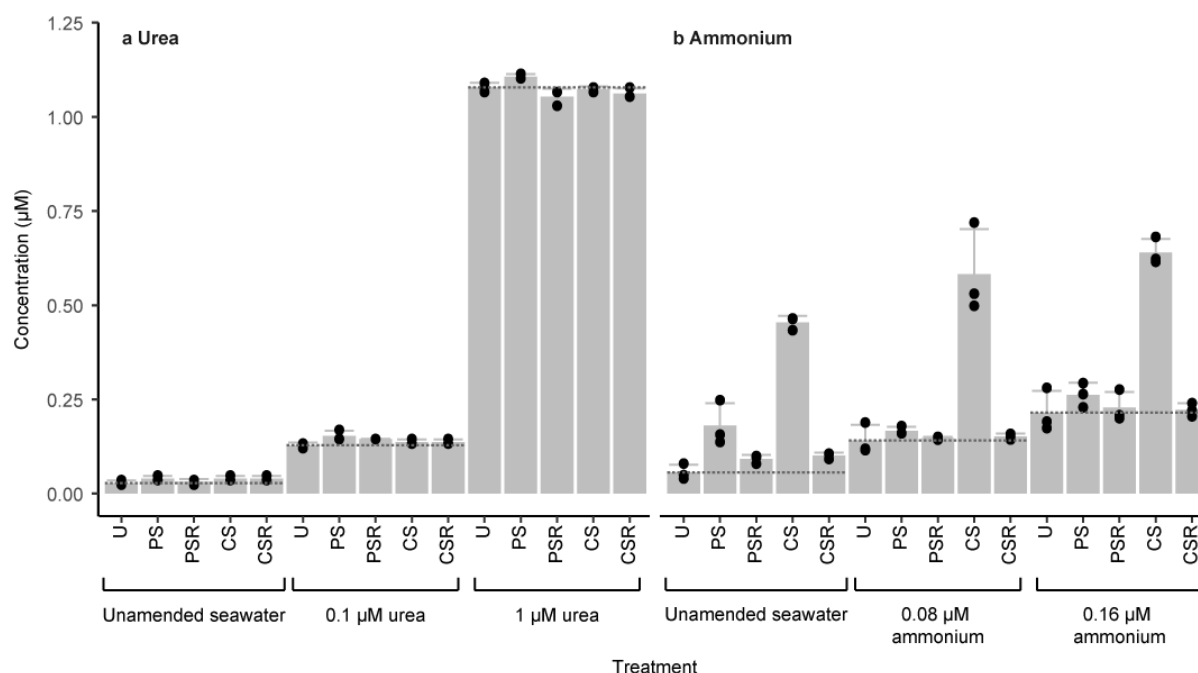
Supplementary Figure 12 UreC diversity obtained from GoM metagenomes. Assembled UreC sequences obtained from GoM metagenomes are indicated in magenta. Black branches are reference UreC sequences. Tree was constructed using IQ-TREE (Nguyen et al. 2015) with automated model selection from near full-length UreC sequences. The scale bar represents amino acid substitutions per site. For the fully annotated tree and a table with the metagenomic and metatranscriptomic read mapping, see Supplementary file 1-6.



Supplementary Figure 13 CynS phylogenetic affiliation and abundance obtained from metagenomics and metatranscriptomics. Assembled, translated CynS sequences obtained from GoM metagenomic data are indicated in magenta. Black branches are reference CynS amino acid (AA) sequences. Translated GoM metagenomic and metatranscriptomic read fragments were mapped onto the alignment and are shown next to the respective branch or sequence cluster as magenta and green circles for metagenomics and metatranscriptomics, respectively. No CynS sequences related to Thaumarchaeota were detected in either metagenomic or metatranscriptomic datasets. Tree was constructed using IQ-TREE(Nguyen et al. 2015) with automated model selection from near full-length CynS sequences. Metatranscriptomic CynS read fragments were fit into the core alignment using the short fragment add option in mafft and confidence was assessed with ultrafast bootstrapping (1,000 iterations). The resulting alignment was used to place short sequences into the core phylogeny using EPA. The scale bar represents amino acid substitutions per site, and bootstrap values > 90 are displayed.



Supplementary Figure 14 ^{15}N -nitrite and ^{15}N -ammonium production from ^{15}N -cyanate by *Nitrosopumilus maritimus*. a) Concentrations of ^{15}N -nitrite, ^{15}N -ammonium and ^{14}N -ammonium in *N. maritimus* culture 1 incubated with $40\ \mu\text{M}$ $^{15}\text{N}^{13}\text{C}$ cyanate. Note the different axes for ^{15}N - and ^{14}N - compounds. b) Production rates of ^{15}N -ammonium in abiotic controls (medium pH 7.2) and in supernatant controls (sterile filtered supernatant of *N. maritimus*) and ^{15}N -nitrite and ^{15}N -ammonium production by *Nitrosopumilus maritimus* cultures. No ^{15}N -nitrite was observed in the abiotic and supernatant controls. Rates for cyanate breakdown in medium controls and culture supernatant were calculated across duplicates and all time points (one-sided t-test, $t=41.6$, $\text{DF} = 4$, $p=9.98\times 10^{-7}$ and $t = 28.31$, $\text{DF}=6$, $p = 6.43\times 10^{-8}$ for medium and culture supernatant, respectively). Rates in *N. maritimus* cultures were calculated across all timepoints of one biological replicate (one-sided t-tests for ammonium / nitrite production rates were $t=14.75 / 4.86$, $\text{DF}=2 / 2$, $p= 2.28\times 10^{-3} / 0.020$; $t = 6.42 / 5.05$, $\text{DF} = 2 / 2$, $p = 0.012 / 0.019$; $t = 28.66 / 4.22$, $\text{DF} = 2 / 2$, $p = 6.08 \times 10^{-4} / 0.026$; and $t = 25.61 / 10.14$, $\text{DF} = 2 / 2$, $p = 7.61\times 10^{-4} / 4.80\times 10^{-3}$ for culture 1, 2, 3 and 4 respectively). c) Measured ^{15}N -nitrite production by *Nitrosopumilus maritimus* cultures, ^{15}N -nitrite production corrected for abiotic breakdown of cyanate and the expected amount of ^{15}N in the nitrite pool assuming that all ^{15}N -nitrite produced in biotic incubations first was released into the extracellular ammonium pool and subsequently oxidized to nitrite (modelled; see Supplementary Discussion). Error bars are the standard errors of the slope across all time points of one biological replicate. Rates were calculated based on linear regressions (one-sided t-tests for ^{15}N -nitrite measured / ^{15}N -nitrite corrected for abiotic breakdown / ^{15}N -nitrite modeled via extracellular NH_4^+ pool were, $t = 4.86 / 6.13 / 10.61$, $\text{DF} = 2 / 2 / 11$, $p = 0.020 / 0.012 / 2.04\times 10^{-7}$; $t = 2.20 / 2.38 / 11.12$, $\text{DF} = 2 / 2 / 11$, $p = 0.079 / 0.070 / 1.27\times 10^{-7}$; $t = 4.22 / 2.22 / 11.23$, $\text{DF} = 2 / 2 / 11$, $p = 0.026 / 0.078 / 1.15\times 10^{-7}$; $t = 10.14 / 3.72 / 11.38$, $\text{DF} = 2 / 2 / 11$, $p = 4.80\times 10^{-3} / 0.033 / 1.00\times 10^{-7}$, for culture 1, 2, 3 and 4, respectively). When data were fitted with an exponential regression, p was <0.001 for all four cultures.



Supplementary Figure 15 Contamination of syringe filters by urea (a) and ammonium (b). The dashed lines indicate mean measured concentrations of urea or ammonium in unfiltered seawater, bars higher than the dashed line stem from contamination by urea or ammonium during the filtration procedure. Error bars are standard deviation of triplicate independent samples. The abbreviations refer to the different filters tested, with and without rinsing with ultrapure water. U refers to unfiltered seawater. PS is the seawater filtered through polyethersulfone filters without ultrapure water rinsing, or with ultrapure rinsing (PSR). CS is seawater filtered through cellulose acetate filters without ultrapure water rinsing, or with ultrapure water rinsing (CSR).

Supplementary tables

Supplementary Table 1 Statistics for rate calculations at all Stations and depths (one-sided t-test). This table is available as an online supplementary dataset; Supplementary Table 1.xlsx (<https://www.nature.com/articles/s41564-018-0316-2#Sec20>) and from K. Kitzinger.

Supplementary Table 2 Thaumarchaeota metagenome-assembled genome (MAG) information and relative MAG abundances. Completeness, contamination and heterogeneity was calculated using CheckM. Abundances per sample are given as percent of fragments mapping to the respective MAGs compared to the total number of fragments per metagenome.

MAG ID	Taxonomy	Completeness (%)	Contamination (%)	Heterogeneity (%)	binned <i>amoA</i>	binned <i>ureC</i>	binned 16S	Station 1, 18m (% FPKM)	Station 2, 12 m (% FPKM)	Station 2, 14 m (% FPKM)	Station 2, 16.5 m (% FPKM)	Station 3, 14m (% FPKM)
GoM MAG1	<i>Nitrosopelagicus sp.</i>	91.26	0.97	0	Present	Present	NA	0.07	0.02	0.06	0.10	0.07
GoM MAG2	<i>Nitrosomarinus sp.</i>	92.72	2.91	66.67	Present	NA	Present	3.14	0.05	0.26	0.72	1.89
GoM MAG3	<i>Nitrosopumilus sp.</i>	95	1.94	50	Present	NA	NA	0.10	0.12	0.43	0.37	0.37
GoM MAG4	<i>Nitrosopumilus sp.</i>	41.91	3.88	83.33	Present	NA	NA	1.29	0.40	1.40	1.82	1.19
GoM MAG5	<i>Nitrosopumilus sp.</i>	93.2	0	0	Present	NA	NA	0.69	0.35	1.24	1.34	0.82
GoM MAG6	<i>Nitrosopumilus sp.</i>	75.9	3.88	40	NA	Present (some)*	NA	1.00	0.14	0.46	0.44	0.94
Sum % FPKM mapping to GoM MAGs								6.30	1.08	3.86	4.79	5.29

**ureC* present in some of the dereplicated GoM MAGs, but not in the best representative

Supplementary Table 3 Determination of direct and indirect rates of urea and cyanate utilization by Thaumarchaeota at station 2. Nitrite production from urea and cyanate could occur either from direct substrate utilization by Thaumarchaeota or as a result of breakdown of urea and cyanate into the extracellular ammonium pool by biotic or abiotic breakdown (indirect utilization). Nitrite production derived from indirect utilization can be calculated by taking into account the abiotic and biotic breakdown rates of urea and cyanate to ammonium, the initial size of the ammonium pool, the ammonia oxidation rate and the ammonium regeneration rate. Together, these parameters provide information on how much urea or cyanate enters the extracellular ammonium pool and how much is then oxidized to nitrite. All of these parameters were determined in incubations carried out *in-situ*, apart from the cyanate abiotic breakdown rates, which were measured in filtered Gulf of Mexico seawater upon return to the laboratory, and cyanate biotic breakdown rates were assumed to be the same as those measured for biotic urea breakdown (see Supplementary Discussion for more details). After taking into account the nitrite production derived from indirect utilization of urea or cyanate, significant production rates of nitrite remained, strongly indicating that direct utilization of urea and cyanate were occurring. For all values a range is shown, which represents the mean value \pm the SE or SD (see Supplementary Discussion). For the modelled direct and indirect utilization rates the range represents two scenarios, one with the highest possible contribution of biotic and abiotic breakdown and one with the lowest possible contribution (see Supplementary Discussion).

	12.0 m depth	14.0 m depth	16.5 m depth
Ammonia oxidation (nM NO ₂ ⁻ d ⁻¹) [§]	834 - 887	2,449 – 2,567	1,658 – 1,791
Ammonium regeneration (nM NH ₄ ⁺ d ⁻¹)*	170 - 680	631 – 1,550	551 – 1,446
Urea oxidation, without added ammonium pool (nM NO ₂ ⁻ d ⁻¹) [§]	24.5 - 27.2	46.5 - 55.6	49.5 - 58.7
Urea oxidation, with added ammonium pool (nM NO ₂ ⁻ d ⁻¹) [§] (ammonium pool incubations)	1.9 - 4.3	12.0 - 16.9	8.9 - 11.4
Biotic urea breakdown to ammonium (nM NH ₄ ⁺ d ⁻¹) [§]	15 - 24	21 - 34	25 - 29
Abiotic urea breakdown to ammonium (nM NH ₄ ⁺ d ⁻¹) [§]	b.l.d.		
Indirect urea oxidation (nM NO₂⁻ d⁻¹)[#]	1.4 - 3.5	5.2 - 8.2	2.8 - 4.9
Direct urea oxidation (nM NO₂⁻ d⁻¹)[#]	1.2 – 1.6	6.2 – 8.5	5.5 – 6.7
Cyanate oxidation, without added ammonium pool (nM NO ₂ ⁻ d ⁻¹) [§]	35.6 - 46.6	49.1 - 58.4	51.3 - 56.5
Cyanate oxidation, with added ammonium pool (nM NO ₂ ⁻ d ⁻¹) [§] (ammonium pool incubations)	7.7 - 11.7	31.5 - 35.4	21.8 - 28.3
Biotic cyanate breakdown to ammonium (nM NH ₄ ⁺ d ⁻¹)	n.d.		
Abiotic cyanate breakdown to ammonium (nM NH ₄ ⁺ d ⁻¹ per μM cyanate) [§]	9.2 - 9.6		
Indirect cyanate oxidation (nM NO₂⁻ d⁻¹)[#]	6.1 - 10.5	20.9 - 29.4	12.8 - 18.8
Direct cyanate oxidation (nM NO₂⁻ d⁻¹)[#]	b.l.d.	b.l.d. - 9.1	b.l.d. - 9.9

§ Measured in this study

*Ammonium regeneration rates were calculated from 15N-ammonium incubations following pool dilution equations (see Supplementary Discussion).

See Supplementary Discussion for further details on how these were modelled, and Supplementary table 4 for the contribution of abiotic cyanate decay only

n.d.: not determined

b.l.d.: below the limit of detection; for abiotic urea breakdown to ammonium the detection limit was (7.9 nM d⁻¹, corresponding to 1.58 nM d⁻¹ per μM urea), for direct cyanate oxidation the detection limit was estimated to be 2.6 nM NO₂⁻ d⁻¹

Supplementary Table 4 Direct and indirect rates of cyanate utilization by Thaumarchaeota at Station 2, assuming only abiotic cyanate breakdown.

	12.0 m depth	14.0 m depth	16.5 m depth
Cyanate oxidation, with added ammonium pool (nM NO ₂ ⁻ d ⁻¹) [§]	7.7 - 11.7	31.5 - 35.4	21.8 - 28.3
Indirect cyanate oxidation (nM NO ₂ ⁻ d ⁻¹), assuming only abiotic cyanate breakdown [#]	4.1 - 5.9	13.3 - 18.7	8.8 - 12.4
Direct cyanate oxidation (nM NO ₂ ⁻ d ⁻¹), assuming only abiotic cyanate breakdown [#]	2.7 – 4.3	11.6 – 17.8	11.2 – 15.1

§ Measured in this study

See Supplementary Discussion for further details on calculations used

Supplementary Table 5 ¹⁵N-¹³C-tracers and ¹⁴N-pools added for process rate determinations.

Compounds Added (5 μM unless otherwise stated)	Investigated process	Measured compound
¹⁵ N-NH ₄ ⁺ , ¹⁴ N-NO ₂ ⁻ , ¹⁴ N-NO ₃ ⁻ , ¹³ C-DIC *	Ammonia oxidation	¹⁵ N-NO ₂ ⁻
¹⁵ N ¹³ C-Urea, ¹⁴ N-NO ₂ ⁻ , ¹⁴ N-NO ₃ ⁻	Urea oxidation	¹⁵ N-NO ₂ ⁻
¹⁵ N ¹³ C-Urea, ¹⁴ N-NH ₄ ⁺ , ¹⁴ N-NO ₂ ⁻ , ¹⁴ N-NO ₃ ⁻	Urea oxidation in ammonium pool incubation	¹⁵ N-NH ₄ ⁺ , ¹⁵ N-NO ₂ ⁻
¹⁵ N ¹³ C-Cyanate, ¹⁴ N-NO ₂ ⁻ , ¹⁴ N-NO ₃ ⁻	Cyanate oxidation	¹⁵ N-NO ₂ ⁻
¹⁵ N ¹³ C-Cyanate, ¹⁴ N-NH ₄ ⁺ , ¹⁴ N-NO ₂ ⁻ , ¹⁴ N-NO ₃ ⁻	Cyanate oxidation in ammonium pool incubation	¹⁵ N-NO ₂ ⁻
Abiotic ¹⁵ N ¹³ C-Urea, ¹⁴ N-NH ₄ ⁺ , ¹⁴ N-NO ₂ ⁻ , ¹⁴ N-NO ₃ ⁻	Abiotic (sterile filtered) Urea oxidation control incubation	¹⁵ N-NH ₄ ⁺ , ¹⁵ N-NO ₂ ⁻
Abiotic ¹⁵ N ¹³ C-Cyanate, ¹⁴ N-NH ₄ ⁺ , ¹⁴ N-NO ₂ ⁻ , ¹⁴ N-NO ₃ ⁻	Abiotic (sterile filtered) Cyanate oxidation control incubation	¹⁵ N-NH ₄ ⁺ , ¹⁵ N-NO ₂ ⁻

¹⁵N-ammonium sulfate (98% ¹⁵N, Sigma), ¹⁵N¹³C-urea (99% ¹³C, 98% ¹⁵N, Sigma), ¹⁵N¹³C-potassium cyanate (95% purity, 99% ¹³C, 98% ¹⁵N, Icon Isotopes), ¹³C-sodium bicarbonate (98% ¹³C, Sigma), ¹⁴N-compounds were all obtained from Sigma
* 200 μM final ¹³C-NaHCO₃ concentration

135

Supplementary Table 6 Sequencing statistics for GoM metagenomes.

Station, Depth	Dataset	#raw reads	#read pairs	# raw bases	#QC-filtered reads	#QC-filtered read pairs	#QC-filtered bases	# scaffolds	Assembly (MB)	Max contig length	N50	L50	GC
Station 1, 18 m	C6-18m_S5	72032256	36016128	17957359367	69541718	34770859	17219021486	747805	794.15	305313	1078	161599	45.9
Station 3, 14 m	CPI-14m_S4	93064228	46532114	23218119059	89295806	44647903	22081997375	775239	868.54	598510	1169	154816	45.5
Station 2, 12 m	I3-11-9m_S1	84917344	42458672	21090538252	82690706	41345353	20490607949	812989	855.73	195763	1070	180428	41.8
Station 2, 14 m	I3-13-9m_S3	58352508	29176254	14547679676	56225882	28112941	13912091527	534261	591.17	232382	1150	106704	43.4
Station 2, 16.5 m	I3-16-4m_S2	104108154	52054077	25988959289	100605890	50302945	24921436191	846173	1000.12	388985	1303	153349	43.9

Supplementary Table 7 Sequencing statistics for metatranscriptomes obtained at Station 2.

Station, Depth	dataset	#raw reads	#read pairs	# raw bases	# rRNA-cleaned reads	# rRNA-cleaned read pairs	# rRNA-cleaned singletons	# rRNA -cleaned fragments	# rRNA-cleaned read bases
Station 2, 12 m	SRR5909422	9359372	4679686	2468604609	3679953	1830450	19053	1849503	933060195
Station 2, 14 m	SRR5909421	19415124	9707562	3505604022	14474989	7223035	28919	7251954	2599248375
Station 2, 16.5 m	SRR5909415	18976144	9488072	3265534600	13108027	6539561	28905	6568466	2243238720

Supplementary Table 8 Phylogenetic affiliation of 16S rRNA gene sequences with perfect match to Thaum726 in SSURef_NR99_128_SILVA_07_09_16.

Group	Perfect Match/all Sequences	Subgroup	Perfect Match/all Sequences
Euryarchaeota/Thermoplasmata/Thermoplasmatales	3/3235	Marine Benthic Group D and DHVEG-1 Marine Group II	1/1106 1/701
WSA2	6/221	2B5 059A02-A-SD-P93 20A-9	1/4 (low sequence quality) 2/8 (low sequence quality) 3/80
Methanosarcinales	3/777	No group Methanobolus	1 1/88
Euryarchaeota/Halobacteria/Halobacteriales	4/2760	Candidatus Methanoperedens Halostagnicola No group	2/83 1/19 3
Woesearchaea	28/520		
Marine Hydrothermal Vent Group	1/91		
Aenigmarchaeota	43/305	Deep Sea Euryarchaeotic Group	43/305
Altiarchaeales	1/38		
Euryarchaeota/Methanobacteria	2/2602	Methanobrevibacter Methanothermobacter	1/2040 1/30
Thaumarchaeota	4318/4952	Marine Group I South African Gold Mine Gp 1 (incl. Nitrosotalea devanattera) Soil Crenarchaeotic Group (incl. Nitrososphaera gargensis) AK31 D-F10	3163/3344 116/126 636/678 42/45 11/12
		FHM11_ terrestrial group	145/230
		Marine Benthic Group A	98/104
		AK59	42/50
		pSL12	9/9
		ZZ73FA48	3/3
		YS18As63	2/2
		AK56	7/10
		OPPD003	5/6
		FS243A-60	8/9
		Papm3A43	2/2
		ITOT-A6-15	3/3
		Group 3c	3/296
Algarhaeota	2/171	Terrestrial Hot Spring Group	2/46
Bathyarchaeota	977/3262		
Crenarchaeota/Thermoprotei	3/614	Thermoproteales/Thermoflaccaceae/Thermofilum	3/46
Ct. Division YNPFFA	2/47		

Supplementary Table 9 Accession numbers of sequences used for 16S rRNA gene tree, *amoA*, *CynS*, *UreC* and genome trees. This table is available as an online supplementary dataset; Supplementary Table 9.xlsx (<https://www.nature.com/articles/s41564-018-0316-2#Sec20>) and from K. Kitzinger.

Supplementary Table 10 CTD data, measured nutrient concentrations, process rates, *Thaumarchaeota* relative abundance based on 16S rRNA gene amplicon sequencing and *Thaumarchaeota* specific CARD-FISH counts. This table is available as an online supplementary dataset; Supplementary Table 10.xlsx (<https://www.nature.com/articles/s41564-018-0316-2#Sec20>) and from K. Kitzinger.

Supplementary Table 11 Parameters for calculation of ammonium regeneration rates in ^{15}N -ammonium incubations at Station 2.

Parameter / Abbreviation	Description
AR	Ammonium regeneration rate (nM d^{-1})
A_t , A_{t-1}	Ammonium concentration at time point t and the previous time point t-1 (nM , ^{15}N + ^{14}N)
T	Time difference between time point t and the previous time point t-1 (d)
AAPE _t and AAPE _{t-1}	Ammonium atom percent excess, ^{15}N atom percent above natural abundance (i.e. 0.37%) at time point t and previous time point t-1 (% excess ^{15}N)

Supplementary Table 12 Parameters for modeling the contribution of abiotic cyanate decay to the observed oxidation rates in ammonium pool incubations at Station 2.

Parameter/Abbreviation	Description	Value range / Calculated from
t	Time (h)	0 -24 h
T	Time interval between t and t-1 (h)	1 h
NAPE _t	¹⁵ N-nitrite concentration above natural abundance stemming from abiotic decay of cyanate at time t (nM, ¹⁵ N)	$NAPE_t = \text{sum}(NAPE_{T(0-t)})$
NAPE _T	¹⁵ N-nitrite increase in nitrite pool above natural abundance stemming from abiotic decay of cyanate during time interval T (nM, ¹⁵ N)	$NAPE_T = AO_{15NT} - AO_T / 100 * 0.37$ equation (4)
AO _{15NT}	¹⁵ N-ammonium oxidized to ¹⁵ N-nitrite during time interval T, at same ¹⁵ N atom% as A% _{15NT} (nM, ¹⁵ N)	$AO_{15NT} = AO_T / 100 * A\%_{15NT}$ equation (5)
AO _T	Total ammonium efflux due to ammonia oxidation during time interval T (nM, ¹⁵ N + ¹⁴ N)	35 – 105 nM h ⁻¹
A% _{15NT}	Atom % ¹⁵ N in ammonium pool at time t (% , ¹⁵ N)	$A\%_{15NT} = A_{15NT} / (A_t)$ equation (6)
A _{15NT}	¹⁵ N-ammonium concentration in ammonium pool at time t (nM, ¹⁵ N)	$A_{15NT} = A_{15NT-1} - AO_{15NT} + A_{15NT}$ equation (7)
A _t	Total ammonium concentration (pool size) at time t (nM, ¹⁵ N + ¹⁴ N)	2,000 – 5,700 nM (time zero) $A_t = A_{t-1} - AO_T + A_{1T}$ equation (8)
A _{15NT}	¹⁵ N-ammonium influx during time interval T (nM, ¹⁵ N, sum of natural abundance ¹⁵ N-ammonium regeneration (AR) and abiotic decay of ¹⁵ N-cyanate to ¹⁵ N-ammonium during time interval T)	0.7 – 2.2 nM h ⁻¹
A _{1T}	Total ammonium influx during time interval T (nM, ¹⁵ N + ¹⁴ N, sum of ammonium regeneration (AR) and abiotic decay of cyanate to ammonium during time interval T)	8 – 65 nM h ⁻¹

Supplementary files

These files are available as online supplementary datasets (<https://www.nature.com/articles/s41564-018-0316-2#Sec20>) and from K. Kitzinger.

Supplementary File 1 UreC tree with bootstrap values. Contains the fully annotated UreC tree containing bootstrap values. Thaumarchaeal GoM metagenome-assembled UreC sequences are depicted in magenta. Apart from bootstrap values, this tree is identical to Supplementary File 3.

Supplementary File 2 UreC tree with bootstrap values. Contains the corresponding Newick tree file to Supplementary File 1, with annotations from Supplementary File 5.

Supplementary File 3 UreC tree with node labels. Contains the fully annotated UreC tree containing node labels used for FPKM mapping of metagenomic and metatranscriptomics ureC read fragments (see Supplementary File 6). Thaumarchaeal GoM metagenome-assembled UreC sequences are depicted in magenta. Apart from node labels, this tree is identical to Supplementary File 1.

Supplementary File 4 UreC tree with node labels. Contains the corresponding Newick tree file to Supplementary File 3, with annotations from Supplementary File 5.

Supplementary File 5 Tree annotation UreC. Contains the tree branch annotations for UreC Newick tree files. The column “Branch_ID” contains the short IDs used for tree calculations, “Accession_Nr/Metagenome_ID” the reference sequence accession numbers or GoM metagenome-assembled UreC IDs, “Final_label” the corresponding branch labels as depicted in the pdf files of the UreC trees.

Supplementary File 6 Read-fragment-mapping UreC. Contains the FPKM mapping from GoM metagenomic and metatranscriptomic datasets to UreC trees. The column “UreC Tree Label / Node ID” refers to the specific node/branch position read fragments were mapped to, “Associated Thaumarchaeota GoM MAG” gives the Thaumarchaeota MAG a specific sequence was binned into/associated with, “Thaumarchaeota affiliated UreC” denotes UreC tree branches or internal nodes associated to Thaumarchaeota, “ureC assembled from GoM metagenome” denotes UreC branches assembled from the GoM metagenomes. FPKM mappings are given separately for metagenomic and metatranscriptomics datasets, and for each Station and depth.

Chapter 4

Single cell analyses reveal contrasting life strategies of the two main nitrifiers in the ocean

Katharina Kitzi^{1,2*}, Hannah K. Marchant^{1*}, Laura A. Bristow^{1,3}, Craig W. Herbold², Cory C. Padilla⁴, Abiel T. Kidane¹, Sten Littmann¹, Holger Daims², Petra Pjevac², Frank J. Stewart⁴, Michael Wagner², Marcel M. M. Kuypers¹

Author affiliations

¹ Max Planck Institute for Marine Microbiology, Celsiusstrasse 1, 28359 Bremen, Germany

² University of Vienna, Centre for Microbiology and Environmental Systems Science, Division of Microbial Ecology, Althanstrasse 14, 1090 Vienna, Austria

³ Department of Biology and Nordic Center for Earth Evolution (NordCEE), University of Southern Denmark, Odense, Denmark

⁴ School of Biological Sciences, Georgia Institute of Technology, 311 Ferst Drive, Atlanta GA 30332-0230, USA

Correspondence: Hannah K. Marchant, hmarchan@mpi-bremen.de and Katharina Kitzi¹, kkitzing@mpi-bremen.de

Author Contributions

K.K., H.K.M., M.M.M.K. L.A.B. and M.W. designed the study. K.K. and L.A.B. performed experiments, K.K. designed the CARD-FISH probe. S.L. and A.K. ran nanoSIMS analyses. K.K., H.K.M. and L.A.B. analyzed samples and data. C.C.P. sampled for molecular analyses, C.W.H. and C.C.P. performed molecular analyses with contribution from F.J.S., P.P. and H.D. The manuscript was written by K.K., H.K.M., M.M.M.K. and L.A.B. with contributions from all co-authors.

In preparation for submission to an international peer-reviewed journal

Abstract

Ammonia oxidizing archaea (AOA) and the nitrite oxidizing Nitrospinae were previously identified as the main nitrifiers in the ocean. Despite their obvious importance for marine N-cycling, little is known about their ecophysiology. Here, stable isotope labeling experiments, molecular and single cell methods were used to compare AOA and Nitrospinae *in situ* growth and substrate utilization in the Gulf of Mexico (GoM). In the GoM, AOA outnumbered Nitrospinae ten to one, even though ammonia and nitrite oxidation rates were similar and Nitrospinae had five-times higher *in situ* growth rates than AOA. The high growth rates and lower abundance of Nitrospinae indicates that they have a higher mortality rate. While AOA mainly assimilated ammonium, more than half of the cellular N-demand of Nitrospinae was met by urea and cyanate. This is in line with the presence of both ureases and cyanases in Nitrospinae metagenome assembled genomes recovered from the GoM. Taken together, the results revealed that Nitrospinae had a 4.5 times higher energy yield than AOA. The high energy yield and utilization of organic N-sources by Nitrospinae are likely important factors for their success in the oceans.

Introduction

Nitrification is a key process in the oceanic N-cycle as it oxidizes ammonium via nitrite to nitrate, which is the main source of nitrogen for many marine primary producers. In the oceans, ammonia is mainly oxidized to nitrite by ammonia oxidizing archaea (AOA) (Francis et al. 2005; Wuchter et al. 2006) and the resulting nitrite is further oxidized to nitrate by nitrite oxidizing bacteria (NOB). Most inorganic fixed N (i.e. nitrate, nitrite and ammonium) in the oceans is present in the form of nitrate (99 %), and less than 0.1 % occurs in the form of nitrite, suggesting that any nitrite formed by ammonia oxidizers is immediately oxidized to nitrate (Kuypers et al. 2018). This has led to the paradigm that ammonia oxidation is the rate-limiting step of nitrification. In light of this, it seems surprising that the AOA can comprise up to 40% of the marine microbial community (Karner et al. 2001), while the NOB usually are far less abundant (Füssel et al. 2012; Beman et al. 2013; Doxey et al. 2015; Pachiadaki et al. 2017; Damashek et al. 2019). This implies that there are stark ecophysiological differences between the two groups of organisms. These likely include the lower energy gain from nitrite oxidation compared to ammonia oxidation (e.g. Bock & Wagner 2006) and the larger cell sizes of NOB compared to AOA (e.g. Watson & Waterbury 1971; Könneke et al. 2005; Pachiadaki et al. 2017). Our understanding of the factors that keep the marine N-cycle in balance is currently hindered by a lack of knowledge concerning the *in situ* ecophysiology of marine nitrite oxidizers, especially in comparison to the AOA. In part, this is because nitrite oxidation is rarely measured as a standalone process in marine systems (e.g. Ward 1987; Füssel et al. 2012; Beman et al. 2013; Bristow et al. 2015; Sun et al. 2017) and nitrite oxidizers are rarely quantified (e.g. Mincer et al. 2007; Beman et al. 2013; Santoro et al. 2010; Damashek et al. 2019). Furthermore, there are only a few marine nitrite oxidizers in culture.

Marine nitrite oxidation is carried out primarily by members of the phylum Nitrospinae (Füssel et al. 2012; Beman et al. 2013; Ngugi et al. 2016; Pachiadaki et al. 2017), and to a lesser extent by members of the genera *Nitrococcus* (Füssel et al. 2012; Füssel et al. 2017) and *Nitrospira* (Haaijer et al. 2013). To date, two Nitrospinae pure cultures are available (Watson & Waterbury 1971; Spieck et al. 2014) that both belong to the genus *Nitrospina*, whilst most Nitrospinae in the marine environment belong to the candidate genus *Nitromaritima* (Nitrospinae Clade 1) and Nitrospinae Clade 2 (Ngugi et al. 2016; Pachiadaki et al. 2017). The two cultivated *Nitrospina* species display high growth rates, with doubling times of approximately one day (Watson & Waterbury 1971; Spieck et al. 2014). One of the species, *Nitrospina gracilis*, has been genome sequenced, which revealed that the

key enzyme for nitrite oxidation, nitrite oxidoreductase (NXR), is closely related to NXR of Nitrospirinae and anammox bacteria (Lücker et al. 2013). Furthermore, *Nitrospina* were shown to use the reductive tricarboxylic acid cycle (TCA) cycle for autotrophic C-fixation (Lücker et al. 2013).

In contrast, the ecophysiology of the environmentally relevant Nitrospirinae genera Nitromaritima (Nitrospirinae Clade 1) and Nitrospirinae Clade 2 is largely unconstrained. A recent *in situ* study has suggested that these Nitrospirinae genera, besides being the main nitrite oxidizers in the oceans, also play a key role in dark carbon (C) fixation, fixing as much as, or more dissolved inorganic C in the ocean than the AOA (Pachiadaki et al. 2017). So far however, direct *in situ* comparisons of C-based growth and assimilation rates of NOB and AOA are lacking. Another largely unexplored facet of Nitrospirinae ecophysiology are their N-assimilation strategies. Genome-based studies have shown that both cultured and many environmental Nitrospirinae encode for the enzymes urease and cyanase, which allow for assimilation of the simple organic N-compounds urea and cyanate (Lücker et al. 2013; Ngugi et al. 2016; Pachiadaki et al. 2017). Direct evidence for *in situ* assimilation of organic N-compounds by nitrite oxidizers is so far missing. However, such organic-N use likely affects the distribution and activity of marine Nitrospirinae and their interactions with the AOA.

Here, we determined the key ecophysiological traits of Nitrospirinae and compare them to those of the AOA in the hypoxic shelf waters of the Gulf of Mexico (GoM). The GoM is an ideal study site to elucidate the *in situ* ecophysiology of these nitrite oxidizers, as it is an area characterized by high nitrite oxidation activity, where Nitrospirinae appear to be the main NOB (Bristow et al. 2015). We investigated nitrite oxidation activity and growth rates of GoM Nitrospirinae by combining metagenomics and metatranscriptomics with stable isotope incubations and single cell techniques. Furthermore, the assimilation of the dissolved organic N (DON) compounds urea and cyanate by Nitrospirinae were investigated under near *in situ* conditions.

Materials and Methods

Sampling

Sampling was undertaken on the Louisiana Shelf in the Northern Gulf of Mexico aboard the *R/V Pelican*, cruise PE17-02, from July 23rd to August 1st, 2016, on a west-east transect from 92°48'4" W to 90°18'7" W, as described previously (Kitzinger et al. 2019). Briefly, seawater was sampled with 20 L Niskin bottles on a rosette equipped with a CTD and an SBE 43 oxygen sensor. Water column nutrient profiles (ammonium, nitrite, nitrate, urea, cyanate) were measured at nine stations (surface to water-sediment interface at max. 19 m). Nitrite oxidation rate measurements, N- and CO₂-assimilation measurements, molecular and FISH analyses were carried out at three of the nine stations (Supplementary Figure 1).

Nutrient sampling and analysis were carried out as previously described (Kitzinger et al. 2019). Briefly, samples for ammonium, nitrite and urea concentrations were measured onboard immediately after collection, following the procedures of Holmes et al. (1999), Grasshoff et al. (1999) and Mulvenna et al. (1992), respectively. Samples for cyanate concentration measurements were derivatized onboard and stored frozen until analysis using high performance liquid chromatography (Dionex, ICS-3000 system coupled to a fluorescence detector, Thermo Scientific, Dionex Ultimate 3000) (Widner et al. 2013). Samples for the determination of nitrate concentrations were stored frozen until analysis following Braman and Hendrix (1989).

Determination of N-assimilation, CO₂-assimilation and nitrite oxidation rates

Assimilation of ammonium, urea, cyanate, nitrite, autotrophic CO₂ fixation, and nitrite oxidation rates were assessed via stable isotope tracer incubations at three stations and three depths in and below

the oxycline as previously described (Bristow et al. 2015; Kitzinger et al. 2019). Briefly, seawater was filled into 250 ml serum bottles from Niskin bottles and allowed to overflow three times to minimize oxygen contamination. Serum bottles were then sealed bubble-free with deoxygenated rubber stoppers (De Brabandere et al. 2012) and stored at *in situ* temperature (28°C) in the dark until the beginning of the experiments (< 7 h). All experimental handling took place under red light to minimize phytoplankton activity.

Tracer amendments (Supplementary Table 1) were made to triplicate serum bottles at each depth to investigate urea ($^{15}\text{N}^{13}\text{C}$ -urea), cyanate ($^{15}\text{N}^{13}\text{C}$ -cyanate), ammonium (^{15}N - NH_4^+), and nitrite (^{15}N - NO_2^-) assimilation and oxidation rates. All amendments were made as 5 μM additions. In the ammonium and nitrite assimilation experiments, 200 μM ^{13}C - NaHCO_3 (dissolved inorganic C, DIC) was added to investigate autotrophic CO_2 fixation. Tracer aliquots were dissolved in sterile filtered seawater at the start of every experiment to minimize abiotic breakdown.

As described in Kitzinger et al. (2019), after tracer addition, a 40 ml helium headspace was set in each serum bottle and oxygen concentrations were adjusted to match *in situ* conditions (Supplementary Table 2). Oxygen concentrations remained within 20% of *in situ* concentrations throughout the incubations, as determined by optode spots in separate bottles (Firesting, Pyroscience). Samples were taken at the start of each experiment to determine the labeling percentage of ^{15}N and ^{13}C -DIC (Holmes et al. 1999; Mulvenna & Savidge 1992; Widner et al. 2013; Grasshoff et al. 1999). Thereafter, serum bottles were incubated in the dark at *in situ* temperature (28°C). After 6 h, 12 h and 24h, 20 ml of seawater was sampled and replaced with He, sterile filtered and frozen. Serum bottle headspaces were again flushed with He and oxygen was added to match *in situ* concentrations. After 24 h, the remaining seawater from triplicate incubations was combined, and 20 ml were fixed and filtered onto 0.22 μm GTTP filters for catalyzed reporter deposition fluorescence *in situ* hybridization (CARD-FISH) and 0.22 μm gold sputtered GTTP filters for nanoSIMS analyses (see below).

Nitrite oxidation rate measurements and determination of ^{13}C -DIC labeling percentage

Nitrite oxidation rates were determined from the increase in ^{15}N -nitrate over time after the addition of ^{15}N -nitrite. Briefly, after the removal of any residual nitrite with sulfamic acid, nitrate was reduced to nitrite using spongy cadmium and subsequently converted to N_2 via sulfamic acid (Füssel et al. 2012; McIlvin & Altabet 2005). The resulting N_2 was then measured by GC-IRMS on a customized TraceGas coupled to a multicollector IsoPrime100 (Manchester, UK). Rates were calculated from the slopes of linear regressions across all time points from the triplicate serum bottles and were corrected for initial ^{15}N -labeling percentage. Only slopes that were significantly different from 0 are reported ($p < 0.05$, one-sided student t-test). When non-significant regressions were found, rates are reported as below detection limit. For the determination and calculation of ammonium oxidation rates see Kitzinger et al. (2019).

^{13}C -DIC labeling percentages were determined from the first time point after sample acidification (Torres et al. 2005) by ^{13}C - CO_2 / ^{12}C - CO_2 measurements using cavity ring-down spectroscopy (G2201-i coupled to a Liaison A0301, Picarro Inc., Santa Clara, USA, connected to an AutoMate Prep Device, Bushnell, USA).

Nitrospinae quantification by CARD-FISH, Nitrospinae growth rates and single cell oxidation rates

To visualize and quantify cells of the Nitrospinae family, a new CARD-FISH probe was designed (Supplementary Text). For Nitrospinae quantification, seawater samples from each station and depth were fixed with 1% paraformaldehyde (final concentration, without methanol, EMS) for 12-24 h at 4°C before filtration (< 400 mbar) onto 0.22 μm GTTP filters (Millipore). Filters were stored frozen at -20°C until analysis. Nitrospinae abundances were determined by CARD-FISH according to Pernthaler

et al. (2004) (Supplementary Text). Samples were additionally screened by CARD-FISH for other marine nitrite oxidizing bacteria of the genera *Nitrospira* (probe Ntspa662, Daims et al. 2001), *Nitrobacter* (probe Nit3, Wagner et al. 1996) and *Nitrococcus* (probe Ntcoc84, Juretschko 2000) at the respective published formamide concentrations.

Nitrospinae growth during the incubation time was assessed by CARD-FISH and growth rates (Equation 1) and doubling times (Equation 2) were estimated according to:

$$GR = \ln(N_t/N_0)/t \quad (\text{Equation 1})$$

$$DT = \ln(2)/GR \quad (\text{Equation 2})$$

where GR is growth rate, N_t the number of Nitrospinae cells at time t (cell counts after incubation), N_0 the number of Nitrospinae cells at time 0 (cell counts *in situ*), t the incubation time (approx. 1 day) and DT is doubling time.

Single cell Nitrospinae nitrite oxidation rates were estimated by combining measured bulk nitrite oxidation rates and the average Nitrospinae cell abundance between Nitrospinae *in situ* counts and Nitrospinae counts after 24 h of incubation, as in Stieglmeyer et al. (2014).

NanoSIMS analyses, calculation of single cell growth rates and single cell C-content

At the end of each incubation experiment, the content of triplicate serum bottles was combined. Water was filtered (< 100 mbar) onto gold sputtered 0.22 μm GTTP filters (Millipore), and fixed in 3% paraformaldehyde (in sterile filtered seawater) for 30 min at room temperature, washed twice in sterile filtered seawater and then stored at -20°C . Before nanoSIMS analysis, cells were stained with DAPI and Nitrospinae were targeted by CARD-FISH (without embedding filters in agarose) after which regions of interest were marked on a laser microdissection microscope (6000 B, Leica).

Single cell ^{15}N - and ^{13}C -assimilation from incubations with ^{15}N -ammonium and ^{13}C -bicarbonate, ^{15}N -nitrite and ^{13}C -bicarbonate, $^{15}\text{N}^{13}\text{C}$ -urea or $^{15}\text{N}^{13}\text{C}$ -cyanate were determined for Station 2, 14m depth, using a nanoSIMS 50L (CAMECA), as previously described (Martínez-Pérez et al. 2016). Instrument precision was monitored daily on Graphite Planchet and regularly on caffeine standards. Due to the small size of most cells in the sample, they were pre-sputtered for only 10 s with a Cs^+ beam (~ 300 pA) before measurements. Measurements were carried out over a field size of $10 \times 10 \mu\text{m}$ or $15 \times 15 \mu\text{m}$, with a dwelling time of 2 ms per pixel and 256×256 pixel resolution over 40 planes. The acquired data was analyzed using the Look@NanoSIMS software package (Polerecky et al. 2012) as previously described (Martínez-Pérez et al. 2016). Ratios of $^{15}\text{N}/(^{15}\text{N}+^{14}\text{N})$ and $^{13}\text{C}/(^{13}\text{C}+^{12}\text{C})$ of Nitrospinae and non-Nitrospinae cells were used for calculation of growth rates only when the overall enrichment Poisson error across all planes of a given cell was < 5%. The variability in $^{15}\text{N}/(^{15}\text{N}+^{14}\text{N})$ ratios across measured Nitrospinae and non-Nitrospinae cells was calculated following Svedén *et al.* (2015) (Supplementary text and Supplementary Figure 2).

Single cell growth rates from nanoSIMS data were calculated as previously described (Martínez-Pérez et al. 2016), where cell ^{15}N - and ^{13}C -atom% excess was calculated by subtracting natural abundance $^{15}\text{N}/(^{15}\text{N}+^{14}\text{N})$ and $^{13}\text{C}/(^{13}\text{C}+^{12}\text{C})$ values (0.37% and 1.11%, respectively). These calculated values are considered conservative, as isotopic dilution of $^{15}\text{N}/(^{15}\text{N}+^{14}\text{N})$ and $^{13}\text{C}/(^{13}\text{C}+^{12}\text{C})$ ratios due to CARD-FISH was not taken into account (Musat et al. 2012; Woebken et al. 2015).

The autotrophic growth rate calculations assume that all newly incorporated ^{13}C as detected from single cell $^{13}\text{C}/(^{13}\text{C}+^{12}\text{C})$ ratios is due to biomass increase. Biomass turnover due to recycling or replacing of cell components without net per cell growth was assumed to be negligible. Nitrospinae autotrophic growth rates were measured in incubations with ^{15}N -ammonium and ^{13}C -bicarbonate

(and an added ^{14}N -nitrite pool), and in incubations with ^{15}N -nitrite and ^{13}C -bicarbonate. Nitrospinae ^{13}C -growth rates did not differ significantly between these two incubations (two-sided, two-sample Wilcoxon test, $W=240$, $p = 0.1113$) and were therefore considered together.

For estimation of the per-cell C-content, cell volumes of Nitrospinae and AOA in the GoM were calculated from nanoSIMS ROI areas. For Nitrospinae, cell shapes were assumed to resemble cylinders topped by two half spheres, AOA cell shapes were assumed to resemble prolate spheroids (Sun & Liu 2003). Nitrospinae and AOA cellular C-content was estimated according to Khachikyan et al. (*in press*), cellular N-content for both groups was calculated from C-content assuming Redfield stoichiometry (C:N = 6.625:1).

N-assimilation (and correspondingly C-assimilation from ^{13}C -bicarbonate) rates were calculated by:

$$\text{N_AssimilationRate [fg-N cell}^{-1} \text{ d}^{-1}] = (^{15}\text{Nat}\%_{\text{excess}_{\text{cell}}}) / (^{15}\text{Nat}\%_{\text{excess}_{\text{label}}}) \times \text{fg-N}_{\text{cell}} \times 1/t \quad \text{Equation (3)}$$

$$\text{N_AssimilationRate [fmol-N cell}^{-1} \text{ d}^{-1}] = \text{N-AssimilationRate [fg-N cell}^{-1} \text{ d}^{-1}] / 14 \quad \text{Equation (4)}$$

where $^{15}\text{Nat}\%_{\text{excess}_{\text{cell}}}$ and $^{15}\text{Nat}\%_{\text{excess}_{\text{label}}}$ are ^{15}N -atom% of a given measured cell and of the ^{15}N -enriched seawater during the incubation after subtraction of natural abundance ^{15}N -atom% (0.37%). $\text{fg-N}_{\text{cell}}$ is the assumed N-content per cell, and t is the incubation time in days (Krupke et al. 2015).

In addition to the directly measured C-assimilation rates from ^{13}C -bicarbonate fixation, C-assimilation rates were calculated from the measured N-assimilation rates, assuming that 6.625 mol of C are assimilated per assimilated mol of N. This was done because the measured ^{13}C isotopic enrichment was likely diluted by the ^{12}C derived from the polycarbonate filter that the cells were filtered and measured on.

DNA and RNA analyses

Samples for DNA and RNA analyses were collected from the same depths and casts sampled for assimilation and oxidation rate experiments as previously described (Kitzinger et al. 2019). For details on nucleic acid extraction please refer to the Supplementary Text.

16S rRNA gene sequencing and analysis

16S rRNA gene diversity was assessed by amplicon sequencing, following an established pipeline (e.g. Padilla et al. 2015; Padilla et al. 2016; Kitzinger et al. 2019), using barcoded primers F515 and R806 (Caporaso et al. 2011). Amplicons were sequenced on the Illumina MiSeq Platform using a Reagent Kit v2 (500-cycles) and a Nano Flow Cell. Details on PCR conditions and bioinformatic analyses are described in the Supplementary Text.

Metagenome sequencing, assembly and binning of metagenome assembled genomes

Metagenomic libraries were constructed and sequenced as previously described (Kitzinger et al. 2019). Read sets were quality filtered using BBduk (BBMap - Bushnell B. - sourceforge.net/projects/bbmap/) and assembled using Metaspades (Nurk et al. 2017) and binned with Metabat2 (Kang et al. 2015) (see Supplementary Text). To improve Nitrospinae binning, the previously obtained metagenomes were re-assembled and re-binned (see Supplementary Text). Nitrospinae metagenome assembled genomes (MAGs) were identified using GTDB-Tk (<https://github.com/ECogenomics/GtdbTk>), which is based on the Genome Taxonomy Database (<http://dx.doi.org/10.1038/nbt.4229>) Metagenome sequencing statistics and information on dereplicated Nitrospinae MAGs are listed in Supplementary Tables 3 and 4, respectively.

Metatranscriptome sequencing

Metatranscriptomes from Station 2 were obtained as previously described (Kitzinger et al. 2019) and analyzed transcription of genes involved in nitrite oxidation. Metatranscriptomes were separated into ribosomal and non-ribosomal partitions using SortMeRNA (Kopylova et al. 2012). Metatranscriptome sequencing statistics are listed in Supplementary Table 5.

Single-gene phylogenetic reconstruction

Single-gene phylogenetic reconstruction was done as described in (Kitzinger et al. 2019) and is described in detail in the Supplementary Text. Briefly, genes of interest, namely the 16S rRNA gene, cyanase (*cynS*), urease alpha subunit (*ureC*) and nitrite oxidoreductase alpha subunit (*nxrA*) bacterial RNA polymerase beta subunit (*rpoB*) were identified in metagenomic assemblies using their respective rfam and pfam HMM models. Alignments were compiled for genes (16S rRNA) and proteins (CynS, UreC, NxrA, RpoB) of interest retrieved from the GoM metagenomes and public databases. These alignments were used for phylogenetic tree calculations using IQ-TREE (Nguyen et al. 2015). The resulting trees were visualized using ITOL (Letunic & Bork 2016). Phylogenetic trees of GoM UreC and CynS have previously been published (Kitzinger et al. 2019), but have been recalculated using the data of the new metagenomic assembly and updated reference sequences.

The abundances of genes of interest in metagenomic and metatranscriptomics datasets were assessed by identifying reads with BLASTX queries against the dataset assembled for phylogenetic analysis and phylogenetic placement into phylogenetic trees using the evolutionary placement algorithm (Berger et al. 2011). Read mapping is reported as fragments per kilobase per million reads (FPKM) values. FPKM values were calculated based on the number of read pairs for which one or both reads were placed into a specified location in the tree, divided by the average gene length in the reference alignment (in kb) divided by the number of total metagenomic read pairs or ribosomal-RNA free metatranscriptomic read pairs (in millions).

The percentage of *ureC*- and *cynS*-containing Nitrospinae was estimated for each metagenomic dataset as in Kitzinger et al. (2019). FPKM for urease or cyanase genes ($FPKM_{ureC/cynS}$) classified as Nitrospinae *ureC/cynS* and the FPKM for Nitrospinae *rpoB* ($FPKM_{rpoB}$) and SSU (16S rRNA genes, $FPKM_{SSU}$) genes were compared, under the assumption that *rpoB* and SSU were universally present in all Nitrospinae as single copy genes. The percentage of *ureC*-/*cynS*-positive Nitrospinae was then calculated as $FPKM_{ureC/cynS} / FPKM_{rpoB}$ and/or as $FPKM_{ureC/cynS} / FPKM_{SSU}$.

Results and Discussion

Nitrite oxidation in the Northern GoM

Nitrite and ammonia oxidation rates were determined during an East-West sampling transect on the Louisiana Shelf of the Gulf of Mexico (GoM) in July 2016. Due to summertime eutrophic conditions (Rabalais et al. 2001), bottom waters were hypoxic at the time (Supplementary Figure 1). Hypoxic bottom waters generally coincided with highest median ammonium (320 nM), urea (69 nM), cyanate (11.5 nM), nitrite (848 nM) and nitrate (2250 nM) concentrations (Figure 1 a - c, Supplementary Figure 3, Kitzinger et al. 2019). These concentrations are similar to previous observations (Bristow et al. 2015).

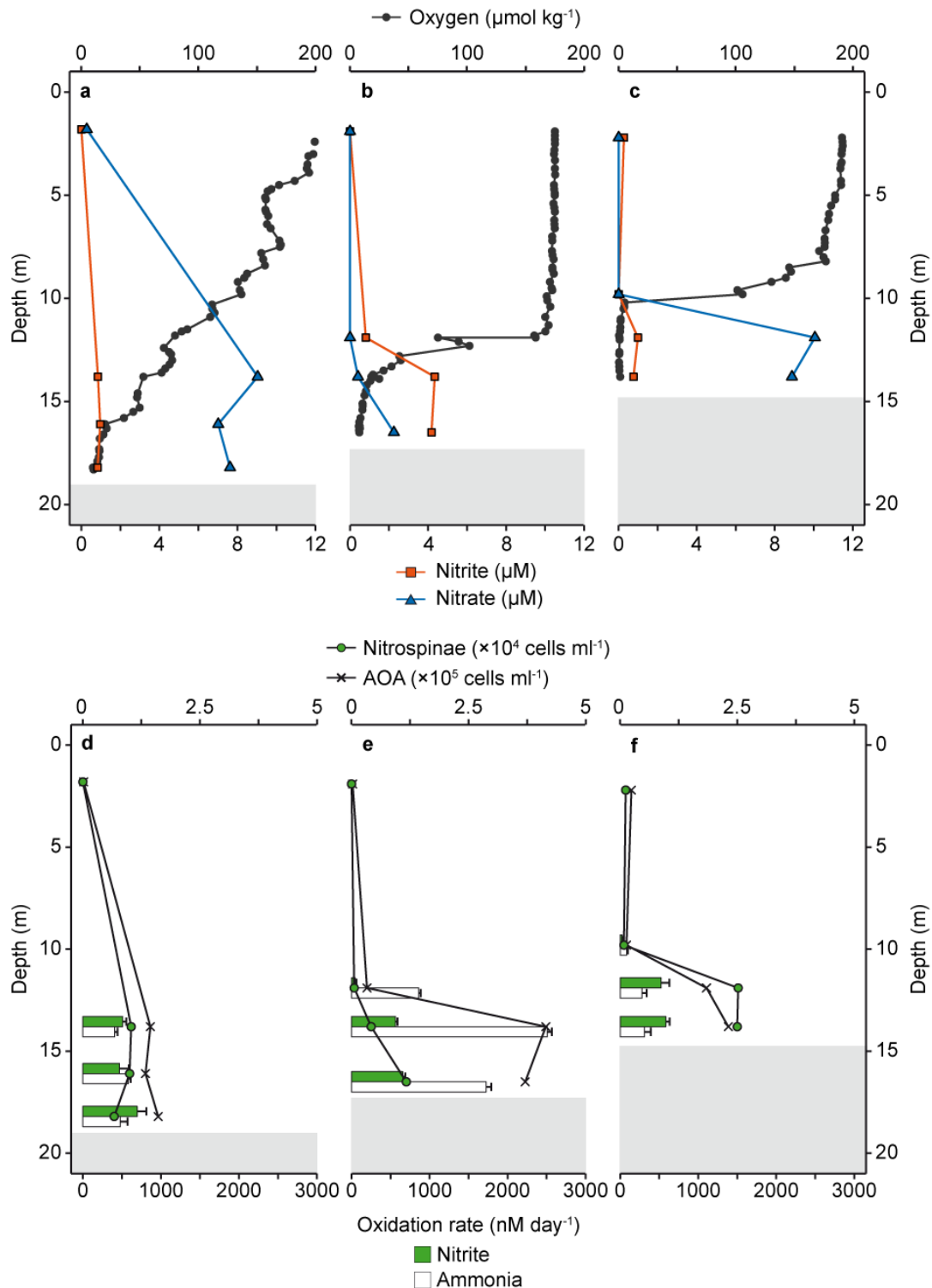


Figure 1 Depth profiles of nutrient concentrations, nitrite and ammonia oxidation rates, and Nitrospinae and AOA cell counts at experimental stations in the Northern GoM. a - c) *In situ* oxygen, nitrite and nitrate concentration profiles at Station 1 (a), 2 (b) and 3 (c). Surface nitrite and nitrate concentrations were taken from the same station, the day before experiments were done. d - f) Nitrite and ammonia oxidation rates and Nitrospinae and AOA CARD-FISH counts at Station 1 (d), 2 (e) and 3 (f). Note the different scales for Nitrospinae and AOA cell counts, respectively. Nitrite and ammonia oxidation rates are depicted as green and white bars, respectively, and were calculated from slopes across all time points of triplicate incubations. Error bars represent standard error of the slope. Shaded grey areas indicate sediment (max. water depth was 18.5 m).

Ammonia and nitrite oxidation rates were comparable, with rates ranging between 80 – 2500 nM day⁻¹ for ammonia oxidation (Kitzinger et al. 2019) and 25 – 700 nM day⁻¹ for nitrite oxidation (Figure 1 d-f). The nitrite oxidation rates were in the range of the few that have been reported previously from the GoM (Bristow et al. 2015) and other oxygen depleted waters (Ward 2008; Füssel et al. 2012; Beman et al. 2013; Sun et al. 2017). The success of NOB in oxygen deficient waters has amongst other factors been attributed to their high affinity for oxygen (Bristow et al. 2016; Sun et al. 2017). Our incubations were carried out at *in situ* oxygen concentrations, ranging from 1 µM to 160 µM. There was no correlation between nitrite oxidation rates and oxygen concentrations (Figure 2c). This indicated that the nitrite oxidizers in the GoM are well adapted to low oxygen concentrations, as observed previously in other regions (Bristow et al. 2016; Sun et al. 2017).

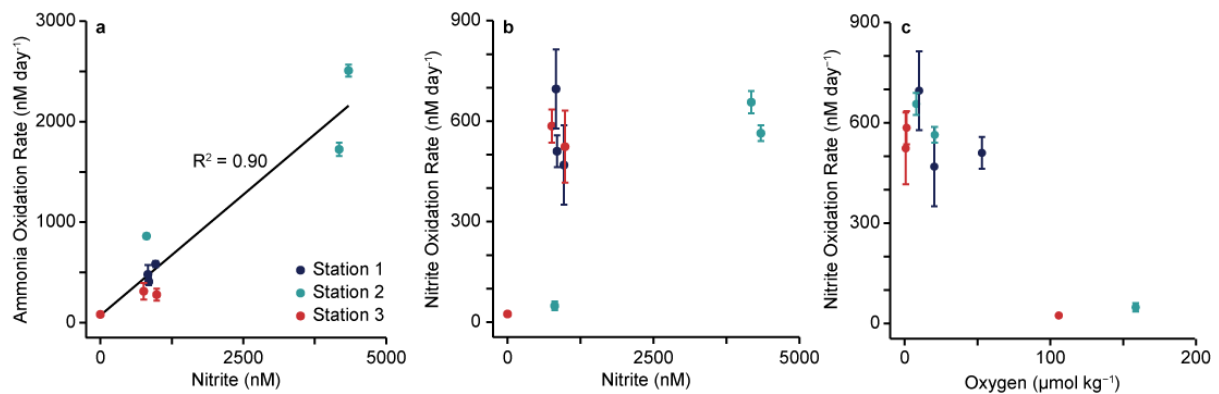


Figure 2 Correlations between ammonia and nitrite oxidation rates and nitrite concentrations and correlation between nitrite oxidation rate and oxygen concentration across experimental stations. a) Correlation between ammonia oxidation rate and nitrite concentration (reproduced from Kitzinger et al. 2019). The black line is the linear regression, R^2 was calculated on the basis of Pearson correlations, and was significant (two-sided t-test, $t = 8.002$, $DF = 7$, $P = 9.10 \times 10^{-5}$) b) Correlation between nitrite oxidation rate and nitrite concentration. c) Correlation between nitrite oxidation rate and oxygen concentration. Error bars represent standard error of the process rates calculated from slopes across all time points and replicates.

There was also no clear relationship between ammonia and nitrite oxidation rates in the GoM (Supplementary Figure 4). For example, ammonia oxidation outpaced nitrite oxidation rates at Station 2, whereas at Station 3, nitrite oxidation rates were higher than ammonia oxidation rates (Figure 1 e, f). This suggests that ammonia and nitrite oxidation are not tightly linked in this region, which is in line with previous observations in the GoM (Bristow et al. 2015). Neither was there a correlation between the nitrite oxidation rates and nitrite concentration (Figure 2b), however, there was a significant correlation between ammonia oxidation rates and nitrite concentrations (Figure 2a, Kitzinger et al. 2019). This indicates that in the GoM, as in most of the ocean, ammonia oxidation, rather than nitrate reduction to nitrite, was the main source of nitrite (Ward 2008).

Nitrite oxidizing community; composition and abundance

To identify the NOB responsible for nitrite oxidation in the GoM, 16S rRNA gene targeted amplicon and deep metagenomic sequencing were performed, and *in situ* metatranscriptomes were obtained. The only detectable NOB based on 16S rRNA gene sequences in both amplicon and metagenome datasets belonged to the phylum Nitrospinae (Figure 3). *Nitrococcus*, another marine NOB that is frequently found in shelf areas (Füssel et al. 2017), was not detected in our dataset. The metagenomes and metatranscriptomes were screened for the presence and transcription of the alpha subunit of nitrite oxidoreductase (*nxrA*), the key gene for nitrite oxidation. In line with the 16S rRNA gene results, almost all identified metagenomic *nxrA* read fragments were affiliated with

Nitrospinae (84 – 98%). 2 – 15% of the metagenomic read fragments mapped to *nxrA* of the NOB genus *Nitrolancea* (Sorokin et al. 2012). These NOB have not been found in the marine environment before, therefore, the fragments mapping to *Nitrolancea nxrA* may represent *nxr*-related genes, e.g. nitrate reductases. Unsurprisingly, given the high nitrite oxidation rates, *nxrA* genes were also highly transcribed *in situ*, and all transcribed *nxrA* genes were affiliated with Nitrospinae.

Based on the retrieved metagenomic Nitrospinae 16S rRNA gene sequences, several co-occurring Nitrospinae were identified, with 85-94 % of the metagenomic Nitrospinae 16S rRNA reads affiliated with Nitrospinae Clade 2, 2-11 % affiliated with *Ca. Nitromaritima* (Nitrospinae Clade 1), and 0.1-2% affiliated with the genus *Nitrospina* (Ngugi et al. 2016; Pachiadaki et al. 2017) (Figure 3). Members of Nitrospinae Clade 2, the most abundant Nitrospinae in our dataset, are environmentally widespread and have previously been found in both open ocean metagenomes and the seasonally anoxic Saanich inlet (Pachiadaki et al. 2017).

To constrain absolute nitrite oxidizer cell numbers, *in situ* cell counts were performed by catalyzed reporter deposition fluorescence *in situ* hybridization (CARD-FISH) using specific probes for *Nitrococcus* (Juretschko 2000), *Nitrospira* (Daims et al. 2001) and *Nitrobacter* (Wagner et al. 1996). Additionally, we designed a new Nitrospinae CARD-FISH probe (Ntspn759), as the published Nitrospinae CARD-FISH probes (Ntspn693, Juretschko 2000, and the recently published probe Ntspn-Mod, Pachiadaki et al. 2017) covered only a fraction of the known Nitrospinae, and did not cover all sequences in our dataset. Our newly developed Ntspn759 probe targeted all of the obtained GoM Nitrospinae 16S rRNA gene sequences. Additionally, it covers 91% of the known 16S rRNA gene diversity of the family Nitrospinaceae, which contains all known Nitrospinae NOB (Supplementary Text). The only NOB in the GoM detectable by CARD-FISH were Nitrospinae, which is in line with the observations from amplicon and metagenomic sequencing that Nitrospinae were the main NOB.

Nitrospinae were hardly detectable at the surface, and numbers increased with depth, reaching up to 2.8×10^4 cells ml⁻¹, just above the sediment. Based on CARD-FISH counts, Nitrospinae constituted at most 1% of the microbial community at all depths and stations (Figure 1, Supplementary Figure 5). Nitrospinae CARD-FISH counts were an order of magnitude lower than those of the AOA in the GoM published previously (Figure 1, Supplementary Figure 6a, Kitzinger et al. 2019). A similar difference in abundance between these two nitrifier groups was also seen in the 16S rRNA gene amplicon dataset and the metagenomic abundance of Nitrospinae and AOA metagenome assembled genomes (MAGs, Supplementary Figure 6 b, c).

The higher abundance of AOA compared to NOB in marine systems has been observed before in metagenome, amplicon, and qPCR-based studies (Mincer et al. 2007; Tolar et al. 2013; Doxey et al. 2015; Lüke et al. 2016; Damashek et al. 2019; Liu et al. 2018; Reji et al. 2019). However, this is one of the first times this has been confirmed by CARD-FISH, a more direct quantification method that is independent of DNA extraction and primer biases. In addition to the *in situ* Nitrospinae counts, CARD-FISH counts were carried out at the end of the ¹⁵N and ¹³C incubations, which revealed that in some incubations, Nitrospinae abundances increased up to 4.7-fold within the incubation period of 24 hours (Supplementary Table 2).

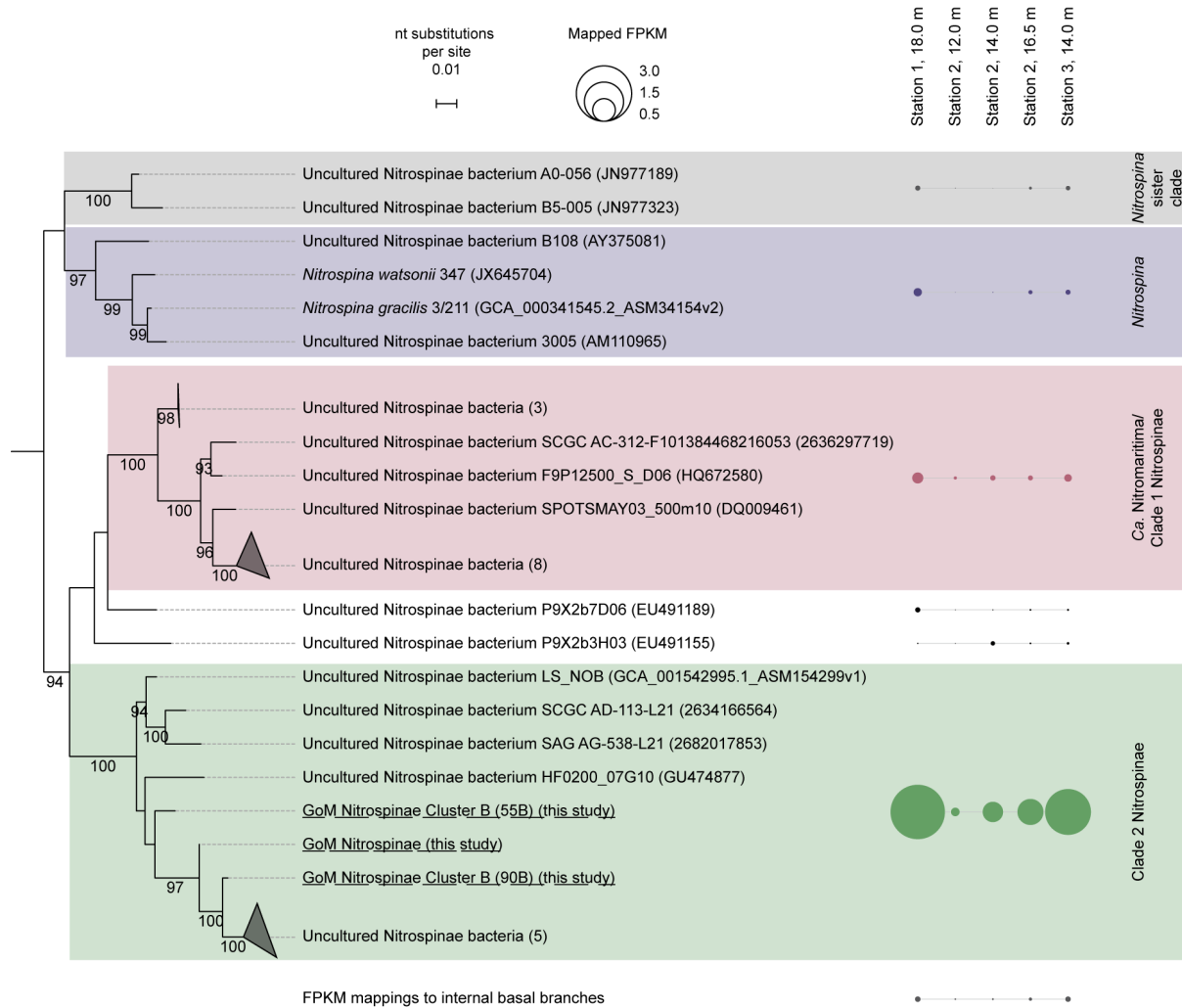


Figure 3 Nitrospinae 16S rRNA gene phylogeny. Nitrospinae 16S rRNA gene sequences retrieved from GoM metagenomes are indicated as “GoM Nitrospinae” and underlined. Outgroup are cultured Deltaproteobacteria. GoM metagenomic read fragments (FPKM) were mapped onto the alignment and are shown next to the respective clades as circles. FPKM mapping to internal basal nodes were grouped and are displayed separately. Tree was constructed using IQ-TREE (Nguyen et al. 2015) with automated model selection from near full-length Nitrospinae 16S rRNA gene sequences and confidence was assessed with ultrafast bootstrapping (1,000 iterations). Metagenomic Nitrospinae 16S rRNA gene read fragments were fit into the core alignment using the short fragment add option in mafft. The resulting alignment was used to place short sequences into the core phylogeny using EPA. The scale bar represents nt substitutions per site, and bootstrap values > 90 are displayed.

Per cell ammonia and nitrite oxidation rates

A factor that could play a key role in determining the abundance of NOB in the environment is their per cell oxidation activity, as this largely determines the energy that can be gained from nitrite oxidation at a single cell level. Such values have not been reported before for the marine environment, as absolute NOB cell numbers are rarely quantified at the same time as bulk nitrite oxidation rates. As the Nitrospinae were the only significant known NOB in the GoM, we were able to calculate per cell nitrite oxidation rates. Assuming that all of the Nitrospinae were active, the increase in CARD-FISH cell counts from the start to the end of the incubation in combination with the bulk nitrite oxidation rates (Supplementary Table 2) indicated that per cell nitrite oxidation rates ranged from 21 – 106 fmol per cell per day. These rates were approximately 14-fold higher than the per cell ammonia oxidation rates of the AOA in the GoM (0.9 – 30.8 fmol-N cell⁻¹ day⁻¹; Kitzinger et al.

2019). To date, no Nitrospinae per cell oxidation rates have been reported for either cultures or environmental populations. However, our rates are in line with those we estimated by combining qPCR data for Nitrospinae 16S rRNA gene abundance and bulk nitrite oxidation rates from the Eastern tropical North Pacific, where Nitrospinae also dominate the NOB community (Beman et al. 2013). These rates ranged from 0 – 107 fmol nitrite per cell per day, assuming that Nitrospinae from the Eastern tropical North Pacific, like *N. gracilis* (Lücker et al. 2013), have a single rRNA operon.

Cellular carbon content of Nitrospinae

Despite their low abundance, Nitrospinae have recently been estimated to be responsible for more dark carbon fixation in marine systems than the highly abundant AOA (Pachiadaki et al. 2017). This could imply that the bulk population carbon content of the Nitrospinae is higher than the bulk population carbon content of the AOA. Both pure culture and *in situ* studies indicate that Nitrospinae are larger than AOA (e.g. Watson & Waterbury 1971; Könneke et al. 2005; Pachiadaki et al. 2017), but the differences in cell and population size has never been quantified *in situ* and subsequently converted to cellular or population carbon content. In order to quantify the carbon content of the NOB and AOA populations in the GoM, cell volumes were calculated from nanoscale secondary ion mass spectrometry (nanoSIMS) measurements. The Nitrospinae were on average four-fold larger than the AOA. By applying a scaling factor for carbon content based on cell biovolume (Khachikyan et al. *in press*), we calculated that the Nitrospinae contained approximately two times as much carbon per cell (100 fg-C cell⁻¹) as AOA (50 fg-C cell⁻¹).

The AOA in the GoM were visibly larger than cultured marine AOA and those normally observed in environmental studies. As such, the GoM AOA cellular carbon content was higher than that previously determined, ranging from 9 – 17 fg-C cell⁻¹ (Herndl et al. 2005; Berg et al. 2015; Bayer et al. 2019b; Khachikyan et al., *in press*).

By combining the *in situ* Nitrospinae and AOA cell abundance and the per cell carbon content, the carbon content of the two nitrifier populations was calculated. The C-content for all investigated stations and depths ranged from 0.08-2.66 bulk- $\mu\text{g-C L}^{-1}$ for the Nitrospinae and 0.72-22.2 bulk- $\mu\text{g-C L}^{-1}$ for the AOA population.

In situ growth rates of Nitrospinae

So far, no *in situ* growth rates have been determined for Nitrospinae. NanoSIMS was performed on samples from Station 2, 14m depth, which were amended with ¹³C-bicarbonate and ¹⁵N-ammonium (or ¹⁵N-nitrite, see methods) to determine single cell Nitrospinae growth rates. Autotrophic growth rates from carbon fixation were 0.25 ± 0.01 (SE) day⁻¹ and ammonium-based growth rates were 0.53 ± 0.03 (SE) day⁻¹ (Figure 4), corresponding to doubling times of 2.8 and 1.3 days, respectively. The discrepancy between C- and N-based growth may be due to C isotope dilution by the CARD-FISH procedure (Musat et al. 2012; Woebken et al. 2015) or due to dilution of the cellular ¹³C by ¹²C derived from the polycarbonate filter surface. Alternatively, this discrepancy could indicate that the Nitrospinae were growing mixotrophically, for which there was some evidence in the Nitrospinae MAGs (see below).

Compared to the Nitrospinae, the AOA in the GoM had significantly lower growth rates based on both ¹³C-bicarbonate assimilation (0.04 ± 0.005 (SE) day⁻¹) and ¹⁵N-ammonium assimilation (0.23 ± 0.01 (SE) day⁻¹) (Figure 4, Kitzinger et al. 2019). It should be noted, that the lower measured AOA autotrophic (¹³C-based) growth rates may also be affected by the smaller cell size of AOA in comparison to Nitrospinae. NanoSIMS measurements were done on cells filtered onto polycarbonate filters, which can lead to a dilution of cellular ¹³C by ¹²C derived from the filter surface. This potential dilution effect could have impacted both the Nitrospinae and AOA ¹³C-enrichment, explaining the

lower ^{13}C -based growth rates compared to the ^{15}N -based rates, but is stronger for smaller cells. The measured lower growth rates of AOA compared to Nitrospinae were however also in good agreement with their lower per cell nitrification rates.

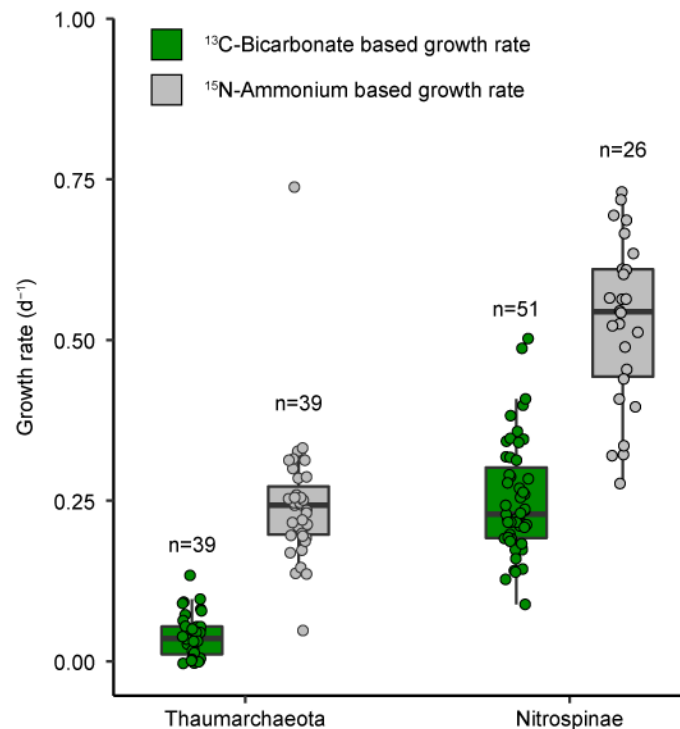


Figure 4 Nitrospinae and AOA autotrophic growth rates calculated from ^{13}C -bicarbonate and ^{15}N -ammonium assimilation measured by nanoSIMS. Nitrospinae ^{13}C -bicarbonate assimilation rates were determined from the water samples after addition of ^{15}N -ammonium and ^{13}C -bicarbonate, and ^{15}N -nitrite and ^{13}C -bicarbonate. AOA data was acquired from the incubation with added ^{15}N -ammonium and ^{13}C -bicarbonate only and was taken from Kitzinger et al. (2019). Number of cells analyzed per population is indicated above each boxplot. Boxplots depict the 25 – 75 % quantile range, with the center line depicting the median (50% quantile); whiskers encompass data points within $1.5 \times$ the interquartile range. Data of each measured cell are shown as points; horizontal position was randomized for better visibility of individual data points. Nitrospinae had significantly higher growth rates than AOA (one-sided, two-sample Wilcoxon test, $W=1984$, $p = 4.04 \times 10^{-16}$ for growth based on ^{13}C -bicarbonate assimilation and $W=1464$, $p = 3.32 \times 10^{-12}$ for growth based on ^{15}N -ammonium assimilation).

***In situ* organic N use by Nitrospinae**

Intriguingly, the ammonium-based growth rate (0.5 day^{-1}) of the Nitrospinae was substantially lower than that calculated from the increase in cell numbers during the incubation period, which corresponded to a growth rate of 1.2 day^{-1} (0.6 days doubling time). This indicates that the Nitrospinae may have been assimilating N-sources other than ammonium. Metagenomic studies and analysis of the *N. gracilis* genome have indicated that some Nitrospinae can use the simple organic N-compounds urea and cyanate as additional N-sources (Lücker et al. 2013; Ngugi et al. 2016; Pachiadaki et al. 2017). To assess whether this is the case in the environment, single cell N-assimilation based on the incorporation of ^{15}N -ammonium, ^{15}N -urea, ^{15}N -cyanate and ^{15}N -nitrite was determined by nanoSIMS.

All measured Nitrospinae cells were significantly enriched in ^{15}N for all tested substrates (Figure 5). Furthermore, the Nitrospinae assimilated significantly more ^{15}N from all these compounds than surrounding microorganisms, including the AOA (Kitzinger et al. 2019). Intriguingly, ammonium and urea were used equally by Nitrospinae, followed by cyanate. Nitrite use by Nitrospinae was much

lower compared to the other tested substrates. We calculated the growth rates of Nitrospinae from N-assimilation of all tested substrates combined, i.e. ammonium, urea, cyanate and nitrite (Supplementary Figure 7). The combined growth rate was 1.2 day^{-1} , which was the same as the cell count based growth rate of 1.2 day^{-1} at Station 2, 14 m depth. This implies that GoM Nitrospinae could meet all of their cellular N-demand by using ammonium, urea and cyanate. In fact, when taken together, urea and cyanate assimilation met more than half of the Nitrospinae N-demand. Utilization of DON for N-assimilation is likely a key factor for the ecological success of Nitrospinae, as it allows them to avoid competition with AOA, whom they depend on for their substrate, nitrite. Thus, from an ecological perspective, utilization of DON as N-source by Nitrospinae is highly advantageous.

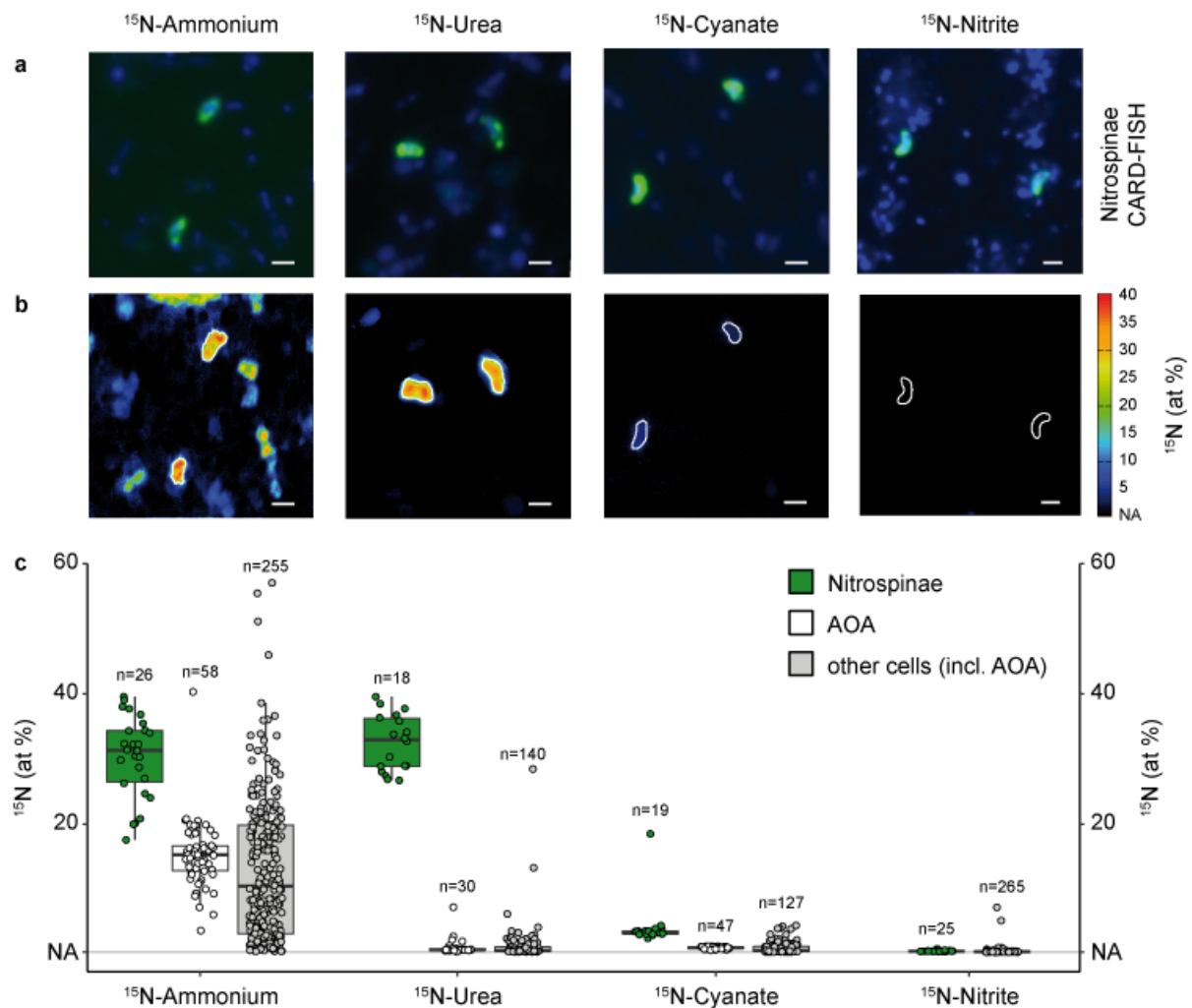


Figure 5 Nitrospinae single cell ^{15}N -assimilation from ammonium, urea, cyanate and nitrite measured by nanoSIMS. a) Representative CARD-FISH images of Nitrospinae (green, stained by probe Ntspn759) and other cells (blue, stained by DAPI). b) Corresponding nanoSIMS image of ^{15}N at% enrichment after addition of ^{15}N -ammonium, urea, cyanate or nitrite. Nitrospinae are marked by white outlines. Scale bar is $1 \mu\text{m}$ in all images. c) ^{15}N at% enrichment of Nitrospinae (green), AOA (white) and other, non-targeted cells (grey) after incubation with ^{15}N -ammonium, ^{15}N -urea, ^{15}N -cyanate or ^{15}N -nitrite. AOA data was taken from Kitzinger et al. (2019) for comparison. Note that non-targeted cells depicted here also include AOA cells, as no specific AOA probe was included in the Nitrospinae nanoSIMS measurements. Number of cells analyzed per category is indicated above each boxplot. Boxplots depict the 25 – 75 % quantile range, with the center line depicting the median (50% quantile); whiskers encompass data points within $1.5 \times$ the interquartile range. NA is the natural abundance ^{15}N at% enrichment value (0.37%).

Nitrospinae MAG analyses

To assess the genomic basis for DON utilization by Nitrospinae, we screened the GoM metagenomes presence of Nitrospinae-like cyanase and urease genes.

From the investigated five deeply sequenced metagenomes, we obtained seven Nitrospinae MAGs, representing three closely related Nitrospinae clusters (hereafter referred to as cluster A, B and C). Nitrospinae cluster A made up 0.003 - 0.358% and cluster B 0.008 - 0.152 % of the metagenomic reads, compared to the lower abundance cluster C with 0.003 - 0.050 % (Supplementary Table 4). All obtained MAGs were affiliated with Nitrospinae Clade 2 (Figure 1, Supplementary Figure 8). In line with the observed assimilation of ^{15}N from ^{15}N -ammonium and ^{15}N -nitrite, the MAGs contained both ammonium and nitrite transporters, as well as assimilatory nitrite reductase genes (Supplementary Table 6). Furthermore, at least one MAG representative of each cluster A, B and C contained urease and/or urea ABC-transporter genes, supporting the observed *in situ* assimilation of urea-derived N (Supplementary Table 6). One of the MAGs (cluster B) contained *cynS*, the gene encoding for cyanase (Supplementary Table 6). The nanoSIMS data implied that all measured Nitrospinae are capable of urea and cyanate use, and thus, all Nitrospinae should encode for both urease (*ureC*) and cyanase (*cynS*) genes. Metagenomic read fragment abundance (FPKM) of Nitrospinae-affiliated *ureC* genes was very similar to FPKM values of Nitrospinae 16S rRNA and *rpoB* gene abundance in all metagenome datasets (average $\text{FPKM}_{ureC} : \text{FPKM}_{SSU} = 1.2$, $\text{FPKM}_{ureC} : \text{FPKM}_{rpoB} = 1.7$), indicating that all GoM Nitrospinae encoded for *ureC*. However, clearly Nitrospinae-affiliated *cynS* genes were much less abundant in the metagenome datasets (average $\text{FPKM}_{ureC} : \text{FPKM}_{SSU} = 0.09$, $\text{FPKM}_{ureC} : \text{FPKM}_{rpoB} = 0.1$). This contrasts the obtained nanoSIMS data, where all measured Nitrospinae incorporated cyanate. The reason for this discrepancy is unknown. However, as *cynS* has previously been shown to undergo horizontal gene transfer (Spang et al. 2012; Palatinszky et al. 2015), it is possible that Nitrospinae contain additional *cynS* not closely related to previously known Nitrospinae *cynS* genes. In addition to urea and cyanate utilization genes, the MAGs also encoded for spermidine, amino acid and (oligo-) peptide ABC-type transporters, which may provide additional N- and C-sources for biomass growth. The presence of a sugar transport system likely taking up sucrose, a fumarate/malate/succinate transporter, as well as many uncharacterized ABC transporter systems further indicated that the GoM Nitrospinae have a potential for mixotrophic growth (Supplementary Table 6). The potential for mixotrophic growth of GoM Nitrospinae could explain the differences observed in ^{13}C -bicarbonate and ^{15}N -based growth rates and may contribute to their environmental success and the high measured growth rates.

There were some indications in the MAGs that the Nitrospinae might have alternative pathways for energy generation. As all other sequenced nitrite oxidizers, including *N. gracilis* (Lücker et al. 2013), the Nitrospinae MAGs encoded a copper containing nitrite reductase (*nirK*). Furthermore, the MAG with the lowest abundance encoded a putative NiFe 3b hydrogenase, similar to the one found in the genome of *N. gracilis* (Lücker et al. 2013). Chlorite dismutase (*clt*) genes were detected in 5 out of the 7 MAGs. Functional chlorite dismutases have been found previously in the genome of the nitrite oxidizer *Nitrospira defluvii* (Maixner et al. 2008), however, this enzyme has a role in detoxification, rather than energy generation.

Overall, the potential for alternative energy generating pathways was low in the obtained MAGs of Nitrospinae Clade 2. However, it cannot be excluded that Nitrospinae Clade 1, which also occur in the GoM at lower abundance, and for which no MAGs were obtained, do have additional metabolic versatility.

Comparison of *in situ* N- and C-assimilation rates between Nitrospinae and AOA

Single cell and population N- and C-assimilation rates were calculated for Nitrospinae and AOA using the ^{15}N -enrichment and their cellular N-content as calculated from their biovolumes. Average Nitrospinae N-assimilation in fmol-N per cell per day was 0.42 ± 0.03 (SE) for ^{15}N -ammonium, 0.43 ± 0.02 (SE) for ^{15}N -urea, 0.05 ± 0.01 (SE) for ^{15}N -cyanate and 0.003 ± 0.0004 (SE) for ^{15}N -nitrite. As the Nitrospinae growth rates calculated by combining ^{15}N -ammonium, ^{15}N -urea, ^{15}N -cyanate and ^{15}N -nitrite assimilation from nanoSIMS measurements were the same as growth rates determined from the increase in cell counts during the incubation, it was assumed that Nitrospinae assimilate all four tested substrates *in situ* to meet their total N-demand for assimilation. Thus, the combined Nitrospinae N-assimilation from all ^{15}N -substrates together was calculated to be 0.91 fmol-N per cell per day.

In comparison to Nitrospinae, the single cell N-assimilation rates (in fmol-N per cell per day) of AOA were significantly lower, with 0.11 ± 0.01 (SE) for ^{15}N -ammonium, 0.005 ± 0.001 (SE) for ^{15}N -urea, 0.004 ± 0.0002 (SE) for ^{15}N -cyanate; and the combined AOA N-assimilation rate from all ^{15}N -substrates together was 0.12 fmol-N per cell per day.

Due to the observed bias in ^{13}C -enrichment measurements, likely due to dilution from the polycarbonate filter (see above), C-assimilation for both Nitrospinae and AOA was estimated from the measured ^{15}N -assimilation rates, following the Redfield ratio of C:N (6.625:1, see Methods). The combined Nitrospinae C-assimilation rate was 6.0 fmol-C per cell per day, compared to a much lower combined AOA C-assimilation rate of 0.76 fmol-C per cell per day. When these values were combined with the Nitrospinae and AOA cell counts, the population C-assimilation was ~ 79 nmol-C per liter per day for the Nitrospinae and ~ 316 nmol-C per liter per day for the AOA.

In addition to ^{15}N -based assimilation rates, the Nitrospinae C-assimilation was calculated from the increase in Nitrospinae cell counts before and after incubation and their cellular C-content. The Nitrospinae population C-assimilation rate from cell count increase was 75 fmol-C per cell per day, which is nearly identical to the values calculated from the ^{15}N -tracer additions.

Contrasting life strategies of Nitrospinae and AOA

From a thermodynamic perspective, ammonia oxidation is a much more exergonic process than nitrite oxidation (e.g. Bock & Wagner 2006). This is also the case under conditions representative for the GoM, where Gibbs free energy release is -262 kJ per mol for ammonia oxidation, compared to -65 kJ per mol for nitrite oxidation (Supplementary Table 7). Therefore, from a thermodynamic perspective, AOA biomass should increase about four times faster than that of the Nitrospinae in the GoM, where bulk ammonia and nitrite oxidation rates are similar (Figure 1). This assumes that they have an equal energy yield (i.e. they are fixing the same amount of C per Joule). Based on the measured bulk nitrification rates at Station 2, 14 m depth (Figure 1), nitrite oxidation provides ~ 0.04 Joule per liter per day, and ammonia oxidation ~ 0.7 Joule per liter per day in the hypoxic GoM waters. This joule energy gain was combined with the population C-assimilation rates of 79 nmol-C per liter per day for the Nitrospinae, and 316 nmol-C per liter per day for the AOA population (Table 1) to calculate the energy yield for nitrite and ammonia oxidation (i.e. the nmol-C fixed per Joule gained). Intriguingly, the energy yield for the Nitrospinae population was ~ 2150 nmol-C per liter per Joule, while AOA population energy yield was only ~ 480 nmol-C per liter per Joule (Table 1). This implies that Nitrospinae are 4.5-fold more efficient in translating the energy gained from the oxidation of nitrite to C-assimilation than the AOA are in translating energy gained from ammonia oxidation. This is surprising considering that AOA use the HP/HB carbon fixation pathway, which is suggested to be the most energy efficient aerobic autotrophic C-fixation pathway (requiring 5 ATP

per generated pyruvate, Könneke et al. 2014). Nitrospinae employ the reverse tricarboxylic acid cycle (rTCA) for autotrophic C-fixation (Lücker et al. 2013). This pathway is highly energy efficient under anaerobic conditions (requiring 2 ATP per generated pyruvate) but is generally highly sensitive to oxygen (Berg 2011). Previous studies have suggested that the Nitrospinae replace the oxygen sensitive enzymes by less oxygen sensitive versions (Lücker et al. 2013). Our results imply that at least under the low oxygen conditions in the GoM, the rTCA cycle in the Nitrospinae is also highly energy efficient.

Table 1 Parameters for estimating energy yield by GoM AOA and Nitrospinae.

Parameter	GoM AOA	GoM Nitrospinae
Cell volume (μm^3)	0.06	0.25
Cell Carbon (fg C cell ⁻¹) (Khachikyan et al. <i>in press</i>)	50	100
Cell abundance (L ⁻¹ , average counts of <i>in situ</i> and end of incubation)	415 000 000	13 200 000
Bulk oxidation rate (nM day ⁻¹)	2508	564
Energy gained per mol oxidized for GoM conditions (kJ mol ⁻¹)	-262	-65
Energy gained from bulk oxidation rates (J day ⁻¹)	0.658	0.037
C-assimilation estimated from N-assimilation per population (nmol-C L ⁻¹ day ⁻¹)	316	79
Energy yield (nM-C J ⁻¹ , using C-assimilation estimated from N-assimilation)	480	2144
Measured C-assimilation from ¹³ C-bicarbonate assimilation per population (nmol-C L ⁻¹ day ⁻¹)	54	17
Energy yield (nM-C J ⁻¹ , using measured C-assimilation from ¹³ C-bicarbonate)	82	464

Additional factors could contribute to the apparent higher efficiency of Nitrospinae in translating energy gain into C-assimilation when compared to the AOA. The Nitrospinae have a short respiratory chain, oxidizing nitrite to nitrate in a single reaction, before transferring electrons to oxygen. In comparison, the AOA must synthesize several enzymes to oxidize ammonia to nitrite (probably at least 3, Carini et al. 2018). During ammonia oxidation, the electrons from hydroxylamine/NO oxidation also need to be shuttled to AMO to activate ammonium, creating more opportunity for energy dissipation not linked to energy conservation. Additionally, the active site of NXR in Nitrospinae is located in the periplasm, therefore, the protons generated during nitrite oxidation directly contribute to the proton motive force, and thus to ATP generation (Lücker et al. 2013). All of these factors could lead to additional metabolic costs in the AOA compared to the Nitrospinae, lowering their energy yield.

A further possibility that could explain the apparent differences in growth yield is that the Nitrospinae were growing mixotrophically, i.e. assimilating organic C in addition to autotrophic C-fixation. In this case, C-assimilation would be uncoupled from the energy gained by nitrite oxidation and the calculated energy yield (which assumes that the measured N-assimilation is matched by autotrophic C-fixation) would be an overestimate. Nevertheless, comparison of the directly measured ¹³C-assimilation from ¹³C-bicarbonate by Nitrospinae and AOA also indicated that the Nitrospinae had a much higher energy yield (465 nmol-C per Joule) than the AOA (82 nmol-C per Joule, Table 1). In principle, the energy yield of the Nitrospinae could also have been overestimated if they were using other electron donors in addition to nitrite, such as sulfur or hydrogen. However,

little to no evidence for the use of alternative electron donors was found in the investigated Nitrospinae MAGs (see above).

It is also possible that the AOA had a higher energy yield than we determined because they released significant amounts of fixed carbon to the environment as dissolved organic C (DOC). Such DOC release has recently been shown for AOA pure cultures (Bayer et al. 2019a) and, if occurring in the environment as well, would have wide ranging implications for our understanding of the impact of the highly abundant AOA on carbon cycling in the dark ocean.

The fact that the AOA outnumber NOB by an order of magnitude in the GoM and other marine systems despite lower growth rates indicates a higher mortality rate for Nitrospinae than for AOA. This mortality could be either due to viral lysis or due to zooplankton grazing. We did not perform experiments to assess the relative importance of these two controlling factors, however, both viral lysis and zooplankton grazing have previously been shown to play a major role in bacterioplankton population control. In fact, the Nitrospinae MAGs encode for prophage genes, a sign of previous or possibly ongoing viral infections.

Our results show that Nitrospinae in the GoM are highly energy efficient, display fast growth rates despite their low *in situ* abundance, and significantly outpace the much more abundant AOA. Maintaining these low *in situ* Nitrospinae cell numbers requires a high mortality rate, likely due to zooplankton grazing and viral lysis. The results presented here show that Nitrospinae meet most of their cellular N-requirement by the assimilation of the DON compounds urea and cyanate, rather than inorganic N. We hypothesize that the combination of high energy efficiency and utilization of DON compounds for growth are likely key factors contributing to the success of Nitrospinae as the main nitrite oxidizer in the ocean.

Acknowledgements

The authors thank the captain and crew of the R/V Pelican PE17-02 cruise. The authors are grateful to P. Hach, G. Klockgether, D. Tienken and D. J. Parris for technical support; W. Mohr, B. Kartal, N. Lehnen, A. Müller and S. Ahmerkamp for fruitful discussions. The authors thank A. Müller for providing *N. gracilis* biomass for CARD-FISH evaluations. This research was funded by the Max Planck Society, the European Research Council Advanced Grant project NITRICARE 294343 (to M.W.), the Austrian Science Fund (DK plus W 1257) and the National Science Foundation grants 1558916 and 1564559 (to F.J.S.).

References

- Bayer B., Hansman R.L., Bittner M.J., Noriega-Ortega B.E., Niggemann J., Dittmar T. and Herndl G.J. 2019a. Ammonia-Oxidizing Archaea Release a Suite of Organic Compounds Potentially Fueling Prokaryotic Heterotrophy in the Ocean. *BioRxiv*, 558726. doi:10.1101/558726.
- Bayer B., Vojvoda J., Reinthaler T., Reyes C., Pinto M. and Herndl G.J. 2019b. Nitrosopumilus Adriaticus Sp. Nov. and Nitrosopumilus Piranensis Sp. Nov., Two Ammonia-Oxidizing Archaea from the Adriatic Sea and Members of the Class Nitrososphaeria. *International Journal of Systematic and Evolutionary Microbiology*, 1–11. doi:10.1099/ijsem.0.003360.
- Beman J.M., Leilei Shih J. and Popp B.N. 2013. Nitrite Oxidation in the Upper Water Column and Oxygen Minimum Zone of the Eastern Tropical North Pacific Ocean. *The ISME Journal* 7. Nature Publishing Group: 2192–2205. doi:10.1038/ismej.2013.96.
- Berg C., Listmann L., Vandieken V., Vogts A. and Jürgens K. 2015. Chemoautotrophic Growth of Ammonia-Oxidizing Thaumarchaeota Enriched from a Pelagic Redox Gradient in the Baltic Sea. *Frontiers in Microbiology* 5: 1–10. doi:10.3389/fmicb.2014.00786.
- Berg I.A. 2011. Ecological Aspects of the Distribution of Different Autotrophic CO₂ Fixation Pathways. *Applied and Environmental Microbiology* 77 (6): 1925–36. doi:10.1128/AEM.02473-10.
- Berger S.A., Krompass D. and Stamatakis A. 2011. Performance, Accuracy, and Web Server for Evolutionary Placement of Short Sequence Reads under Maximum Likelihood. *Systematic Biology* 60 (3): 291–302. doi:10.1093/sysbio/syr010.
- Bock E. and Wagner M. 2006. Oxidation of Inorganic Nitrogen Compounds as an Energy Source. In *The Prokaryotes: Prokaryotic Physiology and Biochemistry*, edited by Eugene Rosenberg, Edward F Delong, Stephen Lory, Erko Stackebrandt, and Fabiano Thompson, 4th ed., 83–118. doi:10.1007/978-3-642-30141-4.
- Braman R.S. and Hendrix S.A. 1989. Nanogram Nitrite and Nitrate Determination in Environmental and Biological Materials by Vanadium(III) Reduction with Chemiluminescence Detection. *Analytical Chemistry* 61: 2715–18. doi:10.1021/ac00199a007.
- Bristow L.A., Dalsgaard T., Tiano L., Mills D.B., Bertagnolli A.D., Wright J.J., Hallam S.J., Ulloa O., Canfield D.E., Revsbech N.P. and Thamdrup B. 2016. Ammonium and Nitrite Oxidation at Nanomolar Oxygen Concentrations in Oxygen Minimum Zone Waters. *Proceedings of the National Academy of Sciences* 113 (38): 10601–6. doi:10.1073/pnas.1600359113.
- Bristow L.A., Sarode N., Cartee J., Caro-Quintero A., Thamdrup B. and Stewart F.J. 2015. Biogeochemical and Metagenomic Analysis of Nitrite Accumulation in the Gulf of Mexico Hypoxic Zone. *Limnology and Oceanography* 60 (5): 1733–50. doi:10.1002/lno.10130.
- Caporaso J.G., Lauber C.L., Walters W.A., Berg-Lyons D., Lozupone C.A., Turnbaugh P.J., Fierer N. and Knight R. 2011. Global Patterns of 16S rRNA Diversity at a Depth of Millions of Sequences per Sample. *Proceedings of the National Academy of Sciences of the United States of America* 108 (suppl. 1): 4516–22. doi:10.1073/pnas.1000080107.
- Carini P., Dupont C.L. and Santoro A.E. 2018. Patterns of Thaumarchaeal Gene Expression in Culture and Diverse Marine Environments. *Environmental Microbiology* 20 (6): 2112–24. doi:10.1111/1462-2920.14107.
- Daims H., Nielsen J., Nielsen P.H., Schleifer K.-H. and Wagner M. 2001. In Situ Characterization of Nitrospira-Like Nitrite-Oxidizing Bacteria Active in Wastewater Treatment Plants. *Applied and Environmental Microbiology* 67 (11): 5273–84. doi:10.1128/AEM.67.11.5273.
- Damashek J., Tolar B.B., Liu Q., Okotie-Oyekan A.O., Wallsgrove N.J., Popp B.N. and Hollibaugh J.T. 2019. Microbial Oxidation of Nitrogen Supplied as Selected Organic Nitrogen Compounds in the South Atlantic Bight. *Limnology and Oceanography* 64 (3): 982–95. doi:10.1002/lno.11089.
- De Brabandere L., L. B.T., Revsbech N.P. and Foadi R. 2012. A Critical Assessment of the Occurrence and Extend of Oxygen Contamination during Anaerobic Incubations Utilizing Commercially Available Vials. *Journal of Microbiological Methods* 88 (1): 147–154. doi:doi:10.1016/j.mimet.2011.11.001.
- Doxey A.C., Kurtz D. a, Lynch M.D., Sauder L. a and Neufeld J.D. 2015. Aquatic Metagenomes Implicate Thaumarchaeota in Global Cobalamin Production. *The ISME Journal* 9: 461–71. doi:10.1038/ismej.2014.142.
- Francis C.A., Roberts K.J., Beman J.M., Santoro A.E. and Oakley B.B. 2005. Ubiquity and Diversity of Ammonia-Oxidizing Archaea in Water Columns and Sediments of the Ocean. *Proceedings of the National Academy of Sciences of the United States of America* 102 (41): 14683–88. doi:10.1073/pnas.0506625102.

- Füssel J., Lam P., Lavik G., Jensen M.M., Holtappels M., Günter M. and Kuypers M.M.M. 2012. Nitrite Oxidation in the Namibian Oxygen Minimum Zone. *The ISME Journal* 6: 1200–1209. doi:10.1038/ismej.2011.178.
- Füssel J., Lückner S., Yilmaz P., Nowka B., van Kessel M.A.H.J., Bourceau P., Hach P.F., Littmann S., Berg J., Spieck E., Daims H., Kuypers M.M.M. and Lam P. 2017. Adaptability as the Key to Success for the Ubiquitous Marine Nitrite Oxidizer Nitrococcus. *Science Advances* 3: 1–9. doi:10.1126/sciadv.1700807.
- Grasshoff K., Kremling K. and Ehrhardt M. 1999. *Methods of Seawater Analysis*. Edited by K Grasshoff, K Kremling, and M Ehrhardt. 3rd editio. Wiley-VCH. doi:10.1016/0304-4203(78)90045-2.
- Haaijer S.C.M., Ji K., van Niftrik L., Hoischen A., Speth D., Jetten M.S.M., Sinninghe Damsté J.S.S. and Op den Camp H.J.M. 2013. A Novel Marine Nitrite-Oxidizing Nitrospira Species from Dutch Coastal North Sea Water. *Frontiers in Microbiology* 4: 1–12. doi:10.3389/fmicb.2013.00060.
- Herndl G.J., Reinthaler T., Teira E., Aken H. Van, Veth C., Pernthaler A. and Pernthaler J. 2005. Contribution of Archaea to Total Prokaryotic Production in the Deep Atlantic Ocean. *Applied and Environmental Microbiology* 71 (5): 2303–9. doi:10.1128/AEM.71.5.2303.
- Holmes R.M., Aminot A., Kérouel R., Hooker B.A. and Peterson B.J. 1999. A Simple and Precise Method for Measuring Ammonium in Marine and Freshwater Ecosystems. *Canadian Journal of Fisheries and Aquatic Sciences* 56: 1801–8.
- Juretschko S. 2000. Mikrobielle Populationsstruktur Und --dynamik in Einer Nitrifizierenden/Denitrifizierenden Belebtschlammanlage. Technische Universität München.
- Kang D.D., Froula J., Egan R. and Wang Z. 2015. MetaBAT, an Efficient Tool for Accurately Reconstructing Single Genomes from Complex Microbial Communities. *PeerJ* 3: e1165. doi:10.7717/peerj.1165.
- Karner M.B., Delong E.F. and Karl D.M. 2001. Archaeal Dominance in the Mesopelagic Zone of the Pacific Ocean. *Nature* 409: 507–10. doi:10.1038/35054051.
- Khachikyan A., Milucka J., Littmann S., Ahmerkamp S., Meador T., Könneke M., Burg T. and Kuypers M.M.M. n.d. Direct Cell Mass Measurements Expand the Role of Small Microorganisms in Nature, 1–28.
- Kitzinger K., Padilla C.C., Marchant H.K., Hach P.F., Herbold C.W., Kidane A.T., Könneke M., Littmann S., Mooshammer M., Niggemann J., Petrov S., Richter A., Stewart F.J., Wagner M., Kuypers M.M.M. and Bristow L.A. 2019. Cyanate and Urea Are Substrates for Nitrification by Thaumarchaeota in the Marine Environment. *Nature Microbiology* 4 (2): 234–43. doi:10.1038/s41564-018-0316-2.
- Könneke M., Bernhard A.E., de la Torre J.R., Walker C.B., Waterbury J.B. and Stahl D.A. 2005. Isolation of an Autotrophic Ammonia-Oxidizing Marine Archaeon. *Nature* 437: 543–46. doi:10.1038/nature03911.
- Könneke M., Schubert D.M., Brown P.C., Hügler M., Standfest S., Schwander T., Schada von Borzyskowski L., Erb T.J., Stahl D.A. and Berg I.A. 2014. Ammonia-Oxidizing Archaea Use the Most Energy-Efficient Aerobic Pathway for CO₂ Fixation. *Proceedings of the National Academy of Sciences of the United States of America* 111 (22): 8239–44. doi:10.1073/pnas.1402028111.
- Kopylova E., Noé L. and Touzet H. 2012. SortMeRNA: Fast and Accurate Filtering of Ribosomal RNAs in Metatranscriptomic Data. *Bioinformatics* 28 (24): 3211–17. doi:10.1093/bioinformatics/bts611.
- Krupke A., Mohr W., LaRoche J., Fuchs B.M., Amann R.I. and Kuypers M.M.M. 2015. The Effect of Nutrients on Carbon and Nitrogen Fixation by the UCYN-A – Haptophyte Symbiosis. *The ISME Journal* 9: 1635–47. doi:10.1038/ismej.2014.253.
- Kuypers M.M.M., Marchant H.K. and Kartal B. 2018. The Microbial Nitrogen-Cycling Network. *Nature Reviews Microbiology* 16 (5): 263–76. doi:10.1038/nrmicro.2018.9.
- Letunic I. and Bork P. 2016. Interactive Tree of Life (iTOL) v3: An Online Tool for the Display and Annotation of Phylogenetic and Other Trees. *Nucleic Acids Research* 44 (W1): W242–45. doi:10.1093/nar/gkw290.
- Liu Q., Tolar B.B., Ross M.J., Cheek J.B., Sweeney C.M., Wallsgrove N.J., Popp B.N. and Hollibaugh J.T. 2018. Light and Temperature Control the Seasonal Distribution of Thaumarchaeota in the South Atlantic Bight. *The ISME Journal* 12: 1473–85. doi:10.1038/s41396-018-0066-4.
- Lückner S., Nowka B., Rattei T., Spieck E. and Daims H. 2013. The Genome of Nitrospina Gracilis Illuminates the Metabolism and Evolution of the Major Marine Nitrite Oxidizer. *Frontiers in Microbiology* 4 (27): 1–19. doi:10.3389/fmicb.2013.00027.
- Lüke C., Speth D.R., Kox M.A.R., Villanueva L. and Jetten M.S.M. 2016. Metagenomic Analysis of Nitrogen and Methane Cycling in the Arabian Sea Oxygen Minimum Zone. *PeerJ* 4: e1924. doi:10.7717/peerj.1924.
- Maixner F., Wagner M., Lückner S., Pelletier E., Schmitz-Esser S., Hache K., Spieck E., Konrat R., Le Paslier D. and Daims H. 2008. Environmental Genomics Reveals a Functional Chlorite Dismutase in the Nitrite-Oxidizing

- Bacterium “Candidatus Nitrospira Defluvii.” *Environmental Microbiology* 10 (11): 3043–56. doi:10.1111/j.1462-2920.2008.01646.x.
- Martínez-Pérez C., Mohr W., Löscher C.R., Dekaezemacker J., Littmann S., Yilmaz P., Lehnen N., Fuchs B.M., Lavik G., Schmitz R.A., LaRoche J. and Kuypers M.M.M. 2016. The Small Unicellular Diazotrophic Symbiont, UCYN-A, Is a Key Player in the Marine Nitrogen Cycle. *Nature Microbiology* 1 (11): 1–7. doi:10.1038/nmicrobiol.2016.163.
- McIlvin M.R. and Altabet M.A. 2005. Chemical Conversion of Nitrate and Nitrite to Nitrous Oxide for Nitrogen and Oxygen Isotopic Analysis in Freshwater and Seawater. *Analytical Chemistry* 77: 5589–95. doi:10.1021/ac050528s.
- Mincer T.J., Church M.J., Taylor L.T., Preston C., Karl D.M. and DeLong E.F. 2007. Quantitative Distribution of Presumptive Archaeal and Bacterial Nitrifiers in Monterey Bay and the North Pacific Subtropical Gyre. *Environmental Microbiology* 9 (5): 1162–75. doi:10.1111/j.1462-2920.2007.01239.x.
- Mulvenna P.F. and Savidge G. 1992. A Modified Manual Method for the Determination of Urea in Seawater Using Diacetylmonoxime Reagent. *Estuarine, Coastal and Shelf Science* 34: 429–38. doi:10.1016/S0272-7714(05)80115-5.
- Musat N., Foster R., Vagner T., Adam B. and Kuypers M.M.M. 2012. Detecting Metabolic Activities in Single Cells, with Emphasis on NanoSIMS. *FEMS Microbiology Reviews* 36: 486–511. doi:10.1111/j.1574-6976.2011.00303.x.
- Ngugi D.K., Blom J., Stepanauskas R. and Stingl U. 2016. Diversification and Niche Adaptations of Nitrospina-like Bacteria in the Polyextreme Interfaces of Red Sea Brines. *The ISME Journal* 10: 1383–99. doi:10.1038/ismej.2015.214.
- Nguyen L.T., Schmidt H.A., Von Haeseler A. and Minh B.Q. 2015. IQ-TREE: A Fast and Effective Stochastic Algorithm for Estimating Maximum-Likelihood Phylogenies. *Molecular Biology and Evolution* 32 (1): 268–74. doi:10.1093/molbev/msu300.
- Nurk S., Meleshko D., Korobeynikov A. and Pevzner P.A. 2017. MetaSPAdes: A New Versatile Metagenomic Assembler. *Genome Research* 27: 824–34. doi:10.1101/gr.213959.116.
- Pachiadaki M.G., Sintés E., Bergauer K., Brown J.M., Record N.R., Swan B.K., Mathyer M.E., Hallam S.J., Lopez-Garcia P., Takaki Y., Nunoura T., Woyke T., Herndl G.J. and Stepanauskas R. 2017. Major Role of Nitrite-Oxidizing Bacteria in Dark Ocean Carbon Fixation. *Science* 358: 1046–51. doi:10.1126/science.aan8260.
- Padilla C.C., Bristow L.A., Sarode N., Garcia-Robledo E., Gómez Ramírez E., Benson C.R., Bourbonnais A., Altabet M.A., Girguis P.R., Thamdrup B. and Stewart F.J. 2016. NC10 Bacteria in Marine Oxygen Minimum Zones. *The ISME Journal* 10: 2067–71. doi:10.1038/ismej.2015.262.
- Padilla C.C., Ganesh S., Gantt S., Huhman A., Parris D.J., Sarode N. and Stewart F.J. 2015. Standard Filtration Practices May Significantly Distort Planktonic Microbial Diversity Estimates. *Frontiers in Microbiology* 6 (547): 1–10. doi:10.3389/fmicb.2015.00547.
- Palatinszky M., Herbold C., Jehmlich N., Pogoda M., Han P., Bergen M. Von, Lagkouvardos I., Karst S.M., Galushko A., Koch H., Berry D., Daims H. and Wagner M. 2015. Cyanate as an Energy Source for Nitrifiers. *Nature* 524: 105–8. doi:10.1038/nature14856.
- Pernthaler A., Pernthaler J. and Amann R. 2004. Sensitive Multi-Color Fluorescence in Situ Hybridization for the Identification of Environmental Microorganisms. In *Molecular Microbial Ecology Manual*, edited by G. Kowalchuk, F. J. de Bruijn, Ian M. Head, A. D. L. Akkermans, and J. D. van Elsas, 2nd ed., 711–26. Dordrecht, Boston, London: Kluwer Academic Publishers. doi:10.1007/978-1-4020-2177-0_311.
- Polerecky L., Adam B., Milucka J., Musat N., Vagner T. and Kuypers M.M.M. 2012. Look@NanoSIMS - a Tool for the Analysis of NanoSIMS Data in Environmental Microbiology. *Environmental Microbiology* 14 (4): 1009–23. doi:10.1111/j.1462-2920.2011.02681.x.
- Rabalais N.N., Turner R.E. and Wiseman W.J. 2001. Hypoxia in the Gulf of Mexico. *Journal of Environment Quality* 30: 320–29. doi:10.2134/jeq2001.302320x.
- Reji L., Tolar B.B., Smith J.M., Chavez F.P. and Francis C.A. 2019. Differential Co-Occurrence Relationships Shaping Ecotype Diversification within Thaumarchaeota Populations in the Coastal Ocean Water Column. *The ISME Journal* 13 (5): 1144–58. doi:10.1038/s41396-018-0311-x.
- Santoro A.E., Casciotti K.L. and Francis C.A. 2010. Activity, Abundance and Diversity of Nitrifying Archaea and Bacteria in the Central California Current. *Environmental Microbiology* 12 (7): 1989–2006. doi:10.1111/j.1462-2920.2010.02205.x.

- Sorokin D.Y., Lückner S., Vejmekova D., Kostrikina N. a, Kleerebezem R., Rijpstra W.I.C., Damsté J.S.S., Le Paslier D., Muyzer G., Wagner M., van Loosdrecht M.C.M. and Daims H. 2012. Nitrification Expanded: Discovery, Physiology and Genomics of a Nitrite-Oxidizing Bacterium from the Phylum Chloroflexi. *The ISME Journal* 6: 2245–56. doi:10.1038/ismej.2012.70.
- Spang A., Poehlein A., Offre P., Zumbrägel S., Haider S., Rychlik N., Nowka B., Schmeisser C., Lebedeva E. V., Rattei T., Böhm C., Schmid M., Galushko A., Hatzenpichler R., Weinmaier T., Daniel R., Schleper C., Spieck E., Streit W., et al. 2012. The Genome of the Ammonia-Oxidizing Candidatus Nitrososphaera Gargensis: Insights into Metabolic Versatility and Environmental Adaptations. *Environmental Microbiology* 14 (12): 3122–45. doi:10.1111/j.1462-2920.2012.02893.x.
- Spieck E., Keuter S., Wenzel T., Bock E. and Ludwig W. 2014. Characterization of a New Marine Nitrite Oxidizing Bacterium, Nitrospina Watsonii Sp. Nov., a Member of the Newly Proposed Phylum “Nitrospinae.” *Systematic and Applied Microbiology* 37: 170–76. doi:10.1016/j.syapm.2013.12.005.
- Stieglmeier M., Mooshammer M., Kitzler B., Wanek W., Zechmeister-Boltenstern S., Richter A. and Schleper C. 2014. Aerobic Nitrous Oxide Production through N-Nitrosating Hybrid Formation in Ammonia-Oxidizing Archaea. *The ISME Journal* 8: 1135–46. doi:10.1038/ismej.2013.220.
- Sun J. and Liu D. 2003. Geometric Models for Calculating Cell Biovolume and Surface Area for Phytoplankton. *Journal of Plankton Research* 25 (11): 1331–46. doi:10.1093/plankt/fbg096.
- Sun X., Ji Q., Jayakumar A. and Ward B.B. 2017. Dependence of Nitrite Oxidation on Nitrite and Oxygen in Low-Oxygen Seawater. *Geophysical Research Letters* 44 (15): 7883–91. doi:10.1002/2017GL074355.
- Svedén J.B., Adam B., Walve J., Nahar N., Musat N., Lavik G., Whitehouse M.J., Kuypers M.M.M. and Ploug H. 2015. High Cell-Specific Rates of Nitrogen and Carbon Fixation by the Cyanobacterium Aphanizomenon Sp. at Low Temperatures in the Baltic Sea. *FEMS Microbiology Ecology* 91 (12): 1–10. doi:10.1093/femsec/fiv131.
- Tolar B.B., King G.M. and Hollibaugh J.T. 2013. An Analysis of Thaumarchaeota Populations from the Northern Gulf of Mexico. *Frontiers in Microbiology* 4 (72): 1–36. doi:10.3389/fmicb.2013.00072.
- Torres M.E., Mix A.C. and Rugh W.D. 2005. Precise $\Delta^{13}\text{C}$ Analysis of Dissolved Inorganic Carbon in Natural Waters Using Automated Headspace Sampling and Continuous-Flow Mass Spectrometry. *Limnology and Oceanography: Methods* 3: 349–60. doi:10.4319/lom.2005.3.349.
- Wagner M., Rath G., Koops H.P., Flood J. and Amann R. 1996. In Situ Analysis of Nitrifying Bacteria in Sewage Treatment Plants. *Water Science and Technology* 34: 237–44.
- Ward B.B. 1987. Nitrogen Transformations in the Southern California Bight. *Deep Sea Research* 34 (5/6): 785–805. doi:10.1016/0198-0149(87)90037-9.
- Ward B.B. 2008. Nitrification in Marine Systems. In *Nitrogen in the Marine Environment*, edited by Douglas G Capone, Deborah A Bronk, Margaret R Mulholland, and Edward J Carpenter, 2nd ed., 199–261. Elsevier Inc. doi:10.1016/B978-0-12-372522-6.00005-0.
- Watson S.W. and Waterbury J.B. 1971. Characteristics of Two Marine Nitrite Oxidizing Bacteria, Nitrospina Gracilis Nov. Gen. Nov. Sp. and Nitrococcus Mobilis Nov. Gen. Nov. Sp. *Archives of Microbiology* 77: 203–30.
- Widner B., Mulholland M.R. and Mopper K. 2013. Chromatographic Determination of Nanomolar Cyanate Concentrations in Estuarine and Sea Waters by Precolumn Fluorescence Derivatization. *Analytical Chemistry* 85: 6661–66. doi:10.1021/ac400351c.
- Woebken D., Burow L.C., Behnam F., Mayali X., Schintlmeister A., Fleming E.D., Prufert-Bebout L., Singer S.W., Cortés A.L., Hoehler T.M., Pett-Ridge J., Spormann A.M., Wagner M., Weber P.K. and Bebout B.M. 2015. Revisiting N₂ Fixation in Guerrero Negro Intertidal Microbial Mats with a Functional Single-Cell Approach. *The ISME Journal* 9: 485–96. doi:10.1038/ismej.2014.144.
- Wuchter C., Abbas B., Coolen M.J.L., Herfort L., van Bleijswijk J., Timmers P., Strous M., Teira E., Herndl G.J., Middelburg J.J., Schouten S. and Sinninghe Damsté J.S. 2006. Archaeal Nitrification in the Ocean. *Proceedings of the National Academy of Sciences of the United States of America* 103 (33): 12317–22. doi:10.1073/pnas.0600756103.

Supplementary information

Supplementary text

Nitrospinae probe design and CARD-FISH conditions

As the previously available probes for Nitrospinae (Juretschko 2000; Pachiadaki et al. 2017) did not target all Nitrospinae OTUs identified in the present study, a new catalyzed reporter deposition (CARD-) FISH probe targeting the Nitrospinae was developed. Nitrospinae 16S rRNA gene amplicon sequences obtained in this study were aligned to the SILVA SSU Ref NR 99 128 alignment (Yilmaz et al. 2014) in Arb version 6.1. using the SINA aligner (Ludwig et al. 2004). To ensure optimal coverage of all Nitrospinae OTUs found in the present study, only sequence positions amplified by the used primer pair (Caporaso et al. 2011) were considered for probe design. A probe (Ntspn759, 5' CCCTGGCTTTCGTATCT 3') was designed using the probe design tool implemented in ARB, further manually refined and evaluated *in silico* using MathFISH (Yilmaz et al. 2011). Competitor probes to non-target organisms with single mismatches were designed manually (Ntspn759_comp1, 5' CCCTGGCTTTCGTACCT 3' and Ntspn759_comp2, 5' CCCTGGCTTTCGCATCT 3') and included in all CARD-FISH experiments. The newly designed probe Ntspn759 targets 93% (280 of 301) Nitrospinae sequences included in SILVA SSU Ref NR 99 128, for comparison, probe Ntspn693 (Juretschko 2000) and Ntspn-Mod (Pachiadaki et al. 2017) target only 12.5% and 79%, respectively (Supplementary Table 8).

Optimal formamide concentration (Manz et al. 1992) of probe Ntspn759 was evaluated for CARD-FISH on a *Nitrospina gracilis* pure culture (Watson & Waterbury 1971) and confirmed on samples from the GoM. Optimal formamide concentration was 15% formamide at 46°C hybridization temperature (Supplementary Figure 9).

Nitrospinae abundances were determined by CARD FISH following Pernthaler et al. (Pernthaler et al. 2004). Briefly, cells were immobilized on the filters by embedding in 0.2% low gelling agarose and endogenous peroxidases were inactivated by incubation in 0.01 M HCl for 10 min. Cells were permeabilized by lysozyme digestion (10 mg ml⁻¹ in 50 mM EDTA and 100 mM Tris-HCl at 37°C for 1 h) and HCl permeabilization (0.1 M HCl for 1 min). Filters were hybridized with horseradish peroxidase labeled oligonucleotide probes at 46°C for up to 3.5 h. Signal amplification was done with OregonGreen labeled tyramides at 48°C for 15 to 30 min. Before enumeration on an epifluorescence microscope (Axioplan 2, Zeiss), cells were counterstained with DAPI. For each CARD-FISH experiment, negative controls with the probe NonEUB (Wallner et al. 1993) were done to exclude non-specific binding of oligonucleotides or insufficient inactivation of endogenous peroxidases.

Analysis of ¹⁵N/(¹⁴N + ¹⁵N) ratio variability in nanoSIMS measurements

We assessed whether sufficient Nitrospinae cells have been measured by nanoSIMS following Sveden et al (2015). Briefly, we calculated the mean and standard error for randomly subsampled Nitrospinae ROIs, where the error of randomly subsampled ROIs of one population should be < 10% to indicate that sufficient cells have been analyzed. Our analysis showed that the standard error for Nitrospinae ¹⁵N/(¹⁴N+¹⁵N) values was <10% after measurement of 3, 2 and 3 cells in the ¹⁵N-ammonium, ¹⁵N-urea and ¹⁵N-nitrite treatments, while for the ¹⁵N-cyanate treatment, one Nitrospinae cell with higher activity caused the error to remain 19% after analysis of all 19 Nitrospinae cells (Supplementary Figure 2). For non-Nitrospinae cells, the standard error of ¹⁵N/(¹⁴N+¹⁵N) values was <10% after measurement of 74, 60, and 185 cells in the ¹⁵N-ammonium,

¹⁵N-cyanate and ¹⁵N-nitrite treatments (Supplementary Figure 2) For ¹⁵N-urea, the standard error did not drop below 10% even after analysis of 140 non-Nitrospinae cells, likely due to the high metabolic variability, with only some able to use urea, in this group (Supplementary Figure 2).

DNA and RNA analyses

Nucleic acid sampling and extraction

1L seawater each was filtered in replicates onto 0.22 µm cartridge filters (Sterivex™, Millipore), filled with lysis buffer (50 mM Tris-HCl, 40 mM EDTA, 0.73 M sucrose) for DNA analyses or RNA stabilizing buffer (25 mM sodium citrate, 10 mM EDTA, 5.3 M ammonium sulfate, pH 5.2) for RNA analyses. Filters were stored at -20°C or flash frozen in liquid nitrogen, for DNA and RNA samples respectively. DNA was extracted using a phenol:chloroform protocol (Padilla et al. 2016). Cells were lysed by adding lysozyme (2 mg in 50 µl of lysis buffer per filter) directly to the cartridges, sealing the cartridges, and incubating for 45 min at 37°C. Proteinase K (1 mg in 100 µL lysis buffer, 100 µl 20% SDS) was added, and the cartridges were resealed and incubated for 2 hours at 55°C. The lysate was removed, and DNA was extracted once with phenol:chloroform:isoamyl alcohol (25:24:1) and once with chloroform:isoamyl alcohol (24:1) and then concentrated by spin dialysis using Ultra-4 (100 kDa, Amicon) centrifugal filters.

RNA was extracted using a modification of the *mirVana*™ miRNA Isolation kit (Ambion) (Frias-Lopez et al. 2008). Cartridges were thawed on ice, RNA stabilizing buffer was then expelled and discarded, and cells were lysed by adding Lysis buffer and miRNA Homogenate Additive (Ambion) directly to the cartridges. Following vortexing and incubation on ice (10 min), lysates were transferred to RNAase-free tubes and processed through an acid-phenol:chloroform extraction according to the kit protocol. The TURBO DNA-free™ kit (Ambion) was used to remove DNA, and the extract was purified using the RNeasy MinElute Cleanup Kit (Qiagen).

16S rRNA gene sequencing and analysis

Relative abundances of microorganisms were assessed via 16S rRNA gene amplicon sequencing. Amplicons were generated by PCR using equal amounts of DNA template (1 ng), Platinum® PCR SuperMix (Life Technologies), and primers F515 and R806 encompassing the V4 region of the 16S rRNA gene (Caporaso et al. 2011). Both forward and reverse primers were barcoded and appended with Illumina-specific adapters. Thermal cycling involved: denaturation at 94°C (3 min), followed by 30 cycles of denaturation at 94°C (45 sec), primer annealing at 55°C (45 sec) and primer extension at 72°C (90 sec), followed by extension at 72°C for 10 min. Amplicons were analyzed by gel electrophoresis to verify size (~400 bp) and purified using Diffinity RapidTip2 pipette tips (Diffinity Genomics, NY). Amplicons from different samples were pooled at equal concentrations and sequenced on an Illumina MiSeq using a 500-cycle Nano kit.

Barcoded sequences were de-multiplexed, trimmed (length cutoff 100 nt), and filtered to remove low quality reads (average Phred score < 25) using Trim Galore! (http://www.bioinformatics.babraham.ac.uk/projects/trim_galore/). Paired-end reads were merged using FLASH (Magoč & Salzberg 2011), with a minimum average length of 250 nt for each read, minimum average length of 300 nt for paired read fragments, and maximum allowable fragment standard deviation of 30 nt. The number of trimmed and merged reads per sample ranged from 11,842 – 21,970. Chimeric sequences were detected by reference-based searches using USEARCH (Edgar 2010) and removed from the sequence pools. Operational Taxonomic Units (OTUs) were defined by clustering at 97% sequence identity using open-reference picking with the UCLUST algorithm (Edgar 2010) in QIIME1 (Caporaso et al. 2010). The average number of sequences assigned

per OTU was 836 (range 646 – 1,138). Taxonomy was assigned to OTUs using the Greengenes database (DeSantis et al. 2006). Singleton sequences and sequences affiliated with mitochondria and chloroplast were removed from any further analysis. Proportional abundances of orders constituting >0.5% of the community were calculated after rarefaction based on the sample with the lowest number of reads (11,842 reads).

Metagenome sequencing and metagenome assembled genome reconstruction

Metagenomic libraries were constructed as previously described (Kitzinger et al. 2019), using NEBNext® UltraTM II FS DNA Library Prep Kit for Illumina, creating average fragment sizes of 550 bp. Samples were sequenced on one lane of an Illumina HiSeq using 2x250 bp cycle kit at Georgia Tech's High-Throughput DNA Sequencing core facility.

bbduk (BBMap - Bushnell B. - sourceforge.net/projects/bbmap/) was used to remove adapters and residual phiX sequences, and to further quality-filter (ktrim=r k=21 mink=11 hdist=2 minlen=149 qtrim=r trimq=15) the paired-end Illumina reads. Quality-filtered reads were assembled with Metaspades (-k 21,33,55,77,99,127) (Nurk et al. 2017). Each individual read set was mapped against each assembly to assist in differential-coverage genome binning using BBMap v. 36.32 (BBMap - Bushnell B. - sourceforge.net/projects/bbmap/). Large (>2 kb) scaffolds were clustered into Metagenome-Assembled Genomes (MAGs) by oligonucleotide frequency (k=4) and read coverage using Metabat2 (Kang et al. 2015). Redundant bins were dereplicated and evaluated using dRep (Olm et al. 2017) (completeness >40%, contamination <10% and genome size >200kb). Nitrospinae MAGs were identified using GTDB-Tk (<https://github.com/Ecogenomics/GtdbTk>), which is based on the Genome Taxonomy Database (<http://dx.doi.org/10.1038/nbt.4229>). MAGs were reassembled/polished by iteratively mapping reads to dereplicated metagenome bins (contigs >2kb) using BBMAP (>98% identity) and reassembling mapped reads with SPAdes v. 3.10.1 (Bankevich et al. 2012) using the previously binned contigs as “trusted-contigs”. Reassembled contigs were filtered based consistency in mapping depth, consistency in tetranucleotide composition and length (> 2kb). Mapping depth and tetranucleotide composition was evaluated through the construction of null models using 2 kb subsequences from the newly reassembled genome. A normally distributed null model for mapping depth was constructed using the mean and standard deviation of median depth for the 2 kb subsequences. P-values were calculated for reassembled contigs based on the null model of mapping depth with pnorm() and corrected for multiple testing using p.adjust(method="BH"). Contigs were rejected if the adjusted p-value < 0.05. A multidimensional null normal distribution for tetranucleotide frequency was constructed by conducting a principle components analysis (PCoA) of log(tetranucleotide counts+1) for 2 kb subsequences and full reassembled contigs. This procedure predicts weighted normalized variance (as a distance from the origin) for each tetranucleotide pattern. P-values were calculated for reassembled contigs based on the null model of tetranucleotide patterns with pnorm() and corrected for multiple testing using p.adjust(method="BH") in R with a FDR of 0.05. Contigs were rejected if the adjusted p-value < 0.05. The rebinning procedure was repeated until reassembly became self-consistent between iterations (based on genome size, completeness and contamination as evaluated with CheckM). Metagenome sequencing statistics and information on dereplicated Nitrospinae MAGs are listed in Supplementary Tables 3 and 4, respectively.

Single-gene phylogenetic reconstruction

16S rRNA gene sequences from metagenomes were identified in metagenomic assemblies using nhmmer against rfam databases for small subunit rRNAs (RFAM: RF00177, RF01959, RF01960),

requiring at least 300 nucleotides to match the model. Sequences were classified using the RDPclassifier (Wang et al. 2007) as implemented in Mothur.

Gene predictions for each metagenomic assembly were made using Prodigal (Hyatt et al. 2010), using the metagenome option (-p meta). Marker genes of urea, cyanate, and nitrite utilization, as well as RNA polymerase genes were extracted from metagenomic assemblies: urease subunit alpha (*ureC*), cyanate lyase/hydratase (*cynS*), nitrite oxidoreductase subunit alpha (*nxrA*) and the β subunit of bacterial RNA polymerase (*rpoB*), respectively. hmmsearch (Eddy 2011) was used to identify genes of interest (*ureC* (PF00449.15), *cynS* (PF02560.14), *nxrA* (PF00384.17), *rpoB* (PF PF00562, RNA_pol_Rpb2_6)), with the requirement that the protein sequence and hmm model align over at least 70% of the length of the model and that the reverse search of the identified protein sequence against the pfam database returned the target model as the best hit.

Reference databases were constructed for *ureC*, *cynS*, *nxrA* and *rpoB* by screening amino acid sequences encoded by all genomes publicly available within the International Nucleotide Sequence Database Collaboration (INSDC - 10.1093/nar/gkx1097) and genomes classified as *Nitrospina* within the Integrated Microbial Genomes & Microbiomes system v.5.0 (doi: 10.1093/nar/gky901). Screening of reference genomes used annotated amino acid sequences when available and were based on amino acid sequences predicted by Prodigal otherwise. Genes of interest were identified using hmmsearch using the same models and criteria as were used for screening the metagenomic assemblies.

Metagenomic-encoded sequences were added to the reference databases and aligned with mafft-linsi (Katoh et al. 2002) and trimmed using trimal -automated1 (Capella-Gutiérrez et al. 2009). Phylogenetic reconstruction was calculated with IQ-TREE (Nguyen et al. 2015) with automated model selection and confidence assessed with ultrafast bootstrapping (1,000 iterations). Resulting trees were used to manually define clades in which Nitrospinae sequences belonged to. Sequences for Nitrospinae-related clades were extracted, realigned and trees were calculated as above. These final trees were visualized using ITOL (Letunic & Bork 2016).

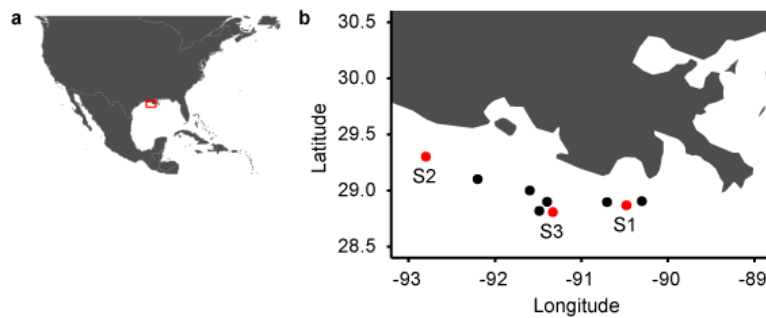
Unassembled metagenomic and metatranscriptomic reads were used to quantify *ureC*, *cynS*, *nxrA* and *rpoB* in these datasets. mRNA reads were screened by BLASTX against the dataset assembled for phylogenetic analysis (see above). Positive BLASTX matches were defined by an e-value $<10^{-6}$, bit score ≥ 50 and alignment length ≥ 30 amino acids. Reads were added to alignments used for calculating phylogeny of each gene of interest using the --add-fragments option in mafft and placed into single gene trees using the evolutionary placement algorithm (Berger et al. 2011). Reads placed into tree with pendant length >0.1 were ignored. The number of reads placed onto individual branches was inferred from integrating classification likelihoods for each branch/read combination. Fragments per kilobase per million reads (FPKM) values were calculated based on the number of inferred read pairs for which one or both reads placed into a specified location in the tree, divided by the median gene length in the reference alignment (in kb) divided by the number of total metagenomic read pairs or ribosomal-RNA free metatranscriptomic read pairs (in millions). Median gene length for calculation of FPKM values was for 1704 nt for *ureC*, 450 nt for *cynS*, 3435 nt for *nxrA* and 4205 nt for *rpoB*.

Supplementary references

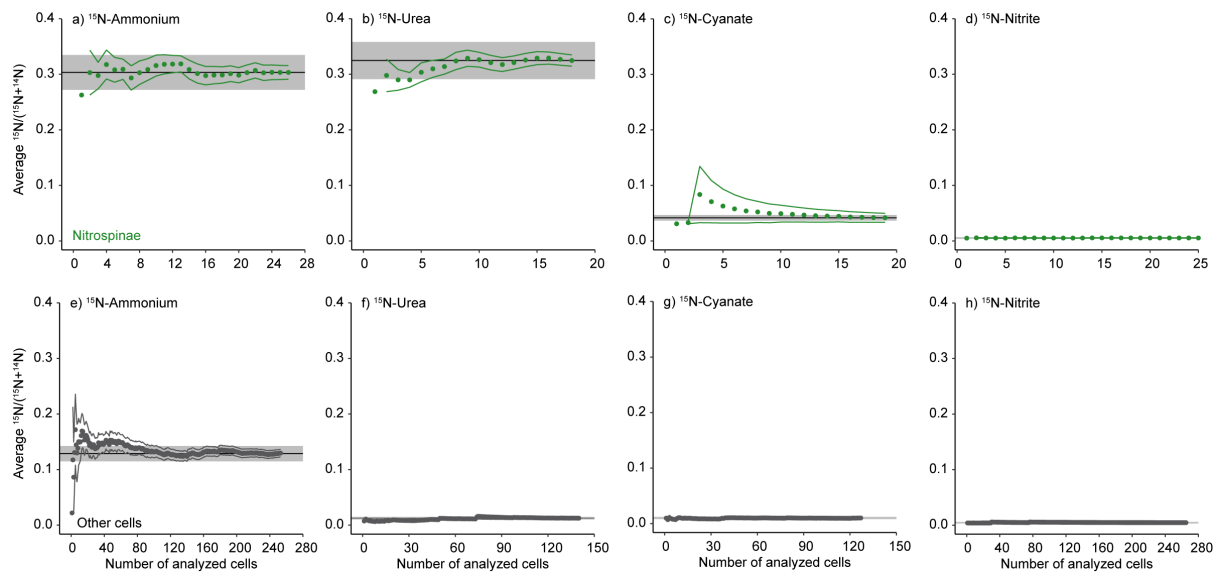
- Bankevich A., Nurk S., Antipov D., Gurevich A.A., Dvorkin M., Kulikov A.S., Lesin V.M., Nikolenko S.I., Pham S., Pribelski A.D., Pyshkin A. V, Sirotkin A. V, Vyahhi N., Tesler G., Alekseyev M.A. and Pevzner P.A. 2012. SPAdes: A New Genome Assembly Algorithm and Its Applications to Single-Cell Sequencing. *Journal of Computational Biology* 19 (5): 455–77. doi:10.1089/cmb.2012.0021.
- Berger S.A., Krompass D. and Stamatakis A. 2011. Performance, Accuracy, and Web Server for Evolutionary Placement of Short Sequence Reads under Maximum Likelihood. *Systematic Biology* 60 (3): 291–302. doi:10.1093/sysbio/syr010.
- Capella-Gutiérrez S., Silla-Martínez J.M. and Gabaldón T. 2009. TrimAl: A Tool for Automated Alignment Trimming in Large-Scale Phylogenetic Analyses. *Bioinformatics* 25 (15): 1972–73. doi:10.1093/bioinformatics/btp348.
- Caporaso J.G., Kuczynski J., Stombaugh J., Bittinger K., Bushman F.D., Costello E.K., Fierer N., Gonzales Peña A., Goodrich J.K., Gordon J.I., Huttley G.A., Kelley S.T., Knights D., Koenig J.E., Ley R.E., Lozupone C.A., McDonald D., Muegge B.D., Pirrung M., et al. 2010. QIIME Allows Analysis of High-Throughput Community Sequencing Data. *Nature Methods* 7 (5). Nature Publishing Group: 335–336. doi:10.1038/nmeth.f.303.QIIME.
- Caporaso J.G., Lauber C.L., Walters W.A., Berg-Lyons D., Lozupone C.A., Turnbaugh P.J., Fierer N. and Knight R. 2011. Global Patterns of 16S rRNA Diversity at a Depth of Millions of Sequences per Sample. *Proceedings of the National Academy of Sciences of the United States of America* 108 (suppl. 1): 4516–22. doi:10.1073/pnas.1000080107.
- DeSantis T.Z., Hugenholtz P., Larsen N., Rojas M., Brodie E.L., Keller K., Huber T., Dalevi D., Hu P. and Andersen G.L. 2006. Greengenes, a Chimera-Checked 16S rRNA Gene Database and Workbench Compatible with ARB. *Applied and Environmental Microbiology* 72 (7): 5069–72. doi:10.1128/AEM.03006-05.
- Eddy S.R. 2011. Accelerated Profile HMM Searches. *PLoS Computational Biology* 7 (10): e1002195. doi:10.1371/journal.pcbi.1002195.
- Edgar R.C. 2010. Search and Clustering Orders of Magnitude Faster than BLAST. *Bioinformatics* 26 (19): 2460–61. doi:10.1093/bioinformatics/btq461.
- Frias-Lopez J., Shi Y., Tyson G.W., Coleman M.L., Schuster S.C., Chisholm S.W. and DeLong E.F. 2008. Microbial Community Gene Expression in Ocean Surface Waters. *Proceedings of the National Academy of Sciences of the United States of America* 105 (10): 3805–10. doi:10.1073/pnas.0708897105.
- Hyatt D., Chen G.-L.L., LoCascio P.F., Land M.L., Larimer F.W. and Hauser L.J. 2010. Prodigal: Prokaryotic Gene Recognition and Translation Initiation Site Identification. *BMC Bioinformatics* 11 (119): 1–11. doi:10.1186/1471-2105-11-119.
- Juretschko S. 2000. Mikrobielle Populationsstruktur Und --dynamik in Einer Nitrifizierenden/Denitrifizierenden Belebtschlammanlage. Technische Universität München.
- Kang D.D., Froula J., Egan R. and Wang Z. 2015. MetaBAT, an Efficient Tool for Accurately Reconstructing Single Genomes from Complex Microbial Communities. *PeerJ* 3: e1165. doi:10.7717/peerj.1165.
- Katoh K., Misawa K., Kuma K. and Miyata T. 2002. MAFFT: A Novel Method for Rapid Multiple Sequence Alignment Based on Fast Fourier Transform. *Nucleic Acids Research* 30 (14): 3059–66. doi:10.1093/nar/gkf436.
- Kitzinger K., Padilla C.C., Marchant H.K., Hach P.F., Herbold C.W., Kidane A.T., Könneke M., Littmann S., Mooshammer M., Niggemann J., Petrov S., Richter A., Stewart F.J., Wagner M., Kuypers M.M.M. and Bristow L.A. 2019. Cyanate and Urea Are Substrates for Nitrification by Thaumarchaeota in the Marine Environment. *Nature Microbiology* 4 (2): 234–43. doi:10.1038/s41564-018-0316-2.
- Letunic I. and Bork P. 2016. Interactive Tree of Life (ITOL) v3: An Online Tool for the Display and Annotation of Phylogenetic and Other Trees. *Nucleic Acids Research* 44 (W1): W242–45. doi:10.1093/nar/gkw290.
- Ludwig W., Strunk O., Westram R., Richter L., Meier H., Yadhukumar A., Buchner A., Lai T., Steppi S., Jobb G., Förster W., Brettske I., Gerber S., Ginhart A.W., Gross O., Grumann S., Hermann S., Jost R., König A., et al. 2004. ARB: A Software Environment for Sequence Data. *Nucleic Acids Research* 32 (4): 1363–71. doi:10.1093/nar/gkh293.
- Magoč T. and Salzberg S.L. 2011. FLASH: Fast Length Adjustment of Short Reads to Improve Genome Assemblies. *Bioinformatics* 27 (21): 2957–63. doi:10.1093/bioinformatics/btr507.

- Manz W., Amann R., Ludwig W., Wagner M. and Schleifer K.H. 1992. Phylogenetic Oligodeoxynucleotide Probes for the Major Subclasses of Proteobacteria: Problems and Solutions. *Systematic and Applied Microbiology* 15: 593–600.
- Nguyen L.T., Schmidt H.A., Von Haeseler A. and Minh B.Q. 2015. IQ-TREE: A Fast and Effective Stochastic Algorithm for Estimating Maximum-Likelihood Phylogenies. *Molecular Biology and Evolution* 32 (1): 268–74. doi:10.1093/molbev/msu300.
- Pachiadaki M.G., Sintés E., Bergauer K., Brown J.M., Record N.R., Swan B.K., Mathyer M.E., Hallam S.J., Lopez-Garcia P., Takaki Y., Nunoura T., Woyke T., Herndl G.J. and Stepanauskas R. 2017. Major Role of Nitrite-Oxidizing Bacteria in Dark Ocean Carbon Fixation. *Science* 358: 1046–51. doi:10.1126/science.aan8260.
- Padilla C.C., Bristow L.A., Sarode N., Garcia-Robledo E., Gómez Ramírez E., Benson C.R., Bourbonnais A., Altabet M.A., Girguis P.R., Thamdrup B. and Stewart F.J. 2016. NC10 Bacteria in Marine Oxygen Minimum Zones. *The ISME Journal* 10: 2067–71. doi:10.1038/ismej.2015.262.
- Pernthaler A., Pernthaler J. and Amann R. 2004. Sensitive Multi-Color Fluorescence in Situ Hybridization for the Identification of Environmental Microorganisms. In *Molecular Microbial Ecology Manual*, edited by G. Kowalchuk, F. J. de Bruijn, Ian M. Head, A. D. L. Akkermans, and J. D. van Elsas, 2nd ed., 711–26. Dordrecht, Boston, London: Kluwer Academic Publishers. doi:10.1007/978-1-4020-2177-0_311.
- Svedén J.B., Adam B., Walve J., Nahar N., Musat N., Lavik G., Whitehouse M.J., Kuypers M.M.M. and Ploug H. 2015. High Cell-Specific Rates of Nitrogen and Carbon Fixation by the Cyanobacterium *Aphanizomenon* Sp. at Low Temperatures in the Baltic Sea. *FEMS Microbiology Ecology* 91 (12): 1–10. doi:10.1093/femsec/fiv131.
- Wallner G., Amann R. and Beisker W. 1993. Optimizing Fluorescent in Situ Hybridization with rRNA-Targeted Oligonucleotide Probes for Flow Cytometric Identification of Microorganisms. *Cytometry* 14: 136–43. doi:10.1002/cyto.990140205.
- Wang Q., Garrity G.M., Tiedje J.M. and Cole J.R. 2007. Naïve Bayesian Classifier for Rapid Assignment of rRNA Sequences into the New Bacterial Taxonomy. *Applied and Environmental Microbiology* 73 (16): 5261–67. doi:10.1128/AEM.00062-07.
- Watson S.W. and Waterbury J.B. 1971. Characteristics of Two Marine Nitrite Oxidizing Bacteria, *Nitrospina gracilis* Nov. Gen. Nov. Sp. and *Nitrococcus mobilis* Nov. Gen. Nov. Sp. *Archives of Microbiology* 77: 203–30.
- Yilmaz L.S., Parnerkar S. and Noguera D.R. 2011. MathFISH, a Web Tool That Uses Thermodynamics-Based Mathematical Models for in Silico Evaluation of Oligonucleotide Probes for Fluorescence in Situ Hybridization. *Applied and Environmental Microbiology* 77 (3): 1118–22. doi:10.1128/AEM.01733-10.
- Yilmaz P., Parfrey L.W., Yarza P., Gerken J., Pruesse E., Quast C., Schweer T., Peplies J., Ludwig W. and Glöckner F.O. 2014. The SILVA and “All-Species Living Tree Project (LTP)” Taxonomic Frameworks. *Nucleic Acids Research* 42 (Database issue): D643–48. doi:10.1093/nar/gkt1209.

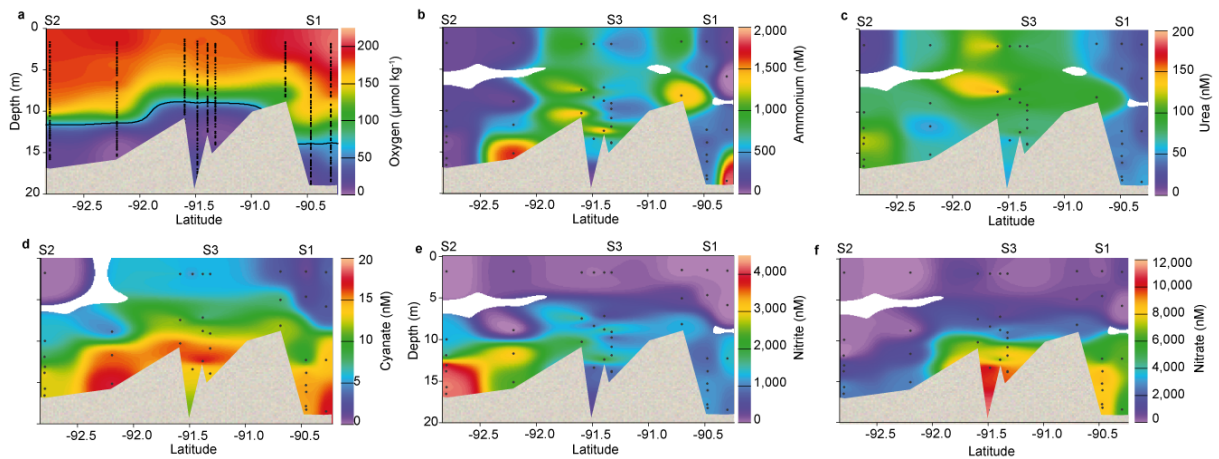
Supplementary figures



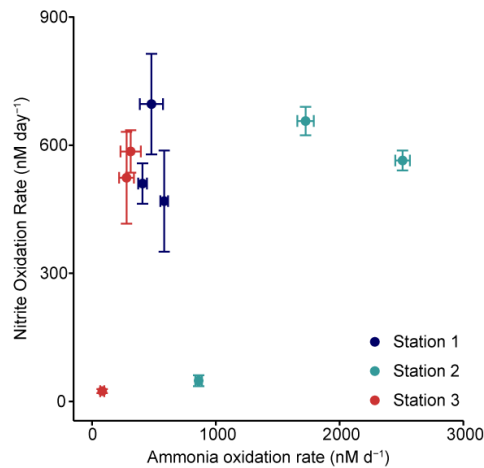
Supplementary Figure 1 Sampling transect in the GoM. a) The GoM sampling location is marked by red square. b) Station locations, experimental stations are indicated with red dots (S1 – S3), stations for nutrient and CTD profiles by black dots. Station map has been reproduced from Kitzing et al. (2019).



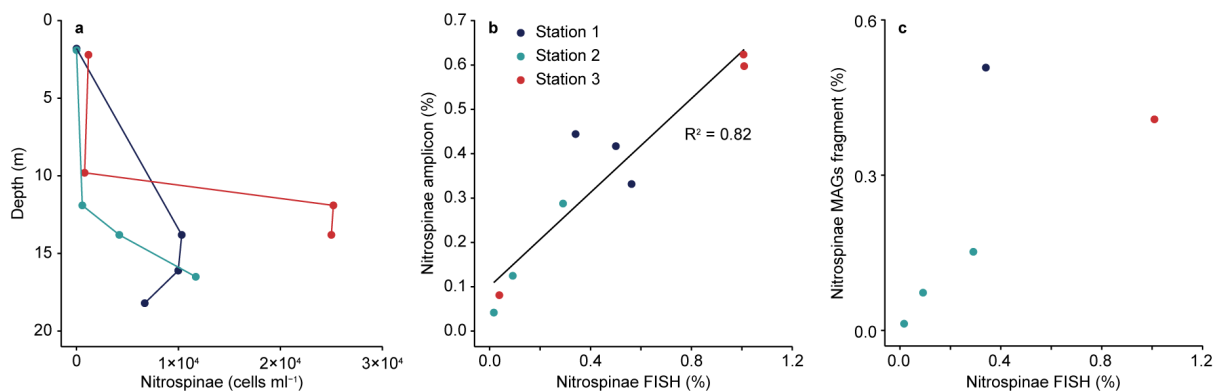
Supplementary Figure 2 Enrichment statistics of Nitrospinae cells (green) and other cells (dark grey) analyzed by nanoSIMS. Dots and solid lines represent the means and standard errors of $^{15}\text{N}/(^{15}\text{N}+^{14}\text{N})$ ratios calculated across randomly subsampled cells. The black line represents the mean across all cells, the light grey area $\pm 10\%$ of the mean. Standard errors for Nitrospinae were $< 10\%$ after analysis of 3, 2 and 3 cells in the ^{15}N -ammonium, ^{15}N -urea and ^{15}N -nitrite treatments, for the ^{15}N -cyanate treatment, one Nitrospinae cell with higher activity caused the error to remain 19% after analysis of all 19 Nitrospinae cells. For other, non-Nitrospinae cells (e-h), the standard error of $^{15}\text{N}/(^{14}\text{N}+^{15}\text{N})$ values was $< 10\%$ after measurement of 74, 60, and 185 cells in the ^{15}N -ammonium, ^{15}N -cyanate and ^{15}N -nitrite treatments. For ^{15}N -urea, the standard error did not drop $< 10\%$ after analysis of 140 non-Nitrospinae cells. The total number of analyzed cells was a) $n = 26$, b) $n=18$, c) $n=19$, d) $n=25$, e) $n=255$, f) $n=140$, g) $n=127$, h) $n=265$.



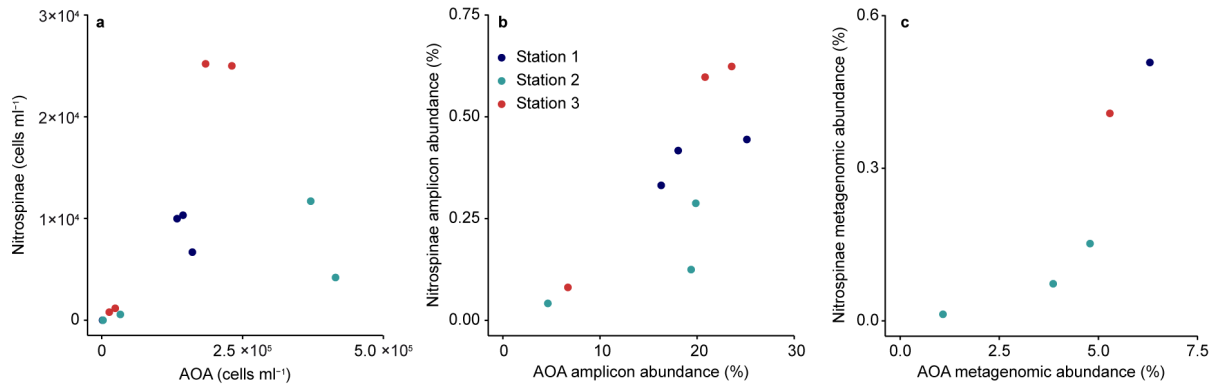
Supplementary Figure 3 Oxygen and nutrient profiles across the sampling transect (shaded area indicates the seafloor). a) Oxygen, b) ammonium, c) urea, d) cyanate, e) nitrite, f) nitrate concentrations. Black dots mark locations of measurements. S1 – S3 mark the position of experimental stations. Plots were generated using Ocean Data View (Schlitzer 2016). Concentration profiles have been reproduced from Kitzing et al. (2019).



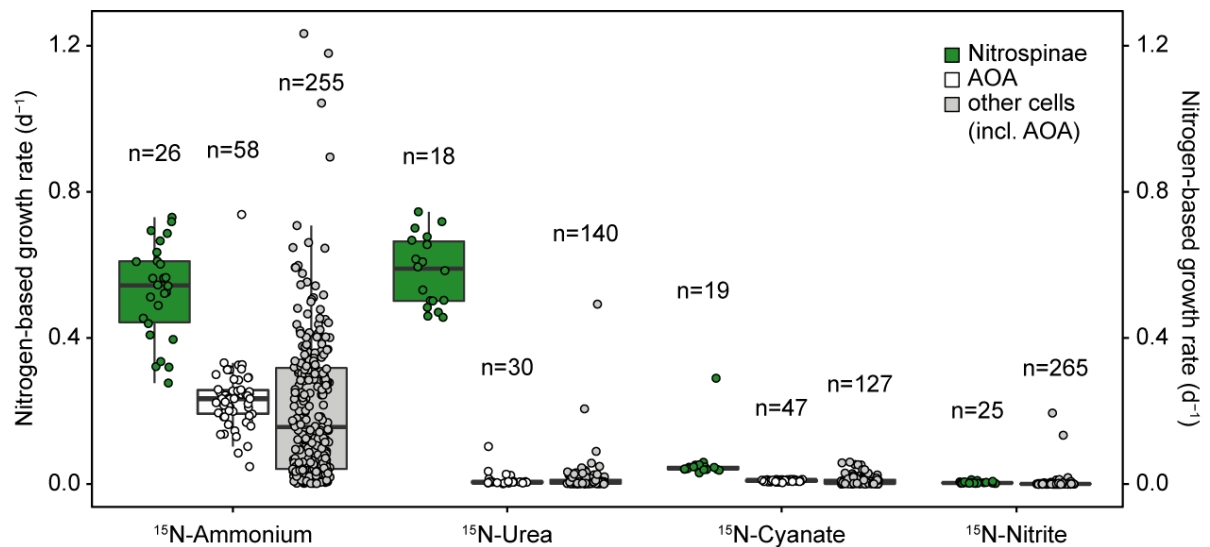
Supplementary Figure 4 Correlation between measured ammonia and nitrite oxidation rates in the GoM.



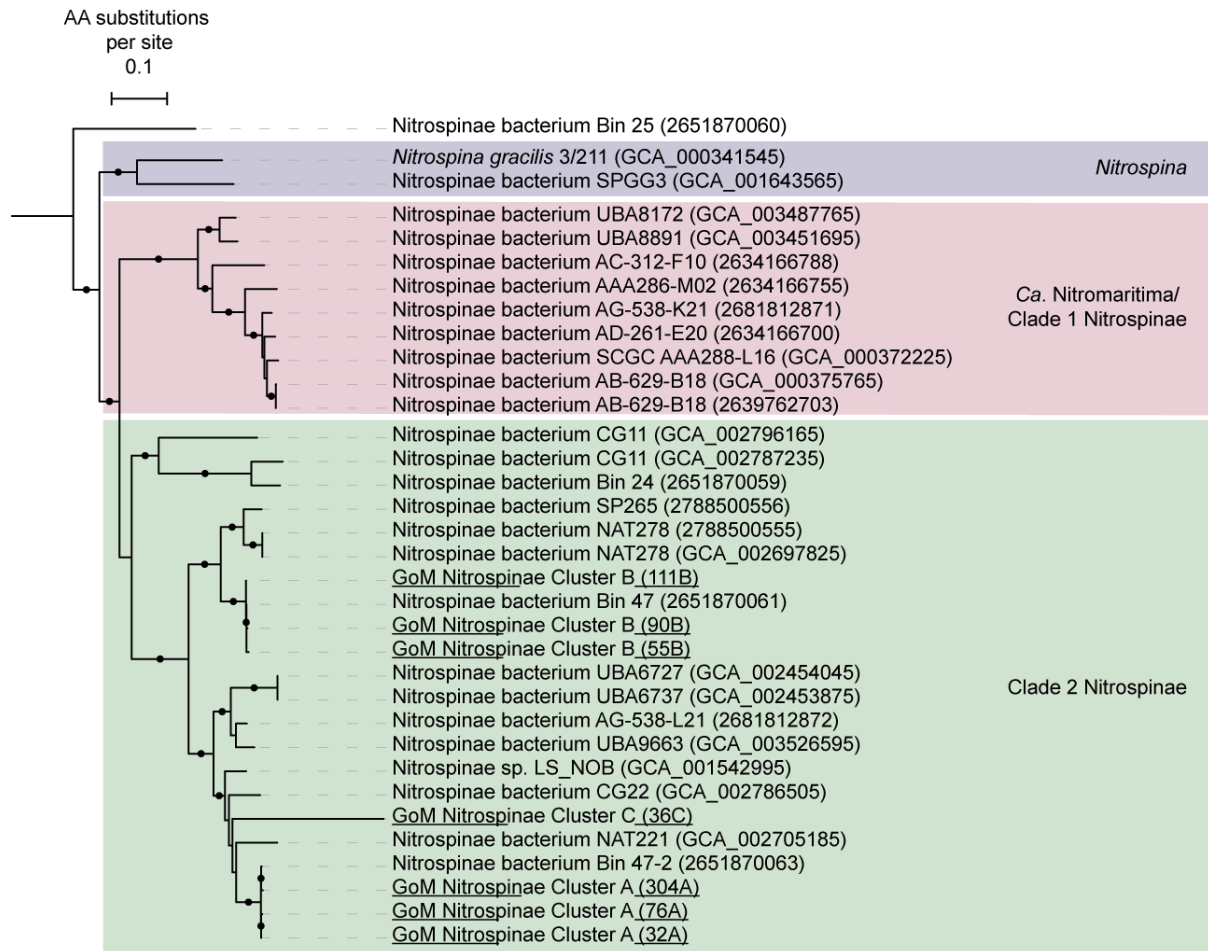
Supplementary Figure 5 Nitrospinae cell abundance based on CARD-FISH (a) and correlation to Nitrospinae relative abundance from 16S rRNA gene amplicon sequencing (b) and Nitrospinae MAG abundance in the metagenomic datasets (c). The black line represents linear regression ($p < 0.05$), R^2 was calculated based on Pearson Correlation.



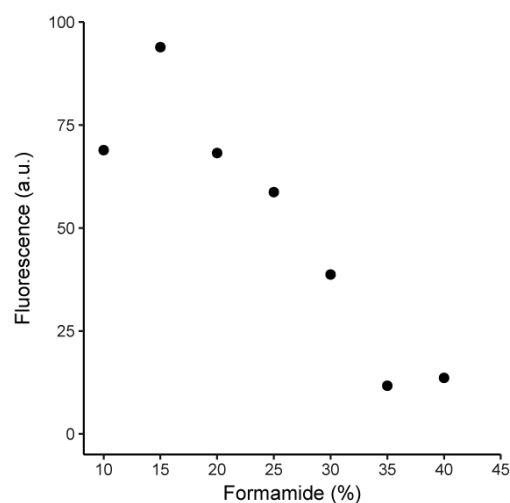
Supplementary Figure 6 Nitrospinae and AOA cell abundance based on CARD-FISH (a), relative abundance from 16S rRNA gene amplicon sequencing b) and MAGs c). Note the different scaling of axes for Nitrospinae and AOA.



Supplementary Figure 7 Nitrospinae single cell growth rates measured by nanoSIMS. Nitrospinae are depicted in green, AOA in white and other, non-targeted cells in grey. Growth rates were calculated from single cell ^{15}N -enrichment after incubation with ^{15}N -ammonium, ^{15}N -urea, ^{15}N -cyanate or ^{15}N -nitrite. AOA data was taken from (Kitzinger et al. 2019) for comparison. Note that non-targeted cells depicted here also include AOA cells, as no specific AOA probe was included in the Nitrospinae experiments. Number of cells analyzed per category is indicated above each boxplot. Boxplots depict the 25 – 75 % quantile range, with the center line depicting the median (50% quantile); whiskers encompass data points within $1.5 \times$ the interquartile range.



Supplementary Figure 8 Nitrospinae genome tree based on 34 universal concatenated marker genes. Nitrospinae GoM metagenome assembled genomes (GoM Nitrospinae) are underlined. Deltaproteobacterial genomes were used as an outgroup. Concatenated alignment was created using CheckM, tree was calculated using IQ-TREE37 with automated model selection. Confidence was assessed with ultrafast bootstrapping (1,000 iterations). Scale bar represents amino acid substitutions per site, and bootstrap values > 90 are displayed.



Supplementary Figure 9 Formamide concentration series for probe Ntspn759. CARD-FISH was performed using different formamide concentrations on a PFA-fixed pure culture of *N. gracilis*. Fluorescence of hybridized cells was recorded under identical conditions for all tested formamide concentrations. Fluorescence intensity dropped at formamide concentrations >20%. a.u., artificial units of fluorescence intensity.

Supplementary tables

Supplementary Table 1 $^{15}\text{N}^{13}\text{C}$ -tracers and ^{14}N -pools added for assimilation and process rate determinations.

Compounds added (5 μM unless otherwise stated)	Processes investigated
$^{15}\text{N-NH}_4^+$, $^{14}\text{N-NO}_2^-$, $^{14}\text{N-NO}_3^-$, $^{13}\text{C-DIC}$ *	Ammonium assimilation, and carbon fixation
$^{15}\text{N}^{13}\text{C-Urea}$, $^{14}\text{N-NO}_2^-$, $^{14}\text{N-NO}_3^-$	Urea assimilation, and carbon fixation
$^{15}\text{N}^{13}\text{C-Cyanate}$, $^{14}\text{N-NO}_2^-$, $^{14}\text{N-NO}_3^-$	Cyanate assimilation, and carbon fixation
$^{15}\text{N-NO}_2^-$, $^{14}\text{N-NO}_3^-$, $^{13}\text{C-DIC}$ *	Nitrite assimilation and oxidation, and carbon fixation
^{15}N -ammonium sulfate (98% ^{15}N , Sigma), $^{15}\text{N}^{13}\text{C}$ -urea (99% ^{13}C , 98% ^{15}N , Sigma), $^{15}\text{N}^{13}\text{C}$ -potassium cyanate (95% purity, 99% ^{13}C , 98% ^{15}N , Icon Isotopes), ^{13}C -sodium bicarbonate (98% ^{13}C , Sigma), ^{14}N -compounds were all obtained from Sigma * 200 μM final $^{13}\text{C-NaHCO}_3$ concentration	

Supplementary Table 2 CTD data, measured nutrient concentrations, oxidation rates, CARD-FISH cell abundance of Nitrospinae and AOA, and metagenomic and amplicon abundance of Nitrospinae and AOA. This table has been omitted from the printed version of this thesis due to space constraints but is provided by K. Kitzinger upon request.

Supplementary Table 3 Sequencing statistics for GoM metagenomes.

Station, Depth	Dataset	# Raw reads	# Raw fragments (read pairs)	# Raw bases	# Total QC fragments (read pairs, merged reads and unpaired reads)	# Total QC bases	# Scaffolds	Scaffold length (MB)	Scaffold N50	Scaffold L50 (KB)	Max scaffold length (KB)
Station 1, 18.0 m	C6-18m_S5	72032256	36016128	17957359367	34754578	16103062180	923189	1332	172469	1.556	408
Station 2, 12.0 m	I3-11-9m_S1	84917344	42458672	21090538252	41340486	17634270666	978822	1352	189985	1.46	377
Station 2, 14.0 m	I3-13-9m_S3	58352508	29176254	14547679676	28095278	12983602885	636633	957	113296	1.695	746
Station 2, 16.5 m	I3-16-4m_S2	1.04E+08	52054077	25988959289	50284474	23548567999	964193	1545	148342	1.921	950
Station 3, 14.0 m	CPI-14m_S4	93064228	46532114	23218119059	44629516	20762427575	931744	1407	162385	1.719	958

Supplementary Table 4 Nitrospinae metagenome assembled genome (MAG) information and relative MAG abundances. Completeness, contamination and strain heterogeneity were calculated using CheckM. Abundances per sample are given as percent metagenomic fragments mapping to the respective MAGs compared to the total number of fragments per metagenome. Note that these mappings were done non-competitively for each MAG. Therefore, average cluster abundances were used for calculating cluster abundance, as MAGs of one cluster represent different strains with very similar genome content. For calculation of the abundance of cluster A, only MAG 32A and 76A were considered, as the binned genome size of 304A is smaller, resulting in lower relative FPKM abundance.

MAG ID	MAG Cluster	Scaffold length (MB)	Completeness (%)	Contamination (%)	Strain heterogeneity (%)	Binned 16S	Binned nxrA	Binned ureC	Binned cynS	Station 1, 18.0 m (%)	Station 2, 12.0 m (%)	Station 2, 14.0 m (%)	Station 2, 16.5 m (%)	Station 3, 14.0 m (%)
GoM_MAG_304 A		1.894	79.62	2.62	0					0.258	0.003	0.016	0.036	0.165
GoM_MAG_32A A		2.546	84.62	2.3	16.67	X	X			0.352	0.003	0.021	0.043	0.229
GoM_MAG_76A A		2.621	93.37	2.56	0	X	X	X		0.364	0.003	0.021	0.044	0.243
GoM_MAG_55B B		2.639	92.49	5.13	0	X	X		X	0.134	0.008	0.046	0.101	0.155
GoM_MAG_90B B		2.653	94.82	4.27	0	X	X	X		0.134	0.008	0.047	0.103	0.154
GoM_MAG_111 B		2.529	91.4	2.71	0	X	X			0.132	0.008	0.044	0.097	0.148
GoM_MAG_36C C		1.926	48.1	2.14	0			X		0.050	0.003	0.008	0.011	0.043
Total percent of fragments mapping to Nitrospinae MAGs														
										0.530	0.016	0.090	0.193	0.443

Supplementary Table 5 Metatranscriptome sequencing statistics.

Station, Depth	Dataset	# Raw reads	# Raw fragments (read pairs)	# Raw bases	# rRNA-free fragments	# rRNA-free bases
Station 2, 12.0 m	SRR5909422	9359372	4679686	2468604609	1843080	1535588485
Station 2, 14.0 m	SRR5909421	19415124	9707562	3505604022	7241278	2599084484
Station 2, 16.5 m	SRR5909415	18976144	9488072	3265534600	6557865	2243101279

Supplementary Table 6 Overview of key genes manually annotated in GoM Nitrospinae MAGs. Green cell shading indicates presence of all gene subunits (for multi-subunit enzymes), orange presence of some subunits.

Gene	GoM_MAG_32A	GoM_MAG_76A	GoM_MAG_304 A	GoM_MAG_55B	GoM_MAG_90B	GoM_MAG_111 B	GoM_MAG_36C
Nitrite oxidoreductase (NxrABC)							
Nitrite reductase, copper containing (NirK)							
Ferredoxin nitrite reductase, assimilatory (NirA)							
Nitrite transporter (NirC)							
Nitrate/nitrite transporter (NirTP)							
Nitrate ABC transporter							
Ammonium transporter (AmtB)							
Urea ABC transporter (Urt-ABCDE)							
Urease accessory proteins (UreDEFG)							
Urease (UreABC)							
Cyanase (CynS)							
Spermidine ABC transporter							
Amino acid ABC transporter							
(Oligo-) Peptide ABC transporter							
Sugar transporter SemiSWEET							
C4-dicarboxylate ABC transporter (fumarate, malate, succinate, oxaloacetate)							
hydrogenase, Nife 3b hydrogenase							
chlorite dismutase (Cld)							

Supplementary Table 7 Gibbs free energy for ammonia oxidation and nitrite oxidation calculated for standard conditions and for conditions in the GoM, i.e. 28°C, salinity 34.8 ppt, pH 7.8, NH_4^+ 0.330 μM , NO_2^- 0.85 μM , NO_3^- 2.25 μM , O_2 10 μM . NH_3 concentration (0.01 μM) was calculated from NH_4^+ concentrations following Beman et al. (Beman et al. 2011) as $\text{NH}_3 = \text{NH}_4^+ * 10^{(\text{pH}-\text{pKa})}$ using pH 7.8 and pKa 9.3.

Process	Reaction	ΔG°	ΔG°
Ammonia Oxidation	$\text{NH}_3 + 1.5\text{O}_2 \rightarrow \text{NO}_2^- + \text{H}_2\text{O} + \text{H}^+$	-271.8	-262.4
Nitrite Oxidation	$\text{NO}_2^- + 0.5\text{O}_2 \rightarrow \text{NO}_3^-$	-82.1	-65.3

Supplementary Table 8 Phylogenetic affiliation of Nitrospinae (target population) and non-Nitrospinae (non-target population) 16S rRNA gene sequences with perfect match to newly designed probe Ntspn759, and previously published probes Ntspn693 (Juretschko 2000) and Ntspn-Mod (Pachiadaki et al. 2017) in Silva_132_SSURef_NR99_13_12_17.

Phylum	Match/total		Class / Order / Family	Match/total		Genus	Match/total												
	Ntspn759	Ntspn-Mod		Ntspn693	Ntspn-Mod		Ntspn759	Ntspn693	Ntspn75	Ntspn-Mod	Ntspn693								
Target																			
Nitrospinae	263/364	228/364	43/364	Nitrospinae/ Nitrospinales/ Nitrospinaceae	263/288	228/288	43/288	Genus <i>Nitrospina</i> LS-NOB (Clade 2)	150/171	128/171	31/171	100/103	98/103	0/103					
Non-Target																			
Spirochaetes	1/4253			Spirochaetia	1/3637														
WOR-1	1/34																		
Planctomycetes	22/9014			Planctomycetacia Phycisphaerae	15/5149														
Marinimicrobia (SAR406 clade)	1/554																		
Chloroflexi		2/9245	21/9245	Dehalococcoidia			2/1606				21/1606								
Patiscibacteria			1/4521	WS6 (Dojkabacteria)			1/162												

Chapter 5

Flow-through stable isotope probing (Flow-SIP) minimizes cross feeding in complex microbial communities

Mooshammer Maria^{1*}, Katharina Kitzinger^{1,2*}, Arno Schintlmeister^{1,4}, Soeren Ahmerkamp², Jeppe Lund Nielsen³, Per Nielsen³, Michael Wagner^{1,4}

* Equal contribution

Author affiliations

¹ University of Vienna, Centre for Microbiology and Environmental Systems Science, Division of Microbial Ecology, Austria

² Max Planck Institute for Marine Microbiology, Bremen, Germany

³ Department of Chemistry and Bioscience, Aalborg University, Denmark

⁴ Large-Instrument Facility for Advanced Isotope Research in Life Sciences, University of Vienna, Austria

Correspondence: Michael Wagner, wagner@microbial-ecology.net and Katharina Kitzinger, kkitzing@mpi-bremen.de

Author Contributions

M.W., M.M. and K.K. designed the study. M.M. and K.K. performed experiments, with support from J.L.N. and P.N., M.M. and K.K. analysed the data. A.S. ran NanoSIMS analyses. S.A. modelled nitrite concentrations around ammonia oxidizer colonies. The manuscript was written by M.M. and K.K. with contributions from all co-authors.

In preparation for submission to an international peer-reviewed journal

Abstract

Stable isotope probing (SIP) is a key tool to identify microorganisms catalyzing the turnover of specific substrates in the environment. However, SIP based studies are subject to the uncertainties posed by cross-feeding, where microorganisms, instead of incorporating the added tracer, incorporate isotopically labelled degradation products released from primary consumers. Here, we introduce a SIP approach that has the potential to eliminate cross-feeding and secondary substrate consumption in complex microbial communities. In this approach, microbial cells on a membrane filter are exposed to a continuous flow through of medium containing isotopically labelled substrates. Thereby, isotopically labelled metabolites and degradation products are constantly removed, preventing consumption of these secondary substrates. A proof-of-concept experiment using nitrifiers in activated sludge showed that Flow-SIP significantly reduces cross-feeding and thus allows to distinguish primary consumers from other members of microbial food webs.

Main text

Stable isotope probing (SIP) is a widely applied tool to link specific microbial populations to metabolic processes in the environment without the prerequisite of cultivation and has greatly advanced our understanding of the role of microorganisms in biogeochemical cycling. SIP relies on tracing the incorporation of specific isotopically labelled substrates (e.g., ^{13}C , ^{15}N , ^{18}O , ^2H) into cellular biomarkers, such as DNA, RNA or phospholipid fatty acids, or into bulk cellular biomass (e.g. Boschker et al. 1998; Radajewski et al. 2000; Orphan et al. 2001; Manefield et al. 2002). SIP is considered a robust technique to identify microbial populations that assimilate the labelled substrate in complex environmental communities. However, cross-feeding can occur when isotopically labelled metabolites are released from a primary consumer and then used by other microorganisms, which subsequently also become isotopically labelled. Thus, cross-feeding leads to erroneous identification of organisms that are not directly responsible for the process of interest, but are rather connected to primary consumers via a microbial food web (Neufeld et al. 2007).

To distinguish primary consumers from other members of microbial food webs, we developed Flow-SIP, an approach that significantly reduces the effect of cross-feeding in SIP studies. In this approach, a monolayer of microbial cells is placed on a membrane filter, and isotopically labelled substrate is supplied by a continuous flow. By means of flow-through, any released labelled metabolites and degradation products are constantly removed, preventing secondary consumption of the labelled substrate. Here, we present a proof-of-concept-experiment using the two-step process of nitrification, where ammonia is first oxidized to nitrite by ammonia oxidizing bacteria (AOB), and nitrite oxidizing bacteria (NOB) subsequently oxidize nitrite to nitrate. The carbon source for both autotrophic nitrifiers (AOB and NOB) is isotopically labelled inorganic carbon (i.e., CO_2 as $^{13}\text{C}\text{-NaHCO}_3$) and as the sole electron donor, ammonium is provided to the nitrifiers. In the flow-through approach, AOB, but not NOB, should be ^{13}C -labelled because the substrate for NOB (nitrite), produced by AOB is continuously removed (Figure 1). We included a control incubation, where the flow-through was recirculated to determine the impact of shear stress on the bacterial cells. Additionally, we included a regular batch incubation to determine the degree of cross-feeding when nitrite is not removed. Cross-feeding is expected to occur in both recirculated and batch control incubations, where the nitrite produced by AOB is not removed and thus both AOB and NOB can gain energy to fix $^{13}\text{C}\text{-CO}_2$. We used fluorescence in situ hybridization (FISH) with rRNA-targeted oligonucleotide probes for identification of AOB and NOB cells in combination with nanoscale secondary ion mass spectrometry (nanoSIMS) for visualization of isotope assimilation at the single-cell level.

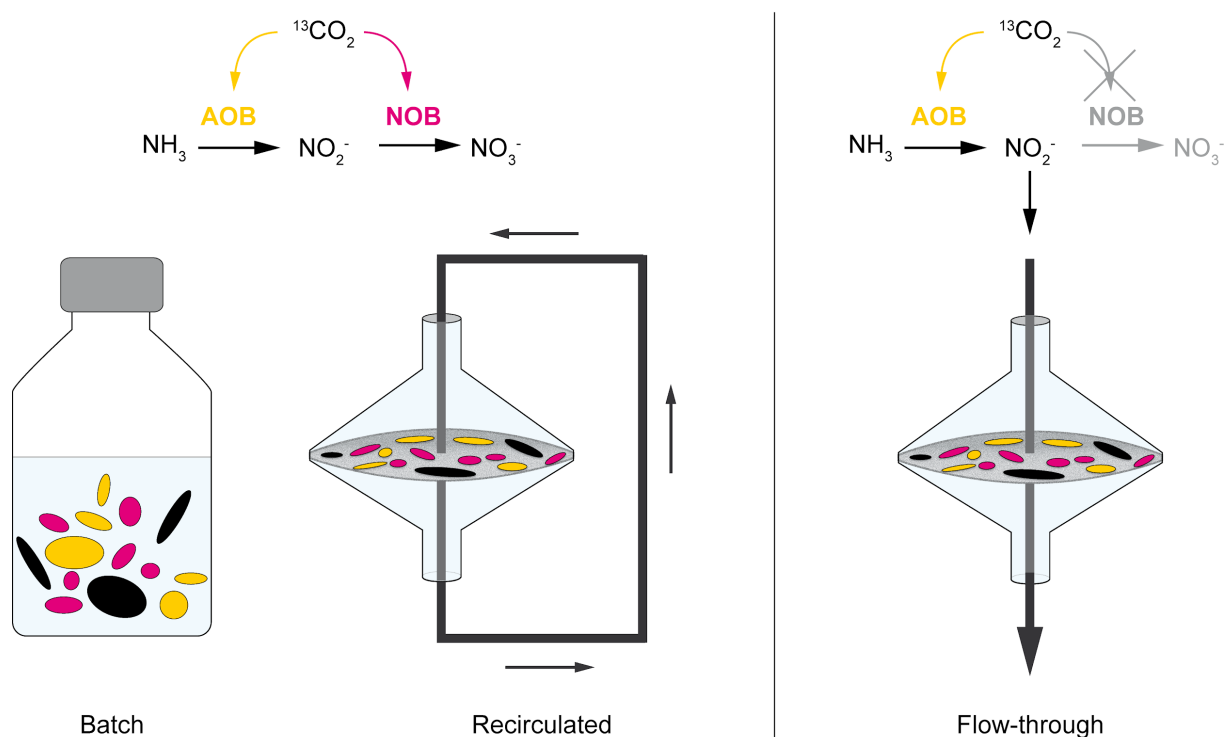


Figure 1 Schematic representation of experimental setup: (left) batch, (center) recirculated and (right) flow-through incubation. In all incubations, the carbon source for both autotrophic nitrifiers (AOB, yellow and NOB, magenta) is isotopically labelled (i.e., CO_2 as $^{13}\text{C}\text{-NaHCO}_3$) and an energy source is provided for AOB only as ammonia (as NH_4Cl). Cross-feeding is expected to occur in the batch and recirculated approaches, where NOB consume nitrite produced by AOB and thus both AOB and NOB incorporate $^{13}\text{C}\text{-CO}_2$. In the flow-through approach, only AOB are expected to be ^{13}C -labeled, as cross-feeding should be eliminated by the continuous removal of nitrite. Non-nitrifier cells are indicated in black.

Cells from activated sludge from a municipal wastewater treatment plant were placed on a membrane filter and additionally inoculated in batch cultures after disruption of flocs by sonication to avoid diffusive cross-feeding in large floc structures. After a starvation period to avoid the use of storage compounds, the membrane filters and batch cultures were incubated in basal mineral medium containing $250 \mu\text{M}$ NH_4Cl and 2 mM $^{13}\text{C}\text{-NaHCO}_3$ (98 atom%) for 24 h at in-situ temperature (14°C). In the flow-through and recirculated incubations, the medium flow was maintained at a rate of 26 mL h^{-1} . This flow rate was the highest flow rate that was tested in a preliminary experiment and it did not significantly inhibited nitrification activity compared to lower flow rates. Modelling advection and diffusion of nitrite at different flow rates showed that, for example, a 10-fold higher flow rate would only marginally reduce nitrite concentrations surrounding the AOB colonies (Figure S1). We carried out two successive experiments using sludge collected from the same plant on different days as replication of experimental results (referred to as E1 and E2). Details on the experimental setup are given in Figure S2 and the Supplementary Text.

In recirculated and batch control incubations, the consumption of ammonium and production of nitrite and nitrate (Figure S3) and single cell ^{13}C -incorporation (Figure 2) indicated that both AOB and NOB were active. In the recirculated incubations, 6 and $14 \mu\text{M}$ (E1) and 2 and $3 \mu\text{M}$ (E2) nitrite and nitrate were produced, respectively, during the 24 h-incubation (Figure S3) In contrast, nitrite and nitrate were non-detectable in flow-through incubations due to the strong dilution by the medium supply. The activity of both AOB and NOB in the recirculated incubation showed that they were not inhibited by the shear stress induced by the flow-through of the medium through the membrane filter. However, nitrification activity (i.e. nitrite and nitrate production) in the recirculated

incubations were reduced by 57% (E1) and 83% (E2) compared to the batch incubations, which was mainly due to lower ammonia oxidation rates resulting in lower nitrite accumulation (Figure S3). The reduced ammonia oxidation activity was also reflected by reduced ^{13}C -incorporation in AOB cells as determined by nanoSIMS in both experiments (Figure 2). In the recirculated setup, we measured mean AOB ^{13}C -incorporation of 3.5 and 3.7 ^{13}C -atom%, in batch incubations 20.3 and 14.4 ^{13}C -atom% for E1 and E2, respectively. AOB in the flow-through incubations also showed lower ^{13}C -enrichment levels (7.9 and 9.6 atom% for E1 and E2, respectively) compared to batch incubations but not as low as in the recirculated incubations.

NOB were enriched in ^{13}C in both the batch (14.9 and 5.2 atom% for E1 and E2, respectively) and recirculated incubations (7.2 and 4.6 atom% for E1 and E2, respectively). In contrast, the flow-through setup resulted in a substantial reduction in ^{13}C -incorporation of NOB (2.0 and 2.3 atom% for E1 and E2, respectively). This shows that nitrite, the secondary substrate, was efficiently removed by means of flow-through, thereby limiting cross-feeding between AOB and NOB. Indeed, in the flow-through incubations, the ^{13}C -enrichment of NOB was not significantly different to the ^{13}C -enrichment of non-nitrifier cells in our setups. We observed a relatively consistent low ^{13}C -enrichment of NOB in the flow-through incubations and of non-nitrifier cells in all incubations. It is unlikely that this is due to ^{13}C -bicarbonate contamination, as all samples were treated with acid before nanoSIMS analysis. It is, however, possible that at least some of the observed ^{13}C -enrichment in NOB is due to anaplerotic reactions leading to C-fixation by background cellular activity rather than substrate induced autotrophic C-fixation (e.g. Li 1982; Roslev et al. 2004).

Our results demonstrate that Flow-SIP is a promising approach to significantly reduce cross-feeding in SIP experiments even in complex microbial communities. Here, we used quantitative single cell isotope probing by combining FISH and nanoSIMS; however, Flow-SIP may also be used in combination with DNA-, RNA- or protein-SIP. These latter methods, unlike FISH, are untargeted and thus potentially allow to identify novel primary consumers of a supplied substrate. Flow-SIP also has the potential to study direct use of chemically unstable substrates, by distinguishing it from consumption of their decomposition products. For example, cyanate, which abiotically decays to ammonium and carbon dioxide, has previously been shown to serve as energy and nitrogen source for ammonia oxidizing archaea (Palatinszky et al. 2015; Kitzinger et al. 2019). Using Flow-SIP, cyanate can be constantly supplied, while abiotically-formed ammonium (as well as ammonium produced by other community members) is constantly removed, which allows to identify ammonia oxidizing microorganisms that directly use cyanate as a substrate. It also reduces the need for control incubations to quantify indirect cyanate use through breakdown to ammonium (Kitzinger et al. 2019). Furthermore, instead of tracing stable isotope assimilation, the presented approach may be coupled to fluorescence-based activity markers, where both a substrate of interest and bioorthogonal non-canonical amino acids are supplied and, subsequently, translationally active cells are visualized on an epifluorescence microscope (BONCAT; Hatzenpichler et al. 2014). Flow-SIP expands the toolbox of microbial ecologists, allowing the direct identification of primary consumers in complex microbial communities without confounding cross-feeding effects. Thereby, this method can yield invaluable insights into the activity and identity of microorganisms catalyzing key processes and element transformations in the environment.

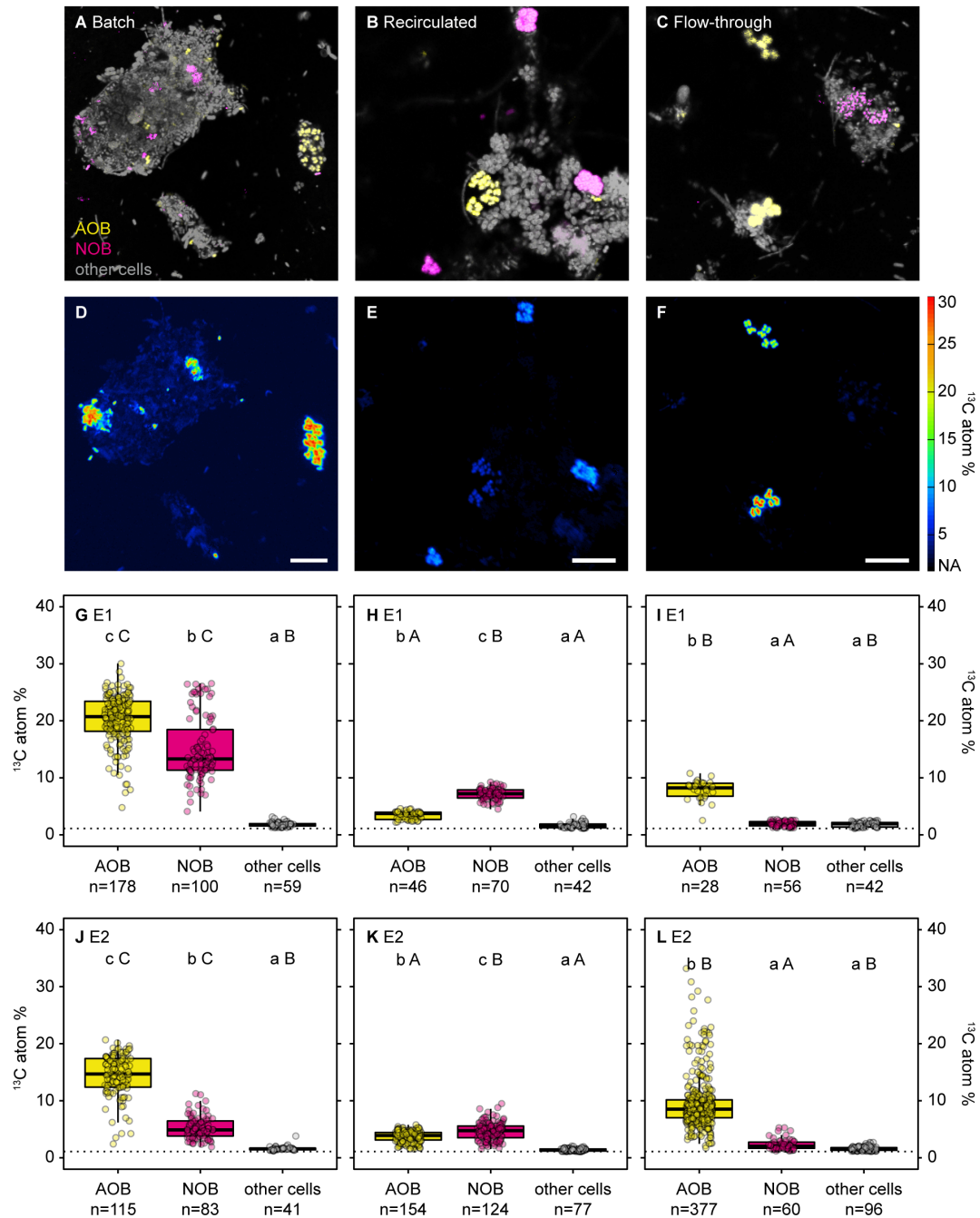


Figure 2 Single cell isotope probing of nitrifiers in batch, recirculated and flow-through incubations. Top panels (A-C) show representative FISH images of E2 (AOB in yellow; NOB in magenta; other cells counterstained by DAPI in grey) of batch, recirculated and flow-through incubations, respectively, and panels (D-F) show the corresponding nanoSIMS image. Scale bar is 10 μm in all images. Bottom panels (G-L) show ^{13}C labelling of AOB, NOB and other cells quantified by nanoSIMS at the single-cell level for E1 (G-I) and E2 (J-L). We used FISH probes targeting AOB (*Nitrosomonas oligotropha* cluster (Cl6a192), *Nitrosomonas eutropha/europea/urea* cluster (NEU)) and NOB (*Nitrotoga* (Ntoga122), *Nitrospira* Lineage 1 (Ntspa1431), and *Nitrospira* Lineage 2 (Ntspa1151)). In (G-L), dashed lines give ^{13}C natural abundance values of the filter surface. Number of cells analyzed per group is indicated below each boxplot. For each experiment, lower case letters indicate significant difference in ^{13}C labelling between groups (AOB, NOB, other cells) within an incubation type and upper case letters indicate significant difference between incubation type for a given group (Kruskal-Wallis test followed by Dunn's test; Statistics are given in Table S2). Boxplots depict the 25–75% quantile range, with the center line depicting the median (50% quantile) and whiskers encompass data points within 1.5 \times the interquartile range.

Acknowledgements

We thank Markus Schmid for help with LMD and CLSM, and Stephanie Eichorst for helpful suggestions for nanoSIMS sample preparation and Marcel Kuypers for fruitful discussions and helpful comments on the manuscript. The study was supported by the ERC Advanced Grant NITRICARE (294343), the Austrian Science Fund (DK plus W 1257) and the Max Planck Society.

References

- Boschker H.T.S., Nold S.C., Wellsbury P., Bos D., De Graaf W., Pel R., Parkes R.J. and Cappenberg T.E. 1998. Direct Linking of Microbial Populations to Specific Biogeochemical Processes by ¹³C-Labeling of Biomarkers. *Nature* 392: 801–4. doi:10.1038/33900.
- Hatzenpichler R., Scheller S., Tavormina P.L., Babin B.M., Tirrell D.A. and Orphan V.J. 2014. In Situ Visualization of Newly Synthesized Proteins in Environmental Microbes Using Amino Acid Tagging and Click Chemistry. *Environmental Microbiology* 16 (8): 2568–90. doi:10.1111/1462-2920.12436.
- Kitzinger K., Padilla C.C., Marchant H.K., Hach P.F., Herbold C.W., Kidane A.T., Könneke M., Littmann S., Mooshammer M., Niggemann J., Petrov S., Richter A., Stewart F.J., Wagner M., Kuypers M.M.M. and Bristow L.A. 2019. Cyanate and Urea Are Substrates for Nitrification by Thaumarchaeota in the Marine Environment. *Nature Microbiology* 4 (2): 234–43. doi:10.1038/s41564-018-0316-2.
- Li W. 1982. Estimating Heterotrophic Bacterial Productivity by Inorganic Radiocarbon Uptake: Importance of Establishing Time Courses of Uptake. *Marine Ecology Progress Series* 8: 167–72. doi:10.3354/meps008167.
- Manefield M., Whiteley A.S., Griffiths R.I. and Bailey M.J. 2002. RNA Stable Isotope Probing, a Novel Means of Linking Microbial Community Function to Phylogeny. *Applied and Environmental Microbiology* 68 (11): 5367–73. doi:10.1128/AEM.68.11.5367.
- Neufeld J.D., Schäfer H., Cox M.J., Boden R., McDonald I.R. and Murrell J.C. 2007. Stable-Isotope Probing Implicates Methylophaga Spp and Novel Gammaproteobacteria in Marine Methanol and Methylamine Metabolism. *The ISME Journal* 1: 480–91. doi:10.1038/ismej.2007.65.
- Orphan V.J., House C.H., Hinrichs K.-U., McKeegan K. and Delong E.F. 2001. Methane-Consuming Archaea Revealed by Directly Coupled Isotopic and Phylogenetic Analysis. *Science* 293: 484–86. doi:10.1126/science.1061338.
- Palatinszky M., Herbold C., Jehmlich N., Pogoda M., Han P., Bergen M. Von, Lagkouvardos I., Karst S.M., Galushko A., Koch H., Berry D., Daims H. and Wagner M. 2015. Cyanate as an Energy Source for Nitrifiers. *Nature* 524: 105–8. doi:10.1038/nature14856.
- Radajewski S., Ineson P., Parekh N.R. and Murrell J.C. 2000. Stable-Isotope Probing as a Tool in Microbial Ecology. *Nature* 403: 646–49. doi:10.1038/35001054.
- Roslev P., Larsen M.B., Jørgensen D. and Hesselsoe M. 2004. Use of Heterotrophic CO₂ Assimilation as a Measure of Metabolic Activity in Planktonic and Sessile Bacteria. *Journal of Microbiological Methods* 59: 381–93. doi:10.1016/j.mimet.2004.08.002.

Supplementary information

Supplementary text

Materials and experimental setup

Schemes of the incubation setup of recirculated and flow-through approaches are shown in Figure S2. For the flow-through approach, the screw caps of the medium reservoir and the waste collection bottle were equipped with two ports, one for the tubing inlet and one for sterile pressure equalization using a membrane filter (0.2 μm). For the recirculated approach, a small bottle was used as medium reservoir with two ports, from which medium was withdrawn and recirculated back, respectively. For both approaches, the medium reservoir was connected to the top of the filter holder (stainless steel, 47 mm, Sartorius) and a peristaltic pump was placed after the filter holder. To open and close the filter holder as well as to remove aliquots of the medium for chemical analysis during the incubation, a three-way valve was connected to the bottom of the filter holder. Material used for both recirculated and flow-through approaches are given in Table S2. All material except for the three-way-valves was sterilized by autoclaving, three-way valves were sterilized by rinsing in 70% ethanol and autoclaved distilled water. Mineral medium was prepared according to Palatinszky et al. (2015), with some modifications: instead of 4 g L⁻¹ CaCO₃, we used 0.01 g L⁻¹ (1 mM), and, as substrate for autotrophic C-fixation, we added ¹³C-NaHCO₃ (98 atom%) with a final concentration of 2 mM, resulting in a final ¹³C-labelling percentage of approximately 66 atom%. For batch and recirculated incubations, 20 mL of medium were inoculated. We accounted for the dead volume of the filter holder and tubing (9 mL) and thus only added 11 mL of medium to the medium reservoir of the recirculated approach. In the flow-through incubations, approximately 624 mL of medium were supplied over 24 h (i.e., flow rate of 26 mL h⁻¹).

Activated sludge was sampled from the nitrification basin of the municipal wastewater treatment plant Aalborg West (luftningstanke, Renseanlæg Vest), Denmark, on March 16th and 18th, 2016. Sludge was disrupted by sonication to yield single cells or colonies to reduce diffusive cross-feeding due to the large 3D-structure of the flocs. 20 ml aliquots of sludge (diluted 1:5 in mineral medium) were sonicated on ice for 120 s using 20% power and 1x cycle settings (Bandelin HD2200, probe MS73), and were allowed to settle for 10 min. The top 15 ml of the sludge suspensions, containing smaller flocs or single colonies and cells, were filtered through 20 μm nylon mesh membrane filters (Magna, Fisher Scientific) to remove residual large flocs. To remove residual substrates from the filtrate, cells were pelleted by centrifugation (20 min, 10°C, 4200 g), supernatant was discarded, and cells were gently resuspended in mineral medium with ¹²C-NaHCO₃ and without ammonium. To avoid the use of storage compounds during the incubation, cells were exposed to a starvation period of approximately 8 - 10 h before start of the incubation. To determine optimal cell density for the incubations, different volumes of sonicated, washed cells were filtered onto 0.2 μm filters, stained by DAPI and inspected by an epifluorescence microscope.

Under sterile conditions, support filters (for E1, glass fibre filters, Advantec, GC50, 47mm, and for E2 nylon membrane filters Magna, Fisher Scientific, 47mm) and membrane filters (0.2 μm polycarbonate, Nucleopore Whatman 47mm) were placed into filter holders (backpressure grids were omitted) fitted with a valve at the filter holder outlet. Filter holders were then filled bubble-free with mineral medium and closed off until cells were applied onto the filter membrane. Using syringes, sonicated, starved cells were gently filtered onto the membranes, discarding the flow-through. To ensure even settling of cells on the membrane surface, additional 20 ml mineral medium

(with $^{12}\text{C-NaHCO}_3$ and without ammonium) were gently pushed through the filter holder, discarding the flow-through. Shortly before the start of the incubation, the medium in the filter holder was replaced by medium containing $^{13}\text{C-NaHCO}_3$ (but no ammonium). Filter holders were then connected to sterile tubing of the incubation setup (Figure S2). The same amount of cells as in the recirculated and flow-through incubations were added to the batch incubations. At the start of the incubation, ammonium was added from a stock solution to batch incubation bottles and into the medium reservoir and fresh medium bottle of the recirculated and flow-through approaches, respectively. Incubations were done in the dark for 24h at in-situ temperature of the nitrification basin in Aalborg Vest (14°C). Immediately after the setup of the incubation, and after approximately 12, 18 and 24 h, subsamples were collected for concentration measurements of ammonium, nitrite and nitrate. In both flow-through and recirculated incubations, samples were collected at the filter holder outlet, and from batch incubations, bulk samples were collected, and cells were removed by centrifugation. Samples were stored at -20°C until analysis.

At the end of the incubation, filter holders were closed off using the valve at the filter outlet, disconnected from the tubing, and cells on the membrane filter inside the filter holders were fixed with formaldehyde (3% formaldehyde in 1x phosphate buffered saline; PBS). To avoid disturbing the cells' position on the membrane filter, 20 ml formaldehyde solution were gently pushed through the filter holders, thereby replacing medium. Filter holders were then closed using the valve connected at the filter holder outlet and incubated for 30 min at room temperature. Formaldehyde was removed by pushing 20 ml 1x PBS through the filter holder, followed by 20 ml distilled water. After pushing out all liquid, filter holders were disassembled, and membrane filters were air-dried and frozen at -20°C until FISH and nanoSIMS analyses. Batch incubation samples were also filtered on a membrane filter, fixed with formaldehyde and stored the same way as the flow-through and recirculated samples.

Nitrification activity was monitored by ammonium consumption, and nitrite and nitrate production. Ammonium, nitrite and nitrate concentrations were quantified after 0, 12, 18 and 24 h by colorimetric procedure as described in Hood-Nowotny et al. (2010) and Garcia-Robledo et al. (2014).

FISH and nanoSIMS analyses

In addition to cells fixed after incubation, bulk activated sludge samples were fixed with formaldehyde as previously described Daims (2009). These samples were used to screen for presence of nitrifier populations by FISH using probes for AOB (probes NEU, Wagner et al. 1995; Nso1225, Mobarry et al. 1996; Nmv/Ncmob Pommerening-Röser et al. 1996; Ncom1025, Juretschko 2000; Cl6a192, Adamczyk et al. 2003) and NOB (Nit3, Wagner et al. 1995; Ntspa1431 and Ntspa1151, Maixner et al. 2006; Ntoga122, Lücker et al. 2015). We detected AOB populations related to *Nitrosomonas oligotropha* (targeted by probe Cl6a192) and *Nitrosomonas eutropha/europea/urea* (targeted by probe NEU). We further detected *Nitrotoga*-affiliated NOB and lineage 1 and 2 *Nitrospira* (targeted by probe Ntspa 1431 and 1151, respectively). Previous metagenomic analyses showed that WWTP Aalborg West does not harbour comammox *Nitrospira* (Albertsen et al. 2012; Munck et al. 2015), whose presence would have confounded the results of our study, as comammox *Nitrospira* are able to oxidise ammonia but are not distinguishable from the canonical lineage 2 *Nitrospira* by FISH. For all FISH and nanoSIMS analyses, we used probe mixes for AOB (Cl6a192 and NEU) and NOB (Ntoga122, Ntspa1431 and Ntspa1151).

Before FISH analysis, laser markings were made on membrane filters using a laser microdissection microscope (Leica LMD 7000, Germany). FISH on sections of the incubated filters was done as previously described by Daims (2009). All FISH probes were double labelled with FitC (AOB in E1; NOB

in E2), Cy3 (NOB in E1), or Cy5 (AOB in E2) fluorophores (Stoecker et al. 2010). We observed strong non-specific binding of the fluorophores, especially of Cy3 and Cy5, to the membrane filter surface. This non-specific binding was overcome by using CARD-FISH hybridization buffer (Pernthaler et al. 2004) instead of normal FISH hybridization buffer in hybridizations of E1 samples. Filter sections of E2 were pre-incubated in 1:10 diluted blocking reagent before hybridization (Pernthaler et al. 2004). After FISH, cells were counterstained with DAPI before fluorescent images were acquired on a confocal laser scanning microscope (SP7, Leica, Germany, equipped with a white light laser).

For nanoSIMS analyses, selected filter sections were attached to antimony-doped silicon wafer platelets (7.1 x 7.1 x 0.11 mm, Active Business Company, Brunthal, Germany) by a commercially available superglue (Loctide®, Henkel, Ireland), and coated with AuPd thin films (30 nm nominal thickness) using a sputter coater (K550X Emitech, Quorum Technologies Ltd., Ashford, UK). In the flow-through incubations, a thin, yellow layer of salt crystals was formed on the filter membranes, which strongly reduced the conductivity of the sample surfaces upon sputtering with AuPd. To remove this layer prior to AuPd coating, the filter membrane sections were washed in 1N HCl or 1N HNO₃ for 10 min, and subsequently rinsed with water (Milli-Q, >18.2 MOhm, Millipore) and 70% ethanol. For comparability and to remove possible ¹³C-bicarbonate contamination, samples from batch and recirculated incubations were also acid washed in the same way.

NanoSIMS measurements were performed on a NanoSIMS 50L (Cameca, Gennevilliers, France) at the Large-Instrument Facility for Advanced Isotope Research at the University of Vienna. Prior to data acquisition, analysis areas were pre-sputtered utilizing a high-intensity, slightly defocused Cs⁺ ion beam (400 pA beam current, ~1,5 μm spot size). Data were acquired as multilayer image stacks by sequential scanning of a finely focused Cs⁺ primary ion beam (approximately 80 nm probe size at 2 pA beam current) over areas between 36 × 36 and 74 × 74 μm² at 512 × 512 pixel image resolution and a primary ion beam dwell time of 5 to 10 msec/(pixel*cycle). The detectors were positioned to enable parallel detection of ¹²C₂⁻, ¹²C¹³C⁻, ¹²C¹⁴N⁻, ³¹P⁻ and ³²S⁻ secondary ions and the mass spectrometer was tuned to achieve a mass resolving power (MRP) of >9.000 (according to Cameca's definition) for detection of C₂⁻ and CN⁻ secondary ions, respectively.

NanoSIMS images were processed using the software WinImage version 2.0.8 (Cameca, France). Prior to stack accumulation, the individual images were aligned to compensate for positional variations arising from primary ion beam and/or sample stage drift. Secondary ion signal intensities were dead time corrected on a per-pixel basis. C isotope composition images displaying the ¹³C/(¹²C+¹³C) isotope fraction, designated as ¹³C atom%, were inferred from the C₂⁻ secondary ion signal intensity distribution images via per-pixel calculation of ¹³C¹²C⁻/(2·¹²C₂⁻+¹³C¹²C⁻) intensity ratios.

Regions of interest (ROIs), referring to individual cells, were manually defined utilizing the nitrogen-, phosphorus- and sulfur-related secondary ion signal intensity distribution maps as indicators of biomass and the respective FISH image. These ROIs were cross-checked by the topographical/morphological appearance of the sampled areas in secondary electron intensity distribution images that were recorded simultaneously with the secondary ion images. Statistical significance of the difference between groups within each approach was analysed by the Kruskal-Wallis test followed by a non-parametric multiple comparison test (Dunn's test), using the R package "dunn.test" (Dinno 2007).

Nitrite diffusion model

In order to determine nitrite distributions surrounding the AOB colonies and to quantify the potential exchange rates with NOB colonies, the flow-condition around a single AOB colony on the flow-SIP filter was simulated.

The steady-state Navier-Stokes equations are given by:

$$\rho(\mathbf{u} \cdot \nabla)\mathbf{u} = -\nabla p + \mu \nabla^2 \mathbf{u}$$

With the continuity equation for incompressible fluids:

$$\nabla \cdot \mathbf{u} = 0,$$

where ρ is the density, μ the dynamic viscosity of water, p the pressure and \mathbf{u} the velocity vector. The stationary scalar transport equations are given by:

$$-D\nabla^2 C + \mathbf{u} \cdot \nabla C = 0,$$

where C is the nitrite concentration and $D = 1.7 \cdot 10^{-9} \text{ m}^2 \text{ s}^{-1}$ is the isotropic diffusion of nitrite. The equations were solved in the COMSOL Multiphysics® software.

Simulating the full 3-dimensional complexity as found on the flow-SIP filter is numerically expensive and requires precise information about the cell and colony structures. Therefore, certain assumptions were made when generating the model domain. First, it is assumed that the AOB colonies are of spherical shape with a radius that can be estimated from measured volumes. For AOB colonies exceeding 50 cells, it was shown that the colony volume can be empirically described using: $V_{col} = n_{cell}^{1.56} e^{-3.28}$, where n_{cell} is the cell number (Coskuner et al. 2005). For colonies with fewer cells no empirical relation exists. Therefore, the volume for 50 cells was linearly scaled down to a theoretical volume of a single cell multiplied with the cell number: $V_{col} = n_{cell} \cdot (50^{0.56} e^{-3.28})$, which is valid for 1-50 cells. Finally, within the domain the reactive, spherical AOB colony was centered in a cylinder. To minimize wall-effects, the radius of the cylinder was adjusted to 120 μm , which is more than 20 times the radius of the AOB colony.

To mimic conditions of the experimental setup, a symmetric outer boundary with a constant inlet flow velocity U_0 and a no-slip boundary condition along the colony's surface was assumed. The inflow nitrite-concentration was adjusted to 0 $\mu\text{mol l}^{-1}$. To simulate the nitrite production of the AOB colonies, a constant normal flux (J_n) was imposed at the surface of the colony, which was calculated based on the cell specific volumetric rates and normalized to the surface area:

$$J_n = \frac{n_{cell} \cdot R_{cell}}{S_{col}}$$

With a cell specific volumetric rate of $R_{cell} = 2.6 \text{ fmol cell}^{-1} \text{ h}^{-1}$ (Laanbroek et al. 1994; Daims et al. 2001; Coskuner et al. 2005; Stieglmeier et al. 2014) and a surface area of $S_{col} = 4\pi r_{col}$. The described approach reduces the decisive parameters to cell numbers and flow velocity. In more than 200 model runs, cell numbers were varied between $n_{cell} = 5, 50, 500$ cells and the imposed flow velocity was sequentially increased from $U_0 = 0 - 100 \mu\text{m s}^{-1}$ in $1.25 \mu\text{m s}^{-1}$ steps.

Post-processing was performed in Matlab (Mathworks 2017b). Briefly, nitrite concentrations were extracted along the equator up to a distance of 100 μm of the colony surface. This procedure was repeated for all imposed flow velocities and subsequently interpolated to an equidistant grid. Subsequently, contour lines were extracted.

Supplementary references

- Adamczyk J., Hesselsoe M., Iversen N., Horn M., Lehner A., Nielsen P.H., Schloter M., Roslev P. and Wagner M. 2003. The Isotope Array, a New Tool That Employs Substrate-Mediated Labeling of rRNA for Determination of Microbial Community Structure and Function. *Applied and Environmental Microbiology* 69 (11): 6875–87. doi:10.1128/AEM.69.11.6875.
- Albertsen M., Hansen L.B.S., Saunders A.M., Nielsen P.H. and Nielsen K.L. 2012. A Metagenome of a Full-Scale Microbial Community Carrying out Enhanced Biological Phosphorus Removal. *ISME Journal* 6 (6). Nature Publishing Group: 1094–1106. doi:10.1038/ismej.2011.176.
- Coskuner G., Ballinger S.J., Davenport R.J., Pickering R.L., Solera R., Head I.M. and Curtis T.P. 2005. Agreement between Theory and Measurement in Quantification of Ammonia-Oxidizing Bacteria. *Applied and Environmental Microbiology* 71 (10): 6325–34. doi:10.1128/AEM.71.10.6325.
- Daims H. 2009. Use of Fluorescence in Situ Hybridization and the Daime Image Analysis Program for the Cultivation-Independent Quantification of Microorganisms in Environmental and Medical Samples. *Cold Spring Harbor Protocols* 4 (7): 1–7. doi:10.1101/pdb.prot5253.
- Daims H., Ramsing N.B., Schleifer K. and Wagner M. 2001. Cultivation-Independent, Semiautomatic Determination of Absolute Bacterial Cell Numbers in Environmental Samples by Fluorescence In Situ Hybridization. *Applied and Environmental Microbiology* 67 (12): 5810–18. doi:10.1128/AEM.67.12.5810.
- Dinno A. 2007. Dunn.Test: Dunn's Test of Multiple Comparisons Using Rank Sums. R Package Version 1.3.2. <http://CRAN.R-Project.Org/Package=dunn.Test>. <http://cran.r-project.org/package=dunn.test>.
- García-Robledo E., Corzo A. and Papaspyrou S. 2014. A Fast and Direct Spectrophotometric Method for the Sequential Determination of Nitrate and Nitrite at Low Concentrations in Small Volumes. *Marine Chemistry* 162: 30–36. doi:10.1016/j.marchem.2014.03.002.
- Hood-Nowotny R., Umana N.H.-N., Inselbacher E., Oswald-Lachouani P. and Wanek W. 2010. Alternative Methods for Measuring Inorganic, Organic, and Total Dissolved Nitrogen in Soil. *Soil Science Society of America Journal* 74 (3): 1018. doi:10.2136/sssaj2009.0389.
- Juretschko S. 2000. Mikrobielle Populationsstruktur Und –dynamik in Einer Nitrifizierenden/Denitrifizierenden Belebtschlammanlage. Technische Universität München.
- Laanbroek H.J., Bodelier P.L.E. and Gerards S. 1994. Oxygen Consumption Kinetics of Nitrosomonas Europaea and Nitrobacter Hamburgensis Grown in Mixed Continuous Cultures at Different Oxygen Concentrations. *Archives of Microbiology* 161: 156–62. doi:10.1007/s002030050036.
- Lücker S., Schwarz J., Gruber-Dorninger C., Spieck E., Wagner M. and Daims H. 2015. Nitrotoga-like Bacteria Are Previously Unrecognized Key Nitrite Oxidizers in Full-Scale Wastewater Treatment Plants. *The ISME Journal* 9: 708–20. doi:10.1038/ismej.2014.158.
- Maixner F., Noguera D.R.D., Anneser B., Stoecker K., Wegl G., Wagner M. and Daims H. 2006. Nitrite Concentration Influences the Population Structure of Nitrospira-like Bacteria. *Environmental Microbiology* 8 (8): 1487–95. doi:10.1111/j.1462-2920.2006.01033.x.
- Mobarry B., Wagner M., Urbain V., Rittmann B.E. and Stahl D. a. 1996. Phylogenetic Probes for Analyzing Abundance and Spatial Organization of Nitrifying Bacteria. *Applied and Environmental Microbiology* 62 (6): 2156–62.
- Munck C., Albertsen M., Telke A., Ellabaan M., Nielsen P.H. and Sommer M.O.A. 2015. Limited Dissemination of the Wastewater Treatment Plant Core Resistome. *Nature Communications* 6: 8452. doi:10.1038/ncomms9452.
- Palatinszky M., Herbold C., Jehmlich N., Pogoda M., Han P., Bergen M. Von, Lagkouravdos I., Karst S.M., Galushko A., Koch H., Berry D., Daims H. and Wagner M. 2015. Cyanate as an Energy Source for Nitrifiers. *Nature* 524: 105–8. doi:10.1038/nature14856.
- Pernthaler A., Pernthaler J. and Amann R. 2004. Sensitive Multi-Color Fluorescence in Situ Hybridization for the Identification of Environmental Microorganisms. In *Molecular Microbial Ecology Manual*, edited by G. Kowalchuk, F. J. de Bruijn, Ian M. Head, A. D. L. Akkermans, and J. D. van Elsas, 2nd ed., 711–26. Dordrecht, Boston, London: Kluwer Academic Publishers. doi:10.1007/978-1-4020-2177-0_311.
- Pommerening-Röser A., Rath G. and Koops H.-P. 1996. Phylogenetic Diversity within the Genus Nitrosomonas. *Systematic and Applied Microbiology* 19: 344–51. doi:10.1016/S0723-2020(96)80061-0.

- Stieglmeier M., Mooshammer M., Kitzler B., Wanek W., Zechmeister-Boltenstern S., Richter A. and Schleper C. 2014. Aerobic Nitrous Oxide Production through N-Nitrosating Hybrid Formation in Ammonia-Oxidizing Archaea. *The ISME Journal* 8: 1135–46. doi:10.1038/ismej.2013.220.
- Stoecker K., Dorninger C., Daims H. and Wagner M. 2010. Double Labeling of Oligonucleotide Probes for Fluorescence in Situ Hybridization (DOPE-FISH) Improves Signal Intensity and Increases rRNA Accessibility. *Applied and Environmental Microbiology* 76 (3): 922–26. doi:10.1128/AEM.02456-09.
- Wagner M., Rath G., Amann R., Koops H.-P. and Schleifer K.-H. 1995. In Situ Identification of Ammonia-Oxidizing Bacteria. *Systematic and Applied Microbiology* 18: 251–64. doi:10.1016/S0723-2020(11)80396-6.

Supplementary figures

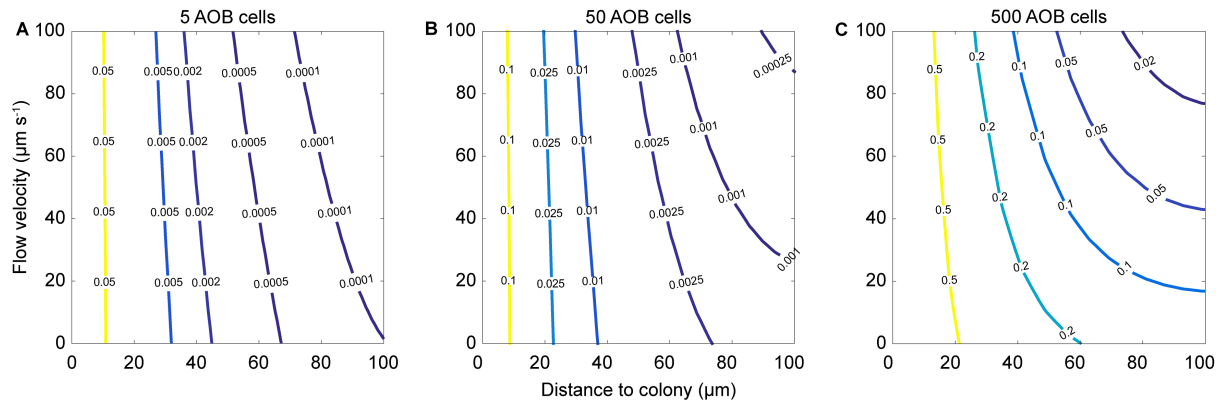


Figure S1 Nitrite diffusion model showing nitrite distribution around AOB colonies on the membrane filter in the flow-through approach, considering different flow velocities. The flow rate of 26 mL h^{-1} used in our experiment corresponds to a flow velocity of $4.2 \mu\text{m s}^{-1}$. The model was run for three different AOB colony sizes, consisting of either (A) 5, (B) 50 or (C) 500 cells. We analyzed AOB colonies ranging from single cell to approximately 250 cells in our experiments. The distance to colony of 0 – 100 μm correspond approximately to the distances between AOB and NOB colonies that we have observed. The contour lines represent nitrite concentration (μM).

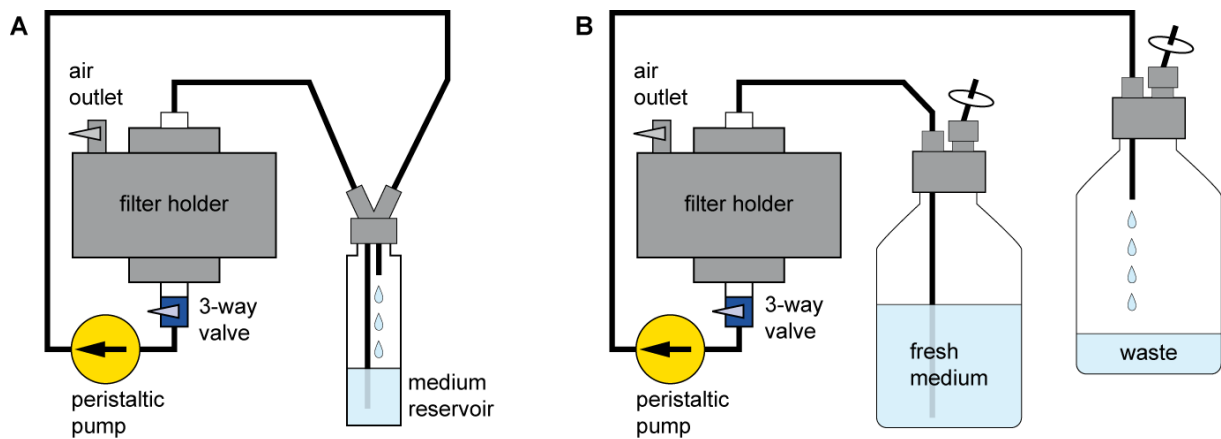


Figure S2 Schemes of incubation setup of recirculated (A) and flow-through approach (B).

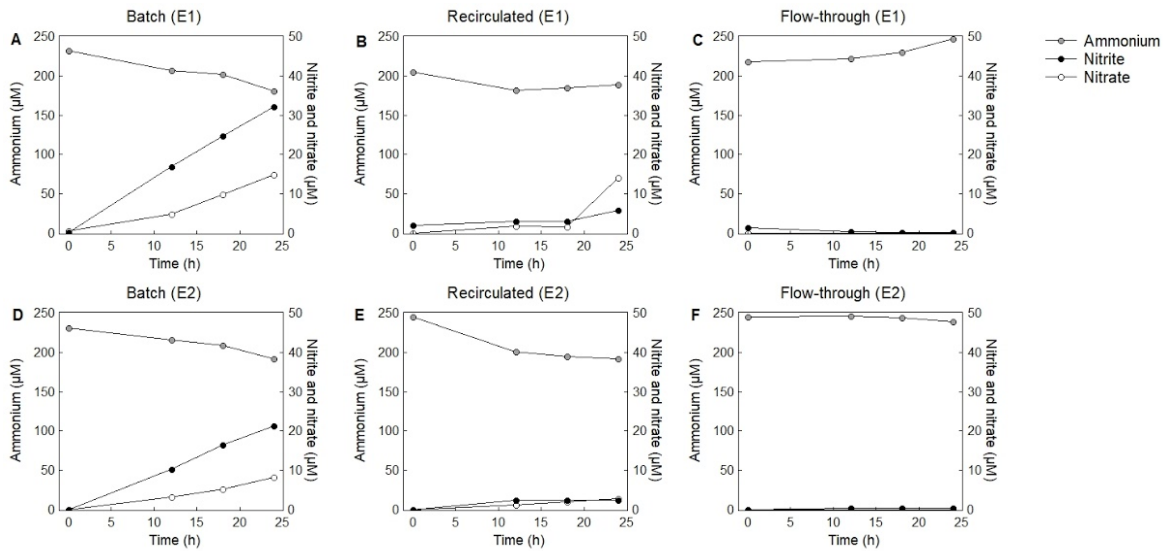


Figure S3 Nitrification activity in batch, recirculated and flow-through incubations of E1 (A-C) and E2 (D-F). Nitrification activity was monitored over the course of the incubation by ammonium consumption, and nitrite and nitrate production. Note that the drop in ammonium concentration in the recirculated treatment between 0 and 12h was not due to ammonium consumption, but due to dilution by ammonium-free medium that was present in the tubing and filter holder at the beginning of the incubation. Nitrite and nitrate were not detectable in the flow-through incubation due to the strong dilution by the medium supply.

Supplementary tables

Table S1. Material used in flow-through and recirculated approaches. Schemes of the setup of both approaches are given in Figure S2.

Item	Comment	Manufacturer	Article number
Ismatec REGLO ICC digital peristaltic pump; 4-channel, 8-roller		Ismatec	ISM4408
Pump tubing, PharMed® Ismaprene, 1.6 mm inner diameter, 4.8 mm outer diameter, 1.6 mm wall thickness		Ismatec	MF0010
2-stop tubing, PharMed® Ismaprene, 1.65 mm inner diameter		Ismatec	SC0331
In-line stainless steel filter holder, 47 mm		Sartorius	16254
Luer lock connector for filter holders		Sartorius	16881
Whatman® Nuclepore™ Track-Etched Membranes; 47 mm diameter, 0.2 µm pore size, polycarbonate		Whatman	WHA111106
Advantec Grade GC50 Glass Fiber Filters, 47 mm diameter, 0.5 µm pore size	Support filter for E1	Advantec	GC5047MM
GVS Life Sciences Magna™ Nylon Membrane Filters, 47 mm diameter, 0.5 µm pore size	Support filter for E2	GVS	1213776
Glass bottle, 1.5 cm inner diameter, 10 cm height, GL25 thread	Medium reservoir for recirculated incubations; custom-made		

Table S2. Test of statistical significance of differences between microbial groups within each approach and differences between approaches within each microbial group. Shown are results of Kruskal-Wallis test and non-parametric multiple comparison test (Dunn's test); *P < 0.05, **P < 0.01, ***P < 0.001.

Within approach		χ^2	df	P-value	Pairwise comparison		
					AOB – NOB	NOB – other cells	AOB – other cells
E1	Batch	182.6	2	< 0.001	***	***	***
	Recirculated	134.7	2	< 0.001	***	***	***
	Flow-through	65.1	2	< 0.001	***		***
E2	Batch	185.4	2	< 0.001	***	***	***
	Recirculated	193.8	2	< 0.001	***	***	***
	Flow-through	327.6	2	< 0.001	***		***

Within microbial group		χ^2	df	P-value	Pairwise comparison		
					Batch – Recirc.	Recirc. – Flow-thr.	Batch – Flow-thr.
E1	AOB	157.0	2	< 0.001	***	*	***
	NOB	184.5	2	< 0.001	***	***	***
	Other cells	7.9	2	0.019	*	*	
E2	AOB	375.0	2	< 0.001	***	***	***
	NOB	98.2	2	< 0.001		***	***
	Other cells	20.3	2	< 0.001	***	***	

Chapter 6

Synthesis and Outlook

Nitrifiers catalyze key processes in biogeochemical Nitrogen (N) cycling in both man-made and natural systems and thus their activity strongly influences the Earth system. Despite their importance, still little is known about their ecophysiology and the traits that underlie their wide environmental distribution and success. Pure culture studies indicate that this environmental success may be due to their broad metabolic versatility. However, there is still limited knowledge about the role that nitrifier metabolic versatility plays in the environment.

In this thesis, I took different methodological approaches to investigate nitrifier metabolic versatility: I studied pure cultures (**Chapter 2 and 3**) and used (meta-) genome analyses (**Chapter 2, 3 and 4**), performed culture-independent *in situ* experiments (**Chapter 3, 4, 5**) and developed new methods to differentiate between direct and indirect use of dissolved organic nitrogen (DON) compounds in complex environmental communities (**Chapter 3 and 5**). The combination of interdisciplinary methods and investigation of processes at different levels – from bulk to single cell activities provided new and important insights into nitrifier metabolic versatility (Figure 1).

Chapter 2 describes the first pure culture of *Nitrotoga*, a nitrite oxidizer isolated from a wastewater treatment plant. This study shed light on the complex evolutionary history of nitrite oxidation, as *Candidatus Nitrotoga fabula* encodes for a new type of nitrite oxidoreductase (NXR) that is phylogenetically related to a clade of uncharacterized enzymes previously thought to represent nitrate reductases (NAR). These closely related enzymes are found in physiologically uncharacterized bacteria and archaea, hinting at the presence of yet unknown nitrite oxidizers in both the bacterial and archaeal domain. Growth of the isolated *Nitrotoga* strain on ultra-pure agarose solid medium facilitates culture handling, and, together with the presence of a plasmid, might in the future allow for the development of a nitrite oxidizer genetic system, which would allow to study the physiology of nitrite oxidizing bacteria (NOB) in even more depth. Furthermore, genome analysis indicated that *Ca. N. fabula* has a versatile metabolism and may be able to use hydrogen and sulfite as alternative electron donors. This study, and another study published shortly after (Boddicker & Mosier 2018), provide evidence that nitrite oxidizers from all genera have the potential for multiple alternative metabolisms, catalyzing processes other than N-redox reactions. This ability could allow nitrite oxidizers to remain active in the environment even when their primary substrates nitrite and oxygen are limiting.

Chapter 3 shows that metabolic versatility also plays an important role for marine ammonia oxidizing archaea (AOA) – both in the environment, the Gulf of Mexico (GoM), and in pure culture. These marine AOA are able to use cyanate and urea both directly and indirectly as additional energy and N-sources, despite lacking known cyanases encoded in their genomes. These findings have important implications for the environment, as the ability to use electron donors and N-sources other than

ammonia/ammonium may allow them to avoid competition for ammonium with other organisms and is likely part of the reason for the high abundance of AOA in the world's ocean (Figure 1). In this study, the development and application of control incubations to tease apart direct and indirect substrate utilization in stable isotope experiments was crucial. Furthermore, this chapter highlights that *in situ* and activity-based experiments are vital to verify a physiological function, as (meta-) genome analyses are not necessarily sufficient to infer an organisms' physiology.

Chapter 4 describes key aspects of the ecophysiology of Nitrospinae, key marine nitrite oxidizers, in comparison to AOA. This showed that despite their low abundance, Nitrospinae in the GoM are highly active, with growth rates exceeding those of the far more abundant AOA. By combining measurements of Nitrospinae and AOA N- and C-assimilation rates with bulk oxidation rates, cell abundances and cellular C-contents, Nitrospinae were shown to be more efficient in converting the energy gained from nitrification to autotrophic C-fixation than the AOA.

Additionally, this study highlighted that DON compounds also play an important role for the ecophysiology of Nitrospinae, that met most of their N-demand for biomass growth from the assimilation of the organic N compounds urea and cyanate, rather than ammonium. This versatility in N-source utilization probably allows Nitrospinae to evade competition with AOA, whom they depend on for their substrate, nitrite. The high growth rates at low Nitrospinae abundance furthermore point to a strong *in situ* control of population size (i.e. a high mortality rate), either due to viral lysis or zooplankton grazing (Figure 1). The combination of high energy efficiency and utilization of DON compounds for growth are likely key factors contributing to the success of Nitrospinae as the main nitrite oxidizer in the ocean.

Chapter 5 takes a step further from the control incubations employed in **Chapter 3** to tease apart direct and indirect substrate use in stable isotope studies. Here, a novel approach to overcome confounding cross-feeding effects in stable isotope incubations was developed, Flow-through stable isotope probing (Flow-SIP). This was achieved by trapping cells on a filter membrane and supplying a constant flow of isotopically labeled substrates. This method allows specific microorganisms to be linked to substrate turnover in the environment and thus significantly expands the toolbox of microbial ecologists and biogeochemists.

The findings presented in this thesis significantly advance our knowledge about the metabolic versatility and physiology of globally relevant nitrifiers through interdisciplinary approaches using culture-dependent and -independent methods. One of the key findings throughout the chapters presented in this thesis was that DON plays a crucial role in the success of nitrifiers in the environment, which allows them to gain energy and/or N for assimilation irrespective of the availability of ammonium.

However, many aspects of nitrifier diversity, physiology and ecology remain unknown. In the following sections, key unconstrained aspects of nitrifier ecology and physiology, and their metabolic versatility that arose during this study are discussed and possible experiments to address them are proposed.

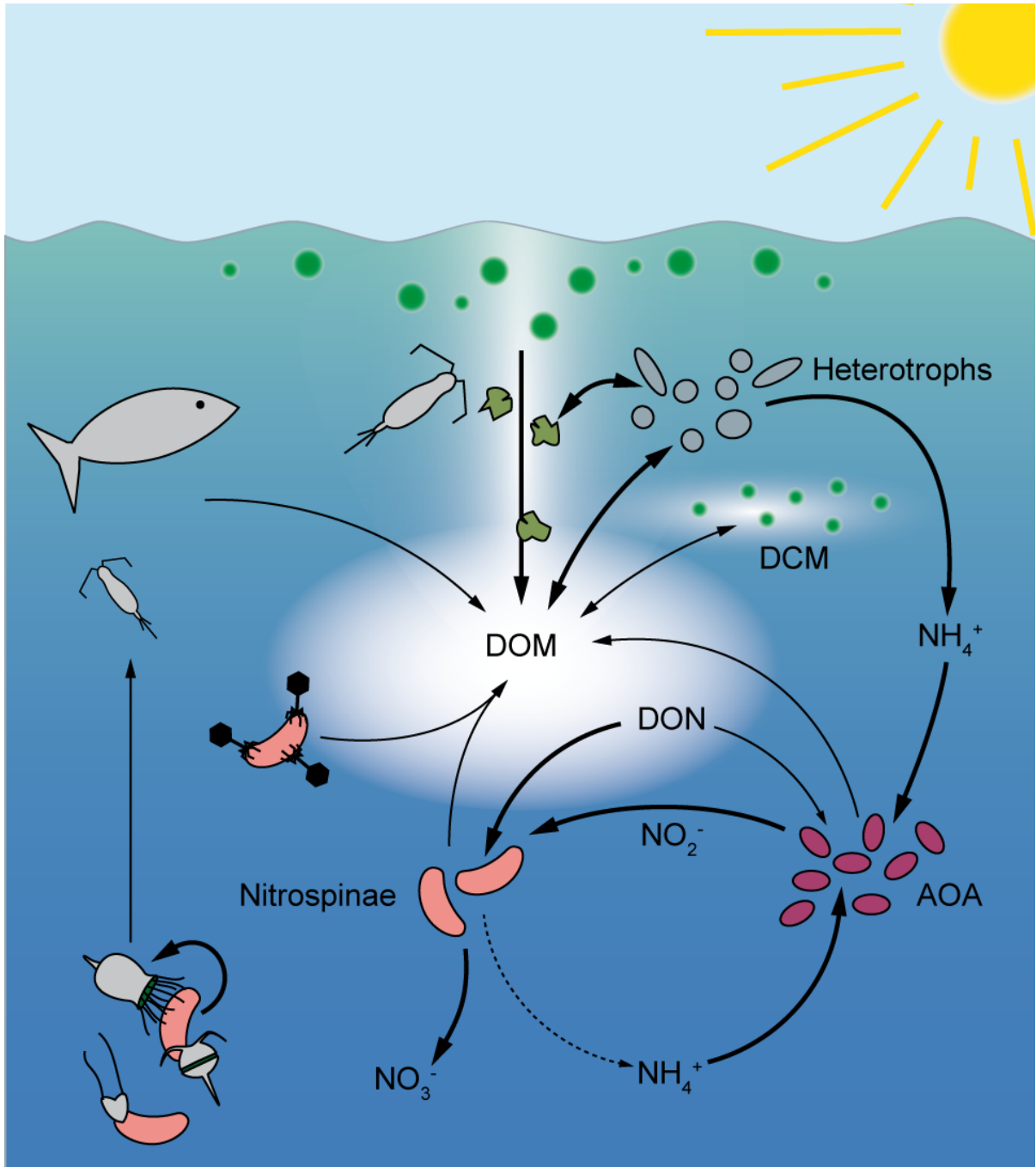


Figure 1 Schematic of dissolved inorganic and organic nitrogen cycling in the marine waters with a special focus on the three main autotrophic groups – phototrophs, ammonia, and nitrite oxidizers. Thickness of arrows corresponds to the flux size. DOM, dissolved organic matter; DCM, deep chlorophyll maximum.

6.1. Key unconstrained aspects of nitrifier ecology and physiology

6.1.1. Uncovering the true diversity of nitrifiers

During the last two decades, the known diversity of nitrifiers has been massively expanded – the ammonia oxidizing archaea were discovered (Treichel et al. 2005; Venter et al. 2004; Könneke et al. 2005); phototrophic nitrite oxidizers were described (Griffin et al. 2007); *Nitrotoga* and *Nitrolancea*, two new NOB genera were found (Alawi et al. 2007; Sorokin et al. 2012); and comammox bacteria, long hypothesized to exist but never identified, were finally shown to exist in the genus *Nitrospira* (Daims et al. 2015; van Kessel et al. 2015). And an even larger nitrifier diversity is likely waiting to be discovered.

It seems that in nature, any metabolism can be found, as long as it is thermodynamically feasible. Therefore, it is surprising that so far, comammox have only been found in terrestrial systems. It might be that in the marine environment, they have so far been missed because we did not look at the right places. Biofilms have been suggested as ideal habitat for comammox (Costa et al. 2006), and these are also common in the marine environment, e.g. on the surface of sand grains (Probandt et al. 2018). Thus, sandy marine sediments may be a prime location to look for marine comammox – bacteria, or, archaea.

Ammonia oxidizers have been identified in both the bacterial and the archaeal domain. Why then should nitrite oxidation be restricted to the bacteria? In **Chapter 2**, first data is presented which hints at the existence of nitrite oxidizing archaea (NOA), based on the presence of a crenarchaeal nitrite oxidoreductase-like gene in a nitrifying enrichment culture without known NOB (Kitzinger et al. 2018). However, just as for marine comammox, direct evidence for the existence of NOA is lacking.

How then could novel nitrifiers be identified? To date, most novel nitrifier groups have been discovered through a cultivation-based approach, as employed in **Chapter 2**. However, new approaches may be needed to bring novel nitrifiers into culture. These could include adjusting the commonly used media composition, enrichment on lower substrate concentrations, or using DON as (co-) substrate instead of only ammonium. Still, most microorganisms may remain part of the uncultivated majority, or, the proportion that is extremely difficult to enrich and isolate.

Metagenomics, as used in **Chapter 3 and 4**, could help to identify microorganisms *in situ* that might nitrify but cannot easily be brought into culture. For example, metagenomics may allow to identify ammonia monooxygenase-like (AMO) or NXR genes in metagenome-assembled genomes of organisms not previously associated with nitrification. Metagenomics may also serve as a guide to more targeted cultivation efforts of putative new nitrifiers, as analysis of their genomes may indicate traits like auxotrophy for cofactors or vitamins, which may then be supplemented in the cultivation media, to better mimic the growth conditions required by the targeted organisms.

It is not unlikely however, that novel nitrifiers employ an enzymatic machinery different to the one of known nitrifiers, rendering metagenomic identification difficult. Additionally, there appears to be no clear-cut separation of NXR and nitrate reductases (Kitzinger et al. 2018), further complicating the meta-omics based identification of nitrifiers.

A cultivation- and metagenome-independent method to identify novel nitrifiers would be to employ Flow-SIP (**Chapter 5**) coupled to DNA or RNA stable isotope probing, using ^{15}N -ammonium or ^{15}N -nitrite and ^{13}C -bicarbonate as sole energy and C-source. Sequencing of the isotopically heavier DNA and/or RNA fractions could give insights into the identity of new nitrifier groups. Furthermore, Flow-SIP could also be used to identify novel comammox microorganisms by employing a dual labeling strategy. First, nitrite could be supplied together with isotopically labeled water (e.g. deuterated water; Berry et al. 2015), then, after a brief starvation period, ammonium and biorthogonal non-

canonical amino acids (BONCAT; Hatzenpichler et al. 2014) could be supplied as sole substrates. Microorganisms which show both deuterium incorporation and a fluorescent signal are possible candidates for comammox metabolism in this setup. These cells could then be identified by combining fluorescence-activated cell sorting to collect cells that incorporated the bioorthogonal amino acids, i.e. cells able to oxidize ammonia, with subsequent Raman sorting of cells showing heavy water incorporation (Berry et al. 2015; Lee et al. 2019), i.e. cells able to oxidize nitrite. DNA analyses on the sorted microorganisms could then reveal their identity.

6.1.2. Factors regulating nitrifier population size *in situ*

In the marine environment, AOA usually outnumber nitrite oxidizers by an order of magnitude. Yet, Nitrospinae in the Gulf of Mexico are both highly energy efficient and display high growth rates – this suggests that Nitrospinae should be far more abundant in the marine environment, unless there was a high mortality rate that keeps their population size small (**Chapter 4**). However, it is unclear what the relative importance of viral vs. zooplankton induced mortality. For other nitrifier groups, the relative importance of viral lysis and zooplankton grazing is also unconstrained – both in the marine environment, and in terrestrial systems. Yet, these are important factors that likely have a large influence on nitrifier distribution and the carbon cycle. The effect of viral lysis and zooplankton grazing on the marine food web is very different – viral lysis channels nutrients and fixed carbon into the microbial loop, while zooplankton grazing transfers them to higher trophic levels. Both of viral lysis and zooplankton grazing could have a strong influence on biogeochemical nutrient cycling and their relative importance for nitrifier mortality should therefore be addressed.

In the marine environment, previous studies have investigated grazing and viral lysis using dilution experiments (Landry & Hassett 1982; Evans et al. 2003). These assume that both the amount of grazing and viral lysis is dependent on encounter rates between “predator” (i.e. zooplankton/viruses) and prey. For dilution experiments, water samples are serially diluted with either sterile filtered water to assess the rate of grazing (Landry & Hassett 1982) or virus free (10 kDa filtered) water to assess the rate of viral lysis (Evans et al. 2003). Prey growth rates are then tracked over time for all dilution series and *in situ* the effect of grazing/viral lysis on the prey growth rates are modeled.

Yet, the effect of viral lysis and grazing has been mainly studied on bulk community level (e.g. Landry & Hassett 1982; Epstein & Shiaris 1992; Baudoux et al. 2008), with much fewer studies addressing the effect of these processes on specific microbial groups (e.g. Evans et al. 2003). These experiments could easily be adapted to investigate the importance of viral lysis and zooplankton grazing for different nitrifier groups.

6.1.3. Differences in nitrifier energy efficiencies

In **Chapter 4**, the *in situ* energy efficiencies (i.e. the amount of Carbon (C) that can be assimilated per Joule gained from nitrite or ammonia oxidation) of Nitrospinae and AOA were directly compared for the first time, by measuring of relevant parameters in one study. These analyses revealed that Nitrospinae are surprisingly energy efficient, even more so than the AOA, which have previously been suggested to harbor the most energy efficient aerobic C-fixation pathway (Könneke et al. 2014).

In the literature, energy efficiency as C-fixed per Joule is rarely reported, instead, the closely related nitrification efficiency or nitrification yield is reported, i.e. C-yield per oxidized mol of ammonia or nitrite. This has been measured previously for AOA (0.1 C:N, Bayer et al. 2019), AOB (0.02-0.09 C:N, Belser 1984; Glover 1985) and the NOB Nitrococcus (0.014-0.031 C/N, Glover 1985) and Nitrobacter (0.023 C:N, Belser 1984). However, for the environmentally important NOB Nitrospinae, Nitrospira and Nitrotoga (as well as Nitrolancea, though its environmental distribution is unclear), no data was

available until now. We report the first nitrification yield calculated for Nitrospinae in the GoM (0.14 C:N, **Chapter 4**).

Constraining the actual energy efficiencies for all nitrifier groups will be vital to gain a better understanding of the underlying mechanisms that control their *in situ* abundance, distribution and activities. As the different C-fixation pathways of nitrifiers are likely associated with different sensitivities to oxygen (e.g. Lücker et al. 2010; Lücker et al. 2013; Sorokin et al. 2012; Kitzinger et al. 2018), the effect of oxygen on energy efficiencies has to be taken into account. Nitrospinae and Nitrospirae use the reverse tricarboxylic acid cycle for C-fixation, which is – at least in anaerobic organisms – highly sensitive to oxygen (Berg 2011). Therefore, these two NOB groups may have a higher energy efficiency at low oxygen concentrations, compared to higher oxygen levels, when energy will be needed to protect the sensitive enzymes from oxygen and/or reactive oxygen species. Energy efficiencies at different oxygen concentrations can be constrained using pure cultures. However, more importantly, energy efficiencies of relevant nitrifiers in the environment need to be examined to better constrain their ecophysiology – e.g. by using nitrification rates and relating them to single cell C-fixation rates at different oxygen levels.

6.1.2. Nitrifier biochemistry and physiology

The underlying biochemistry for both ammonia and nitrite oxidation and the different C-fixation pathways are key factors in determining the energy efficiencies of nitrifiers. There are still large knowledge gaps regarding the basic nitrifier biochemistry and physiology (see below).

Most of the current knowledge on gene function and metabolic pathways in microorganisms stems from insights gained through analyses of mutant strains – mainly using the genetic model organism *Escherichia coli*. While ammonia oxidizing bacteria (AOB) can be genetically modified (Sayavedra-Soto & Stein 2010), for NOB and AOA, no genetically tractable model organisms have been obtained to date. However, availability of such model systems would allow targeted analyses to answer key questions about their biochemistry and physiology such as:

- How do the AOA and NOB electron transport chains function?
- Which enzymes are responsible for hydroxylamine oxidation to NO and/or nitrite in AOA?
- Can one type of NXR be substituted by a different type, or even a NAR? What are the associated oxidation kinetics and energetic consequences (e.g. cytoplasmic vs. periplasmic NXR)?
- Which NXR subunits are required for nitrite oxidation?
- What is the physiological role of the universally present chlorite dismutase genes in NOB?

With the availability of the pure culture betaproteobacterial nitrite oxidizer *Ca. Nitrotoga fabula* (**Chapter 2**; Kitzinger et al. 2018), that harbors a plasmid and is able to grow on solid medium, we may now be a step closer to developing a genetic system for NOB. In contrast, to date, none of the available AOA isolates have been reported to grow on solid medium, although genetic systems have been established for the related Crenarchaeota, efforts to establish an AOA genetic system have not been successful.

6.2. Key unconstrained aspects of nitrifier metabolic versatility

6.2.1. Cyanate utilization by AOA lacking canonical cyanases

Chapter 3 shows that AOA in the GoM and cultured marine AOA are able to directly use cyanate as a substrate despite lacking canonical cyanases (*cynS*) (Kitzinger et al. 2019). The mechanism of cyanate utilization, however, is unresolved. In the following section possible mechanisms are discussed and experiments to elucidate how cyanate is utilized by AOA are proposed.

Cyanate utilization might be conferred by a cyanase-like enzyme that lacks homology to canonical cyanases. An alternative cyanase (*cynH*) has recently been found in some *Synechococcus* strains (Kamennaya & Post 2011). GoM AOA and *Nitrosopumilus maritimus* may encode for yet another enzyme with cyanase activity. As the genomes of AOA contain a plethora of genes without known function (e.g. >40% of *N. maritimus*' genes have no predicted function; Walker et al. 2010), there is ample opportunity for potential alternative cyanases. Upregulation of a potential alternative cyanase could be tested by performing comparative transcriptomic or proteomic experiments using *N. maritimus* grown on cyanate and *N. maritimus* grown on ammonium.

Alternatively, cyanate utilization may not be conferred by a dedicated cyanase-like enzyme, but by a moonlighting enzyme – an enzyme performing multiple functions (Huberts & van der Klei 2010). Cyanate, as a linear molecule, appears to also fit the active sites of several enzymes primarily acting on other linear molecules. For example, Fe-Mo nitrogenase catalyzes the breakdown of cyanate/isocyanic acid to ammonium and CO (Rasche & Seefeldt 1997), and cyanate acts as inhibitor for carbon monoxide dehydrogenase (Seravalli et al. 1995) and carbonic anhydrase (Supuran et al. 1997; Lindskog 1997). Therefore, cyanate breakdown may be facilitated by a constitutively expressed enzyme with a primarily different metabolic function in AOA. This could be tested using a random expression cloning approach (Gabor et al. 2004), where AOA genes are randomly cloned and expressed in a suitable genetic system and potential enhanced growth on cyanate as sole N-source or cyanate breakdown to ammonium is measured.

However, cyanate utilization in marine AOA might also be facilitated non-enzymatically. As abiotic cyanate breakdown is enhanced at low pH (Kamennaya et al. 2008; Palatinszky et al. 2015), low pH micro-environments in AOA cells may facilitate cyanate breakdown.

The AOA tested in this thesis all appeared to be able to use cyanate as a substrate, yet, it is unknown whether this finding extends to further marine AOA in culture and in the environment. This trait may even be common in other nitrifying or non-nitrifying microorganisms, which lack known cyanases, but nonetheless are able to use cyanate as energy and/or N-source.

6.2.2. Utilization of DON compounds other than cyanate, urea, amino acids and polyamines

To date, DON use by nitrifiers has been shown for cyanate, urea and – although it is presently unclear whether these are used directly or indirectly – polyamines and amino acids (e.g. Ouverney & Fuhrman 2000; Teira et al. 2006; Alonso-Saez et al. 2012; Palatinszky et al. 2015; Bayer et al. 2016; Tolar et al. 2017; Kitzinger et al. 2019; Damashek et al. 2019). However, the DON pool encompasses an enormous diversity of molecules, and it remains to be seen how much of the abundant DON pool can be used by nitrifiers.

Due to the chemical and structural diversity of the DON pool (e.g. Antia et al. 1991), any targeted experiment to assess the use of one specific DON compound by nitrifiers is a “trial and error” approach of whether one specific compound is actually used. Selecting DON compounds for targeted experiments based on their detection in seawater in high concentrations is likely not the best approach, as compounds undergoing rapid turnover may only be present at low concentrations. To a

certain extent, presence of genes encoding for the degradation of specific DON compounds in nitrifier genomes can serve as an important guide to which DON compounds may be relevant (e.g. Palatinszky et al. 2015; Koch et al. 2015; Bayer et al. 2016). However, as shown in **Chapter 3** for cyanate use by AOA, the absence of a known DON utilization gene does not necessarily mean that a specific DON compound cannot be used.

One way to identify use of specific DON compounds by nitrifiers in a non-targeted approach could be to perform incubation experiments using nitrifier isolates and incubating them in presence of bulk DON (e.g. cell lysate or complex DON extracted from the environment). Tracking the concentration decrease in specific DON compounds over time, e.g. by combining high performance liquid chromatography (HPLC)-based approaches for low molecular weight DON and Fourier transform ion cyclotron resonance mass spectrometry (FT-ICR-MS) for high molecular weight DON (Dittmar & Stubbins 2014), could allow to identify additional DON compounds that are relevant for nitrifiers.

Another factor that is largely unexplored and could be addressed in such an experiment is whether nitrifiers are only able to use simple DON compounds, with a low C:N ratio, or whether they can also use larger DON compounds with higher C:N ratios. The larger DON compounds are, the more C they contain relative to N, the more competition nitrifiers might face from heterotrophs that utilize DON as both C- and N-source. On the other hand, Damashek and colleagues found a tendency towards increasing ammonia oxidation rates from polyamine-N with increasing C-skeleton length (Damashek et al. 2019).

Further research is needed to establish whether there is a preference among different microbial groups for different DON compounds, and whether these patterns differ depending on region, nutrient conditions, or season.

6.2.3. Differential DON utilization between co-occurring clades of nitrifiers

DON use patterns may not only differ between nitrifiers and heterotrophs. Different, co-occurring nitrifiers may also specialize on distinct DON compounds to avoid inter-clade competition and thus occupy different substrate-based niches. Of two *Nitrosopumilus* species that both were enriched from the Mediterranean Sea, only one encoded urease, while the other appeared to be better equipped for a particle-associated lifestyle (Bayer et al. 2016). This could suggest that differential DON use can indeed confer an ecological niche. Also in the environment, different proportions of the AOA community encoded for urease in different geographic regions (Tolar et al. 2017). However, it is unclear if AOA lacking urease can instead use other DON compounds.

The analyses performed in this thesis (**Chapter 3 and 4**) mainly targeted the GoM AOA and the GoM Nitrospinae populations as a whole, rather than looking at individual sub-groups. However, this data suggested that while some AOA are able to directly use urea, also non-urease encoding AOA indirectly benefit from urea-derived N via cross-feeding. In contrast, the use of ammonium and cyanate as N-sources was similar across all measured GoM AOA. GoM Nitrospinae, despite the presence of several co-occurring species, appeared to display rather uniform assimilation rates of the tested substrates ammonium, urea and cyanate.

These combined findings indicate that GoM nitrifiers differentiate their ecological niches based on additional factors than mere ammonium, urea and cyanate utilization patterns. Future studies will reveal whether or not this is a general feature of marine nitrifiers and holds true across different oceanic regions.

6.2.4. Importance of DON utilization in oligotrophic environments

The Louisiana shelf of the GoM, where AOA and Nitrospinae DON utilization was studied (**Chapter 3 and 4**) is a nutrient-rich system compared to the vast majority of the ocean's waters, which are oligotrophic. Concentration ratios of DON:ammonium tend to be lower in coastal or shelf areas compared to more oligotrophic waters, indicating that relative DON availability in oligotrophic systems may be higher (Antia et al. 1991). This implies that AOA might experience a stronger ammonium limitation in oligotrophic systems and possibly rely even more on the use of alternative substrates, i.e. DON, to sustain their high cell numbers throughout the ocean (Herndl et al. 2005; Teira et al. 2006; Church et al. 2010). However, it is still unclear if AOA in the oligotrophic ocean indeed display a proportionally higher utilization rate of DON compared to nutrient rich shelf systems. Preliminary data (data not shown) from our work in the Mediterranean and the Angola Gyre indicate that AOA may indeed meet a large part of their energy need by utilizing DON in oligotrophic oceanic regions.

Compared to the GoM AOA, GoM Nitrospinae appeared to cover a much larger proportion of their cellular N-requirement from urea and cyanate. Single cell amplified genomes indicate that also in oligotrophic systems, many Nitrospinae contain ureases and cyanases (Pachiadaki et al. 2017). This implies that the use of these N-sources may be important for Nitrospinae throughout the ocean.

Comparing the relative contribution of ammonium and DON to AOA and Nitrospinae energy and/or N-assimilation requirements across different nutrient regimes and oceanic regions will reveal important insights into the ecophysiology of these ubiquitous nitrifiers.

6.2.5. Nitrifier DON affinities

Previous work has shown that both cultured and environmental AOA have an exceptionally high affinity for their primary substrate, ammonium/ammonia (Martens-Habbena et al. 2009; Horak et al. 2013). It is generally assumed that this is a key factor explaining their high abundance in marine systems. Data presented in this thesis (**Chapter 3 and 4**) and findings of other groups (e.g. Tolar et al. 2017; Santoro et al. 2017; Damashek et al. 2019) have shown that both AOA and Nitrospinae can meet a significant portion of their energy and/or N-assimilation requirements from organic N-compounds. However, one aspect that has not been addressed so far, is, how the nitrifiers' affinities for DON compare to their affinity for ammonium. This however, has important implications. Can nitrifiers scavenge low concentrations of DON compounds as efficiently as low concentrations of ammonium? Or is their affinity for DON even higher than that for ammonium? If so, nitrifiers may even preferentially utilize DON over ammonium in some regions of the ocean.

Urea, polyamines and amino acids are frequently taken up from the environment by ABC-type transporters, which can have exceptionally high affinities for their substrates (Hosie & Poole 2001; Valladares et al. 2002; Shah & Swiatlo 2008). If nitrifiers' DON uptake and degradation machinery has a sufficiently high affinity, these traits may allow them to remain active by using DON compounds as energy source, even when ambient ammonium concentrations were below their apparent K_m for ammonium.

Another important but unconstrained aspect is to compare the DON affinities of nitrifiers to those of other microorganisms, as this will ultimately determine whether nitrifiers can efficiently compete for DON with other members of the microbial community.

6.2.6. Utilization of alternative electron donors by nitrite oxidizers

Metabolic versatility of nitrifiers, and, more specifically, NOB, is not limited to the use of DON compounds as an additional N-source for biomass growth. Both *Nitrotoga* (**Chapter 2**) and marine Nitrospinae (**Chapter 4**) encode for genes that likely allow them to use sulfite and/or hydrogen as

additional electron donors in addition to nitrite. This is not a unique feature found only in these two studies, indeed, many nitrite oxidizers have the genetic potential to use hydrogen (Sorokin et al. 2012; Lücker et al. 2013; Koch et al. 2014; Füssel et al. 2017) and sulfur compounds (Sorokin et al. 2012; Lücker et al. 2013; Füssel et al. 2017). While hydrogen and sulfide oxidation have been tested on NOB isolates (Koch et al. 2014; Füssel et al. 2017), it is unconstrained whether these alternative metabolisms are environmentally relevant for NOB, and whether some NOB may even actually be hydrogen oxidizers with the additional capacity to also oxidize nitrite (Daims et al. 2016).

Testing the environmental relevance of these alternative metabolic processes – e.g. using stable isotope incubations linked to single cell analyses, as done in **Chapter 3 and 4**, or using Flow-SIP, as in **Chapter 5** – will be important aspects of NOB research in the future, as these reactions could provide energy for NOB in times of nitrite depletion or anoxia, and thereby could substantially expand their ecological niche.

The findings presented in this thesis give first important insights into key physiological traits of nitrifiers, both in culture and in the environment. One prominent outcome was the importance of the DON compounds urea and cyanate for both AOA and Nitrospinae. As DON is by far the most abundant reduced N-source in the marine environment (Gruber 2008), it is highly advantageous to use DON in addition to ammonium for autotrophs relying on reduced N as their energy source. Therefore, it is not surprising that nitrifiers have developed and/or acquired the enzymatic machinery to utilize DON as an additional source of energy and N for assimilation. However, many oceanic ecosystem models currently account for nitrification solely as a function of the environmental ammonium concentration (e.g. Yool et al. 2007; Yool 2010). The results presented here, together with the high abundance of DON in the world oceans indicates that this approach may be insufficient to accurately represent global nitrification activity in ocean models. Furthermore, nitrifiers are not the only chemolithoautotrophs with large effects on biogeochemical N-cycling that rely on reduced N-compounds. Anammox bacteria also depend on the availability of reduced N and have recently been implicated in DON utilization (Babbin et al. 2017; Ganesh et al. 2018).

There is ample opportunity for future research on metabolic versatility and DON utilization patterns in both nitrifiers and anammox, which hopefully eventually allows us to understand how these globally important microorganisms keep biogeochemical N-cycling in balance.

References

- Alawi M., Lipski A., Sanders T., Pfeiffer E.M. and Spieck E. 2007. Cultivation of a Novel Cold-Adapted Nitrite Oxidizing Betaproteobacterium from the Siberian Arctic. *The ISME Journal* 1 (3): 256–64. doi:10.1038/ismej.2007.34.
- Alonso-Saez L., Waller A.S., Mende D.R., Bakker K., Farnelid H., Yager P.L., Lovejoy C., Tremblay J.-E., Potvin M., Heinrich F., Estrada M., Riemann L., Bork P., Pedros-Alio C. and Bertilsson S. 2012. Role for Urea in Nitrification by Polar Marine Archaea. *Proceedings of the National Academy of Sciences of the United States of America* 109 (44): 17989–94. doi:10.1073/pnas.1201914109.
- Antia N.J., Harrison P.J. and Oliveira L. 1991. The Role of Dissolved Organic Nitrogen in Phytoplankton Nutrition, Cell Biology and Ecology. *Phycologia* 30 (1): 1–89. doi:10.2216/i0031-8884-30-1-1.1.
- Babbin A.R., Peters B.D., Mordy C.W., Widner B., Casciotti K.L. and Ward B.B. 2017. Multiple Metabolisms Constrain the Anaerobic Nitrite Budget in the Eastern Tropical South Pacific. *Global Biogeochemical Cycles* 31: 258–71. doi:10.1002/2016GB005407.
- Baudoux A.C., Veldhuis M.J.W., Noordeloos A.A.M., Van Noort G. and Brussaard C.P.D. 2008. Estimates of Virus- vs. Grazing Induced Mortality of Picophytoplankton in the North Sea during Summer. *Aquatic Microbial Ecology* 52: 69–82. doi:10.3354/ame01207.
- Bayer B., Vojvoda J., Offre P., Alves R.J.E., Elisabeth N.H., Garcia J. AL, Volland J.-M., Srivastava A., Schleper C. and Herndl G.J. 2016. Physiological and Genomic Characterization of Two Novel Marine Thaumarchaeal Strains Indicates Niche Differentiation. *The ISME Journal* 10. Nature Publishing Group: 1051–63. doi:10.1038/ismej.2015.200.
- Bayer B., Vojvoda J., Reinthaler T., Reyes C., Pinto M. and Herndl G.J. 2019. Nitrosopumilus Adriaticus Sp. Nov. and Nitrosopumilus Piranensis Sp. Nov., Two Ammonia-Oxidizing Archaea from the Adriatic Sea and Members of the Class Nitrososphaeria. *International Journal of Systematic and Evolutionary Microbiology*, 1–11. doi:10.1099/ijsem.0.003360.
- Belser L.W. 1984. Bicarbonate Uptake by Nitrifiers: Effects of Growth Rate, PH, Substrate Concentration, and Metabolic Inhibitors. *Applied and Environmental Microbiology* 48 (6): 1100–1104.
- Berg I.A. 2011. Ecological Aspects of the Distribution of Different Autotrophic CO₂ Fixation Pathways. *Applied and Environmental Microbiology* 77 (6): 1925–36. doi:10.1128/AEM.02473-10.
- Berry D., Mader E., Lee T.K., Woebken D., Wang Y., Zhu D., Palatinszky M., Schintlmeister A., Schmid M.C., Hanson B.T., Shterzer N., Mizrahi I., Rauch I., Decker T., Bocklitz T., Popp J., Gibson C.M., Fowler P.W., Huang W.E., et al. 2015. Tracking Heavy Water (D₂O) Incorporation for Identifying and Sorting Active Microbial Cells. *Proceedings of the National Academy of Sciences of the United States of America* 112 (2): 194–203. doi:10.1073/pnas.1420406112.
- Boddicker A.M. and Mosier A.C. 2018. Genomic Profiling of Four Cultivated Candidatus Nitrotoga Spp. Predicts Broad Metabolic Potential and Environmental Distribution. *ISME Journal* 12. Springer US: 2864–82. doi:10.1038/s41396-018-0240-8.
- Church M.J., Wai B., Karl D.M. and DeLong E.F. 2010. Abundances of Crenarchaeal AmoA Genes and Transcripts in the Pacific Ocean. *Environmental Microbiology* 12 (3): 679–88. doi:10.1111/j.1462-2920.2009.02108.x.
- Costa E., Pérez J. and Kreft J.-U. 2006. Why Is Metabolic Labour Divided in Nitrification? *Trends in Microbiology* 14 (5): 213–19. doi:10.1016/j.tim.2006.03.006.
- Daims H., Lebedeva E. V., Pjevac P., Han P., Herbold C., Albertsen M., Jehmlich N., Palatinszky M., Vierheilig J., Bulaev A., Kirkegaard R.H., von Bergen M., Rattei T., Bendinger B., Nielsen P.H. and Wagner M. 2015. Complete Nitrification by Nitrospira Bacteria. *Nature* 528 (7583): 504–9. doi:10.1038/nature16461.
- Daims H., Lüscher S. and Wagner M. 2016. A New Perspective on Microbes Formerly Known as Nitrite-Oxidizing Bacteria. *Trends in Microbiology* 24 (9): 699–712. doi:10.1016/j.tim.2016.05.004.
- Damashek J., Tolar B.B., Liu Q., Okotie-Oyekun A.O., Wallsgrove N.J., Popp B.N. and Hollibaugh J.T. 2019. Microbial Oxidation of Nitrogen Supplied as Selected Organic Nitrogen Compounds in the South Atlantic Bight. *Limnology and Oceanography* 64 (3): 982–95. doi:10.1002/lno.11089.
- Dittmar T. and Stubbins A. 2014. Dissolved Organic Matter in Aquatic Systems. In *Treatise on Geochemistry*, edited by Heinrich D Holland and Karl K Turekian, 2nd ed., 12:125–56. Oxford: Elsevier Ltd. doi:10.1016/B978-0-12-382182-9.00014-1.

- Epstein S.S. and Shiaris M.P. 1992. Size-Selective Grazing of Coastal Bacterioplankton by Natural Assemblages of Pigmented Flagellates, Colorless Flagellates, and Ciliates. *Microbial Ecology* 23: 211–25. doi:10.1007/BF00164097.
- Evans C., Archer S.D., Jacquet S. and Wilson W.H. 2003. Direct Estimates of the Contribution of Viral Lysis and Microzooplankton Grazing to the Decline of a *Micromonas* Spp. Population. *Aquatic Microbial Ecology* 30: 207–19.
- Füssel J., Lücker S., Yilmaz P., Nowka B., van Kessel M.A.H.J., Bourceau P., Hach P.F., Littmann S., Berg J., Spieck E., Daims H., Kuypers M.M.M. and Lam P. 2017. Adaptability as the Key to Success for the Ubiquitous Marine Nitrite Oxidizer *Nitrospira*. *Science Advances* 3: 1–9. doi:10.1126/sciadv.1700807.
- Gabor E.M., Alkema W.B.L. and Janssen D.B. 2004. Quantifying the Accessibility of the Metagenome by Random Expression Cloning Techniques. *Environmental Microbiology* 6 (9): 879–86. doi:10.1111/j.1462-2920.2004.00640.x.
- Ganesh S., Bertagnolli A.D., Bristow L.A., Padilla C.C., Blackwood N., Aldunate M., Bourbonnais A., Altabet M.A., Malmstrom R.R., Woyke T., Ulloa O., Konstantinidis K.T., Thamdrup B. and Stewart F.J. 2018. Single Cell Genomic and Transcriptomic Evidence for the Use of Alternative Nitrogen Substrates by Anammox Bacteria. *The ISME Journal* 12: 2706–22. doi:10.1038/s41396-018-0223-9.
- Glover H.E. 1985. The Relationship between Inorganic Nitrogen Oxidation and Organic Carbon Production in Batch and Chemostat Cultures of Marine Nitrifying Bacteria. *Archives of Microbiology* 142: 45–50.
- Griffin B.M., Schott J. and Schink B. 2007. Nitrite, an Electron Donor for Anoxygenic Photosynthesis. *Science* 316: 1870. doi:10.1126/science.1139478.
- Gruber N. 2008. The Marine Nitrogen Cycle: Overview and Challenges. In *Nitrogen in the Marine Environment*, edited by Douglas G Capone, Deborah A Bronk, Margaret R Mulholland, and Edward J Carpenter, 2nd ed., 3:1–50. Elsevier. doi:10.1128/microbe.3.186.1.
- Hatzenpichler R., Scheller S., Tavormina P.L., Babin B.M., Tirrell D.A. and Orphan V.J. 2014. In Situ Visualization of Newly Synthesized Proteins in Environmental Microbes Using Amino Acid Tagging and Click Chemistry. *Environmental Microbiology* 16 (8): 2568–90. doi:10.1111/1462-2920.12436.
- Herndl G.J., Reinthaler T., Teira E., Aken H. Van, Veth C., Pernthaler A. and Pernthaler J. 2005. Contribution of Archaea to Total Prokaryotic Production in the Deep Atlantic Ocean. *Applied and Environmental Microbiology* 71 (5): 2303–9. doi:10.1128/AEM.71.5.2303.
- Horak R.E.A., Qin W., Schauer A.J., Armbrust E.V., Ingalls A.E., Moffett J.W., Stahl D.A. and Devol A.H. 2013. Ammonia Oxidation Kinetics and Temperature Sensitivity of a Natural Marine Community Dominated by Archaea. *The ISME Journal* 7: 2023–33. doi:10.1038/ismej.2013.75.
- Hosie A.H.F. and Poole P.S. 2001. Bacterial ABC Transporters of Amino Acids. *Research in Microbiology* 152: 259–70. doi:10.1016/S0923-2508(01)01197-4.
- Huberts D.H.E.W. and van der Klei I.J. 2010. Moonlighting Proteins: An Intriguing Mode of Multitasking. *Biochimica et Biophysica Acta* 1803: 520–25. doi:10.1016/j.bbamcr.2010.01.022.
- Kamennaya N.A., Chernihovsky M. and Post A.F. 2008. The Cyanate Utilization Capacity of Marine Unicellular Cyanobacteria. *Limnology and Oceanography* 53 (6): 2485–94. doi:10.4319/lo.2008.53.6.2485.
- Kamennaya N.A. and Post A.F. 2011. Characterization of Cyanate Metabolism in Marine *Synechococcus* and *Prochlorococcus* Spp. *Applied and Environmental Microbiology* 77 (1): 291–301. doi:10.1128/AEM.01272-10.
- Kitzinger K., Koch H., Lücker S., Sedlacek C.J., Herbold C., Schwarz J., Daebeler A., Mueller A.J., Lukumbuzya M., Romano S., Leisch N., Michael Karst S., Kirkegaard R., Albertsen M., Nielsen P.H., Wagner M. and Daims H. 2018. Characterization of the First “*Candidatus Nitrotoga*” Isolate Reveals Metabolic Versatility and Separate Evolution of Widespread Nitrite-Oxidizing Bacteria. *MBio* 9 (4): e01186-18. doi:10.1128/mBio.
- Kitzinger K., Padilla C.C., Marchant H.K., Hach P.F., Herbold C.W., Kidane A.T., Könneke M., Littmann S., Mooshammer M., Niggemann J., Petrov S., Richter A., Stewart F.J., Wagner M., Kuypers M.M.M. and Bristow L.A. 2019. Cyanate and Urea Are Substrates for Nitrification by Thaumarchaeota in the Marine Environment. *Nature Microbiology* 4 (2): 234–43. doi:10.1038/s41564-018-0316-2.
- Koch H., Galushko A., Albertsen M., Schintlmeister A., Gruber-Dorninger C., Lücker S., Pelletier E., Le Paslier D., Spieck E., Richter A., Nielsen P.H., Wagner M. and Daims H. 2014. Growth of Nitrite-Oxidizing Bacteria by Aerobic Hydrogen Oxidation. *Science* 345 (6200): 761–63.
- Koch H., Lücker S., Albertsen M., Kitzinger K., Herbold C., Spieck E., Nielsen P.H., Wagner M. and Daims H. 2015. Expanded Metabolic Versatility of Ubiquitous Nitrite-Oxidizing Bacteria from the Genus *Nitrospira*.

- Proceedings of the National Academy of Sciences of the United States of America* 112 (36): 11371–76. doi:10.1073/pnas.1506533112.
- Könneke M., Bernhard A.E., de la Torre J.R., Walker C.B., Waterbury J.B. and Stahl D.A. 2005. Isolation of an Autotrophic Ammonia-Oxidizing Marine Archaeon. *Nature* 437: 543–46. doi:10.1038/nature03911.
- Könneke M., Schubert D.M., Brown P.C., Hügler M., Standfest S., Schwander T., Schada von Borzyskowski L., Erb T.J., Stahl D.A. and Berg I.A. 2014. Ammonia-Oxidizing Archaea Use the Most Energy-Efficient Aerobic Pathway for CO₂ Fixation. *Proceedings of the National Academy of Sciences of the United States of America* 111 (22): 8239–44. doi:10.1073/pnas.1402028111.
- Landry M.R. and Hassett R.P. 1982. Estimating the Grazing Impact of Marine Micro-Zooplankton. *Marine Biology* 67: 283–88. doi:10.1007/BF00397668.
- Lee K.S., Palatinszky M., Pereira F.C., Nguyen J., Fernandez V.I., Mueller A.J., Menolascina F., Daims H., Berry D., Wagner M. and Stocker R. 2019. An Automated Raman-Based Platform for the Sorting of Live Cells by Functional Properties. *Nature Microbiology*. doi:10.1038/s41564-019-0394-9.
- Lindskog S. 1997. Structure and Mechanism of Carbonic Anhydrase. *Pharmacology and Therapeutics* 74 (1): 1–20. doi:10.1016/S0163-7258(96)00198-2.
- Lücker S., Nowka B., Rattei T., Spieck E. and Daims H. 2013. The Genome of Nitrospina Gracilis Illuminates the Metabolism and Evolution of the Major Marine Nitrite Oxidizer. *Frontiers in Microbiology* 4 (27): 1–19. doi:10.3389/fmicb.2013.00027.
- Lücker S., Wagner M., Maixner F., Pelletier E., Koch H., Vacherie B., Rattei T., Sinninghe Damsté J.S., Spieck E., Le Paslier D. and Daims H. 2010. A Nitrospira Metagenome Illuminates the Physiology and Evolution of Globally Important Nitrite-Oxidizing Bacteria. *Proceedings of the National Academy of Sciences of the United States of America* 107 (30): 13479–84. doi:10.1073/pnas.1003860107.
- Martens-Habbena W., Berube P.M., Urakawa H., de la Torre J.R. and Stahl D.A. 2009. Ammonia Oxidation Kinetics Determine Niche Separation of Nitrifying Archaea and Bacteria. *Nature* 461: 976–79. doi:10.1038/nature08465.
- Ouverney C.C. and Fuhrman J. a. 2000. Marine Planktonic Archaea Take up Amino Acids. *Applied and Environmental Microbiology* 66 (11): 4829–33. doi:10.1128/AEM.66.11.4829-4833.2000.
- Pachiadaki M.G., Sintés E., Bergauer K., Brown J.M., Record N.R., Swan B.K., Mathyer M.E., Hallam S.J., Lopez-Garcia P., Takaki Y., Nunoura T., Woyke T., Herndl G.J. and Stepanauskas R. 2017. Major Role of Nitrite-Oxidizing Bacteria in Dark Ocean Carbon Fixation. *Science* 358: 1046–51. doi:10.1126/science.aan8260.
- Palatinszky M., Herbold C., Jehmlich N., Pogoda M., Han P., Bergen M. Von, Lagkouvardos I., Karst S.M., Galushko A., Koch H., Berry D., Daims H. and Wagner M. 2015. Cyanate as an Energy Source for Nitrifiers. *Nature* 524: 105–8. doi:10.1038/nature14856.
- Probandt D., Eickhorst T., Ellrott A., Amann R. and Knittel K. 2018. Microbial Life on a Sand Grain: From Bulk Sediment to Single Grains. *The ISME Journal* 12: 623–33. doi:10.1038/ismej.2017.197.
- Rasche M.E. and Seefeldt L.C. 1997. Reduction of Thiocyanate, Cyanate, and Carbon Disulfide by Nitrogenase: Kinetic Characterization and EPR Spectroscopic Analysis. *Biochemistry* 36: 8574–85. doi:10.1021/bi970217e.
- Santoro A.E., Saito M.A., Goepfert T.J., Lamborg C.H., Dupont C.L. and Ditullio G.R. 2017. Thaumarchaeal Ecotype Distributions across the Equatorial Pacific Ocean and Their Potential Roles in Nitrification and Sinking Flux Attenuation. *Limnology and Oceanography* 62: 1984–2003. doi:10.1002/lno.10547.
- Sayavedra-Soto L.A. and Stein L.Y. 2010. Genetic Transformation of Ammonia-Oxidizing Bacteria. In *Methods in Enzymology*, 1st ed., 486:389–402. Elsevier Inc. doi:10.1016/B978-0-12-381294-0.00017-1.
- Seravalli J., Kumar M., Lu W.P. and Ragsdale S.W. 1995. Mechanism of CO Oxidation by Carbon Monoxide Dehydrogenase from *Clostridium thermoaceticum* and Its Inhibition by Anions. *Biochemistry* 34: 7879–88. doi:10.1021/bi00024a012.
- Shah P. and Swiatlo E. 2008. A Multifaceted Role for Polyamines in Bacterial Pathogens. *Molecular Microbiology* 68 (1): 4–16. doi:10.1111/j.1365-2958.2008.06126.x.
- Sorokin D.Y., Lücker S., Vejmekova D., Kostrikina N. a, Kleerebezem R., Rijpstra W.I.C., Damsté J.S.S., Le Paslier D., Muyzer G., Wagner M., van Loosdrecht M.C.M. and Daims H. 2012. Nitrification Expanded: Discovery, Physiology and Genomics of a Nitrite-Oxidizing Bacterium from the Phylum Chloroflexi. *The ISME Journal* 6: 2245–56. doi:10.1038/ismej.2012.70.

- Supuran C.T., Conroy C.W. and Maren T.H. 1997. Is Cyanate a Carbonic Anhydrase Substrate? *Proteins: Structure, Function and Genetics* 27: 272–78. doi:10.1002/(SICI)1097-0134(199702)27:2<272::AID-PROT12>3.0.CO;2-J.
- Teira E., van Aken H., Veth C. and Herndl G.J. 2006. Archaeal Uptake of Enantiomeric Amino Acids in the Meso- and Bathypelagic Waters of the North Atlantic. *Limnology and Oceanography* 51 (1): 60–69. doi:10.4319/lo.2006.51.1.0060.
- Tolar B.B., Wallsgrove N.J., Popp B.N. and Hollibaugh J.T. 2017. Oxidation of Urea-Derived Nitrogen by Thaumarchaeota-Dominated Marine Nitrifying Communities. *Environmental Microbiology* 19 (12): 4838–4850. doi:10.1002/elsc.201200179.
- Treusch A.H., Leininger S., Kietzin A., Schuster S.C., Klenk H.P. and Schleper C. 2005. Novel Genes for Nitrite Reductase and Amo-Related Proteins Indicate a Role of Uncultivated Mesophilic Crenarchaeota in Nitrogen Cycling. *Environmental Microbiology* 7 (12): 1985–95. doi:10.1111/j.1462-2920.2005.00906.x.
- Valladares A., Montesinos M.L., Herrero A. and Flores E. 2002. An ABC-Type, High-Affinity Urea Permease Identified in Cyanobacteria. *Molecular Microbiology* 43 (3): 703–15. doi:10.1046/j.1365-2958.2002.02778.x.
- van Kessel M.A.H.J., Speth D.R., Albertsen M., Nielsen P.H., Op den Camp H.J.M., Kartal B., Jetten M.S.M. and Lücker S. 2015. Complete Nitrification by a Single Microorganism. *Nature* 528: 555–59. doi:10.1038/nature16459.
- Venter J.C., Remington K., Heidelberg J.F., Halpern A.L., Rusch D., Eisen J.A., Wu D., Paulsen I., Nelson K.E., Nelson W., Fouts D.E., Levy S., Knap A.H., Lomas M.W., Nealson K., White O., Peterson J., Hoffman J., Parsons R., et al. 2004. Environmental Genome Shotgun Sequencing of the Sargasso Sea. *Science* 304: 66–74. doi:10.1126/science.1093857.
- Walker C.B., de la Torre J.R., Klotz M.G., Urakawa H., Pinel N., Arp D.J., Brochier-Armanet C., Chain P.S.G., Chan P.P., Gollabgir A., Hemp J., Hügler M., Karr E.A., Könneke M., Shin M., Lawton T.J., Lowe T., Martens-Habbena W., Sayavedra-Soto L.A., et al. 2010. Nitrosopumilus Maritimus Genome Reveals Unique Mechanisms for Nitrification and Autotrophy in Globally Distributed Marine Crenarchaea. *Proceedings of the National Academy of Sciences of the United States of America* 107 (19): 8818–23. doi:10.1073/pnas.0913533107.
- Yool A. 2010. Modeling the Role of Nitrification in Open Ocean Productivity and the Nitrogen Cycle. In *Methods in Enzymology*, 1st ed., 486:3–32. Elsevier Inc. doi:10.1016/B978-0-12-381294-0.00001-8.
- Yool A., Martin A.P., Fernández C. and Clark D.R. 2007. The Significance of Nitrification for Oceanic New Production. *Nature* 447: 999–1002. doi:doi: 10.1038/nature05885.

Author contributions

Chapter 2 – Characterization of the first “*Candidatus Nitrotoga*” isolate reveals metabolic versatility and separate evolution of widespread nitrite-oxidizing bacteria

Katharina Kitzinger, Hanna Koch, Sebastian Lücker, Christopher J. Sedlacek, Craig Herbold, Jasmin Schwarz, Anne Daebeler, Anna J. Mueller, Michael Lukumbuzya, Stefano Romano, Nikolaus Leisch, Søren Michael Karst, Rasmus Kirkegaard, Mads Albertsen, Per Halkjær Nielsen, Michael Wagner, Holger Daims

Detailed author contributions

I designed the study with H.D., H.K. and M.W. I enriched and isolated *Ca. Nitrotoga fabula*, and maintained the culture with help of J.S. I extracted DNA and performed fluorescence *in situ* hybridization experiments. S.M.K., R.K. and P.H.N. sequenced the genome. I annotated the genome with support from S.L., H.K. and H.D. I performed all physiological experiments and data analyses (except for microrespirometry measurements) and calculated the 16S rRNA gene phylogeny. Microrespirometry measurements were performed by C.J.S. Electron microscopy was performed by A.D., N.L. and S.R. Cultivation, DNA extraction and genome analyses of the crenarchaeal enrichment was done by A.D., A.J.M., M.L., H.D., M.A. and C.H. Nxr phylogenetic trees were calculated by C.H. and S.L. I assembled and interpreted the data and wrote the manuscript together with H.D., with contributions from all co-authors. *Ca. N. fabula* was isolated during my MSc thesis (<http://othes.univie.ac.at/36778/>), all other experiments were performed during my doctoral thesis.

Published in mBio 2018, 9 (4) e01186-18

Chapter 3 – Cyanate and urea are substrates for nitrification by Thaumarchaeota in the marine environment

Katharina Kitzinger, Cory C. Padilla, Hannah K. Marchant, Philipp F. Hach, Craig W. Herbold, Abiel T. Kidane, Martin Könneke, Sten Littmann, Maria Mooshammer, Jutta Niggemann, Sandra Petrov, Andreas Richter, Frank J. Stewart, Michael Wagner, Marcel M. M. Kuypers, Laura A. Bristow

Detailed author contributions

I, L.A.B., H.K.M., M.M.M.K. and M.W. designed the study. I performed experiments onboard R/V Pelican with L.A.B. I prepared samples for mass spectrometry measurements, NanoSIMS and performed fluorescence *in situ* hybridization experiments. *N. maritimus* was provided by S.P. and M.K. I performed experiments with *N. maritimus* cultures with H.K.M. and L.A.B. NanoSIMS analyses were done by S.L. and A.T.K. I assembled and analyzed all data with help of L.A.B., H.K.M. and P.F.H. C.C.P. sampled for and did molecular analyses with contribution from C.W.H. and F.J.S. Cyanate concentrations were measured by M.M. and A.R.; total dissolved nitrogen was analyzed by J.N. I assembled and interpreted the data and wrote the manuscript together with L.A.B. and H.K.M., with contributions from all co-authors.

Published in Nature Microbiology 2019, 4, 234–243

Chapter 4 – Single cell analyses reveal contrasting life strategies of the two main nitrifiers in the ocean

Katharina Kitzinger, Hannah K. Marchant, Laura A. Bristow, Craig W. Herbold, Cory C. Padilla, Abiel T. Kidane, Sten Littmann, Holger Daims, Petra Pjevac, Frank J. Stewart, Michael Wagner, Marcel M. M. Kuypers

Detailed author contributions

I designed the study with H.K.M., M.M.M.K., L.A.B. and M.W. I performed experiments onboard R/V Pelican with L.A.B. I designed the new fluorescence *in situ* hybridization probe, prepared samples for mass spectrometry measurements, incl. NanoSIMS and performed fluorescence *in situ* hybridization for cell counts. S.L. and A.T.K. ran nanoSIMS analyses. I assembled and analyzed all data with help of H.K.M. and L.A.B. C.C.P. sampled for molecular analyses, C.W.H. performed molecular analyses with contribution from F.J.S. and P.P. I manually annotated key genes in Nitrospinae metagenome assembled genomes with help from H.D. I wrote the manuscript with H.K.M., L.A.B. and M.M.M.K., with contributions from all co-authors.

In preparation for submission to an international peer-reviewed journal

Chapter 5 – Flow-through stable isotope probing (Flow-SIP) minimizes cross feeding in complex microbial communities

Mooshammer Maria*, Katharina Kitzinger*, Arno Schintlmeister, Soeren Ahmerkamp, Jeppe Lund Nielsen, Per Nielsen, Michael Wagner

* equal contribution

Detailed author contributions

I, M.M. and M.W. designed the study. I and M.M. developed the experimental setup and performed all experiments, with support from J.L.N. and P.N. NanoSIMS measurements were done by A.S. I and M.M. analyzed and assembled all data. S.A. modelled nitrite concentrations around ammonia oxidizer colonies. The manuscript was written by M.M. and me, with contributions from all co-authors.

In preparation for submission to an international peer-reviewed journal

Versicherung an Eides Statt / *Affirmation in lieu of an oath*

**gem. § 5 Abs. 5 der Promotionsordnung vom 18.06.2018 /
according to § 5 (5) of the Doctoral Degree Rules and Regulations of 18 June, 2018**

Ich / I, Katharina Kitzinger, Roonstrasse 59, 28203 Bremen, Mat.-Nr. 3049824
(Vorname / First Name, Name / Name, Anschrift / Address, ggf. Matr.-Nr. / student ID no., if applicable)

versichere an Eides Statt durch meine Unterschrift, dass ich die vorliegende Dissertation selbständig und ohne fremde Hilfe angefertigt und alle Stellen, die ich wörtlich dem Sinne nach aus Veröffentlichungen entnommen habe, als solche kenntlich gemacht habe, mich auch keiner anderen als der angegebenen Literatur oder sonstiger Hilfsmittel bedient habe und die zu Prüfungszwecken beigelegte elektronische Version (PDF) der Dissertation mit der abgegebenen gedruckten Version identisch ist. / *With my signature I affirm in lieu of an oath that I prepared the submitted dissertation independently and without illicit assistance from third parties, that I appropriately referenced any text or content from other sources, that I used only literature and resources listed in the dissertation, and that the electronic (PDF) and printed versions of the dissertation are identical.*

Ich versichere an Eides Statt, dass ich die vorgenannten Angaben nach bestem Wissen und Gewissen gemacht habe und dass die Angaben der Wahrheit entsprechen und ich nichts verschwiegen habe. / *I affirm in lieu of an oath that the information provided herein to the best of my knowledge is true and complete.*

Die Strafbarkeit einer falschen eidesstattlichen Versicherung ist mir bekannt, namentlich die Strafandrohung gemäß § 156 StGB bis zu drei Jahren Freiheitsstrafe oder Geldstrafe bei vorsätzlicher Begehung der Tat bzw. gemäß § 161 Abs. 1 StGB bis zu einem Jahr Freiheitsstrafe oder Geldstrafe bei fahrlässiger Begehung. / *I am aware that a false affidavit is a criminal offence which is punishable by law in accordance with § 156 of the German Criminal Code (StGB) with up to three years imprisonment or a fine in case of intention, or in accordance with § 161 (1) of the German Criminal Code with up to one year imprisonment or a fine in case of negligence.*

Bremen, 13. Mai 2019
Ort / Place, Datum / Date

Signature

